Methodologies for evaluating exposure and response of stone masonry to wind-driven rain

Scott Allan Orr

St Cross College

University of Oxford

A thesis submitted for the degree of

Doctor of Philosophy

in

Science and Engineering in Arts, Heritage, and Archaeology

Trinity 2018

Abstract

Wind-driven rain (WDR) is a main moisture source and weathering factor for monumental and vernacular stone masonry in the UK. To conserve and manage these structures, especially as weather events are predicted to become more intense during the 21st century, methodologies are needed that: (a) characterise environmental WDR exposure, and (b) non-destructively monitor the response of moisture regimes within stone masonry.

This thesis aims to address exposure and response between WDR and stone masonry, integrating characterisation and methodological development with an emphasis on data handling and visualisation. Semi-empirical approaches are employed to characterise current and future WDR exposure in the UK to evaluate existing standards and metrics. The use of non-destructive electromagnetic techniques for moisture measurement is explored for comparative advantages when applied for stone masonry.

Extreme value analysis (EVA) is used to evaluate severe WDR exposure in the UK at eight sites. While reinforcing established trends (e.g. prevailing wind directions) this research highlighted the impact of wall orientation on the volume of water and consistency within WDR spells and their quantity and duration. The EVA demonstrated that current standards (ISO 15927-3 and BS 8104) underestimate extreme exposure. A combination of UKCP09 Weather Generator output with probabilistic processes demonstrated that existing contrasts between sites will be magnified by predicted climatic changes and become more seasonally polarised, providing an impetus to improve current standards by incorporating extreme value analysis and temporal metrics.

A novel, cost- and time-effective method of laboratory gravimetric calibration using 'isolated diffusion' was validated, which produced calibrations of radar and microwave techniques for three UK building stones that matched modelled behaviour. The combined use of microwave and radar techniques in field studies on two stone masonry constructions characterised localised moisture regimes within stone masonry *systems* (stone units and mortar joints), demonstrating that technique selection is optimised with consideration for material properties and the investigation objective. Innovative data handling and visualisation strategies demonstrated their utility for these scenarios of stone masonry composed of different materials.

By developing methodologies for semi-empirical evaluation and non-destructive techniques, as well as characterising environmental and hygric properties/behaviour of stones and stone masonry, this thesis has contributed to both progress in scientific research and practical aspects of heritage conservation in the context of a changing 21st century climate.

"From where we stand the rain seems random.
If we could stand somewhere else,
we would see the order in it."

– TONY HILLERMAN (1990, p. 214)

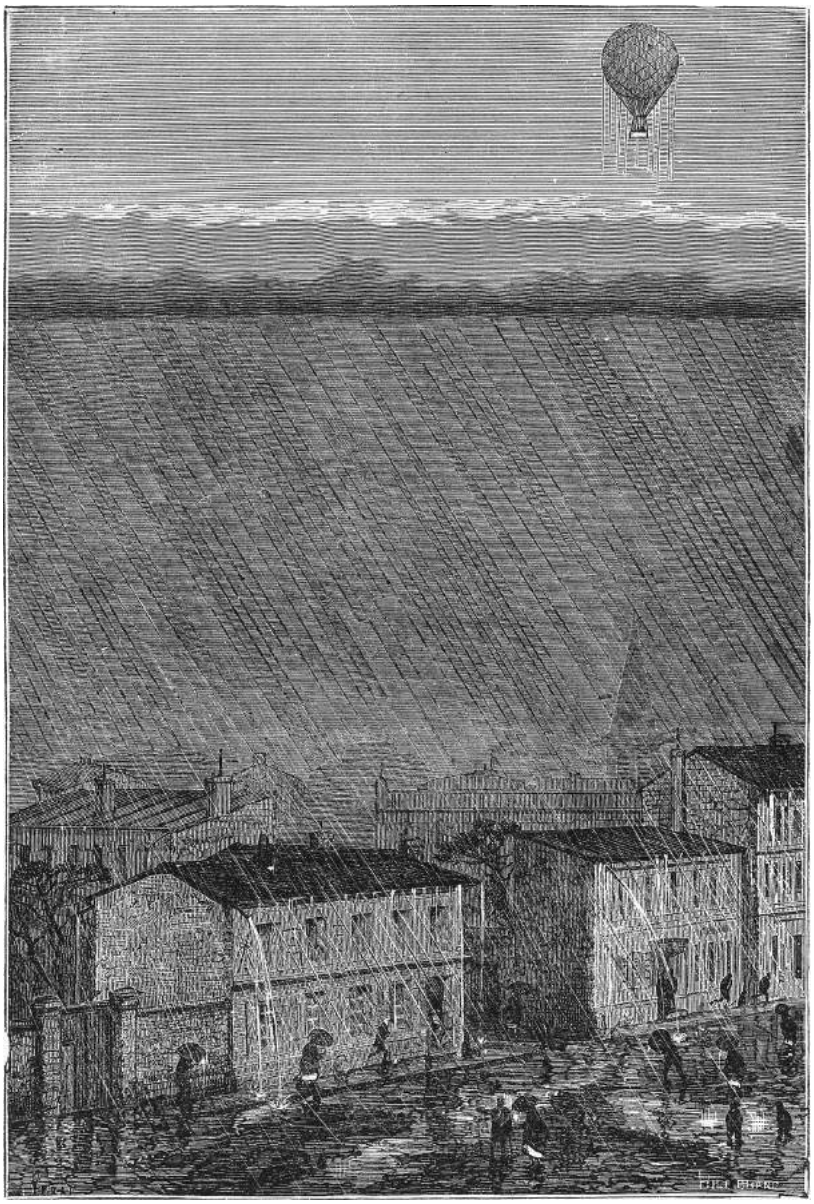

Coupe de l'Atmosphère pendant une pluie.
Source: *L'atmosphère et les grands phénomènes de la nature* (1905, p. 297)

Dedicated to every teacher
who has told a misfit
they can achieve anything:

it can mean so much.

Acknowledgements

Most doctoral students only dream of having a supervisor like Heather Viles: inspiring but exacting, and yet eternally supportive and encouraging. I will cherish the discussions we shared: they challenged me in ways I could not have foreseen. I take from them a broad vision of the scientific endeavour and a deepened understanding of what it truly means to be human.

I am indebted to several people for professional contributions: Alick Leslie, Dawson Stelfox, Maureen Young, and Joanne Curran for advice and guidance (and the support of Historic Environment Scotland and the Consarc Design Group); Mona Edwards and Hong Zhang, for their advice and support during laboratory experiments; Sabine Kruschwitz and Jens Wöstmann for their supervision and support during my placement at the German Bundesanstalt für Materialforschung und -prüfung (BAM); Iain Williams and his team, for going beyond professional duties to enable my site work in Edinburgh (and ensuring my continued survival while clambering around scaffolding); Colin Burns and William Revie for constructing test specimen walls, and Callum Graham, Sarah Hamilton, and Thomas Batchelor for contributing to data collection.

I would like to acknowledge the following organisations for financial support: the UK Engineering and Physical Sciences Research Council through the Centre for Doctoral Training in Science and Engineering in Arts, Heritage, and Archaeology (SEAHA CDT); the Natural Sciences and Engineering Research Council of Canada; Historic Environment Scotland; the Canadian Centennial Scholarship Fund; the York Consortium for Conservation and Craftsmanship; the University's School of Geography and the Environment; St Cross College; and the University's Santander Academic Travel Award scheme for enabling my placement at BAM. Finally, I would like to acknowledge Historic England for indirectly contributing to my research through the construction of laboratory test specimens for a parallel project that were of great benefit to my own work.

To conclude, personal gratitude is extended to[1]: the dazzling Lucie Fusade, for always being there; my inspiring colleagues within the Oxford Rock Breakdown Laboratory and SEAHA CDT (90% commiseration, 10% laughter—or perhaps the opposite); the effervescent Dr Robyn Pender, for challenging me to think about the big questions, and all those with whom I have lived, who put up with me and my shenanigans. Finally, to my family, who have always put up with me and my shenanigans. I could never thank you enough.

[1] Among countless others, which limitations of space do not permit me to explicitly acknowledge: you know who you are.

Table of Contents

Table of Contents i

List of Figures vii

List of Tables xi

I Research context and design 1

1 Introduction 3

1.1 Context . . . 3
1.2 Rationale . . . 4
1.3 Research aims and objectives . . . 9
1.4 Thesis structure . . . 10

2 Literature review 13

2.1 Stone in the UK built environment . . . 13
2.1.1 Stone weathering . . . 15
2.1.2 Behaviour of stone masonry systems . . . 17
2.2 Wind-driven rain . . . 20
2.2.1 Impacts . . . 21
2.2.2 Methods of assessment . . . 22
2.2.3 Semi-empirical evaluation of WDR . . . 24
2.2.4 Climate change and future uncertainty . . . 26
2.3 Characterising moisture regimes within stone masonry . . . 31
2.3.1 Principle of non-destructive moisture measurement . . . 32
2.3.2 Gravimetric calibration . . . 33
2.3.3 Guidance in the literature . . . 36
2.3.4 Measurement principles . . . 40
2.3.5 Combinative survey methods . . . 46

2.4 Conclusion 47

3 Research framework **49**

3.1 Structure 49

3.1.1 Components 52

3.1.2 Strategies 52

3.2 Method selection 54

3.2.1 Exposure to wind-driven rain 54

3.2.2 Response of stone masonry 55

II Semi-empirical evaluations of exposure to wind-driven rain **59**

4 Characterisation of building exposure to wind-driven rain in the UK and evaluation of current standards **61**

4.1 Introduction 63

4.2 Methods 66

4.2.1 Climate and sites 66

4.2.2 Calculating WDR exposure from meteorological data 68

4.3 Results 79

4.3.1 Annual frequency of wind-driven rain spells 79

4.3.2 Duration of wind-driven rain spells 81

4.3.3 Amount of wind-driven rain 82

4.3.4 Applicability of current standards 84

4.4 Discussion 92

4.5 Conclusion 93

5 Wind-driven rain and future risk to built heritage in the United Kingdom: novel metrics for characterising rain spells **95**

5.1 Introduction 97

5.2 Methods 100

5.2.1 The ISO model 100

5.2.2 Meteorological data 104

5.2.3 Sites 108

5.3 Results 109

5.3.1 Model validation 109

5.3.2 Annual characteristics 114

5.3.3 Spell volumes . . . 116
5.3.4 Spell durations and inter-spell characteristics . . . 120
5.3.5 Intra-spell characteristics . . . 124
5.4 Discussion . . . 125
5.4.1 Factors impacting calculations and predictions of wind-driven rain . . . 126
5.4.2 Implications for risks to cultural heritage and built infrastructure . . . 129
5.5 Conclusion . . . 135

III Non-destructive measurement of the response of moisture regimes within stone masonry 137

6 An 'isolated diffusion' gravimetric calibration procedure for radar and microwave moisture measurement in porous building stone 139
6.1 Introduction . . . 141
6.2 Material and methods . . . 144
6.2.1 Stones . . . 144
6.2.2 Procedure . . . 146
6.2.3 Equipment . . . 146
6.2.4 Gravimetric calibration . . . 153
6.3 Theory/Calculation . . . 155
6.4 Results . . . 160
6.4.1 Dry material dielectric constants . . . 160
6.4.2 Radar calibrations . . . 162
6.4.3 Microwave calibrations . . . 167
6.5 Discussion . . . 169
6.5.1 Calibration procedures . . . 169
6.5.2 Comparison of radar and microwave measurements . . . 172
6.6 Conclusion . . . 174

7 Moisture monitoring of stone masonry: a comparison of microwave and radar on a granite wall and a sandstone tower 177
7.1 Introduction . . . 179
7.2 Material and methods . . . 181
7.2.1 Experimental design . . . 181
7.2.2 Oxford experiment: purpose-built granite test wall . . . 183
7.2.3 Edinburgh experiment: New College, Edinburgh . . . 184

7.2.4 Percentile representation of measurements . . . 188
7.3 Results . . . 190
7.3.1 Oxford experiment . . . 191
7.3.2 Edinburgh experiment . . . 198
7.4 Discussion . . . 204
7.4.1 Comparative advantages of radar and microwave techniques . . . 204
7.4.2 Data visualisation and presentation . . . 207
7.5 Conclusion . . . 208

IV Implications for scientific research and practical heritage conservation 211

8 Discussion, synthesis and future work 213
8.1 Exposure to wind-driven rain . . . 214
8.1.1 Improving semi-empirical evaluation of wind-driven rain exposure . . . 214
8.1.2 Climate change during the 21st century . . . 218
8.2 Response of stone masonry . . . 220
8.2.1 Identifying regions with higher prevalence of wind-driven rain . . . 220
8.2.2 Characterising the potential impact of periodicity on moisture monitoring 221
8.2.3 Assessing the impact of urban scale and building geometry . . . 222
8.3 Data handling and visualisation . . . 223
8.3.1 Data handling . . . 223
8.3.2 Visualisation strategies . . . 226
8.4 Final remarks on discussion, synthesis, and future work . . . 228

9 Conclusion 229
9.1 Exposure to wind-driven rain . . . 229
9.2 Response of moisture regimes within stone masonry . . . 232
9.3 *Finale ultimo* . . . 234

References 237

V Appendices 317

A Geological Strata of Great Britain 319

B Supplementary Information to Paper IV: normalised value representation of moisture measurement data 321

C Pilot study: comparability of non-destructive moisture measurement techniques on masonry during simulated wetting 325

D Statements of substantive contributions from paper co-authors 339

List of Figures

2.1 A selection of moisture movement pathways for an uninsulated solid wall stone masonry structure with a rubble core 19
2.2 Conceptual shapes of gravimetric calibration curves for commercial geophysical devices 34
2.3 An overview of different measurement principles and techniques for non-destructive measurement of moisture 41

3.1 The research framework for this thesis 50

4.1 The sites selected to evaluate current WDR exposure and standards . . . 67
4.2 Prevailing wind directions (represented by relative occurrence) for eight UK sites 69
4.3 The number of wind-driven rain spells occurring at different sites in the UK from 1986 to 2015, as a function of average annual precipitation and wall orientation 79
4.4 Frequency of occurrence of wind-driven rain spells of different lengths for eight UK sites at 12 wall orientations between 1986 and 2015 82
4.5 Wind-driven rain exposure at eight UK sites for 12 different wall orientations (0^o = north) between 1986 and 2015 84
4.6 Wind-driven rain exposure for eight UK sites for 12 different wall orientations (0^o = north) from 1959 to 1991 and absolute changes in in I_A and $I_{S,\mathrm{EVA}}$ for 1986 to 2015 from 1959 to 1991 86
4.7 A comparison of the 'once every three years' spell calculated from ISO 15927, BS 8104, and extreme values analysis for 1959 to 1991 and 1986 to 2015 89
4.8 The probabilities of exceeding the 'once every three years' spells calculated from ISO 15927 and BS 8104 in any given year 91

5.1 An example of a driving rain spell, as defined in ISO 15927-3:2009. . . . 103

5.2 Study sites used to evaluate future WDR exposure, representing the variability of exposures to precipitation and wind across the UK. 110
5.3 Comparison of the generated baseline time series (1960–1990) to the recorded meteorological data at sites within their respective prediction regions for eight UK sites. 112
5.4 Comparison of the mean hourly wind speed distribution for the generated baseline time series (1961–1990) to the recorded meteorological data . . 114
5.5 The predicted changes in average exposures of wind-driven rain, presented for annual behaviour and for individual seasons. 116
5.6 The volumes of the mean and the worst spell likely to occur once every three years at each site during different periods 119
5.7 The current and future frequency of wind-driven rain spells of different lengths at eight UK sites. 123

6.1 A demonstrative A-scan taken on an oven-dry sample of Portland limestone 150 mm×150 mm×150 mm 148
6.2 Dielectric constants for three UK building stones at 1.6 GHz over the ambient saturation range of water contents 164
6.3 Surface wave amplitude for three stone types at 1.6 GHz over the ambient saturation range of water contents, as calculated from radar measurements taken on two calibration procedures 165
6.4 Modelled reflection and transmission coefficients, R and T respectively, for two configurations of layered systems of a porous materials 166
6.5 Microwave sensor indices for three stone types over the ambient saturation range of water contents for ambient drying and isolated diffusion 168

7.1 The two masonry constructions evaluated for moisture regimes in Paper IV 183
7.2 The measurement areas for the Edinburgh experiment, demonstrating the four zones in Scenario A and Scenario B 186
7.3 Spatial representations of a granite masonry wall drying after simulated WDR exposure, represented with percentiles 192
7.4 Temporal representations of components of a granite masonry wall during drying after simulated WDR exposure during the Oxford experiment . . 194
7.5 Spatial representations of moisture variation (in percentiles) across a granite masonry wall after simulated WDR exposure demonstrating penetration through joints and depth-focused electromagnetic measurements 197

7.6 Spatial representations of moisture measurements during simulated WDR exposure for a part of New College, Edinburgh following four spell intensities 199
7.7 Temporal representations of moisture measurements during for a part of New College, Edinburgh following simulated WDR exposure at four spell intensities 200
7.8 Measurement percentiles for two microwave sensors and a radar variable for mortar joint configurations within the sandstone façade of New College, Edinburgh 202

8.1 Predicted changes in summer and winter precipitation for the 21st century under a high emissions scenario 219

A.1 The geological strata of Great Britain 319

B.1 Spatial representations of a granite masonry wall drying after simulated WDR exposure, represented with normalised values 322
B.2 Temporal representations of components of a granite masonry wall during drying after simulated WDR exposure during the Oxford experiment . . 323
B.3 Measurement percentiles for two microwave sensors and a radar variable for mortar joint configurations within the sandstone façade of New College, Edinburgh 324

C.1 The monoliths (limestone and sandstone) and the traditional masonry construction, with an example of the simultaneous instrument set-up with positions of the mortar joints 328
C.2 Transformed meter readings $\Delta\nu$ and ERT depth moisture profiles ρ' for two iterations of the limestone monolith moisture regimes. 334
C.3 NNLS regression results for handheld meters: Coefficients and quantity of regression models incorporating depth 335
C.4 A distinct transfer of significant moisture migration at monolith edges mid-drying and collected base water at 48 h 336
C.5 Differential instrument readings above and below mortar joints within the stone for the electrical resistance meter, the microwave meter, and ERT . 337

D.1 Co-author statement from Professor Heather Viles 340
D.2 Co-author statement from Dr Maureen Young 341
D.3 Co-author statement from Mr Dawson Stelfox 342
D.4 Co-author statement from Dr Joanne Curran 343

D.5 Co-author statement from Dr Alick Leslie 344
D.6 Co-author statement from Ms Lucie Fusade 345

List of Tables

2.1 Processes of stone weathering, with environmental factors, observed impacts, and relevant literature . . . 16
2.2 Methods of assessing wind-driven rain exposure, presented with advantages, disadvantages, and key literature . . . 24
2.3 Percentage change in total precipitation amount from 1961–2006 by season and area, based on a linear trend . . . 28
2.4 Change (days) in days of rain $\geq$ 1 mm from 1961–2006 by season and area, based on a linear trend . . . 28
2.5 Literature that provides an overview of measurement principles and techniques for moisture in building materials . . . 37
2.6 Common techniques for non-destructively measuring moisture in building materials and structures, presented with advantages, disadvantages, and relevant literature . . . 43

4.1 Climatic data availability and basic meteorological and geographical characteristics of the study sites used to evaluate current WDR exposure and standards in Paper I . . . 68
4.2 Annual maxima series (AMS) values for a north-oriented wall in Stornoway between 1986 and 2015 . . . 77
4.3 Sites WDR exposures characterised by group properties according to the amount and distribution across wall orientations . . . 83

5.1 The parameters employed to calculate the frequency of different meteorological conditions used in the comparison of the baseline generated time series and the recorded meteorological data . . . 111
5.2 Annual indices (I_A, total exposure to wind-driven rain) during the baseline (1961–1990) and under the prediction scenario (2070–2099) at the eight sites for all wall orientations . . . 116
5.3 Predicted change in the annual spell index I_A (total wind-driven rain exposure) from 1961–1990 to 2070–2099 for all wall orientations . . . 117

5.4 Predicted percent change in exposures to wind-driven rain from 1961–1990 to 2070–2099, for all wall orientations 118
5.5 Period of time elapsing between sequential wind-driven rain spells from 1961–1990 and 2070–2099, with changes 122
5.6 Mean fraction of hours within spell with wind-driven rain 125
5.7 Likely change in predicted occurrence of mechanisms impacting building performance in 2070–2099 due to changes in wind-driven rain spells and temperature under a high emissions scenario 131

6.1 Hygric and physical properties of the three stone types investigated in the calibration study (Paper III) 144
6.2 Typical dimensional representations of GPR data 147
6.3 Dielectric constants for three dry stone types ($n = 1$) at 1.6 GHz calculated from radar travel times measured from two different calibration procedures 161
6.4 Linear regression models for the calibrations developed from measurements taken with a metal back as a function of air-back measurements . . 167
6.5 Linear regression model R^2 values for the measured microwave sensor indices as a function of modelled reflection coefficients R 169

7.1 Experimental design of simulated WDR exposure to compare microwave and radar moisture measurement techniques 182
7.2 Experimental design of the two scenarios designed for simulated WDR exposure of the sandstone tower 187
7.3 A summary of recommended techniques and variables to use for specific investigation objectives depending on the masonry context 205

Part I

Research context and design

1 | Introduction

"During human progress, every science is evolved out of its corresponding art."

– HERBERT SPENCER (1861, p. 77)

Architecture constitutes an irreplaceable component of tangible cultural heritage, which represents a unifying past (Council of Europe, 1985) and forms an integral component of the building stock in countries such as the United Kingdom (Ross, 2003, pp. 1–6). The imminent acknowledgement of the Anthropocene as a geological age when human activity has made a significant global influence (Waters et al., 2016) strengthens the importance of historical and traditional buildings—especially stone-built structures—in the environment; Gómez-Heras and McCabe (2015) argue that while they are assets to preserve, they are also recorders of past and present environmental change. As a result, their conservation and management should be interwoven with dialogue on environmental impact, sustainability, and climate change (Cassar, 2005; Solli et al., 2011).

1.1 Context

There is economic incentive for preserving stone-built heritage and maintaining traditional buildings, which also support sustainability and citizen wellbeing. Heritage tourism and the maintenance of traditional buildings are significant economic drivers. For example, direct, indirect, and induced effects of heritage tourism represented 2% of the UK's

GDP in 2011 (El Beyrouty and Tessler, 2013). In the year previous to that, repair and maintenance on English historic buildings accounted for 10% of the total value of the country's construction industry (Ecorys, 2012). Stone is also an important component of the UK's diverse portfolio of domestic vernacular architecture: in 2016, at least 8.2 million UK dwellings incorporated solid wall construction (Ministry of Housing, Communities & Local Government, 2016), which are primarily 18th and 19th century stone-built or brick-built structures (Vadodaria et al., 2010). Historical and traditional buildings contribute to sustainable development by recognising the embodied energy in the materials that were used in their construction (Jackson, 2005). In addition, there are environmental and resource implications associated with their demolition (*Ibid.*) and subsequent sourcing, and transportation of materials for replacement new-build structures (Stubbs, 2004). Additionally, engaging with heritage, even infrequently, contributes to improvements in citizen mental and physical wellbeing (Wheatley and Bickerton, 2017). In the context of creating links with heritage and the past, economic benefit, and improved wellbeing, it is important to maintain and conserve historical and traditional buildings if they are to fulfil their role in society.

1.2 Rationale

Stone has been employed in the built environment globally for millennia (Ashurst and Dimes, 1998, pp. 19–20) for its aesthetic qualities, workability, and durability (Lott, 2013,

p. 1; English Heritage, 2012, chap. 1). Stone that is exposed to the environment is subjected to weathering processes of physical change that decrease strength and longevity (Winkler, 1987), including chemical attack, transformation stress from freeze-thaw cycles, crystallisation stress and biodegradation (Brimblecombe, 1994). These processes often occur in complex combinations (Antill and Viles, 2003; Steiger, Charola and Sterflinger, 2011), and are underpinned by the presence and movement of moisture (English Heritage, 2012, p. 63). It is important to consider how the spatial patterning of different weathering processes and their respective rates might be influenced by the building envelope, i.e. elements which make up the entirety of a built structure such as roofs, gutters, and other drainage implements. This is especially applicable to stone masonry, in which the combination of stone units with mortar joints as a 'system' can create moisture pathways that foster weathering mechanisms (Liberatore, Spera and Cotugno, 2003). Properly-selected mortars can also help to regulate moisture regimes within stone masonry (Hughes et al., 2012), thus mortars for repair and repointing need to selected in such a way that balances their various properties (Forster and Carter, 2011). Therefore, it is important to be able to characterise moisture regimes in both stone units and mortar joints within stone masonry systems.

Wind-driven rain is precipitation given a horizontal component by the wind (Blocken and Carmeliet, 2004), which represents the main source of moisture and agent of deterioration for building façades (Erkal, D'Ayala and Sequeira, 2012). The ingress of

water through stone masonry building fabric can introduce moisture to 'reservoirs' (Singh, 1994), exacerbate existing moisture problems (English Heritage, 2014, p. 76), produce thermal bridges across the building envelope (Bomberg and Shirtliffe, 1978; Benavente, Cultrone and Gómez-Heras, 2008), increase the risk of condensation (Garratt and Nowak, 1991), and enable precipitation to reach parts of the building façade that would otherwise not be impacted (Lacy, 1977). These can result in conditions that negatively impact occupant health and comfort (Davis, McGregor and Enfield, 2016) and support mould growth (Vereecken and Roels, 2012).

The twenty-first century UK is predicted to be 'warmer and wetter' (Jenkins, Perry and Prior, 2009, p. 17) and perhaps 'windier' (Brimblecombe, 2014), with more extreme precipitation events (Kharin et al., 2007). These changes suggest that increased volumes and intensities of extreme wind-driven rain exposure can be expected to occur more frequently. The resilience of stone-built architecture to these changes is uncertain, as the predicted variations are likely to cause long-term damage due to more frequent physical, chemical, and biological attack (Sabbioni, Brimblecombe and Cassar, 2010) and increased magnitude and wider variation of cycles of moisture migration (Hall et al., 2011).

To assess the impact of wind-driven rain, semi-empirical approaches to evaluate wind-driven rain exposure have been developed into standards. These use long-term hourly climate data to characterise annual and episodic (spell) behaviour with the quantity of water impacting a theoretical surface. Spells are periods of time separated by a certain number

of hours, based on the dynamics of masonry drying. BS 8104 (1992) is specific to the UK and provides reference maps based on 20th century climate data, while ISO 15927-3 (2009) provides generalised calculation procedures. In the context of a changing climate, it is uncertain whether these are adequately capturing current and future wind-driven rain exposure and the temporal characteristics of wind-driven rain.

To further understand weathering processes that may be impacting stone masonry due to exposure to wind-driven rain, it is necessary to characterise the 'response' of stone masonry with respect to spatial and temporal aspects of moisture regimes (Alves et al., 2011). Non-destructive techniques can be used for this purpose as alternatives to invasive sampling or destructive techniques, as they align with 'minimally-invasive' policies common within heritage management (e.g. Drury and McPherson, 2008). These techniques use a diverse range of physical phenomena as proxies for water contents and are typically evaluated with reference gravimetric calibration which can be costly and time-intensive (Camuffo and Bertolin, 2012). Many measurement principles are derived from medical imaging; these are appropriate for laboratory-scale investigations of fluid transport in porous media, e.g. magnetic resonance imaging (Camaiti, Bortolotti and Fantazzini, 2015) and x-ray tomography/neutron radiography (Masschaele et al., 2004), but are not scalable to building surveys. In contrast, tools appropriated from geological sciences or contemporary civil and geomatic engineering including radar (Lai, Dérobert and Annan, 2018) and microwave (see Kupfer, 1997) propagation are suitable for characterising

moisture regimes at a façade scale.

An ideal technique for moisture measurement in field studies would have the capability to scan large areas of the surface and determine changes in moisture in specific locations at different depths. The measurements would be repeatable, accurate, independent of the material, and unaffected by its inhomogeneity or irregular texture. The device would also be portable, safe to operate, efficient and affordable enough for regular and prolonged use. However, no measurement technique fits this ideal (Pinchin, 2008).

Non-destructive techniques are effectively employed when chosen for their comparative advantages, with awareness for their weaknesses; the practical application of NDT methods therefore depends on the investigation objectives (Válek et al., 2010), and moisture regimes relevant to the situation. Despite an established body of guidance available on their measurement principles (e.g. Wormald and Britch, 1969; Dill, 2000; Camuffo, 2013; Nilsson, 2018, among many others), there is a lack of methodological procedures for technique selection, multi-method approaches, data handling, and visualisation practice.

In the context of more intense wetting events, it is crucial to have adequate guidance and metrics for assessing current and future building exposure to wind-driven rain. Equally, there is an imperative "to develop new combinations of moisture sensors sensitive to both wetting and drying at varying rates over a range of depths, and which can be used both to quantify moisture content at a point and to map changes in spatial distribution over time" (Smith et al., 2011b, p. 56). Of special interest are "techniques which can provide localised

estimates of water content and therefore allow water content distributions to be mapped" (Hall and Hoff, 2012, p. 32) within stone masonry systems.

1.3 Research aims and objectives

This thesis aims to evaluate the relationship between wind-driven rain and stone masonry. It examines both exposure to wind-driven rain and the response of the moisture regimes within stone masonry. These components are linked by: 1) methodological evaluation and development, and 2) environmental and material characterisation, alongside hygric behaviour. To this end, this thesis aims to address the two aforementioned components of the relationship between wind-driven rain and stone masonry, integrating characterisation and methodological development. In both exposure and response assessment, the first objective explores and validates a methodology that provides a platform on which to expand through the second. The primary objectives, within two components, are:

1. Exposure to wind-driven rain

Objective A. To investigate current wind-driven rain exposure in the UK and evaluate the applicability of existing standards.

Objective B. To explore future wind-driven rain exposure in the UK and characterise the temporal attributes of wind-driven rain to develop new metrics.

2. Response of moisture regimes within stone masonry

Objective C. To determine dielectric properties of three UK building stones and validate a rapid and cost-effective method of gravimetric calibration for non-destructive techniques.

Objective D. To characterise moisture regimes within stone masonry systems based on comparative advantages of non-destructive electromagnetic techniques, and propose effective data handling and visualisation strategies.

This thesis has been collaboratively undertaken with Historic Environment Scotland and the Consarc Design Group, to emphasise aims and objectives that are relevant to practical aspects of heritage conservation and building management.

1.4 Thesis structure

This thesis is comprised of four parts. Part I places the research in context and presents its overall structure, after the introduction provided within this chapter. Chapter 2 surveys the literature within relevant fields and demonstrates the gaps that motivate the undertaken research. Section 2.1 discusses stone in the built environment, emphasising its prevalence in the UK, moisture-dependent weathering mechanisms, and the hygric behaviour of stone masonry systems. Section 2.2 describes the potential impacts of wind-driven rain and assessment methods, demonstrating their importance in the context of a changing UK

climate. Finally, Section 2.3 outlines the principles of non-destructive testing to monitor moisture regimes with stone masonry and gravimetric calibration, after which surveys of the body of guidance on measurement principles and literature on techniques commonly applied in façade-scale investigations are presented. Chapter 3 lays out the framework for the research undertaken and the 'paper-based' approach for this thesis. It also provides rationale for the selection of primary methods employed in Parts II and III.

Part II pertains to semi-empirical evaluation of exposure to wind-driven rain. This is explored through two papers:

- Paper I (Chapter 4) characterises the amount of annual WDR exposure and the frequency and duration of directional WDR spells for eight sites in the UK from 1986 to 2015. The utility of BS 8104 (1992) and ISO 15927 (2009) for evaluating extreme WDR exposure at those sites is assessed by representing the worst spell likely to occur in any given three-year period using a 'return period' approach from extreme value analysis (EVA).

- Paper II (Chapter 5) combines UKCP09 Weather Generator predictions with a probabilistic process to create hourly time series of climate parameters under a high-emissions scenario for 2070–2099 at eight UK sites. Exposure to WDR at these sites for baseline and future periods is calculated from semi-empirical models based on long-term hourly meteorological data using ISO 15927 (2009). The future

characteristics of spells of wind-driven rain are explored alongside a discussion of the relevant temporal metrics.

Part III pertains to non-destructive measurement of the response to wind-driven rain. This is explored through two papers:

- Paper III (Chapter 6) proposes a cost- and time-effective 'isolated diffusion' gravimetric calibration procedure in which a set of samples are sealed at specific water contents and equilibrated. The procedure is compared to ambient drying over 120 h for three UK building stones and evaluated with modelled reflection coefficients and relative permittivities.

- Paper IV (Chapter 7) explores the comparative advantages of microwave and radar measurements in two field experiments of exposure to short (but intense) simulated wind-driven rain exposure to demonstrate when and how they are most effectively employed. A novel method of representing data as percentiles is explored to facilitate effective communication of moisture measurements.

Part IV presents implications for scientific research and practical heritage conservation and concludes the thesis. Chapter 8 creates connections between the four papers, stimulates broader discussion, and recommends future directions for research. Chapter 9 briefly summarises the findings of the thesis and places them in the wider context of building sustainability and heritage science.

2 | Literature review

"Our relationship to water is ambivalent.
Neither humans nor buildings can
tolerate too little or too much of it."

– ALAN OLIVER (1997, p. 1)

This chapter sets this thesis in the context of the relevant field(s) and demonstrates the gaps that motivate the undertaken research. It provides further rationale for the objectives introduced in Chapter 1. Topics and methods (along with relevant bodies of literature) specific to each paper are covered in their respective chapters (see Chapter 3).

2.1 Stone in the UK built environment

Stone – a term for rock that has been shaped for anthropogenic use (Siegesmund and Snethlage, 1994, p. 1) – is often perceived as a material of permanence, which is exemplified by its selection for important buildings and war memorial gravestones (Lott, 2011; Viles, 2013). There is a great diversity of geological strata in the UK (Woodcock and Strachan, 2012; see also Appendix A), which is reflected in a rich variety of stone types employed for building purposes, or 'essays in local geology' (Bianco, 2017). There was a historical motivation to use local stone: one estimate suggests that if medieval stone was transported overland for a distance of twelve miles its price doubled (Salzman, 1992, p. 119). Thus, larger distances were only feasible if water-based transport could be

easily used. This local use of stone is reflected in the country's portfolio of monumental ecclesiastical, fortified, and educational structures; for example: York Minster in Tadcaster dolostone (Historic England, 2017), parts of the Tower of London in Kentish Ragstone (Bonazza et al., 2007), many buildings within the University of Oxford and its colleges of Headington limestones (Arkell, 1947).

In contrast, many stone types have found widespread use beyond their local areas across the UK and abroad (Morris, 2004). Portland limestone, which originates from the south coast of England, has been acknowledged as a Global Heritage Stone Resource (Hughes et al., 2013), having been employed for many important buildings, including St Paul's Cathedral, London (Inkpen et al., 2012). Similarly, Clipsham limestone (from Lincolnshire) has commonly been employed as a replacement stone for other limestones in southeast England. Prominent examples include the Palace of Westminster, i.e. the UK's House of Parliament (Lott and Richardson, 1997) and many buildings within the University of Oxford (Oakeshott, 1975). It is not uncommon to find clusters of structures of the same type of imported stone, such as Binny sandstone in central Edinburgh (British Geological Survey, 2015).

Stone is also an important component of the diversity of vernacular architecture across the UK. For example, in 2016, at least 35% of UK dwellings (approximately 8.2 million) were comprised (in part or in whole) of solid wall construction (Ministry of Housing, Communities & Local Government, 2016). These dwellings were primarily built during the

late 18th and 19th centuries with structural solid walls 23 cm thick or greater, either in stone or brick (Vadodaria et al., 2010). The significant presence of solid wall construction within the current building stock represents the extent to which stone masonry is widespread, and an integral component of sustainable growth and managing the UK's housing shortage, especially with regards to energy retrofits (Bergman and Foxon, 2018).

2.1.1 Stone weathering

Early investigations into stone deterioration focused on describing permanent physical change (Warnes, 1926; Schaffer, 1932). These continued to be investigated alongside mitigation techniques (Clarke and Ashurst, 1972; Schmidt, 1976; Timmons, 1976; Gauri, 1978). This progressed to further quantification of weathering and its relationship with atmospheric conditions, including dose-response and damage functions (Colman, 1981; Kralj, Pande and Middleton, 1991; Cooke, Inkpen and Wiggs, 1995; Hoke and Turcotte, 2004), which was furthered in subsequent decades (Kucera et al., 2007; Tidblad and Kucera, 2007). These studies often focus on a single process, but what has emerged in the literature—for its utility and versatility—is the quantification of internal moisture as an broad indicator of the potential for multiple weathering processes.

Masonry is susceptible to physical and chemical weathering processes (Table 2.1), which often occur simultaneously (Antill and Viles, 2003; Steiger, Charola and Sterflinger, 2011). Almost all weathering is initiated or supported by the presence of moisture, or

Table 2.1. Processes of stone weathering, with environmental factors, observed impacts, and relevant literature. Processes and environmental factors adapted from Brimblecombe (1994).

Process	Environmental factors	Observed impact(s)*	Literature
Erosion	polishing/cleaning, dust, air and water movement (e.g. wind-driven rain, surface run off etc.)	loss of surface detail, exfoliation, sanding, powdering, crumbling, alveolisation, abrasion	Young, Urquhart and Laing, 2003; Tang et al., 2004; Erkal, D'Ayala and Sequeira, 2012; El-Sherbiny, 2018
Soiling	dust, humidity, electrical charge, air flow	blackening, loss of contact, changes in colour, patina formation	Beloin and Haynie, 1975; Grossi et al., 2003; Ashurst, 2016
Freezing	temperature, water	mechanical failure, spalling, delamination	Litvan, 1980; Bayram, 2012; Martínez-Martínez et al., 2013
Crystallisation stress	soluble salts, water	mechanical failure, exfoliation, blistering	Schaffer, 1932; Goudie and Viles, 1997; Charola, 2000; Doehne, 2002; Ruedrich and Siegesmund, 2007; Franzen and Mirwald, 2009; Espinosa-Marzal and Scherer, 2010
Chemical transformation stress or attack	pollutants, notably SO_2, trace gases, humidity, air flow, catalytic particles	sulfation of stone, crust formation, exfoliation, patina formation, blistering, delamination, scaling, peeling, efflorescence, subfloresence	Winkler, 1966; Lewry et al., 1994; Camuffo, 1995; Charola and Ware, 2002; Steiger, 2003; Smith and Viles, 2006
Dissolution	water flow, solutes (e.g. dynamics of rising damp)	loss of surface detail, loss of material	Winkler, 1966; Hall and Hoff, 2007
Biodegradation	organisms, light, high humidity, optimal temperature	mold, lichen growth, loss of detail, dissolution, mechanical failure, pitting, deposit, film formation, algal growth	Griffin, Indictor and Koestler, 1991; Warscheid and Braams, 2000; Bjelland and Thorseth, 2002; Smith et al., 2011a; Viles, 2012; McCabe et al., 2013; Traversetti, Bartoli and Caneva, 2018
Differential thermal/hygric expansion	temperature, water (e.g. hygric swelling)	mechanical failure, spalling, delamination	Franzini, Gratziu and Spampinato, 1984; Rodriguez-Navarro et al., 1997; Gómez-Heras, Smith and Fort, 2008; Sebastián et al., 2008

*Terminology based on the *ICOMOS Illustrated Glossary on Stone Deterioration Patterns* (2008)

rather: "water is the most important factor in stone deterioration" (English Heritage, 2012, p. 63). For each process, the important factors are a combination of absolute water contents, time of wetness (McCabe et al., 2013), depth of penetration and frequency of wetting and drying.

There are other processes that can significantly impact stone in the built environment, but these are less directly associated with moisture. These include catastrophic events such as earthquakes (Binda and Anzani, 1997) and terrorism (Holtorf, 2006). Less catastrophic impacts of human behaviour have been noted, including erosion from bicycles leaning against masonry (Thornbush and Viles, 2005) and cracks/fractures created by bullet impacts

(Mol et al., 2017).

2.1.2 Behaviour of stone masonry systems

Stone masonry is deteriorated by many processes, including those discussed in Section 2.1.1. However, there are contextual considerations that distinguish stone masonry from rock weathering in a natural context, including building elements and material combinations. Most contextual aspects of stone masonry are intended to be protective against weathering, but can be deteriorative if the implementation is based on misunderstanding of material and/or construction principles or mismanagement.

Stone masonry for structural purpose is generally composed of at least two material types in specific geometries.[1] The most common type of structural stone masonry is core-and-veneer, comprised of two parallel walls and a core between them filled with rubble or other infill; it is described in *De Architectura*, demonstrating its use from (at least) the Roman period onwards (Vitruvius, n.d.). It is also common to find walls without a core, composed of single or double layers of ashlar units. The masonry units are set into mortar, traditionally based on lime and natural aggregate (Holmes and Wingate, 2002). It was not until the 1920s that this masonry technique was superseded by cavity wall constructions (University of the West of England, 2011), which replace the core with an air gap and typically incorporate moisture-repellent barriers (Weber, 2013). These 20th

[1] This contrasts dry stone walling, which is often homogenous in its material types and primarily used for boundary delineation (Radford, 2001).

century masonry structures behave differently to core-and-veneer systems, since they are designed to inhibit the movement of moisture through the wall depth.

There are a number of moisture ingress and egress pathways in core-and-veneer stone masonry systems (Figure 2.1). Moisture can come from external sources (e.g. wind-driven rain and other precipitation, and water from the ground), and internal sources such as domestic activities (Christian, 1993). The same pathways exist in solid wall constructions without a rubble core, in which case the transfer between external and internal environments occurs directly through the ashlar units and mortar joints. Singh (1994) covers sources of dampness in buildings in great detail: external sources include roof leakage, defective flashing, uncapped chimneys, and under-performing drainage elements (e.g. gutters and drainpipes); domestic activities that contribute to internal sources include spillage, condensation from cooking and cleaning, and plumbing leaks. All of these elements are part of what is considered the 'building envelope' (English Heritage, 2014, p. 54), which is an important concept for understanding interactions between moisture and stone masonry.

A number of moisture regimes and movements can exist simultaneously within stone masonry. Moisture can be present within masonry units and mortar joints in both liquid and vapour form, with exchange occurring between them seeking their respective equilibrium moisture contents (Camuffo, 2013, pp. 81–89). Of particular concern is the penetration through mortar joints through to the interior (Liberatore, Spera and Cotugno, 2003);

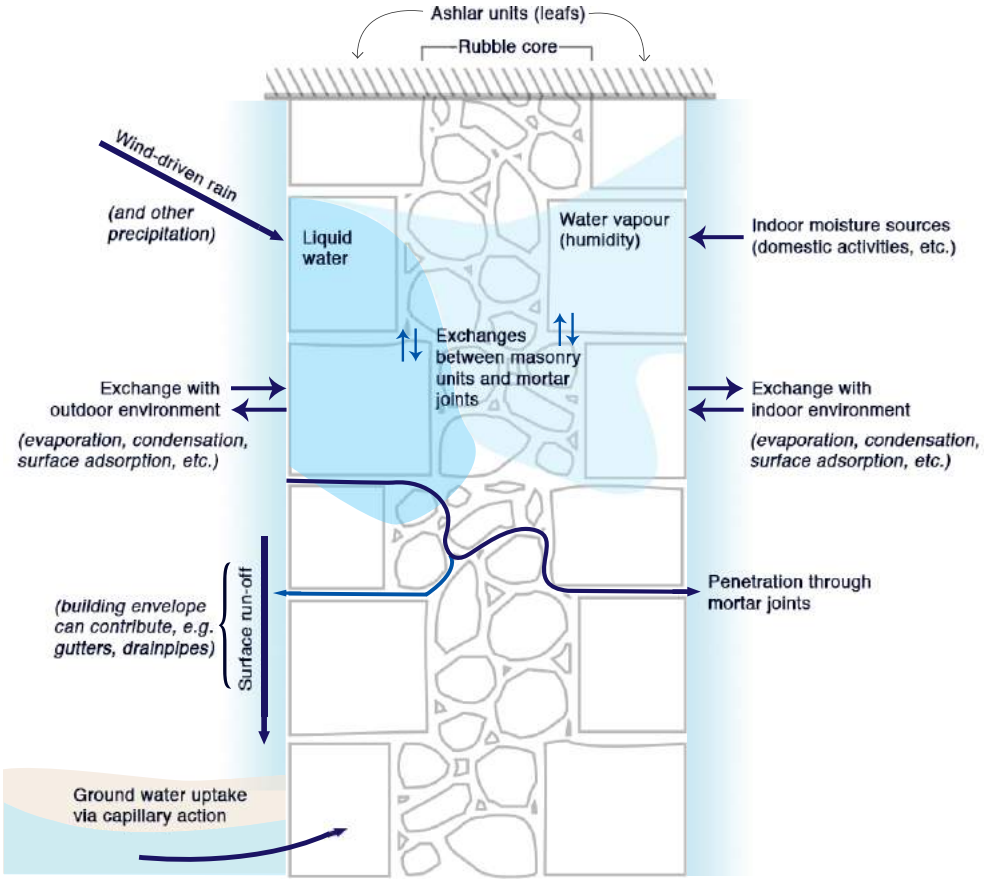

Figure 2.1. A selection of moisture ingress pathways for an uninsulated solid wall stone masonry structure with a rubble core. *Source: Author's own.*

however, properly selected mortars can also help to regulate moisture regimes within stone masonry (Hughes et al., 2012). Thus, mortars for repair and repointing need to selected in such a way that balances their various properties (Forster and Carter, 2011). These static and dynamic aspects of the presence and movement of water within porous building materials are part of hygric behaviour, which must be characterised to understand moisture regimes and weathering.

2.2 Wind-driven rain

Wind-driven rain (WDR) is rain that is given a horizontal velocity component by wind. Wind-driven rain intensity depends both on the level of rainfall and on wind speed and direction. In the UK, the highest rates and intensities of WDR are to be expected in areas with the wettest and windiest conditions. Directional trends will be apparent based on prevailing wind directions: for most of the UK, higher wind speeds from the south and west result in higher intensities of WDR, although this is not true of the entire country, especially near the east coast (Lacy, 1977). The intensity of WDR impacting a façade will vary greatly depending on the context, which might induce reductions or magnifications of both wind and precipitation exposure. While the former is intuitive, the latter could be introduced by urban canyons and channeling of rainfall due to poorly-functioning drainage, respectively. Estimates of wind speed and direction are influenced by several sources of uncertainty, including the aforementioned local obstacles, large variability in wind speed in space and time (Jain and Singh, 2003, p. 78), and subsampling (e.g. "the average speed and direction over the ten minute period leading up to the reporting time", UK Met Office, 2018).

Current standards and practice typically divide exposure to WDR into time periods referred to as 'spells', considered to be "periods of driving rain during which the risk of penetration through masonry increases, i.e. a period in which the input of water due to

the driving rain exceeds the loss due to evaporation" (ISO, 2009, p. 12). This definition of a spell is most appropriate for the dynamics of water movement in porous building materials, but rain spells can be defined in many ways, depending on the particular subject of focus (especially in the context of larger-scale infrastructure and natural environments): for example, a period of five days with (i) at least 15 mm of precipitation and no day with less than 1 mm or (ii) at least 20 mm with one such day or (iii) at least 25 mm with two such days (Lowndes, 1962).

2.2.1 Impacts

Wind-driven rain can have a range of impacts on both the broader behaviour of the building environment and the building fabric itself. It has long been associated with the penetration of water through the building fabric (Garden, 1963; Eldridge, 1976; Marsh, 1977; Straube, 2002; Rüther and Time, 2015). This can have several consequences for the building environment/envelope:

- transferring moisture to 'reservoirs', e.g. temporary or semi-permanent receptors for moisture (Singh, 1994), such as other elements of the building fabric;
- exacerbating existing moisture problems, due to existing water flow paths (English Heritage, 2014, p. 76);
- producing thermal bridges across the building envelope, due to water's lower

thermal capacity compared to most building materials (Bomberg and Shirtliffe, 1978; Benavente, Cultrone and Gómez-Heras, 2008);

- increasing the risk of condensation, due to lowered internal temperatures (Garratt and Nowak, 1991);

- enabling precipitation to reach many parts of the building façade it otherwise would not impact, due to the addition of the horizontal component (Lacy, 1977).

Many of these result in conditions that can negatively impact occupant health and comfort (Platt et al., 1989; Davis, McGregor and Enfield, 2016; Mendell, Macher and Kumagai, 2018) and support mould growth (Abuku, Janssen and Roels, 2009; Vereecken and Roels, 2012). These impacts are in addition to the aforementioned weathering processes (Section 2.1.1) that can affect components of stone masonry (e.g. Tang et al., 2004; Erkal, D'Ayala and Sequeira, 2012; D'Ayala and Aktas, 2016). Additionally, there are several links between wind-driven rain, vegetation, and urban microclimates, especially with regards to assessing urban water cycles and interactions with thermal dynamics (Derome et al., 2017).

2.2.2 Methods of assessment

Three approaches for assessing wind-driven exposure are experimental measurement, semi-empirical evaluation, and numerical methods based on Computational Fluid Dynamics

(CFD) (Blocken, 2014; see Table 2.2). Assessing the intensity of WDR on building façades is complex because it is influenced by a wide range of parameters, including building geometry, environment topography, position on the building facade, wind speed, wind direction, turbulence intensity, rainfall intensity and raindrop-size distribution. How different modelling approaches address these parameters is covered in detail by Blocken and Carmeliet (2010).

Measurements have been the primary tool in WDR research, although systematic experimental approaches of WDR exposure are less feasible than other methods (Moonen et al., 2012). Due to strict guidelines recommended for rigorous evaluation of WDR exposure (Blocken and Carmeliet, 2005, 2006a), semi-empirical representations with origins in the mid-twentieth century (Hoppestad, 1955; Lacy and Shellard, 1962) have been further developed and remained common since then. The limitations of both these methods motivated the development of numerical methods with CFD for evaluating steady-state WDR exposure by Choi (1991, 1993, 1994a, 1994b, 1997), which was subsequently expanded into the time domain (Blocken and Carmeliet, 2002). Despite the many advantages of CFD approaches demonstrated since 2002, the application of CFD for WDR studies in practice has remained very limited (Blocken, 2014).

Acknowledging the potential inaccuracies of measurement methods, recent studies have used specialised rigs to simulate wind-driven rain exposure (Lopez, 2011; Fister et al., 2012). Although the latter focused on soil erosion, both studies strive to reproduce

Table 2.2. Methods of assessing wind-driven rain exposure, presented with advantages, disadvantages, and key literature, representing an international body of work over the relevant time periods.

Method	Advantages	Disadvantages	Literature
Wind-tunnel measurement	accounts for turbulence, controllable environment and experimental design	specialised equipment, expensive, simplified or scaled geometry	Rodgers et al., 1974; Sandberg, 1974; Beijer, 1977; Rodgers, 1977; Hilaire and Savina, 1988
On-site measurement	accommodates all building geometries (with the right gauge placement), realistic exposures	easily suffer from large errors, time-consuming, expensive, measurements on a particular building site have very limited application to other sites	Beckett, 1938; Lacy, 1951, 1965; Newman, 1987; Brown, 1988; Prior and Newman, 1988; Osmond, 1995; Osmond, 1996; Kerr, Matthews and Kirmayr, 1997, 1998; Högberg, Kragh and Mook, 1999; Mook, 2002; Blocken and Carmeliet, 2005, 2006a; Lopez, 2011; Scholten et al., 2011; Baheru et al., 2014; Ge, Chiu and Stathopoulos, 2017
Semi-empirical evaluation	ease of use, applicable to sites for which appropriate data is available	estimates WDR exposure	Hoppestad, 1955; Lacy and Shellard, 1962; Lacy, 1977; BSI, 1992; CEN, 1997; Straube and Burnett, 2000; Sanders, 2004; ISO, 2009; Pérez-Bella et al., 2012, 2013; Pérez-Bella et al., 2014; Narula, Sarkar and Azad, 2017; Pérez-Bella et al., 2017; Ge et al., 2018; Tsoka and Thiis, 2018
Numerical methods (incorporating CFD)	accurate, accounts for all parameters in WDR exposure	computationally demanding, geometry specific, specialised skills/tools needed	Souster, 1979; Choi, 1991, 1993, 1994a, 1994b, 1997; Blocken and Carmeliet, 2002; Tang et al., 2004; Persoon et al., 2008; Abuku, Janssen and Roels, 2009; Briggen, Blocken and Schellen, 2009; Huang and Li, 2010; Hooff, Blocken and Harten, 2011; Kubilay et al., 2013, 2015

characteristics of wind-driven rain exposure, including droplet diameters, quantities of rainfall impacting the surface, and duration.

2.2.3 Semi-empirical evaluation of WDR

Semi-empirical models of driving rain are based on experimental observations that WDR on façades increases approximately proportionally with wind speed and vertical rainfall. These indices were first developed and applied in the UK and Norway in the mid-twentieth century (Hoppestad, 1955; Lacy and Shellard, 1962). This simple calculation of the product of mean annual values of wind speed and vertical precipitation remains a common metric used to assess wind-driven rain exposure, (e.g. Sabbioni, Brimblecombe and Cassar, 2010). In 1985 this was converted into a method (Prior, 1985) as background to a draft standard

(BSI, 1984). These documents developed what was formerly an index (units of $m^2\ s^{-1}$) into a quantity indicative of exposure in L m^{-2} for specific time periods, based on: hourly wind speed and direction and precipitation, façade orientation, and factors to incorporate terrain roughness, local topography, obstructions and building geometry. This was superseded by BS 8104 (1992), which remains the current reference for assessing wind-driven rain exposure in the UK.

BS 8104 served as the basis for the European normal 13013-3 (1997) but was supplemented with a new method for scenarios where rainfall and wind are not measured at the same location (Sanders, 2004). This method is based on 'wetting' and 'drying' half days which are derived from wind speed, humidity and the observers' assessment of whether or not it was raining (Sacre, 1982; Beguin, 1986). This method was included as a secondary approach to calculating indices in the current ISO 15927-3 (2009; henceforth ISO 15927), which has been harmonised as a European and international (ISO) standard. Lacy (1977) investigated a range of 'intense' wind-driven rain events, which were characterised by both duration and frequency. Despite this, current standards do not use duration or other temporal qualities (except to delineate between different spells) to characterise rain events. The implication of this is that extreme WDR spell exposure is characterised only by the quantity of water during the spell, without consideration for the 'rate' of exposure (i.e. a volume over time).

The two main semi-empirical methods for evaluating wind-driven rain exposure are

what can be referred to as the ISO 15927 (2009) and the Straube and Burnett (2000; S&B) models. The S&B model requires a 'rain admittance factor'—or 'driving rain factor/function' (Straube and Burnett, 1997; Straube, 1998; Straube and Burnett, 2000)—from simultaneous free-field and wall measured WDR, which are provided for a limited set of three types of building geometry and setting. This limits the situations in which it can be applied, unless appropriate (typically simultaneous) measurements are available for the site of interest.

ISO 15927 (2009) remains the current international standard for semi-empirically evaluating WDR exposure. It includes both annual metrics and procedures for determining extreme WDR events. Several developments have taken place since its publication. Specifically, by improving factors for building/wall geometry (e.g. Blocken and Carmeliet, 2006a; Ge et al., 2018; Tsoka and Thiis, 2018). As well, there have been developments of methods for evaluating extreme WDR events (Pérez-Bella et al., 2012, 2013), in which assessments are also made of the similarly between analyses done between hourly and daily meteorological data.

2.2.4 Climate change and future uncertainty

Wind-driven rain has been acknowledged as a phenomenon that can affect buildings since at least the beginning of the 20th century (Keim, 1902, p. 4). The changing characteristics of both precipitation and wind have made it an important topic within assessing future

climate risk to cultural heritage (Sabbioni, Brimblecombe and Cassar, 2010; Nik et al., 2015). The common catchline "warmer and wetter" (Jenkins, Perry and Prior, 2009, p. 17), and perhaps ‘windier’ (Brimblecombe, 2014) distills much of the current consensus on the UK climate towards the end of the 21st century. In 2011, BRE Scotland advised (Reid and Garvin, 2011) the Scottish Government that the present climate had not changed enough from that presented in exposure reference maps published in 1992 (BSI, 1992) based on conditions in 1959–1991 to warrant an update. Despite this, many heritage organisations (such as Historic Environment Scotland, 2018) are actively considering how to manage the impact of a changing climate on heritage sites over the 21st century.

2.2.4.1 Precipitation

The consensus that rates of precipitation will, on average, increase suggests that quantities of wind-driven rain exposure should also increase. However, measured climatic conditions from 1961–2006 demonstrate that this is valid for some regions of the UK during certain seasons (Tables 2.3 and 2.4): in the beginning of the 21st century (as compared to the 20th), many regions of the UK have experienced lowered average annual precipitation and decreased days with $\geq$ 1 mm rain. These measured changes in precipitation and days during which $\geq$ 1 mm of precipitation occurred demonstrate that there is not a direct relationship between them. This is an important outcome for wind-driven rain exposure, which is typically assessed with annual and spell-based metrics: it suggests that

Table 2.3. Percentage change in total precipitation amount from 1961–2006 by season and area, based on a linear trend (bold type indicates significance of the trend at the 95% level). Adapted from Jenkins, Perry, and Prior (2009, p. 77).

Area	Spring	Summer	Autumn	Winter	Annual
South West England	4.0	-8.8	28.6	15.9	9.7
South East England	-6.5	-13.1	20.6	23.3	5.4
London	-7.0	-16.7	19.4	22.7	2.5
Wales	8.4	-5.6	22.3	27.0	13.6
East of England	-1.7	4.9	21.6	17.7	9.3
West Midlands	-1.4	-5.2	29.8	10.9	7.6
East Midlands	-4.6	2.6	28.7	11.0	8.1
Northern Ireland	9.5	2.5	-0.7	12.5	5.2
Yorkshire and Humberside	-0.3	-1.1	10.2	24.3	7.1
North West England	6.3	-13.2	5.6	**43.0**	8.8
North East England	4.6	-6.9	12.4	**29.6**	8.7
West Scotland	23.2	4.3	11.0	**58.6**	**23.2**
East Scotland	14.3	-3.6	28.0	**35.9**	**18.7**
North Scotland	22.6	-5.0	11.1	**65.8**	**23.0**

Table 2.4. Change (days) in days of rain $\geq$ 1 mm from 1961–2006 by season and area, based on a linear trend. Adapted from Jenkins, Perry, and Prior (2009, p. 85).

Area	Spring	Summer	Autumn	Winter	Annual
South West England	-1.4	-1.3	4.1	2.2	1.9
South East England	-3.4	-1.8	3.4	2.6	-0.9
London	-2.5	-0.7	3.5	2.6	1.3
Wales	0.5	-0.7	2.9	4.6	5.7
East of England	-2.8	0.6	2.9	2.1	0.9
West Midlands	-2.7	-1.8	3.6	1.9	-0.7
East Midlands	-2.6	-0.2	3.0	1.4	-0.2
Northern Ireland	0.5	-0.7	0.5	3.2	2.5
Yorkshire and Humberside	-2.0	-0.2	1.4	2.2	-0.1
North West England	0.4	-1.1	2.9	6.8	7.5
North East England	-1.9	-1.8	2.4	2.7	0.1
West Scotland	2.6	0.8	2.9	8.6	14.1
East Scotland	0.8	0.4	2.4	3.4	5.8
North Scotland	2.8	-1.9	-0.6	8.4	7.7

rates of change characterised by annual metrics and extreme WDR spell exposures might experience different changes. This is supported by predicted increases in the frequency of localised extreme precipitation events in summer months (Jenkins, Perry and Prior, 2009, p. 12; Kendon et al., 2014).

How these changes in precipitation will manifest specifically in wind-driven rain exposure has not yet been studied in detail. However, observed seasonal polarisation of precipitation, which is predicted to become more severe throughout the 21st century (Fowler and Ekström, 2009), suggests that annual metrics currently used to assess wind-

driven rain will not capture this variability. Similarly, metrics that identify high levels of volumetric exposure might not capture short (but intense) WDR spells.

2.2.4.2 Wind speed and direction

The North Atlantic Oscillation has varied considerably for the past 150 years, but there has been no significant trend (Jenkins, Perry and Prior, 2009, p. 16). Wind speed changes well above the surface in the driving models are dependent on the ocean conditions (Sexton and Murphy, 2010) so certainty regarding changes is low.

Storms are of particular concern for their relationship with wind-driven rain. Strong wind speeds and heavy precipitation in the winter in the UK, of particular relevance to extreme wind-driven rain exposure, are associated with extratropical cyclones, commonly referred to as storms. Data from the most recent IPCC report suggest that an appropriate description for changes in the North Atlantic storm track is an extension into Europe, rather than the poleward shift more common elsewhere and during other seasons (Chang, Guo and Xia, 2012; Christensen et al., 2013; Zappa et al., 2013). There is a projected small increase in the number of storms and individual storms are associated with increased precipitation (Zappa et al., 2013). While change in winds associated with individual storms is near-zero (*Ibid.*), the increased number of storms may increase the number of days with high winds. Confidence in these projections of cyclones and their impact on weather at the earth's surface is low due to model deficiencies and a lack of understanding of conflicting

processes occurring in the North Atlantic (Christensen et al., 2013). Future improvements in model resolution may provide new information on these projected storm track changes. For example, a high resolution model identified projected increases for a particular type of storm over Europe that was not well simulated at a lower resolution (Haarsma et al., 2013). Storms have a tendency to 'cluster', i.e. the occurrence of storms is unevenly distributed over time. This clustering of wind driven rain may cause an added risk to buildings, and provide further evidence for seasonal deep-seated wetting (Smith et al., 2011a).

Convective storms are periods of high wind speeds and rates of precipitation that can result in short, but intense WDR exposure. They are the result of strong updrafts of wind (Houghton, 1968) that result in localised intense periods of rainfall characterised by large droplet diameters (Houze Jr, 1997). Accurate verification of operationally produced rainfall estimates of convective rainfall events is difficult due to the extreme variations in the temporal and spatial distribution of convective precipitation (Ray, 1986, p. 142). However, this can be improved by supplementing meteorological measurements with statistical approaches (Stein et al., 2015) and satellite imagery (Xu, Adler and Wang, 2014). Additionally, although all forms of precipitation, including convective-related events, are represented in UKCP09 weather projections (UK Climate Projections, 2014), the coarse resolution (25 km) of many of the projections will likely not reflect localised convective precipitation events (Kendon et al., 2015).

2.3 Characterising moisture regimes within stone masonry

In the built heritage context, a measurement approach can provide useful information for characterising how a stone masonry system functions. Non-destructive approaches are the most logical application when invasive testing and sampling are not simply implemented (for administrative or logistical reasons). Non-destructive techniques can be based on a wide range of measurement principles – each which has their respective benefits and trade-offs.

There are two main methods for assessing the response of stone masonry to wind-driven rain that can be implemented 'non-destructively': modelling and measurement. One of the most common types of the former are simulations based on differential equations, (e.g. WUFI, see Künzel and Kiessl, 1996; Antretter et al., 2011), which has frequently been employed to assess internal moisture contents of stone masonry (Holm and Künzel, 2003; De Rose et al., 2014) and validated against field measurements (Künzel and Kiessl, 1996; Wilkinson et al., 2009). Another commercial software that has been employed for the same purpose is DELPHIN (Nicolai et al., 2008; see also Twelmeier, Sperbeck and Budelmann, 2008; Skora et al., 2009).

2.3.1 Principle of non-destructive moisture measurement

Initial moisture survey techniques were based on visual detection and/or destructive or semi-destructive techniques. The former may be sufficient in some instances, but can be deceptive (Doehne and Price, 2010, p. 21) and is purely qualitative. Common destructive techniques include borehole samples (e.g. Weritz et al., 2009) and embedded wooden dowels (e.g. Sass and Viles, 2006). These cause permanent change within a structure, are point-based (e.g. cover a limited spatial range), and are often only placed within mortar joints. The deficiencies of this type of methods motivate interest in techniques that can non-destructively measure moisture.

Non-destructive testing (NDT) refers to a group of techniques used in science and technology to evaluate the properties of a material or system without using invasive sampling (Cartz, 1995). It has been used extensively for diagnostic testing of the structural condition of built cultural heritage (Livingston, 1999), since it is in accordance with 'minimally-invasive' policy within heritage management (e.g. Drury and McPherson, 2008). With respect to moisture detection, most non-destructive testing measurement principles are indirect, i.e. the reading/output from a technique is a proxy for the presence of moisture that is used as a relative level or is translated into moisture content or state of water in some way, usually with a calibration (Nilsson, 2018, p. 15).

2.3.2 Gravimetric calibration

Calibration of any measurement device assesses instrument bias relative to an accepted standard. This bias is then accommodated in subsequent use to adjust as closely as possible to the accepted standard response (ASTM International, 2013a). Gravimetric calibrations of non-destructive moisture measurement devices use the mass of water as an accepted standard of the absolute measurement of the quantity of water present in a sample. Although calcium carbide is specified as another 'accepted standard' in ASTM D4944 – 11 (ASTM International, 2018), it is a destructive reference and therefore not suitable for calibrations over a range of water contents (Camuffo and Bertolin, 2012). Gravimetric calibrations ideally result in mathematical relationships between water content and device readings. This is important for cases in which moisture thresholds are of interest. In other scenarios, it might be more important to characterise general behaviours or 'curve shapes', as demonstrated elsewhere (Eklund et al., 2013). A subset of these are conceptually represented in Figure 2.2. These allow an operator to understand how the device readings relate to water contents more broadly for a given material, without necessarily converting to quantitative water content.

Figure 2.2 (a) represents the ideal calibration curve, with a consistent linear relationship. In this scenario, the device is equally sensitive to the entire range of water contents of interest. (b) shows non-linear relationships in which there is greater sensitivity at

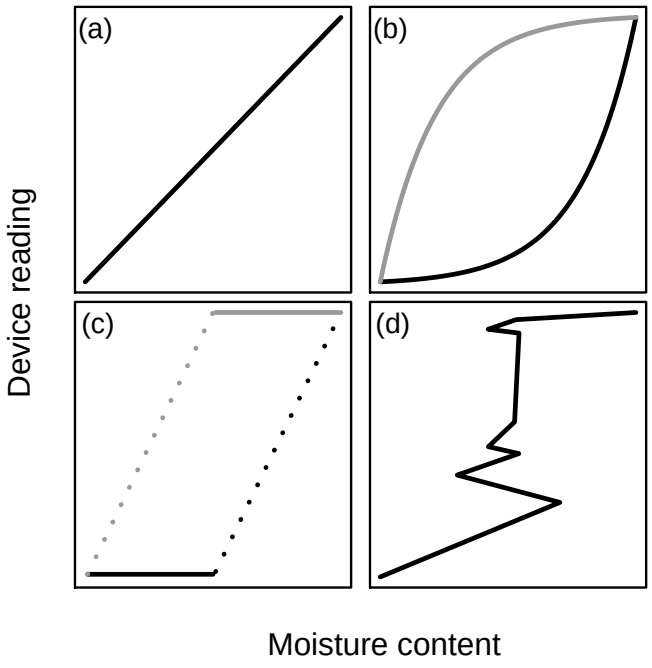

Figure 2.2. Conceptual shapes of gravimetric calibration curves for commercial geophysical devices.

higher water contents (black) and lower water contents (grey). In (c), a device that has thresholds of detection within the water content range of interest (black: lower, grey: upper); the nature of the relationship is uncertain, as it might be closer to those in (a) or (b), or a combination thereof. In (d), a generally related trend in device readings that is inconsistently related to water content. These inconsistencies can be due to a number of factors, including operator error, limitations of the technique and/or device, and material properties.

Gravimetric techniques determine the moisture content in a sample by monitoring weight change during controlled drying and calibrating these to the volumetric moisture content. The results of these tests are taken to be the most accurate method of moisture quantification (Hall and Hoff, 2012, p. 31), and used as the basis for other sampling

methods. Gravimetric techniques can be destructive or non-destructive. To create accurate calibration curves for specific specimens, core or surface samples are extracted, isolated from the atmosphere (Sandrolini and Franzoni, 2006), and then analysed in a laboratory setting (Weritz et al., 2009; Cardani et al., 2013; Kilic, 2014). However, promising results using previous calibration data (Sass and Viles, 2010b) or similar stone specimens (Martinho et al., 2012) demonstrate that gravimetric calibration does not necessarily need to compromise the specimen. Care must be taken with the employment of proxies that physical ageing, weathering, and defects are considered. Camuffo and Bertolin (2012) caution against the use of gravimetric techniques for calibrating signal-based methods because it is a volumetric measure, while the remainder of NDT methods surveyed are spatially resolved. In this way the calibration can only be considered valid if the material and moisture distribution is assumed to be homogenous.

Many standards are concerned with measuring moisture contents of traditional building materials (e.g. ISO, 2003; ASTM International, 2016; BSI, 2017). However, these are designed to quantify water contents in obtained samples through gravimetry, and do not contain procedures for calibrating non-destructive techniques.

Standards that do contain procedures for gravimetric calibration (e.g. ASTM International, 2013a, 2013b) are designed for wooden materials and primarily intended for use with electrical resistance and capacitive techniques. The current state-of-the-art recommends calibration be done by producing a range of relative humidity conditions

using salt solutions and climatic chambers (Climent, Lindmark and Nilsson, 2018). These techniques require specialised facilities and equipment that can be costly to implement and operate, while also requiring significant amounts of time to develop calibrations.

2.3.3 Guidance in the literature

There is a prolific body of guidance that summarises methods of measuring moisture in building materials (Table 2.5); the challenge for the interested reader is identifying which are in relevant domains and provide an appropriate level of detail and technical content. The measurement principles listed in Table 2.5 have also been applied in soil measurement (e.g. Su, Singh and Baghini, 2014) and food science applications (e.g. Divya and Ramanathan, 2017), further expanding the potential guidance available on moisture measurement in porous materials. Similarly, guidance on specific techniques that discusses a range of applications beyond moisture measurement (e.g. ground penetrating radar; see Lai, Dérobert and Annan, 2018) further confounds the issue of finding appropriate information. It should be noted that wood behaves very differently to most porous building materials, and is generally considered separately in literature (e.g. Niemz and Mannes, 2012).

Table 2.5. Literature that provides an overview of measurement principles and techniques for moisture in building materials (presented in chronological order, capturing the state of the art over time through 'snapshots').

Title	Citation	Format	Domain	Intended audience	Summary of content
The measurement of moisture movements in building materials	Barrow, 1927	Article	Building science	Scientists	Gravimetry
Physical methods of moisture measurement [in four parts]	Pande and Pande, 1962	Article	Metrology	Scientists	Indirect methods, emphasis on micro-scale focused but includes techniques common in current field practice
Measurement of moisture in concrete and masonry with special reference to neutron scattering techniques	Waters, 1965	Article	Building science	Scientists	Indirect methods, microwave/electrical properties, neutron scattering
Methods of measuring moisture content applicable to building materials	Wormald and Britch, 1969	Article	Building science	Scientists	Indirect methods, laboratory- and field-scale principles: electrical and thermal, vapour pressure
Moisture measurement in concrete	Hundt and Buschmann, 1971	Enquiry summary (article)	Building science	Scientists, Practitioners	indirect dielectric and thermal methods, survey evaluation
State of moisture content measurement in the building materials industry	Roife, 1980	Article	Building science	Scientists	dielectric and neutron methods
Materialfeuchtemessung [Moisture content measurement]	Kupfer, 1997	Book [in German]	Building science	Scientists	Principles, measurement principles, laboratory and field applications, standards
Dampness in buildings, 2nd Ed.[2]	Oliver, 1997, pp. 256–268	Book portion	Building science, conservation	Practitioners	Inspection, moisture meters (electrical resistivity, dielectric, etc.)
An Overview of Principles and Techniques of Moisture Properties Measurement for Building Materials and Components	Tada and Watanabe, 1998	Conference paper	Building science	Scientists	Various methods: nuclear, thermal, electric, ultrastonic, also theory of moisture transport
A review of testing for moisture in building elements	Dill, 2000	Report	Building science	Practitioners	Specifications and standards, selecting the appropriate test method, field-scale techniques, automated long-term monitoring
Methods for the assessment of moisture content of envelope assemblies	Derome, Teasdale-St-Hilare and Fazio, 2001	Conference proceedings	Building science	Practitioners	Various methods: thermal, dielectric, ultrasonic, spectroscopic analysis, guidance of technique selection
Moisture Measurement Guide for Building Envelope Applications	Saïd, 2004	Report	Building science	Practitioners	Various methods: thermal, electric, field-scale techniques, examples of measurements
A comparison of different techniques to quantify moisture content profiles in porous building materials	Roels et al., 2004	Article	Building science, conservation	Scientists	Micro-scale techniques: NMR, MRI, γ-ray, etc. with examples
Non-Destructive Field Tests in Stone Conservation. Final Report for the Research and Development Project #3	Svahn, 2006, pp. 34–38	Report	Conservation	Conservators	Context of stone conservation, direct methods, field-scale indirect methods (electrical, microwave, thermal, NMR, wooden dowels)
Measurement Methods of Moisture in Building Envelopes – A Literature Review	Saïd, 2007	Article	Building science	Practitioners	Embedded probes, electric and microwave techniques, surface wetness sensors

continued on next page…

[2] 1st Ed. published in 1988

Table 2.5 – *continued from previous page*

Title	Citation	Format	Domain	Intended audience	Summary of content
Moisture measurement in building materials: an overview of current methods and new approaches	Phillipson et al., 2007	Article	Building science	Scientists, Practitioners	Principles, techniques in common use in field-scale measurement, [research] micro-scale techniques
Techniques for monitoring moisture in walls	Pinchin, 2008	Article	Conservation	Conservators	Field indirect methods: dielectric, microwave, radar, NMR, thermal, ultrasonic, etc. Side-by-side comparison of various aspects of each technique, environmental monitoring
Time-domain reflectometry method and its application for measuring moisture content in porous materials: A review	Cerný, 2009	Article	Materials science	Scientists	Time-domain relfectometry with theory and application, principles of dielectric measurement
Electromagnetic techniques for moisture content determination of materials	Kaatze and Hübner, 2010	Article	Building science	Scientists	Electromagnetic techniques (e.g. TDR, microwave, spectroscopy, etc), theory and principles, time- and frequency-based approaches
Stone Conservation: An Overview of Current Research	Doehne and Price, 2010, pp. 6–9	Report	Conservation	Conservators	Field and laboratory techniques in common practice, with relevant references
State of the art — Methods to measure moisture in concrete	Quincot et al., 2011	Article	Building science	Practitioners	Direct and indirect methods, embedded sensor, resistivity, dielectric, thermal, infrared, and neutron-based techniques, nanotechnology and micro-electromechanical systems
Towards standardisation of moisture content measurement in cultural heritage materials	Camuffo and Bertolin, 2012	Article	Conservation	Conservators	Standards, direct and indirect methods in common practice with measurement principles, field- and laboratory micro-scales
Water Transport in Brick, Stone and Concrete, 2nd Ed.[3]	Hall and Hoff, 2012, pp. 33–40	Book portion	Building science	Scientists	Direct methods, indirect methods: microscale laboratory techniques and field-scale electrical techniques
Microclimate for Cultural Heritage: Conservation, Restoration, and Maintenance of Indoor and Outdoor Monuments, 2nd Ed.[4]	Camuffo, 2013, pp. 454–464	Book portion	Conservation	Scientists, Practitioners	Standards, direct and indirect methods, field- and laboratory micro-scale techniques
Methods for measuring rock surface weathering and erosion: A critical review	Moses, Robinson and Barlow, 2014	Article	Geomorphology	Scientists	Techniques that have been used in recent past (from time of publication), electrical/dielectric measurements, laboratory and field investigations
BS EN 16682: Conservation of cultural heritage – Guide to the measurements of moisture content in materials constituting movable and immovable cultural heritage	BSI, 2017	Standard	Conservation	Practitioners	Principles, absolute [direct] and relative [indirect] methods, field and laboratory micro-scale techniques
Methods of Measuring Moisture in Building Materials and Structures	Nilsson, 2018	Book	Building science	Scientists, Practitioners	Principles: measurement principles of direct and indirect methods, field- and micro-scale techniques, applications

[3] 1st Ed. published in 2002

[4] 1st Ed. published in 1998

Most guidance tends to focus on either laboratory (micro-) or field-scale techniques; this is especially apparent in mid-20th century literature when emphasis within the field was characterising the microscale dynamics of moisture movement (as opposed to applying technologies *in situ* to inform management and conservation). From approximately the turn of the millenium the variety of measurement principles of techniques included in guidance remains more or less the same. Typically, most guidance has been written for measurements on concrete and other materials most commonly used in contemporary construction. However, more recent attention has been devoted to applying techniques in a heritage setting (BSI, 2017), and especially for rock and stone (Svahn, 2006; Doehne and Price, 2010; Moses, Robinson and Barlow, 2014).

There is a wide range of technical knowledge required to comprehend difference guidance, which results in a polarisation between applicability to scientists or practitioners, but infrequently both. This manifests as a divide between reporting and interpreting using the measured physical properties (e.g. electrical resistivity) or manipulated values (e.g. arbitrary scales). This represents a contrast between the quantitative detection of water contents and the determination of variation of moisture levels across an area of interest. Using relative readings, as discussed by Dill (2000) and elsewhere, e.g. Burkinshaw and Parrett (2003), is applicable in the latter case, since it supports decision making in building management without requiring calibration of specific materials. This is also represented

in a shift in terminology within BS 16682 (2017) from 'direct or indirect' to 'absolute or relative' measurement techniques.

What is noticeably lacking from this body of guidance literature is information pertaining to procedures for data handling, and visualisation practice. However, a few recent sources provide specific guidance on technique selection: Dill (2000) emphasises matching techniques and measurement principles based on the investigation objectives and materials at hand, as well as scenarios in which long-term minimally-invasive monitoring would produce more satisfactory results. Derome, Teasdale-St-Hilare and Fazio (2001) provide guidance on technique selection, with emphasis on accuracy, response time, and their source(s) of errors. The only techniques they consider appropriate from field studies are electrical resistance and dielectric approaches. There is also a gap in guidance on how non-destructive technique should be implemented techniques into field-scale (practical building conservation) investigations of stone masonry and stone masonry systems. Even in the detailed and comprehensive volume recently edited by Nilsson (2018), the use of non-destructive techniques in a masonry context is not emphasised to any significant degree (despite nine chapters focused on applications).

2.3.4 Measurement principles

Changes in the water content of a porous building material affect nearly every bulk physical property, which has resulted in a great number of techniques being applied to minimally-

invasive and/or non-destructive measurement moisture in building materials (Figure 2.3).

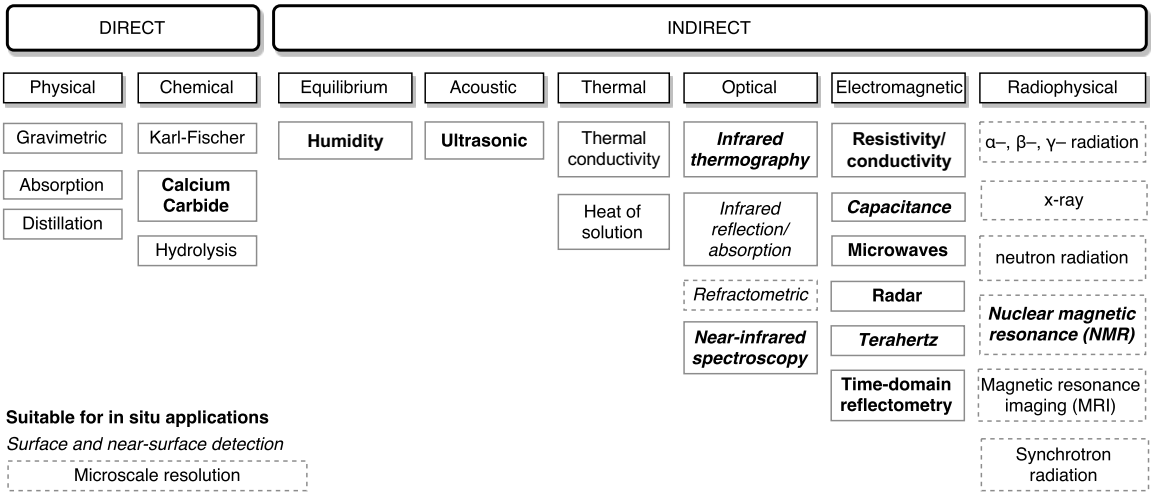

Figure 2.3. An overview of different measurement principles (sub-headings beneath direct and indirect methods) and techniques (within each principle) for non-destructive measurement of moisture.[5] Adapted from Kupfer (1997, p. 19).

NDT techniques are optimised when they are selected for their strengths in acknowledgement of their weaknesses. The practical application of NDT methods therefore depends on the objective of investigation (Válek et al., 2010), and the relative concern regarding moisture regimes. One key issue is the detection of surface, near surface, and deep-seated moisture within constructions of porous building materials (Wilhelm, 2016, p. 52). As introduced in Section 2.3.3, many techniques operate on the micro-scale; these are not appropriate for *in situ* applications since they require specialised set ups (and often include radiation sources). Details of the measurement principles and implementation of these techniques (and others not applicable to straightforward *in situ* applications) techniques can be found in the guidance listed in Table 2.5 (p. 37). Many techniques in

[5] Those techniques indicated in italics are exclusively capable of detecting surface and near-surface moisture levels, whereas others not specifically indicated can also provide information on these regions (in addition to others) under the right conditions.

Figure 2.3, although suitable on site, can be classified as 'minimally-invasive' (but are by definition destructive):

- Calcium carbide: determines moisture content from powder acquired by drilling through a change in pressure caused by a chemical reaction with acetylene (Slight, 1989);
- Equilibrium humidity: infers moisture from the moisture content of dowels inserted into drill holes (typically cellulosic), measured by resistivity or mass (Walker, Pavía and Dalton, 2016);
- Time-domain reflectometry (TDR): calculating the dielectric constant from an electromagnetic signal travel time between two embedded rods (Cerný, 2009).

Excluding these techniques, there are a range of non-destructive (surface, i.e. one-sided) approaches commonly used to measure moisture in building materials and stone masonry based on acoustic, optical, electromagnetic, and radiophysical principles (Table 2.6). The areal capture (surficial and at depth) of these techniques depends on the device design and construction, commercial or otherwise. For example, it is possible to apply infrared thermography on a single point, using a handheld thermometer (or similar device). However, in practice it is more common to use a camera that provides a gridded output of thermal measurements covering a spatial area. Similarly, the depth of sensitivity for resistivity is a function of the separation of the prongs, i.e. it is significantly different for a

handheld meter with a prong spacing of 1.5 cm than for a transect with maximum electrode spacing of 1.5 m. Analogues can be drawn for most other techniques.

Ultrasonic techniques have been used to assess moisture levels, but are more typically employed to assess physical and mechanical properties of building materials (e.g. Vasconcelos et al., 2008).

Table 2.6. Common techniques for non-destructively measuring moisture in building materials and structures, presented with advantages, disadvantages, and relevant literature.

Principle / Technique	Description	Advantages	Disadvantages	Relevant literature
Acoustic				
Ultrasonic	Low frequency (typically 0.1-50 MHz) waves are generated; various properties of measured, including travel time and attenuation; higher moisture levels increase both parameters	high depth penetration, immediate results (which support spot decisions)	Difficult to apply to rough or irregular surfaces, requires couplant gel and a clean and sturdy surface	Wang, 1990; Ross and Pellerin, 1994; Kahraman, 2007; Cotic et al., 2013; Verstrynge et al., 2014
Optical				
Infrared thermography	Measures radiance converting it into an apparent surface temperature (Camuffo and Bertolin, 2012); areas with higher moisture levels have higher thermal capacities, resulting in variation in apparent temperature	Large spatial range, quick data acquisition, independent of subsurface metal (in so far as this would affect surface temperatures)	Proxy of a proxy (i.e. using radiance as an indirect measure of temperature), highly dependent on environmental conditions during *in situ* use, requires known emissivities for accurate results (Kylili et al., 2014)	Rosina and Grinzato, 2001; Santos et al., 2003; Capitani et al., 2009; Grinzato et al., 2011; Lerma, Cabrelles and Portalés, 2011; Edis, Flores-Colen and Brito, 2015; Barreira, Almeida and Delgado, 2016
Near-infrared (NIR) spectroscopy	Analyses absorbance between 780–2500 nm; strong peaks are caused by the presence of H_2O, suggesting higher moisture levels in a porous media	Inexpensive	Requires post-processing of spectra, limited spatial scale, more suitable for organic materials	Ghandehari et al., 2012; Leblon et al., 2013; Tsuchikawa and Kobori, 2015; Zahiri, Laefer and Gowen, 2018
Electromagnetic				
Resistivity (and conductivity)	Measures the electrical impedence between electrodes or pins (Pinchin, 2008); higher resistance implies lower moisture levels	Handheld meters are easy to operate	Potential impact from salts, pin- and electrode-based approaches can cause permanent change to surface (indents and staining, respectively)	Knowler, 1927; Archie, 1942; Sass and Viles, 2006, 2010b; Kruschwitz et al., 2012; Martinho et al., 2012; Eklund et al., 2013; Martínez-Garrido et al., 2018
Capacitance	Measures capacitance (the ability to store electric charge), which is dependent on the dielectric constant a component of permittivity (BSI, 2017); capacitance is proportional to the dielectric constant (Kupfer, 1997, p. 85), i.e. higher capacitance higher levels of moisture	Handheld meters are easy to operate	Limited depth penetration	Cerný et al., 1995; Howell, 1995; Trotman and Harrison, 2004; Larsen, 2012; Eklund et al., 2013

continued on next page...

Table 2.6 – *continued from previous page*

Principle / Technique	Description	Advantages	Disadvantages	Relevant literature
Microwave	A wide frequency band (0.3 to 300 GHz), various properties of measured, primarily reflection (Lataste and Göller, 2018): higher moisture levels increase all three parameters; typically 1-10 GHz is used, to balance signal penetration depth and sensitivity to moisture	Negligible impact from salinity, Simultaneous surface and depth measurements with the appropriate applicators	Uncertain range of detection, more sensitive to surface moisture than depth (Camuffo and Bertolin, 2012)	Hauschild and Menke, 1998; Bläuer and Rousset, 2009; Weritz et al., 2009; Göller, 2012; Kruschwitz, 2015
Radar	A wide frequency band (0.3 to 300 GHz), various properties of measured, including travel time, attenuation, and wave amplitudes (Lai, Dérobert and Annan, 2018); higher moisture levels affect three parameters in different ways; typically 0.5-10 GHz is used in commercial applications, to balance signal penetration depth and sensitivity to moisture	Simultaneous surface and depth measurements, visual output available immediately, quantitative output possible	Expensive, requires data processing for conclusive results (typically off-site)	Maierhofer and Leipold, 2001; Binda, 2005; Maierhofer et al., 2008; Cardani et al., 2013; Cotic et al., 2013; Lai et al., 2014; Cetrangolo et al., 2017; Martínez-Garrido et al., 2018
Radiophysical				
Nuclear magnetic resonance (NMR)	generates a magentic field: the amplitude of the echo envelope, or equivalently by the integral of the relaxation time distribution function is sensitive to moisture (Blümich, Perlo and Casanova, 2008)	High spatial resolution, accuracy, and precision	High set-up time, specialised operation	Gummerson et al., 1979; Brocken, Adant and Pel, 1997; Tedoldi, 2002; Blümich et al., 2003; Bortolotti et al., 2006; Proietti et al., 2006; Litti et al., 2015

Infrared thermography is a very common technique, but is typically used to produce visual output (and not assessed quantitatively); see Young (2015). However, Lerma et al. (2011) have demonstrated the value of signal processing in reducing the impact of varying material properties on identifying variations in moisture across a façade. It is important to note that infrared thermography uses a proxy for surface temperature, which is in turn used as a proxy for moisture levels. This additional degree of separation from the absolute presence of moisture can increase imprecision. Near-infrared spectroscopy is unique in Table 2.6, as it is most commonly used for assessing moisture contents in wood, due to its applicability to organic papers – including extensive use in paper science (Tsuchikawa and Kobori, 2015).

The electromagnetic techniques are based on the same principle, but measure different parameters within the interaction of waves with porous media (e.g. permittivity, conductivity, reflection coefficients) at different frequencies. The literature presented in Table 2.6 for these techniques is a mix of research-grade tools (e.g. Kruschwitz et al., 2012) and more accessible tools commonly used in building surveying (e.g. Eklund et al., 2013). The electromagnetic techniques presented require different levels of technical knowledge to operate and evaluate. At most operating frequencies, microwave and radar techniques will be negligibly impacted by salinity, whereas electrical and capacitive techniques can be influenced by the presence of salts within building materials (Wilhelm, Viles and Burke, 2016).

Nuclear magnetic resonance (NMR) imaging has been used to characterise the dynamics of moisture since the 1970s (Gummerson et al., 1979). More recently, a commercial tool, the NMR-MOUSE^{TM} (Eidmann et al., 1996) that can be used on-site has resulted in frequent *in situ* use (see Table 2.6).

Other techniques (but based on one of the aforementioned principles) have been applied to non-destructively evaluate moisture in building materials, e.g. self potential (Martinho et al., 2014), evanescent field dielectometry (Di Tullio et al., 2010; Olmi et al., 2011), but are less prevalent in both literature and common practice.

New techniques are continually being developed for application to building material moisture measurement. For example, Terahertz imaging has demonstrated potential

utility (Federici, 2012; DiGiovanni et al., 2013; Krügener et al., 2015) but has not been commercially developed for widespread use within building assessment. More recently, the sensitivity of bluetooth (Moldenhauer et al., 2017) and laser scanning (Suchocki and Katzer, 2018) to varying moisture contents within building materials has been demonstrated. These techniques hold promise for rapid, high-resolution detection of moisture variation within a building façade, but have not yet been commercially developed or implemented into common practice.

2.3.5 Combinative survey methods

The benefits of employing multiple NDT techniques are widely acknowledged. Studies have shown that applying a suite of techniques, including slower quantitative and faster, more qualitative methods will often provide the most information, yielding the best assessments (Di Tullio et al., 2010; Martinho et al., 2014). This is complicated not only by the difficulty of interpreting results from a single method but also the harmonisation of the results (Binda, Cantini and Tedeschi, 2013). In many cases, multi-sensor approaches have been focused on selecting the most accurate technique based on a selection criteria (e.g. Smith et al., 2011b; Zhao et al., 2012).

Although Camuffo and Bertolin (2012, p. 31) outline that "it is theoretically incorrect to perform calibrations by comparing methodologies based on different physical principles", others have demonstrated that reasonable agreement and (in some cases) correlations can

be established between testing methods (Weritz et al., 2009; Solla et al., 2012; Martinho et al., 2014) as well as gravimetrically-derived moisture contents (Nguyen et al., 2008; Sass and Viles, 2010b; Chabriac et al., 2014; Pel, 1995, chp. 3). Regardless of numerical agreement, what is integral to NDT surveys is that in most cases the methods provide consistent qualitative output, despite being based on different physical principles (Válek et al., 2010).

2.4 Conclusion

Stone masonry is an important part of monumental and vernacular heritage in the UK, contributing to economic development and sustainability. Stone is susceptible to weathering by several processes, many of which are dependent on the presence and movement of water. These can be exacerbated within a stone masonry context, so it is important to characterise moisture regimes within the building envelope, especially with regards to the function of mortar joints within the system.

Wind-driven rain is one of the most important sources of moisture for the UK's built environment. In addition to the aforementioned stone weathering processes, wind-driven rain can impact the performance of the building envelope and affect occupant health and comfort. Measurement, numerical methods, and semi-empirical evaluation are three common assessment techniques. Semi-empirical evaluation has been extensively used in the UK since the mid-20th century for practical purposes of building management and risk

assessment. In the context of a changing and uncertain climate, it is important to ensure that current guidance (especially standards) and metrics used to semi-empirically evaluate wind-driven rain exposure can accurately characterise current and future wind-driven rain exposure.

Characterising moisture regimes within stone masonry is an important part of understanding the response to wind-driven rain. Numerical methods (modelling) and non-destructive measurement are two approaches commonly employed. Non-destructive testing methods use a diverse range of physical phenomena as proxies for the presence of moisture; these are commonly related to gravimetric calibration to understand the relationship of the measured properties of arbitrary values to an absolute moisture content. An abundance of guidance (for both technical and practical audiences) can confound selecting the most appropriate technique for a given scenario. Several techniques, including electrical resistivity and electromagnetic techniques, are especially applicable to *in situ* field studies (particularly in combinative use). However, there is a need for better guidance for more accessible calibration techniques, methods of data handling and visual representation.

3 | Research framework

"White. A blank page or canvas.
The challenge: bring order to the whole.
Through design. Composition. Tension. Balance. Light.
And harmony."

– STEPHEN SONDHEIM (2000, pp. 17–18)

This thesis uses a four-unit structure to evaluate the relationship between wind-driven rain and stone masonry. It examines the **exposure** to wind-driven rain and the **response** of moisture regimes within stone masonry. These structural components are linked by two approaches: 1) the evaluation and development of **methodology**, and 2) **characterisation** of the environment, material properties, and hygric behaviour. This section introduces these dimensions of the thesis, and also provides rationale for the particular approaches chosen (i.e. the semi-empirical exposure assessment method and electromagnetic non-destructive moisture measurement techniques).

3.1 Structure

The core aim of this thesis is to explore the exposure and response of stone masonry to wind-driven rain (Figure 3.1). It is not intended to create direct relationships between these two components i.e. an exposure of x will produce a response y in the stone masonry. Rather, the aim is to characterise relevant physical phenomena and properties and develop assessment methods that individually address each component. This reflects the two-part

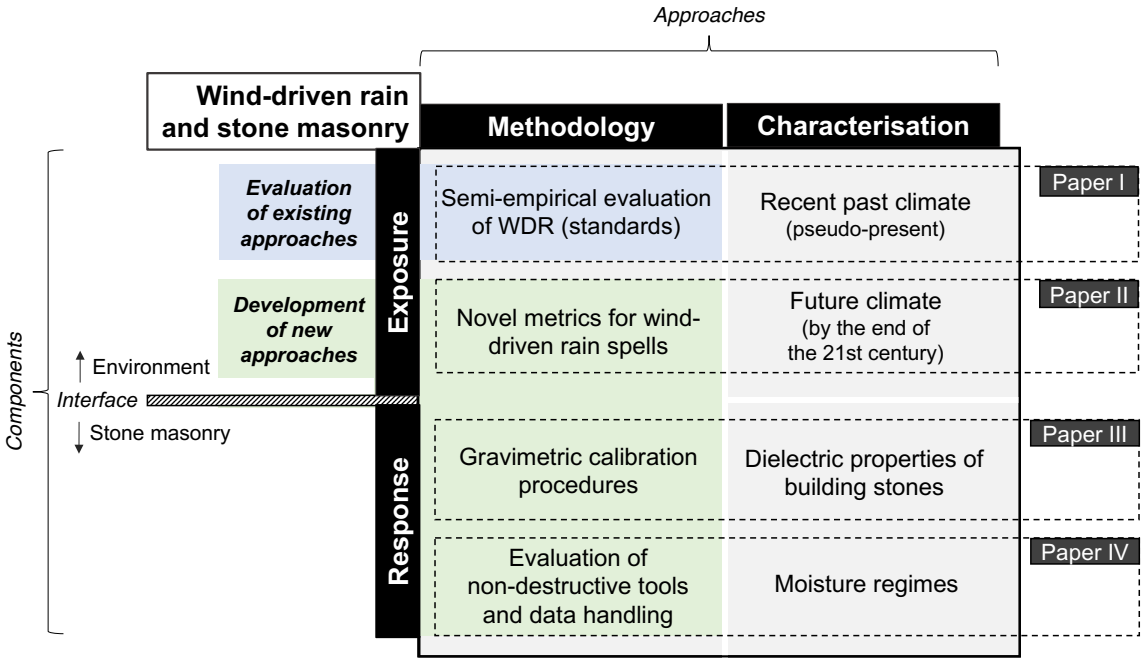

Figure 3.1. The research framework for this thesis, demonstrating the four-part approach employed to characterise the relationship between wind-driven rain and stone masonry.

structure of research within building engineering related to wind-driven rain: 1) assessment of the impinging wind-driven rain intensity, and 2) assessment of the response of the building façade to the impinging wind-driven rain (Blocken et al., 2009). The synthesising discussion in Chapter 9 identifies synergies between components.

Each Paper included in Figure 3.1 is presented as a main body chapter. These chapters are written as stand-alone manuscripts that are at various stages of publication in relevant peer-reviewed journals. According to departmental regulations, three of these papers have been submitted to (or published in) international peer-reviewed journals. Paper IV (Chapter 7) has been drafted as a manuscript suitable for submission in a similar manner but has not yet been submitted. The candidate has made a substantive contribution to each paper, which is attested to by first authorship and signed statements from each co-author (Appendix D).

The status of publication is presented at the beginning of each chapter along with an abstract and names of co-authors. Therefore, each main body chapter includes an introduction and brief literature review to provide context, methods, theory and calculations (when applicable), results, and discussion. Papers I to IV are presented in the following chapters:

- Paper I: Characterisation of building exposure to wind-driven rain in the UK and evaluation of current standards (Chapter 4);
- Paper II: Wind-driven rain and future risk to built heritage in the United Kingdom: novel metrics for characterising rain spells (Chapter 5);
- Paper III: An 'isolated diffusion' gravimetric calibration procedure for radar and microwave moisture measurement in porous building stone (Chapter 6);
- Paper IV: Moisture monitoring of stone masonry: a comparison of microwave and radar on a granite wall and a sandstone tower (Chapter 7).

Through the EPSRC Centre for Doctoral Training in Science and Engineering in Arts, Heritage, and Archaeology, the project is undertaken collaboratively with Historic Environment Scotland and the Consarc Design Group. These organisations have contributed to the scientific direction of this thesis and helped to steer the aims and objectives toward practical elements of heritage conservation and building management.

3.1.1 Components

The **exposure** of stone masonry to wind-driven rain is defined here as encompassing all environmental factors (e.g. aspect, built context, precipitation, wind speed and direction) which influence the amount of water arriving at the masonry surface.

The **response** of stone masonry to wind-driven rain exposure is defined here as the processes in which water is absorbed into a stone masonry system, moves within it, and is returned to the atmosphere (e.g. penetration through joints, evaporation, etc). The rates of these processes vary over space and time, resulting in uneven distributions of water within a façade. Longer term responses of stone masonry, such as deterioration and material loss, are not discussed in this thesis. However, as they depend largely on moisture migration the work presented in this thesis will help improve understanding of them in future.

3.1.2 Strategies

The strategies used to investigate the exposure and response of stone masonry to wind-driven in this thesis are methodological development and characterisation. Characterisation is secondary to developing methodologies, but serves three purposes:

1. to provide evidence supporting the need for methodological development

2. to demonstrate the informational benefit of the proposed methodologies

3. to create new information that is useful in practical heritage conservation and

building management

Environmental conditions of the recent past (a pseudo-present climate, characterised over long periods of time to account for annual variability) furthers understanding of the current climate (Paper I). This motivates a critical assessment of the current standards used to estimate wind-driven rain exposure, which suggests changes that could be implemented to improve existing approaches. By characterising predicted environmental conditions in a severe climate change scenario (Paper II), this thesis preemptively identifies future methodological needs of the built environment sector and demonstrates the utility of novel temporal metrics for characterising wind-driven rain spells.

Both papers that evaluate the response of stone masonry to WDR (Papers III and IV) propose novel techniques and approaches. This thesis does not focus on developing new technologies that non-destructively detect the presence of moisture within a construction. Instead, it emphasises:

(a) laboratory procedures for calibrating existing techniques (Paper III);

(b) field-appropriate implementation techniques for efficient survey planning (Paper IV);

(c) *how* existing techniques are used (Papers III and IV);

(d) strategies of data handling and visualisation of moisture measurement data to encourage them to be used as an integral part of monitoring the built environment (Paper IV).

3.2 Method selection

Several methods exist for assessing wind-driven rain exposure and non-destructively measuring moisture in building materials. Each of these components has been addressed with a 'primary' method. The rationale for the selection of each method is explored.

3.2.1 Exposure to wind-driven rain

There are there main methods to assess the amount and intensity of wind-driven rain exposure (Section 2.2.2). Measurements and numerical methods – especially if the former incorporates computational fluid dynamics, e.g. Briggen, Blocken and Schellen, 2009 – can be costly, resource-intensive, and applied to a specific scenario of limited spatial scale. Semi-empirical models are based on climatic data from meteorological monitoring stations, and can incorporate the anthropogenic and natural context by applying factors, which are being continually improved (Ge et al., 2018). This facilitates comparisons between locations for which data is available, without requiring WDR-specific instrumentation at each site (Papers I and II). Exposure maps based on semi-empirical models are commonly used in building assessment and design practice. It is important to ensure these maps are relevant to the current climate and based on state-of-the-art techniques (Paper I). It is also imperative to sustainability to establish the suitability of these methods and standards for assessing predicted future climates and suggest future developments for their continued

relevance (Paper II). For these reasons, a semi-empirical evaluation of wind-driven rain was employed in this thesis (Papers I and II). It is also used to inform the methods used to assess the response of WDR (Paper IV).

3.2.2 Response of stone masonry

There are two main methods for assessing the response of stone masonry to wind-driven rain: modelling and measurement (Section 2.3). Regardless of the commercial software employed, modelling approaches are hindered by two challenges in heritage applications:

- Material properties – to produce valid results, these softwares require accurate numerical input of accurate hygrothermal material properties. In heritage applications, this can be difficult if insufficient quantities of building material samples can be sourced. Additionally, the increased heterogeneity of building materials caused by *in situ* weathering processes can result in varying accuracy of modelled behaviour;

- Aspects of workmanship and realistic geometry – these softwares represent idealised constructions that do not account for structural deficiencies, such as cracks (and other microscale features) in mortar joints which can provide rapid ingress points for wind-driven rain.

In a built heritage context, a measurement approach can provide useful information for characterising the functioning of a stone masonry system. An early component of this study

(Appendix C) demonstrated the logistical difficulties of collecting rapid measurements with both point- and transect-based electrical techniques. In contrast, the electromagnetic tools showed strong potential for being implemented into moisture measurement methodologies. There are several additional practical motivations for developing methodologies based on non-destructive electromagnetic techniques:

- they are one of the most common measurement principles for handheld moisture meters as they include capacitive and dielectric devices (Pinchin, 2008);
- they typically use commercially available frequencies (ITU, 2016), meaning they do not require special licenses to be operated;
- within this frequency range, the effect of conductivity (which is dependent on salinity), is negligible compared to the presence of fresh water (Klein and Swift, 1977);
- a range of antenna and applicators can be implemented in commercial design, which enables investigation at various areal ranges and depths.

For these reasons, among others, the methodologies for assessing the response of stone masonry to wind-driven rain are primarily driven by the characteristics of devices based on electromagnetic measurement principles (Papers III and IV). The methodologies developed assess the validation and calibration of commercial sensors (Paper III) based on laboratory

evaluation, as well as practical aspects of implementing them into surveys of the historic building environment (Paper IV).

Electromagnetic measurement can account for the potential variation induced by these types of structural heterogeneity is preferential. These can incorporate measurements of physical structures (Papers III and IV). In the ideal scenario, the structures are produced to a high standard and can therefore be well characterised from a material and structure perspective (Paper IV). More realistically, structures with a complex and uncertain history of ambient weathering are investigated *in situ* for which comprehensive environmental and material characterisation is less feasible (Paper IV).

Part II

Semi-empirical evaluations of exposure to wind-driven rain

4 | Characterisation of building exposure to wind-driven rain in the UK and evaluation of current standards

"The storm starts, when the drops start dropping
When the drops stop dropping then the storm starts stopping."

– DR SEUSS [Theodor 'Seuss' Geisel] (1979, final page)

Published as: Orr, S. A. and H. Viles. (2018). 'Characterisation of building exposure to wind-driven rain in the UK and evaluation of current standards'. *Journal of Wind Engineering and Industrial Aerodynamics*, 180:88–97. doi:10.1016/j.jweia.2018.07.013

Abstract

One method of estimating WDR exposure is semi-empirical formulae based on hourly meteorological data including ISO 15927-3:2009 and BS 8104:1992. These provide protocols to estimate extreme WDR exposure, such as the worst spell likely to occur in any given three-year period. This study characterises the amount of annual WDR exposure and the frequency and duration of directional WDR spells for eight sites in the UK from 1986 to 2015. To assess the utility of these standards for evaluating extreme WDR exposure at those sites, the worst spell likely to occur in any given three-year period is determined using a 'return period' approach from extreme value analysis (EVA). It is shown that in the context of the prevailing wind patterns in the UK wall orientation is an important factor in determining the frequency and duration of WDR spell properties. EVA is applied for eight sites in the UK from 1959 to 1991 to evaluate the methods and climatic data used in BS 8104:1992 and their relevance to current climate. Both standards underestimate the volumetric exposure of the 'once every three years' spell compared to EVA for methodological reasons but are useful tools to assess annual exposure and compare between sites.

This manuscript is reprinted exactly as published (Orr and Viles, 2018a).

4.1 Introduction

Wind-driven rain (WDR) or driving rain is rain given a horizontal velocity component by the wind and falling obliquely (Blocken and Carmeliet, 2004). WDR represents the main source of moisture and agent of deterioration for building façades (Erkal, D'Ayala and Sequeira, 2012).

One method of evaluating the exposure of a building façade to WDR is semi-empirical formulae. In the mid-twentieth century, it was found that the quantity of rainfall with a horizontal component that would hit a wall surface is proportional to both precipitation and wind speed (Hoppestad, 1955; Lacy and Shellard, 1962). Subsequently, this product was used to estimate relative annual exposures across the UK (Lacy, 1976), relevant to assessing average moisture contents in walls (BSI, 1992) and the potential for deep-seated wetting (Smith et al., 2011a; McCabe et al., 2013).

Many mechanisms that can physically alter porous building materials–such as salt migration, crystallisation stress, and biological growth–are dependent on the presence and movement of water. Additionally, intense spells are associated with rain penetration through edges of doors or windows (ISO, 2009). For these reasons, a rain spell approach was developed by the UK Met Office and the Building Research Establishment to evaluate building exposures and relative risk for regions of the country (BSI, 1984; Prior, 1985).

Building on the 1976 annual exposure maps (Lacy, 1976) and a rain spell methodology,

isoline maps of wind-driven rain were produced for the UK in BS 8104 (1992) based on hourly meteorological data from 1959 to 1991. The spell indices represent the worst spell likely to occur in any three year period. BS 8104 remains the current reference for WDR exposure in the UK.

ISO 15927-3 (2009; henceforth ISO 15927) was developed from the methods underpinning BS8104 as a generalised calculation procedure for assessing wind-driven rain exposure, which can be applied for time periods and locations for which appropriate data is available. The worst spell likely to occur in any three year period is represented by a percentile of the spell amounts occurring in a given time period for a specific wall orientation.

Methods based on extreme value analysis (EVA) acknowledge that weather events are rarely represented by normal distributions. Therefore, traditional statistical representations (i.e. percentiles) of weather events might be skewed by extreme random phenomena and are thus not suitable for characterising extreme WDR events. Current approaches to representing extreme wind-driven events use the Gumbel distribution (Nadarajah and Kotz, 2004) and the concept of return periods (Gumbel, 1941). Return periods are a well-established method originally used to assess flood risk that statistically represents the probability of a certain recurrence of events. The Gumbel distribution is "perhaps the most widely applied statistical distribution for problems in engineering " (Nadarajah and Kotz, 2004, p. 13), and frequently used for climate applications (Nadarajah, 2006).

Return periods combined with the Gumbel distribution have been used in conjunction to evaluate extreme WDR exposure (Pérez-Bella et al., 2012; Giarma and Aravantinos, 2014). However, these studies used scalar estimations of WDR exposure, which do not incorporate wind direction and wall orientation. This is important for assessing WDR exposure in the UK, as the polar jet stream introduces strong directional trends in wind speeds and prevailing wind directions.

Accurate assessments of building exposure to extreme rainfall events (e.g. the worst spell likely to occur every three years) are a crucial component of building management. WDR spells are becoming more important with expected increases in rainfall intensity and frequency in the 21st century (IPCC, 2013, p. 23). In a 2011 report evaluating the need for new guidance on wind-driven rain (Reid and Garvin, 2011), BRE Scotland advised that the UK climate had not changed sufficiently to render BS 8104 irrelevant. No mention of the opacity of calculation methods is made. These changes in climate challenge the relevance and applicability of the data and methods upon which current standards are based.

This paper characterises wind-driven rain exposure for eight UK sites (Figure 4.1) between 1986 and 2015. It explores the frequency of occurrence of different spells as a function of annual precipitation and wall orientation. The validity of methods used in current standards to calculate the 'once every three years' spell are compared with extreme value analysis. A similar comparison to extreme value analysis to evaluate extreme WDR exposure from 1959 to 1991 assesses whether the data and methods that are the basis for

BS 8104 are representative of the current UK climate. Guidance is provided on how to interpret ISO 15927-3 and BS 8104 for design and risk assessment.

4.2 Methods

4.2.1 Climate and sites

The UK has a temperate maritime climate, characterised by westerly air flows and depressions which particularly influence the western margins. Eight sites that experience different climates were selected to be studied (Figure 4.1 and Table 4.1). These sites exhibit individual trends in prevailing wind directions but also reflect the general prevalence of south-westerly winds (Figure 4.2).

Long-term hourly meteorological measurements for these eight sites from 1986 to 2015 were obtained from the UK Met Office (UK Met Office, 2006a, 2006b), and used to evaluate the current conditions of WDR exposure. Thirty years of hourly data has been used in the majority of works in the field (Fazio, Mallidi and Zhu, 1995; DEFRA, 2009) and is considered the ideal period of measurements for using ISO 15927 (2009). Using many years of data accounts for inter-annual variability to capture the general behaviour, and 30 is the recommended length for presenting statistical parameters by the World Meteorological Organisation (Guttman, 2010).

Figure 4.1. The sites evaluated in this study.

A secondary study period of 1959[1] to 1991 was used; this enabled an evaluation of BS 8104 (1992) using periods of data comparable to that upon which it was based. For three of the study sites (Boulmer, Leuchars, and Nottingham), the appropriate data format was not available during this period. Data from the nearest sites with appropriate data were

[1]Limited availability for Leeming, 1965 to 1991.

Table 4.1. Climatic data availability and basic meteorological and geographical characteristics of the study sites.

Name	Time period		Average precipitation*	Elevation	Approximate distance from coast
	1959-1991	1986-2015	mm year^{-1}	m	km
Stornoway	X	X	1187	14	<5
Leuchars		X	695	12	<5
Turnhouse	X		646	35	<5
Aldergrove	X	X	854	62	20
Boulmer		X	701	24	<5
Leeming	X		535	33	50
Heathrow	X	X	681	25	100
Nottingham		X	849	118	100
Elmdon	X		651	95	150
Plymouth	X	X	967	45	<5
Valley	X	X	836	11	<5

**Over the specified time periods*

used as substitutes (Leeming, Turnhouse, and Elmdon, respectively; see Figure 4.1). These 'proxy' sites are used to approximate the climatic conditions for Boulmer, Leuchars, and Nottingham, as they experience similar (but not identical) climates.

4.2.2 Calculating WDR exposure from meteorological data

4.2.2.1 ISO 15927-3:2009

ISO 15927 specifies two procedures for providing an estimate of the quantity of water likely to impact on a wall of any given orientation. It uses at least 10 (but ideally 20 to 30) years of hourly measurements of precipitation, wind speed, and wind direction to calculate the WDR exposure.

The wind-driven rain exposure I in an hour is calculated as:

$$I = \frac{2}{9} v r^{8/9} cos(D-\theta) \qquad [\mathrm{L\ m^{-2}}] \tag{4.1}$$

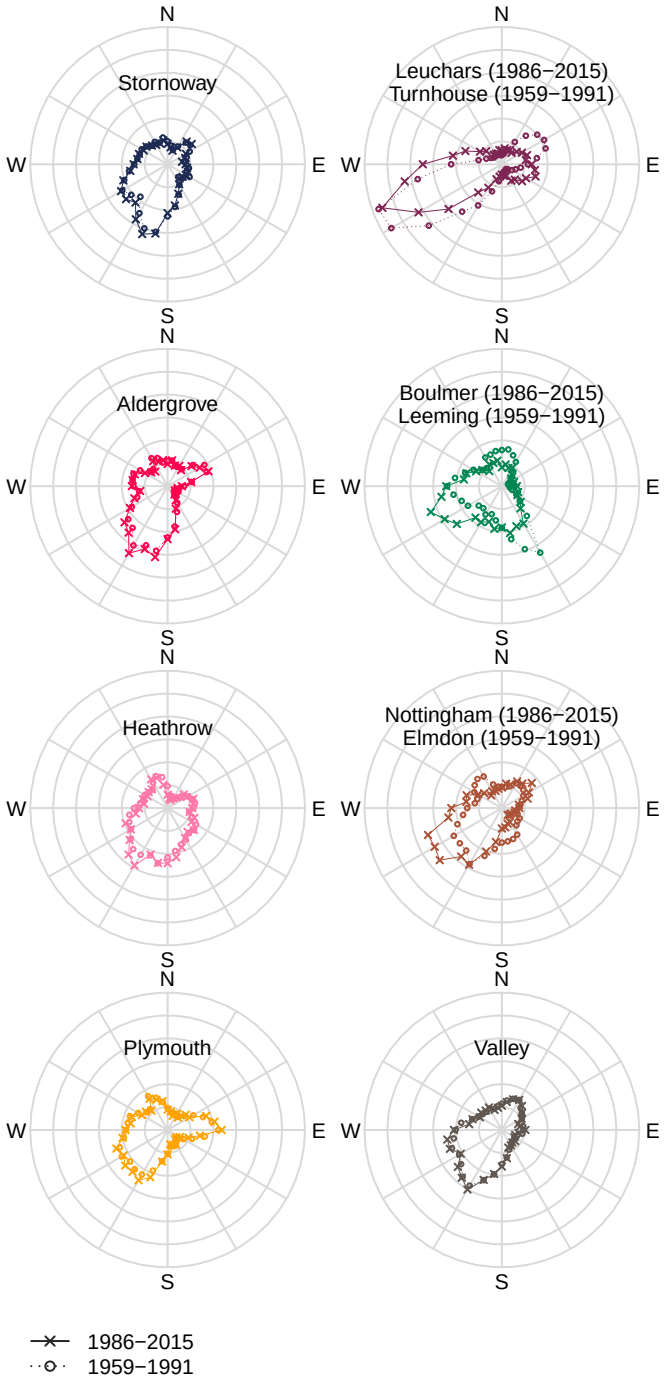

Figure 4.2. Prevailing wind directions (represented by relative occurrence) for eight UK sites, based on measured hourly wind directions (UK Met Office, 2006b) from 1986 to 2015 and 1959 to 1991. For three sites, approximate 'proxy' climatic data from nearby sites has been used due to data availability.

from average hourly wind speed v (m s^{-1}), hourly precipitation r (mm), hourly mean wind direction D (^{o}) for a specific wall orientation θ (^{o}). This semi-empirical formula "yields the amount of WDR passing through a vertical surface in an undisturbed airstream" (Blocken and Carmeliet, 2004, p. 1102), and is therefore reflective of the amounts of water that are expected incident to a vertical surface, ignoring obstacles and topography. This formula for wind-driven rain loads represents a realistic estimate of the exposure of a façade, as it is derived from the average characteristics of rain drops and their aerodynamic properties (Blocken and Carmeliet, 2004).

The **annual index** I_A is the average annual WDR exposure, defined as:

$$I_A = \frac{\sum \frac{2}{9} v r^{8/9} cos(D-\theta)}{N} \qquad [\text{L m}^{-2}] \tag{4.2}$$

where the summation of I is taken over all hours for which $cos(D-\theta)$ is positive for N years, i.e. wind is intersecting the wall orientation. I_A is synonymous to the summation of Equation 4.1 meeting the condition $cos(D-\theta) > 0$ divided by the N years of data. The annual index I_A should be used for "considering the average moisture content of exposed building material or when assessing the likely growth of mosses and lichens" (BSI, 1992, p. 4).

A **spell-specific index** I'_S is calculated for periods of WDR exposure which are

separated by 96 h or more of no wind-driven rain exposure:

$$I'_S = \sum \frac{2}{9} v r^{8/9} cos(D-\theta) \qquad [\text{L m}^{-2}] \tag{4.3}$$

where the summation is taken over all hours for which $cos(D-\theta)$ is positive, i.e. wind is intersecting the wall orientation.

The **spell index** I_S represents the worst spell likely to occur in any given three year period. ISO 15927 represents I_S as the 67th percentile of the I'_S values, i.e. the value for which 33% of the I'_S values are higher. The spell index is representative of the risk of "rain penetration through masonry, which requires a prolonged input of water" (ISO, 2009, p. 12).

Using percentiles to represent an event with a respective rate of occurrence implies that the frequency of events in a given time period n is known. For example, if there are 60 spells occurring in one year, the worst spell likely to occur could be represented by the amount of WDR exposure below which 59 of the spell amounts may be found, i.e. $59/60 \times 100\% = 98.\overline{3}$. More generally, this percentile P is represented by $(n-1)/n \times 100\%$. If there were 75 spells occurring in a three year period, the worst spell (highest amount) to occur in that period would be represented by $(75-1)/75 \times 100\% = 98.\overline{6}$. Therefore, the percentile representing the worst spell likely to occur in a three year period is dependent on the frequency of occurrence, i.e. how many spells are occurring. Although ISO 15927 does not

use $(n-1)/n$ to determine the percentile that represents the worst spell likely to occur in any three year period, this formula and example demonstrate the potential effect of natural variation in annual event occurrence on extreme events determined from percentiles.

Equations 4.1, 4.2, and 4.3 include the wall orientation as part of the calculations. This means that the annual index and the spell index are directional metrics that do not apply to all orientations of a wall at a given site. Both I_A and I_S as presented here represent airfield conditions: WDR that would occur at a height of 10 m above ground level in the middle of an airfield with no other obstructions. To estimate the exposure for a specific façade, factors are provided in ISO 15927 that can be applied to the indices to account for terrain roughness, topography, obstructions, and the wall context.

4.2.2.2 BS 8104:1992

BS 8104 uses reference isoline maps to calculate WDR exposure in the UK. The reference maps divide the UK into subregions of similar WDR characteristics centred around pivotal sites. The subregions are divided further into geographical increments i to represent local variation. As in ISO 15927, the annual index I_A and spell index I_S are used. The procedure to determine values of I_A and I_S for a location is (BSI, 1992):

1. Look at the appropriate wind-driven rain map in Appendix B of BS 8104. Find the subregion in which the site is located. Find the geographical increment i for the site of interest. These increments are shown between contour lines.

2. Examine the rose for the particular subregion and method (I_A or I_S). Each rose gives 12 values corresponding to different orientations. Select the rose value r nearest to the orientation of the façade of interest

3. Add the rose value to the geographical increment to obtain the map value of I_A ($m_A = r_A + i$) and/or I_S ($m_S = r_S + i$).

If a site lies on a boundary of a subregion, contour, or orientation, the higher of the two figures should be taken. If desired, reducing factors can be applied to account for terrain roughness, topography, obstruction, and wall context.

The map value $m = i + r$ is provided for either the spell (m_s) or annual (m_a) index, which represents the conditions for a given wall orientation at a pivotal site, modified slightly to account for local variation. The annual index I_A in L m^{-2} can be calculated from its respective map value m_A:

$$m_A = 6 + 19.93\log_{10}(I_A/200) \tag{4.4}$$

The spell index I_S in L m^{-2} can be similarly calculated from its respective map value m_S:

$$m_S = 10 + 19.93\log_{10}(I_S/20) \tag{4.5}$$

The formula used to estimate hourly wind-driven rain exposure in BS 8104 is a simpler

representation of WDR exposure than that used in ISO 15927 (Equation 4.1). It is the product of hourly velocity and precipitation with the cosine of the prevailing wind direction and the wall orientation $I = rv\cos(D-\theta)$. This provides a "reasonably precise method of comparing different sites with respect to total amounts of WDR on walls" (Lacy, 1977), but does not estimate the actual exposure to WDR (Lacy, 1965).

4.2.2.3 Applying extreme value analysis to WDR spell exposure

To assess extreme WDR exposure, this study applied extreme value analysis (Fisher and Tippett, 1928; Smith, 1990). It is an established method used in environmental applications (e.g. Smith, 1989) to evaluate extreme deviations from the median of probability distributions. There are two practical approaches to using this technique to evaluate weather events:

- Generating an 'Annual Maxima Series' (AMS; see Cunnane, 1973), i.e. the maximum values of the weather event occurring in individual years
- Using the 'Peak Over Threshold' method (Leadbetter, 1991), where peak values over a certain threshold are recorded

It is difficult to define thresholds for WDR exposure that would represent clear impacts on a building envelope. Penetration through masonry constructions is a complex process that is dependent on a number of variables in addition to the amount of water hitting a

surface during the spell. For this reason, the AMS is more appropriate for assessing WDR events.

The AMS approach can be combined with the concept of 'return periods', a classic technique to evaluate the occurrence of extreme weather events such as floods (Gumbel, 1941). A return period is an estimate of the likelihood of an event, which can also be thought of as an 'expected frequency'. It can be converted into a probability of exceeding that value in any given year. For example a 'once every three years' spell has the probability p of occurring in any given year equal to $1/3 = 0.3\bar{3}$. It is likely that the 67th percentile in ISO 15927 is representing the value for which 1/3 of amounts are higher. However, probabilities and percentiles should not be directly compared. A probability represents the likelihood of exceeding a spell amount in a single year within a given three-year period, but this does not imply that this value will be exceeded every three years (or in any specific three-year period). As discussed in Section 4.2.2.2, a percentile representing the occurrence of an extreme event is based on an amount of WDR that was exceeded once in a specific three-year period and is dependent on the number of spells.

The AMS method has previously been applied to evaluate the 'once every three years' spell in Spain (Pérez-Bella et al., 2012, 2013). The semi-empirical calculation from ISO 15927 of hourly exposure (Equation 4.1) is used, with periods of 96 h or more without WDR exposure between spells. This representation is analogous to the 'wind-driven rain relationship' described by Blocken and Carmaliet (2004).

Pérez-Bella et al. used a scalar daily parameter, but defined spells as separated by 4 days (96 h) without precipitation (Pérez-Bella et al., 2012, 2013). This daily scalar value was found to correlate well with I'_S values calculated from hourly [scalar] data. However, this method does not incorporate the directional properties of WDR spells, which are an important consideration in the UK context (see Section 4.2.1).

The 'expected frequency' approach can be combined with a probability distribution of extreme values, such as the Gumbel distribution (Gumbel, 1958). In this way, it is possible to determine the spell exposure likely to be exceeded in any given three year period. One benefit of the AMS method is that the results are independent of the 'population size' (number of spells), i.e. comparisons can be made between sites and time periods that experience different numbers of spells.

Worked example of the AMS method

768 WDR spells were calculated to occur in Stornoway between 1986 and 2015 for a wall oriented north[2]. From these, the AMS values (the highest spell exposure occurring in each year) can be determined (Table 4.2).

The cumulative distribution function for the Gumbel distribution is (Gumbel, 1941, 1958):

$$f(\alpha, x^*, u) = e^{-e^{-\alpha(x^*-u)}} \tag{4.6}$$

[2]Spells that occurred across calendar years were allocated to the year in which the majority of the hours within the spell occurred.

Table 4.2. AMS values for a north-oriented wall in Stornoway between 1986 and 2015.

Year	Maximum value of I'_S L m^{-2}	Year	Maximum value of I'_S L m^{-2}
1986	44.95	2001	59.51
1987	121.8	2002	67.39
1988	106.8	2003	100.4
1989	151.7	2004	55.38
1990	31.26	2005	184.2
1991	56.79	2006	160.0
1992	63.71	2007	141.4
1993	106.9	2008	101.7
1994	40.44	2009	109.3
1995	67.78	2010	63.08
1996	99.76	2011	49.48
1997	66.79	2012	63.13
1998	162.6	2013	56.77
1999	69.65	2014	95.98
2000	73.94	2015	59.96

in which x^* is the WDR exposure likely to be exceeded in the return period. The average of the AMS values $\bar{x} = 87.75$ has a standard deviation $\sigma_x = 40.19$. u is the mode. α is the dispersion parameter, which is a ratio of the standard deviations of the population and a reduced variable population:

$$\alpha = \frac{\sigma_y}{\sigma_x} = \frac{\sqrt{\sum \frac{(x_i - \bar{x})^2}{N}}}{\sqrt{\sum \frac{(y_i - \bar{y})^2}{N}}} \tag{4.7}$$

The reduced variable is only a function of the number of years N, indicated by $i = 1, 2, \ldots, 30$:

$$y_i = -ln\left(ln\left(\frac{N+1}{i}\right)\right) \tag{4.8}$$

for which the reduced variable data average from $\bar{y}$ = 0.536 and standard deviation σ_y

= 1.131. Therefore $\alpha = \sigma_y/\sigma_x = 0.02815$. The mode u is calculated by:

$$u = \bar{x} - \bar{y}\frac{1}{\alpha} = 68.70 \tag{4.9}$$

A return period of three years implies a probability of occurrence $p \approx 0.67$. Therefore, the WDR x^* that is likely to exceeded once every three years = $1 - p = 0.33$:

$$\begin{aligned} 0.33 &= 1 - f(\alpha, x^*, u) \\ &= e^{-e^{-\alpha(x^* - u)}} \\ &= e^{-e^{-0.02815(x^* - 68.70)}} \end{aligned} \tag{4.10}$$

which can be solved to show $x^* = 100.8$ L m^{-2}. This represents I_S: the WDR exposure likely to be exceeded once in any given three year period. A generalised and rearranged form can be used to calculate the I_S from a set of AMS values:

$$x^* = \frac{-1}{\alpha} ln\left(ln\left(\frac{1}{1-p}\right)\right) + u \tag{4.11}$$

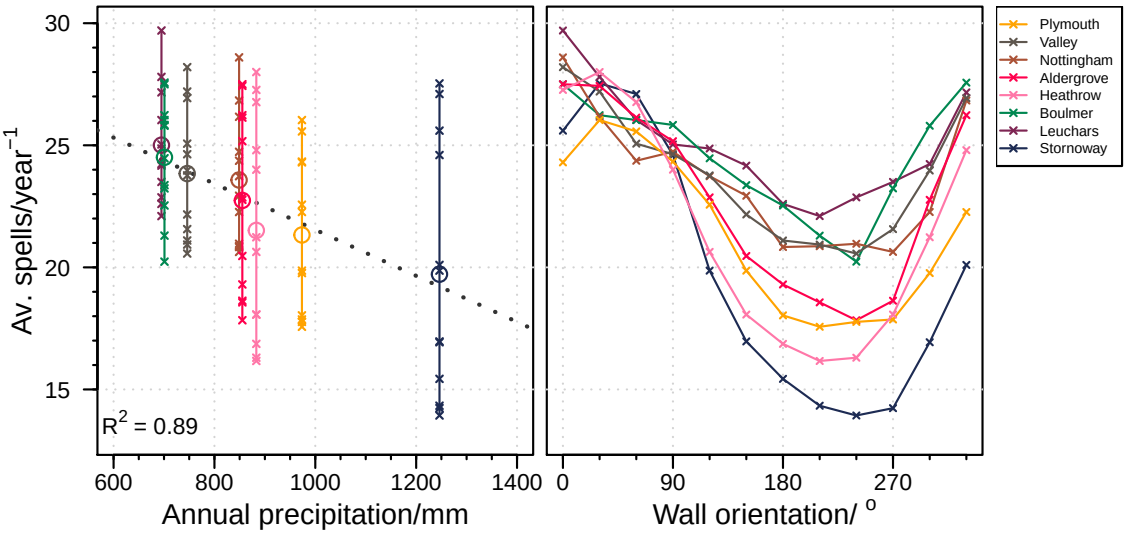

Figure 4.3. The number of wind-driven rain spells occurring at different sites in the UK from 1986 to 2015, as a function of average annual precipitation (left) and wall orientation (right). The linear fit of annual precipitation and average number of spells per year was taken on the average value across all wall orientations, represented by open circles. Smaller x's represent the average annual number of spells for different orientations at the respective site.

4.3 Results

4.3.1 Annual frequency of wind-driven rain spells

These eight sites across the UK experience an average of 14 to 30 WDR spells per year, depending on the annual precipitation and wall orientation (Figure 4.3). How many rain spells there are in a given year is determined by several factors. By definition, it is dependent on the grouping and frequency of precipitation, as well as predominant wind directions. Figure 4.3 demonstrates that there is an inverse relationship between the average annual precipitation and the numbers of spells that occur. The higher the precipitation, the less likely it is that there will be a period of 96 h or more without any WDR exposure.

In general, fewer but longer spells are experienced by south-western oriented façades, as they are hit more frequently by prevailing winds in the UK. Exposed locations such as Stornoway have fewer rain spells than other sites, as periods of 96 h or more without driving rain are less frequent due to higher annual precipitation.

For wall orientations that do not intersect with prevailing wind directions (i.e. θ = 0–90^{o}, northerly and easterly façades) the number of spells per year is between 24 and 30. There is a greater variation between the sites for southwestern façades (14 to 23) and there is consistently fewer spells occurring than on their northeasterly counterparts. If a scalar (non-directional) index is used (e.g. Pérez-Bella et al., 2012), fewer spells could be expected. This is because a scalar representation of WDR exposure incorporates all precipitation as WDR exposure. In contrast, a directional representation of WDR exposure allows for precipitation to occur without having WDR exposure, if the wind direction is not intersecting with a given wall orientation.

The significant variation in the number of spells occurring for different sites and wall orientations demonstrates the limitations of percentile representation of extreme WDR events, since the percentiles representing extreme events are dependent on their frequency of occurrence. As well, percentiles are only accurate for determining the frequency of events if the exact number of spells occurring during the period are known. If long-term averages of annual frequency are extrapolated to a three year period, calculations resulting from percentiles will be estimations of extreme events. For example, from 1986 to 2015 a

façade oriented to 120° in Stornoway experienced an average of approximately 20 spells per year. If this is extrapolated to 2002 to 2004, the 'once every three years' spell is represented by $P = (60-1)/60 \times 100\% = 98.3$. However, from 2013 to 2015 this site only experienced 54 spells (as defined by ISO 15927). Then, the accurate percentile representation of the 'once every three years' spell would be the $P = (54-1)/54 \times 100\% = 98.1$. Based on accurate event occurrence at this site and orientation from 1997 to 1999 $P = 98.5$ (n = 69). In both of these cases, using n = 60 would approximate, but not represent, the worst spell that occurred in these three year periods. For the sites and orientations included here, the 'once every three years' spell could be represented by percentiles ranging from P = 97.6–98.8. In these cases, the percentiles could be heavily influenced by extreme random phenomena.

4.3.2 Duration of wind-driven rain spells

Based on the assessment of spell length at eight sites from 1986 to 2015, short spells are most common. The distribution of the duration of WDR spells is primarily driven by the wall orientation (and therefore prevailing wind direction), but is also dependent on the annual precipitation (Figure 4.4). By comparing Figures 4.3 and 4.4, it can be seen that spells tend to be longer for wall orientations that experience fewer spells. Exposed regions with higher annual precipitation will have more longer spells compared to sites with lower levels of precipitation. For example, Figure 4.4 shows that a south-facing façade

at Stornoway experienced 40 WDR spells lasting between 1000 and 2000 h, while a façade oriented similarly at Heathrow experienced 10. Conversely, the same wall orientation in Stornoway experienced 200 spells lasting less than 100 h while its Heathrow counterpart experienced twice as many. The average time between sequential WDR spells was between 7.38 to 11.5 days. There is no clear relationship between this inter-spell time and annual precipitation, wall orientation, or prevailing wind directions.

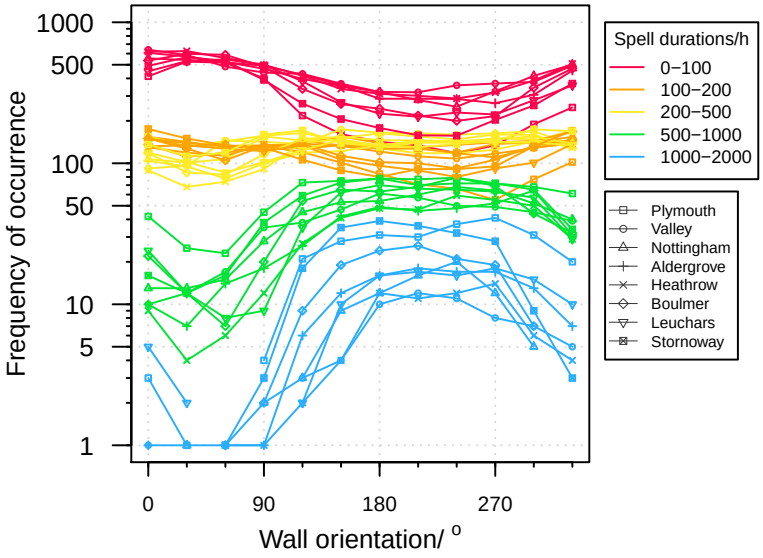

Figure 4.4. Frequency of occurrence of wind-driven rain spells of different lengths for eight UK sites at 12 wall orientations between 1986 and 2015.

4.3.3 Amount of wind-driven rain

The amount of annual indices $I_{A,\mathrm{ISO15927}}$ (as calculated from ISO 15927, i.e. Equation 4.2 applied to the hourly meteorological data) and spell indices $I_{S,\mathrm{EVA}}$ (from extreme value analysis) varied between 110 and 1212 L m^{-2} and 31 and 494 L m^{-2}, respectively, across the eight sites from 1986 to 2015 (Figure 4.5). This was dependent on site characteristics

Table 4.3. Sites WDR exposures characterised by group properties according to the amount and distribution across wall orientations.

Group	Sites	WDR exposure (I_A and I_S)	Modal distribution
Western coastal sites	Plymouth, Valley, Stornoway	very high annual and spell exposure	steep, modes at 180-240^o
Eastern sites	Heathrow and Nottingham	low annual and spell exposure	broad, modes at 210^o
Eastern coastal sites	Leuchars and Boulmer	low annual and spell exposure	broad, modes at 90^{o*}
No group	Aldergrove	mid-range annual exposure, low spell exposure	broad, mode at 180^o

**more prominent for annual index* I_A

and wall orientations. The most extreme exposures impacted southern and western wall orientations for western coastal sites. In contrast, the exposures for northern and eastern wall orientations were more homogenous across sites.

The WDR exposures can be characterised by group properties according to the amount and distribution across wall orientations (Table 4.3). The distinctions are driven primarily by a contrast between eastern and western sites, with an influence from coastal proximity. Additionally, the sites do not universally experience the highest exposures for southern and eastern wall orientations. Specifically, the eastern coastal sites (Leuchars and Boulmer) have the highest exposures for eastern façades, despite having southern and western prevailing wind directions. This is likely influenced by increased wind speeds for these orientations: even though easterly winds are occurring less frequently, they are more likely occurring in conjunction with higher wind speeds.

The $I_{S,\mathrm{EVA}}$ values as determined from extreme value analysis are a significant component of the total (annual) exposure. Across all wall orientations the WDR exposure during the 'once every three years' spell is equivalent to at least 25% of the average annual

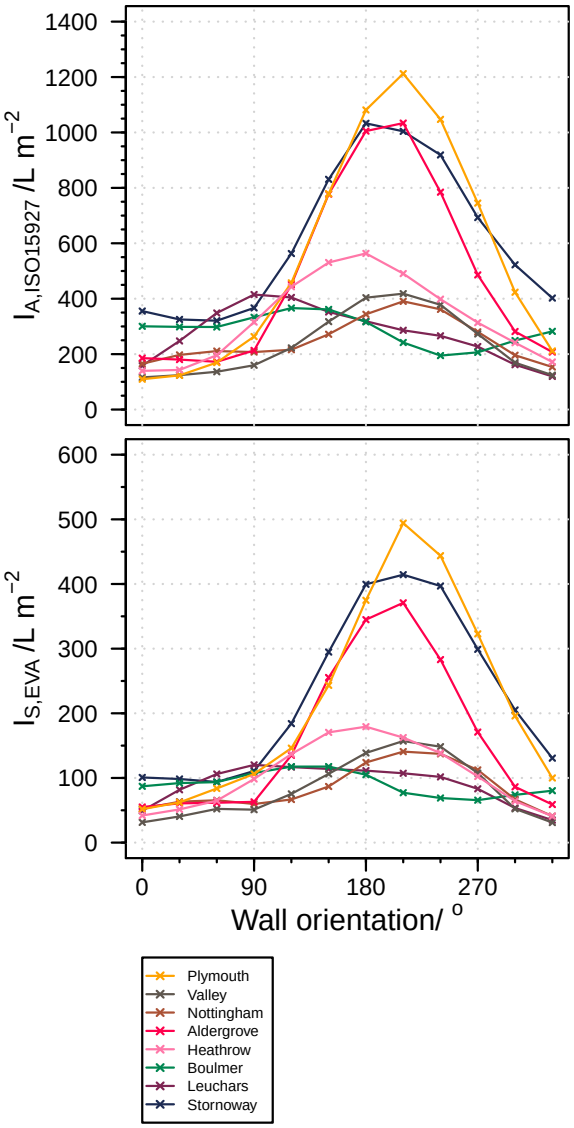

Figure 4.5. Wind-driven rain exposure at eight UK sites for 12 different wall orientations (0^{o} = north) between 1986 and 2015. Upper: Annual index I_A. Lower: Spell index ($I_{S,\mathrm{EVA}}$), which is the statistical 'once every three years' spell.

exposure ($I_{A,\mathrm{ISO15927}}$), and can be as much 50% in Plymouth.

4.3.4 Applicability of current standards

Two aspects of semi-empirical WDR standards affect their applicability to current design and risk analysis: changes in climate and calculation methodologies. To assess the

similarity of the data used as the basis for BS 8104 to the more recent climate, the methods described in Section 4.2.2.3 are employed for meteorological data from 1959 to 1991. The amount of the annual ($I_{A,\mathrm{ISO15927}}$) and spell indices ($I_{S,\mathrm{EVA}}$) are compared to the equivalent indices for 1986 to 2015 (Section 4.3.4.1). The methods for calculating extreme event exposure are investigated by comparing the I_S values from 'once every three years' spell in BS 8104 and ISO 15927 with spell amounts from extreme value analysis during both time periods.

4.3.4.1 Change in climate

BS 8104 is based on climatic data from 1959 to 1991. As BS 8104 is a current tool used for design and assessment, it is important to determine if the conditions of WDR exposure during this period are representative of a more recent climate. To this end, $I_{A,\mathrm{ISO15927}}$ and $I_{S,\mathrm{EVA}}$ have been calculated for the same (or nearby) sites from 1959 to 1991.

For most sites the difference between $I_{A,\mathrm{ISO15927}}$ and $I_{S,\mathrm{EVA}}$ values between 1959 to 1991 and 1986 to 2015 was less than 50 L m^{-2}, regardless of wall orientation (Figure 4.6). More recently Plymouth experienced significantly higher 'once every three years' spell for southern and western façades, while Stornoway saw a significant decrease in these extreme events for similar façades. Valley also experienced a more moderate (100 L m^{-2}) increase in the $I_{S,\mathrm{EVA}}$ exposure for southern façades. The Met Office records do not indicate any changes in the location of these monitoring stations (UK Met Office, 2006a, 2006b),

suggesting that these changes in $I_{S,\mathrm{EVA}}$ are attributable to a change in climate.

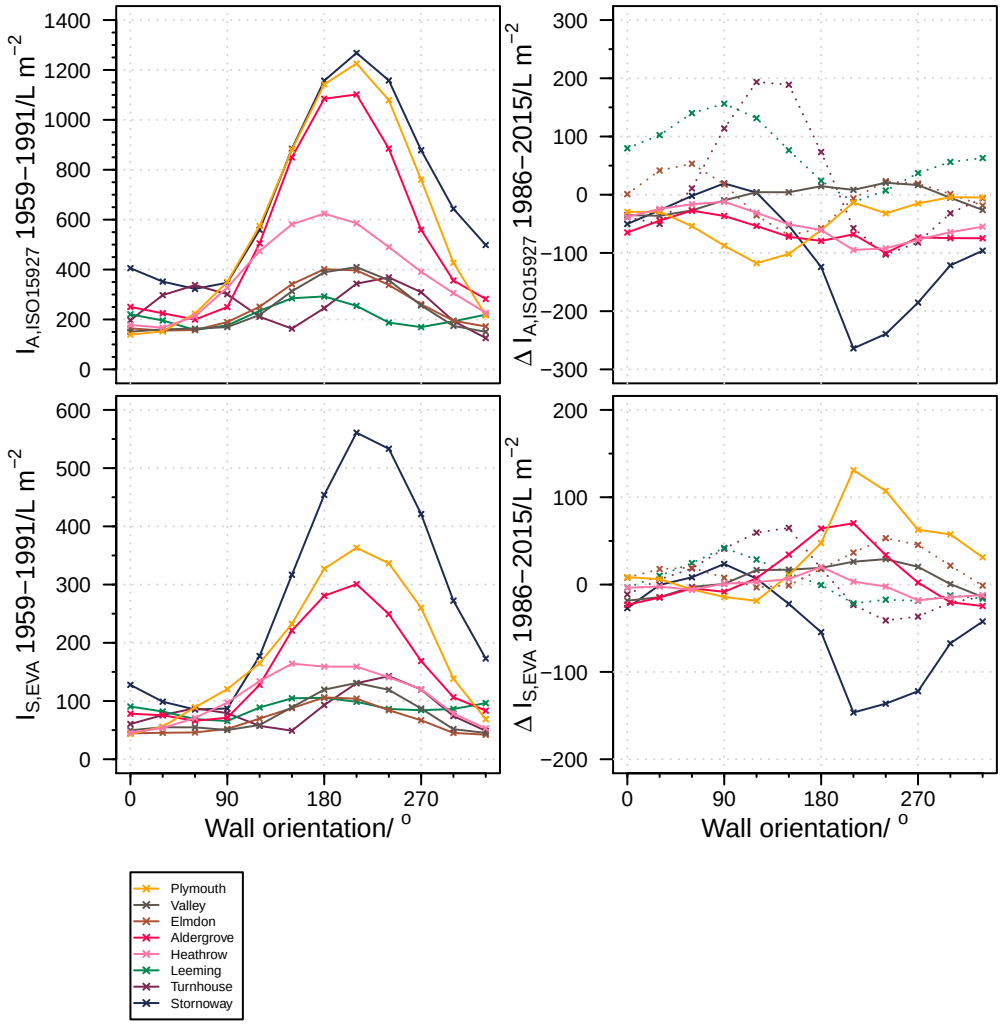

Figure 4.6. Left: wind-driven rain exposure for eight UK sites for 12 different wall orientations (0° = north) from 1959 to 1991. Right: absolute changes in in I_A and $I_{S,\mathrm{EVA}}$ for 1986 to 2015 from 1959 to 1991.

The changes in $I_{A,\mathrm{ISO15927}}$ and $I_{S,\mathrm{EVA}}$ represented by dashed lines in Figure 4.6 are affected by local climate variation and should be taken with caution. They were calculated from different sites for the two periods due to data availability (see Figure 4.1). This is demonstrated by the distributions of $\Delta I_{A,\mathrm{ISO15927}}$ and $\Delta I_{S,\mathrm{EVA}}$ across wall orientations experienced at these sites' for 1959 to 1991 (Figure 4.6). Turnhouse appears to be bimodal,

with a prominent mode around 240° equal to that observed around 90° from 1986 to 2015. In 1959 to 1991 the mode of the distribution for Leeming $I_{A,\mathrm{ISO15927}}$ is shifted to 120 to 150°, contrasting that identified for Boulmer from 1986 to 2015 centred around 90°. The distribution of spell durations and inter-spell periods do not vary significantly between 1959 to 1991 and 1986 to 2015. Although it is unknown how weather systems or the position of storm tracks are expected to change during the twenty-first century (Murphy et al., 2009), this supports the current consensus that weather patterns are not changing and that natural variability has a greater impact than climate change (Eames, Kershaw and Coley, 2011b). This is likely due to negligible expected change in established wind patterns in the UK, including the dominating effect of the polar jet stream.

The comparison of $I_{A,\mathrm{ISO15927}}$ and $I_{S,\mathrm{EVA}}$ values between the two timelines suggests the meteorological data used to produce BS 8104 is representative of more recent characteristics of the UK climate. However, the significant changes for the country's most extreme exposures perhaps indicates that these standards might be increasingly out of date for design and risk assessment. The validity of mid-to-late twentieth century meteorological data for representing the current climate should be revisited periodically to determine whether they remain a relevant tool.

4.3.4.2 Evaluation of current standards' methods for calculating extreme event exposure

BS 8104 and ISO 15927 include procedures to determine the 'once every three years' spell. Using the climatic data used to determine $I_{S,\mathrm{EVA}}$ from extreme value analysis, the 'once every three years' spell is calculated from each of these standards. These are compared to the values of $I_{S,\mathrm{EVA}}$ to evaluate their methodologies of calculating extreme event exposure.

The methods in BS 8104 and ISO 15927 are underestimating the 'once every three years' spell amounts, compared to extreme value analysis (Figure 4.7). For ISO 15927, taking the 67th percentile of I'_S values as the 'once every three years' spell is underestimating I_S exposure in the UK by roughly an order of magnitude. The reference maps used in BS 8104 are much closer to the $I_{S,\mathrm{EVA}}$ values calculated from EVA. However, distances from the 1:1 ratio line in Figure 4.7 can represent significant differences, and must be interpreted according to the logarithmic axis.

During both study time periods, the higher exposures of western coastal sites (Stornoway, Valley, and Plymouth) are significantly underestimated. For example, the comparison of I_S values in the bottom-left plot of Figure 4.7 is based on meteorological data from 1959 to 1991. The values of $I_{S,\mathrm{EVA}}$ for Stornoway (wall orientations 180 to 240°) range from approximately 400 to 600 L m^{-2}. In contrast, BS 8104 calculations estimate these exposures to range from 180 to 200 L m^{-2}. Similar conclusions can be drawn for Plymouth

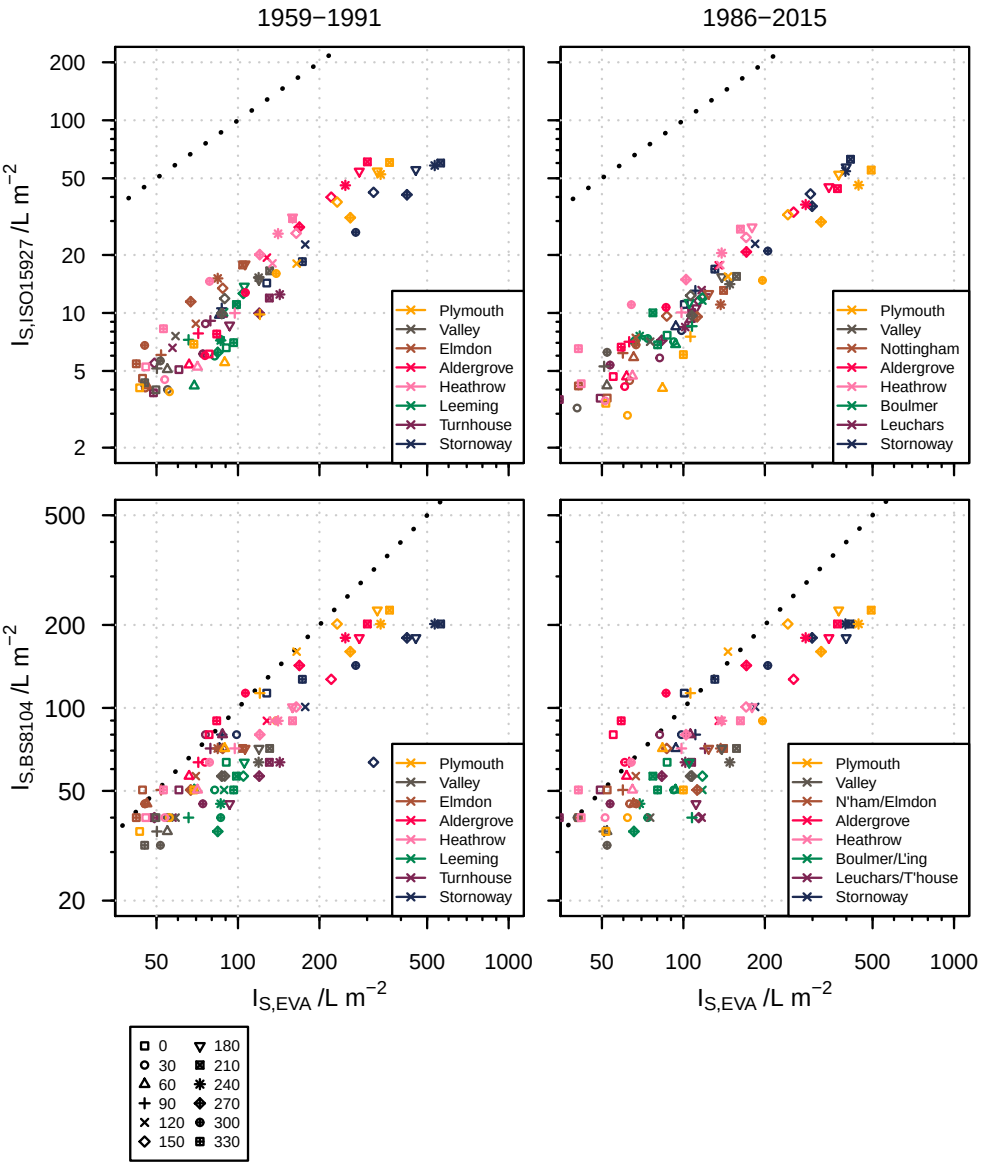

Figure 4.7. A comparison of the 'once every three years' spell calculated from ISO 15927, BS 8104, and extreme values analysis for 1959 to 1991 and 1986 to 2015. The black dotted line denotes a 1:1 ratio. In the bottom right plot, the legend items with two names refer to the site for BS 8104 and EVA, respectively.

and Valley during both time periods.

The BS 8104 I_S exposures calculated from 1959 to 1991 are more similar to those calculated from EVA during 1986 to 2015 than those calculated from the same time period. Although many aspects of the development of BS 8104 are documented (through Lacy,

1976; Prior, 1985 etc.), how the 'once every three years' spell was determined is unclear. Without more information on this, it is difficult to discuss contrasts between BS 8104 and EVA in greater detail.

Comparing the calculated values of I_S from BS 8104 and ISO 15927 with $I_{S,\mathrm{EVA}}$ is one method of evaluating the amount of WDR exposure determined by these standards. Another method is to convert the $I_{S,\mathrm{BS8104}}$ and $I_{S,\mathrm{ISO15927}}$ into equivalent return periods. This can be done by taking x^* in Equation 4.11 to be the calculated 'once every three years' spell from each standard. u and α are determined from the AMS series determined from extreme value analysis for that site and wall orientation. Then, the value of p can be solved for: this represents the probability that the value is exceeded in any given year. The 'equivalent return period' is represented by $1/p$. In this way, the equivalent return period is indicative of a point on the probability distribution function of annual maxima as determined from AMS. If the I_S calculated from a standard were equivalent to those calculated from EVA the probability of exceeding them in any given year would be 1/3, equivalent to a return period of 3 years. It should be noted that the 'equivalent return periods' are based on distributions determined from the AMS series, which do include the I_S values calculated from BS 8104 and ISO 15927: these 'equivalent' values should be considered as indicative values.

The probabilities of exceeding the 'once every three years' spells from ISO 15927 and BS 8104 and equivalent return periods are presented in Figure 4.8. The probability of

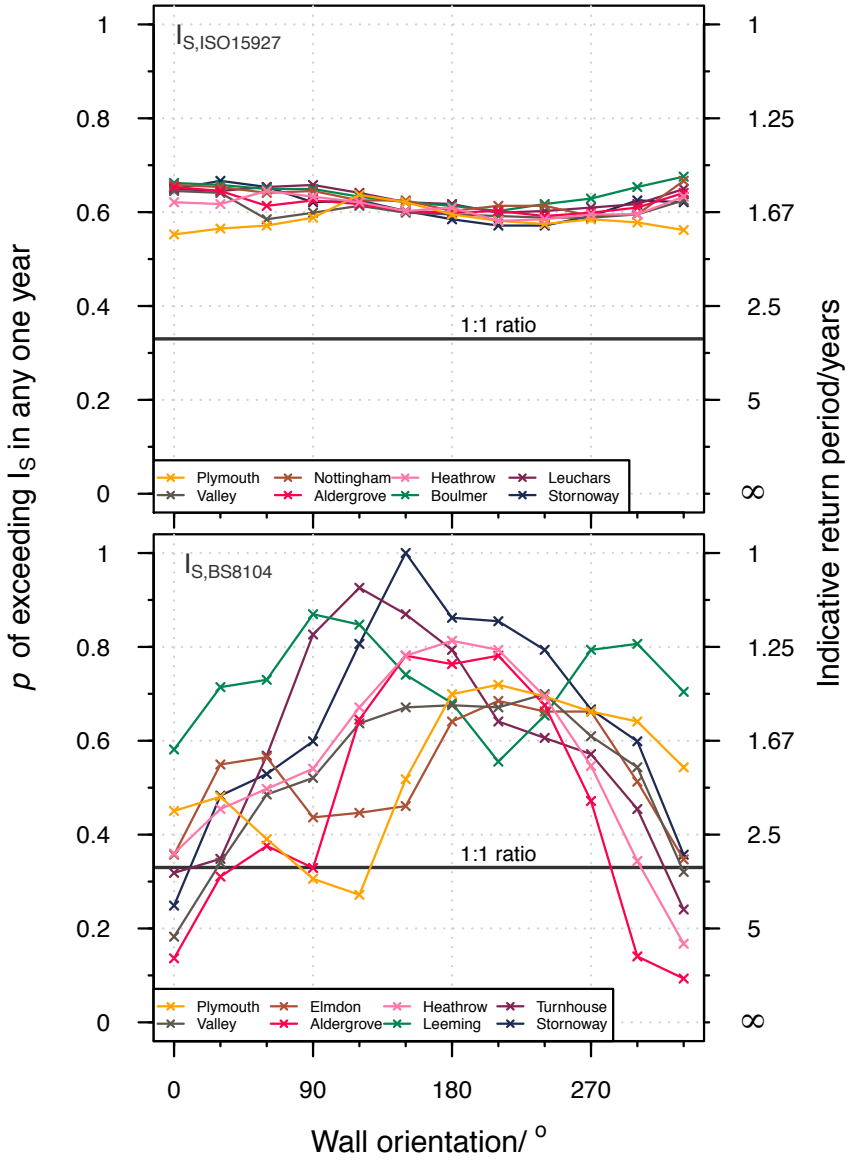

Figure 4.8. The probabilities of exceeding the 'once every three years' spells calculated from ISO 15927 and BS 8104 in any given year. The equivalent return periods are presented on the right axis.

exceeding I_S as calculated from ISO 15927 in any one year is minimally variable, and is within 0.55 and 0.65. This is equivalent to a range of return periods between 1.48 and 1.81 years. The probability of exceeding I_S as calculated from BS 8104 exhibits a wider range and a strong dependency on wall orientation. The equivalent return periods range between 1 and 10 for $I_{S,\mathrm{BS8104}}$. Figure 4.8 suggests that the unclear methods originally

used to compute the ‘once every three years’ spell in BS 8104 are especially unsuitable for wall orientations that typically have higher exposures, i.e. southern and western façades.

4.4 Discussion

The results presented here demonstrate that extreme WDR events for some regions of the UK are likely underestimated by ISO 15927 and BS 8104 when compared to the extreme value analysis approach. This section provides guidance on interpreting their output and discusses their applicability in current use.

WDR indices were originally proposed and developed for comparative purposes: “The annual mean WDR index gives, it is believed, a reasonably precise method of comparing different sites with respect to total amounts of WDR on walls. It enables a designer to compare the exposure of a place with that at another with which he is already familiar.” (Lacy, 1976, p. 108). By this definition, they remain a useful tool for design, because the extreme WDR spells calculated with BS 8104 and ISO 15927 have a reasonably proportional relationship with those calculated from EVA. However, this relationship is much less applicable for sites with more extreme climates and climatic variation. In these cases, using ISO 15927 and BS 8104 could lead to substantial under-designing for building elements exposure risks.

The annual index from both standards used to indicate average moisture contents and the likelihood of biological growth remain useful tools for these purposes. For BS 8104,

this is because extreme WDR exposure appears to have not changed significantly since 1959 to 1991. This is in contrast to a gradual linear increase in UK temperatures observed from 1961 to 2006 (Jenkins, Perry and Prior, 2009). For ISO 15927, the annual index is a non-trivial summation of a set of exposures within a year and is not influenced by percentiles or the frequency of spells.

4.5 Conclusion

This paper employed extreme value analysis by combining return periods with a Gumbel distribution to evaluate extreme wind-driven rain exposure for eight sites across the UK. It was shown that the directional aspect (i.e. wall orientation) of exposure produces significant variation in the quantity, duration, and amount of wind-driven rain spells experienced in the UK.

WDR exposure at the eight study sites from 1986 to 2015 demonstrated that the western coastal sites had high annual and spell exposure, especially for southern and western wall orientations in line prevailing wind directions. The intensity of exposure for northern and eastern wall orientations was more homogenous across the eight sites; the eastern coastal sites notably experienced the highest WDR exposure for eastern façades, demonstrating that wind speeds can have a dominating effect over prevailing wind directions.

The current standards are underestimating extreme wind-driven rain events such as the worst spell likely to occur in any given three year period when compared to a method based

on extreme value analysis. In the case of BS 8104, this shortcoming is likely caused by a poorly understood methodology to identify extreme events, as current wind-driven rain exposures are not significantly different from those of the mid-to-late twentieth century for many sites in the UK. For ISO 15927, this is influenced by its protocol that incorporates percentiles. Despite this, they remain a useful semi-qualitative tool for characterising annual exposure for average moisture contents and comparing relative exposures between sites.

Assessment of WDR exposure for design and risk analysis needs to incorporate methods that are not affected by random weather phenomena, such as extreme value analysis. The approach employed herein of return periods combined with Gumbel distributions and probability can be a powerful tool to evaluate extreme WDR exposure. Being able to use meteorological data to evaluate the risks posed by WDR is an importance component of efficient and effective management and conservation of the historic built environment.

5 | Wind-driven rain and future risk to built heritage in the United Kingdom: novel metrics for characterising rain spells

"The arrogance of success is to think that what you did yesterday will be sufficient for tomorrow."

– C William Pollard (2000, p. 114)

Published as: Orr, S. A., M. Young, D. Stelfox, J. Curran, and H. Viles. (2018). 'Wind-driven rain and future risk to built heritage in the United Kingdom: Novel metrics for characterising rain spells'. *Science of the Total Environment*, 640:1098–1111. doi:10.1016/j.scitotenv.2018.05.354.

Abstract

Wind-driven rain (WDR) is rain given a horizontal velocity component by wind and falling obliquely. It is a prominent environmental risk to built heritage, as it contributes to the damage of porous building materials and building element failure. While predicted climate trends are well-established, how they will specifically manifest in future WDR is uncertain. This paper combines UKCP09 Weather Generator predictions with a probabilistic process to create hourly time series of climate variables under a high-emissions scenario for 2070–2099 at eight UK sites. Exposure to WDR at these sites for baseline and future periods is calculated from semi-empirical models based on long-term hourly meteorological data using ISO 15927-3:2009. Towards the end of the twenty-first century, it is predicted that rain spells will have higher volumes, i.e. a higher quantity of water will impact façades, across all 8 sites. Although the average number of spells is predicted to remain constant, they will be shorter with longer of periods of time between them and more intense with wind-driven rain occurring for a greater proportion of hours within them. It is likely that in this scenario building element failure – such as moisture ingress through cracks and gutter over-spill – will occur more frequently. There will be higher rates of moisture cycling and enhanced deep-seated wetting. These predicted changes require new metrics for wind-driven rain to be developed, so that future impacts can be managed effectively and efficiently.

This chapter is slightly modified from Orr et al. (2018b). The methods have been shortened to reduce repetition from Chapter 3.

5.1 Introduction

The IPCC was virtually certain[1] in 2013 that the troposphere has warmed since the mid-20th century and had high confidence[2] that global precipitation patterns have changed – trends that are likely to continue over the twenty-first century (IPCC, 2013). These changes pose threats to natural and built heritage (Cassar, 2005), especially in the United Kingdom where more intense and frequent precipitation events are very likely[3].

The presence and movement of water contributes to the weathering and deterioration of porous materials and other aspects of building performance. Traditional building materials such as stone and mortar, as well as concrete, are affected by many weathering processes in which water is implicated, such as chemical weathering (Charola and Ware, 2002), freeze-thaw weathering (Hall, 1999), salt weathering (Doehne, 2002) and biological weathering (Warscheid and Braams, 2000; Crispim and Gaylarde, 2005).

Wind-driven rain (WDR) or driving rain is rain given a horizontal velocity component by the wind and falling obliquely (Blocken and Carmeliet, 2004). WDR represents the main moisture source and cause of deterioration on most building façades (Erkal, D'Ayala and Sequeira, 2012), as it is implicated in both long-term deep-set wetting (Smith et al., 2011a; McCabe et al., 2013) and short-term risks of building element failure, e.g. rain

[1] 99–100% probability
[2] Defined as high agreement based on robust evidence
[3] 90–100% probability

penetration through edges of doors or windows (ISO, 2009) and additionally junctions and gaps.

Wind-driven rain exposure can be assessed in many ways. To evaluate local and microscale conditions omni-directional gauges and wall-mounted pressure plates have been used since the 1930s (Lacy, 1951), more recently in combination with numerical simulations of computational fluid dynamics (e.g. Briggen, Blocken and Schellen, 2009; Pettersson et al., 2016). To determine regional characteristics, semi-empirical models of WDR have been developed. These are indices or relationships representing the volume of WDR exposure over a specific time period based on values of wind speed and direction and precipitation. As these variables are frequently measured by meteorological monitoring stations, WDR can be estimated for locations where this data is available. The aforementioned measurement, modelling, and semi-empirical techniques evaluate exposure to WDR. The susceptibility of building components to ingress can be assessed experimentally (e.g. BSI, 1970, 2001) or by using coupled heat and moisture transport differential equations models (e.g. WUFI Nik et al., 2015).

Wind-driven rain in the UK is expected to increase gradually over the twenty-first century, based on predicted increases of annual precipitation and days with intense rainfall (Brimblecombe, 2014; Holmes, 2015) under various emission scenarios. This raises doubt about the applicability and relevance to future conditions of current metrics and exposure maps to future conditions. In 2011 BRE Scotland advised that the present climate had

not changed enough from the exposure reference maps published in 1992 (BSI, 1992) based on conditions in 1959–1991 to warrant an update (Reid and Garvin, 2011); practical experience suggests that changes in building performance during this century are already noticeable (Stelfox, 2018) compared to the twentieth century. While work has been done on site-level intervention techniques for increasing the resilience of traditional masonry (Laycock and Wood, 2014), little to date has evaluated how the characteristics of WDR might change during the twenty-first century.

The potential impact of climate change on cultural heritage is a growing academic concern (Fatoric and Seekamp, 2017), of interest for practical assessments undertaken at the site-specific level (Historic Environment Scotland, 2018). Using models or predictions is a crucial component of a robust moisture risk assessment, and should be considered as a tool for exploring possible risk (May and Sanders, 2017).

Semi-empirical evaluations of future WDR risk have been undertaken for Nordic regions including Sweden (Nik and Sasic Kalagasidis, 2014; Nik, 2017) and Finland (Pakkala et al., 2016). These studies have applied ISO 15927 or similar formulae (e.g. ASHRAE, 2009) to generated hourly data for future weather conditions. However, these studies have used 'morphing' (scaling) or unspecified processes to produce the future hourly time series (Nik, 2017 and Pakkala et al., 2016, respectively) which might not reflect the future temporal variation of WDR exposure. Nik and Kalagasidis (2014) have presented evaluations of future climate as annual means, which are generally more indicative annual

variability and not of long-term climate changes. They have also presented a single future scenario, whereas the use of at least 100 different projected scenarios is advisable to robustly characterise future conditions. This type of analysis has not yet been undertaken for the UK, which will experience climate changes distinct from the aforementioned regions.

This paper assesses a predicted future scenario of wind-driven rain and risk to built heritage for eight locations in the UK in 2070–2099, based on generated time series of climate conditions from the UKCP09 weather generator (UK Climate Projections, 2012) and a probabilistic process of producing hourly time series (Eames, Kershaw and Coley, 2011a; Eames, Kershaw and Coley, 2011b). The changing characteristics of wind-driven rain are assessed with standard indices and novel metrics based on additional attributes of wind-driven rain spells that emphasise temporal variability. A discussion of the implications of these changes for built heritage follows, considering building element failure, biological growth, near-surface cycling and deep-seated wetting.

5.2 Methods

5.2.1 The ISO model

ISO 15927 includes two driving rain indices that should be calculated from at least 10 years (and preferably 20 or 30) of continuous hourly data:

- **annual index** I_A: should be used for "considering the average moisture content of exposed building material or when assessing the likely growth of mosses and lichens" (BSI, 1992, p. 4);

- **spell index** I_S: "defined in terms of rain penetration through masonry, which requires a prolonged input of water" (ISO, 2009, p. 12).

It is important to note that neither of these directly reflects rain penetration through building elements (e.g. window frames, junctions, cracks, etc...), which are dependent on short but intense WDR (ISO, 2009, p. v).

The volume of wind-driven rain that would hit a square metre in a 1 h period is calculated from:[4]

$$I = \frac{2}{9} v r^{8/9} cos(D-\theta) \quad [\text{L m}^{-2}] \tag{5.1}$$

from average hourly wind speed v (m s^{-1}), hourly precipitation r (mm), and hourly mean wind direction D^{o} for a specific wall orientation θ^{o}. These hourly exposures are used to calculate the indices in ISO 15927, and referred to as volumes hereafter.

The **annual index** I_A is calculated by the $\Sigma I/N$ for all hours in which $cos(D-\theta) > 0$, i.e. when the wind is blowing against the wall; N is the number of years of data available. This is referred to as an *airfield* index in ISO 15927 as it represents WDR that would

[4] Alternative units of the analogous mm h^{-1} are sometimes used. This has not been employed to avoid confusion between the vertical rainfall (precipitation) and the calculated WDR exposure.

occur at a height of 10 m above ground level in the middle of an airfield with no other obstructions. According to ISO 15927, this is calculated as:

$$\mathrm{I}_A = \sum \frac{\frac{2}{9} v r^{8/9} cos(D-\theta)}{N} \quad [\mathrm{L\ m^{-2}}] \tag{5.2}$$

where the summation is taken over all the hours in which there is active WDR, i.e. $cos(D-\theta) \geq 0$, and N is the number of years the summation is taken over.

A **spell-specific index** I'_S is calculated for an individual spell ΣI for all hours in which $cos(D-\theta) > 0$ within that spell, also in L m^{-2}. Spells are separated by periods of at least 96 h for which $v r^{8/9} cos(D-\theta) \leqslant 0$, i.e. in which there is no WDR impacting a specific wall orientation. This is representative of airfield conditions, as described above for the annual index. See Figure 5.1 for an example of a rain spell, as defined in ISO 15927. Experimental work by Caton at the UK Meteorological Office showed that up to 96 consecutive hours with no driving rain are necessary before evaporative losses will exceed water ingress from rain exposure (Prior, 1985); 96 h is also sufficient to bridge the gap between succeeding depressions in a weather sequence in the UK (Prior, 1983). In contrast to current standards, Caton distinguished between spells using periods of $\geqslant$ 96 h without 'appreciable' driving rain, for which an approximate value of one tenth of the expected index for a once in three year spell for each orientation (Prior, 1985). 96 h is arguably an arbitrary delimiter between spells. It does not imply that 96 h is sufficient for all moisture ingress to exit the building

envelope.

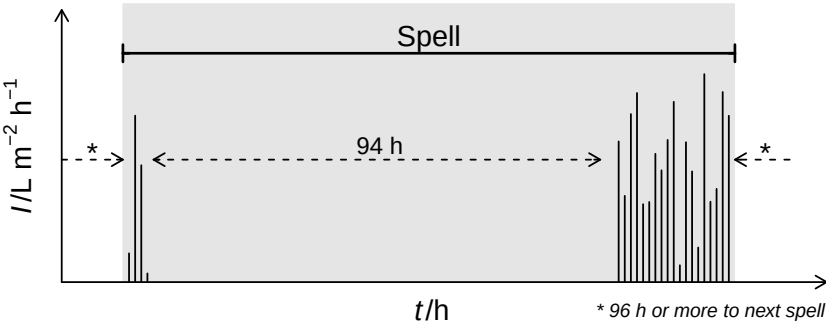

Figure 5.1. An example of a driving rain spell, as defined in ISO 15927-3:2009.

The **spell index** I_S is defined as the 66th percentile of all spells' I'_S in ISO 15927. Using percentiles to represent extreme events is dependent on their frequency of occurrence. Instead this was calculated from an Annual Maxima Series approach using 'return periods' and the Gumbel distribution (Pérez-Bella et al., 2012, 2013; Orr and Viles, 2018a; the latter is reprinted in Chapter 4). The benefit of this approach is that it is less affected by extreme random weather phenomena and can be applied to sets of event occurrence that have difference frequencies of occurrence, e.g. sites and orientations that experience different average quantities of spells per year.

The calculation-based approach of ISO 15927 has the advantage over BS 8104 that WDR may be assessed at any location or time for which appropriate data or predictions are available. However, the indices do not reflect other characteristics of the annual or spell behaviour, including:

- spell duration;

- fraction of hours for which there was active wind-driven rain within a spell (the 'active fraction');

- the length of time between sequential spells (inter-spell period).

Some of these additional properties have been discussed for rain spells across the United States (Underwood and Meentemeyer, 1998), but have not been explored for the UK. It should also be noted that output from the semi-empirical model in Equation 5.1 does not reflect localised microclimates, such as those common in urban environments. The context of building façade can have a significant impact on the level of exposure, which can be explored with CFD.

5.2.2 Meteorological data

5.2.2.1 Baseline period data

As discussed in Section 5.2.1, long-term hourly data is required to calculate WDR indices. A baseline reference period of 1961–1990 was used, as this closely resembles the period of observations used to formulate BS 8104 (1959–1991) and 1960 is also a frequently used comparison basis for climate projections by the IPCC (2013). Similarly, 1961–1990 is the basis for the UK Climate Impacts Programme (UKCIP) and the 2009 UK Climate Projections (UKCP09) Weather Generator tool (see Section 5.2.2.2).

5.2.2.2 Creation of future probabilistic design weather years

To assess future WDR characteristics, the most recent 2009 UK Climate Projections (UKCP09) have been used to create probabilistic meteorological conditions (DEFRA, 2009) for 2070–2099 under an A1 high emissions scenario. This scenario was selected from the IPCC Special Report on Emissions Scenarios (Nakicenovic and Swart, 2000): it characterises a scenario of high fossil fuel use with rapid economic growth and introduction of new and more efficient technologies (Murphy et al., 2009, pp. 134–135).

UKCP09 includes a Weather Generator that is a stochastic rainfall model (Wilks and Wilby, 1999) to produce artificial time series under various emission scenarios – other weather variables are then generated according to the precipitation and inter-variable relationships on the previous day. These relationships contribute to maintaining the consistency between and within each variable (Jones et al., 2009). The Weather Generator creates hundreds or thousands of future 30-year statistically equivalent time series representative of predicted behaviour. The time series represent future characteristics but would not be expected to reflect actual measurements over their respective time horizons. Using 100 or more Weather Generator outputs allows a range of plausible scenarios to be explored that represent the probability distribution.

The Weather Generator provides generated time series for a baseline period (1961–1990) and the future scenario (2070–2099) for 5 km $\times$ 5 km grid cells over the UK. The

daily time series contain the following variables, among others:

- precipitation, mm;
- maximum temperature, ^{o}C;
- minimum temperature, ^{o}C;
- sunshine fraction;
- vapour pressure, Pa;
- potential evapotranspiration (PET), mm day^{-1}.

Precipitation, maximum and minimum temperatures, vapour pressure, and radiation parameters are produced at the hourly resolution using simple disaggregation rules from the estimated daily parameters (Jones et al., 2009, p. 31).

Using ISO 15927, hourly time series of wind direction, wind speed, and precipitation are required to evaluate WDR indices. The output from the UKCP09 Weather Generator has been adapted to produce the necessary hourly time series required as input to building simulation software (Watkins, Levermore and Parkinson, 2011; Du, Underwood and Edge, 2012; Mylona, 2012). The limitations of the Weather Generator approach is that not all variables required for simulation or calculation purposes are created at the hourly resolution.

Eames et al. have developed a process using probabilistic models to produce the necessary variables for WDR indices at an hourly resolution from the Weather Generator output (Eames, Kershaw and Coley, 2011a; Eames, Kershaw and Coley, 2011b). The generation process requires a reference hourly time series with the relevant variables to

use as a 'training' data set for the algorithms. In this paper, measured data from the 'Met Office Integrated Data Archive System' (MIDAS) Land and Marine Surface Stations Data (1853–current) (UK Met Office, 2012) for 1961–1990 was used. This was selected so that it covered the same years as the baseline period. The process can be summarised as:

1. Calculate average daily wind speed from PET (Ekström et al., 2007);

2. Generate 24 h of hourly wind speeds: extract 24 h measurements from the closest average daily wind speed occurring during the same season (DJF, MAM, JJA, SON) in the reference data set;

3. Generate 24 h of hourly wind direction: every 6 h, generate a random probabilistic wind direction from the corresponding season and daily wind speed, linearly interpolate between generated values;

4. Linearly interpolate between any missing data in the time series.

Eames et al. showed this process to reproduce measured data very well for a range of sites across the UK (Eames, Kershaw and Coley, 2011a; Eames, Kershaw and Coley, 2011b). This assumes that, in future, the relationships between rainfall volume and other weather variables remains consistent, i.e. greater amounts or frequencies of precipitation will be reflected in proportional increases in wind speeds. Wind directions in the UK are dominated by the south-westerly jet streams: although they have shown significant

variability in the twentieth century, there is little evidence to suggest a changing trend over the past few decades (Jenkins, Perry and Prior, 2009).

This generation process has been validated against the CIBSE Test Reference Years for Plymouth (Chartered Institute for Buildings Services Engineers, 2017), 1983–2004 (Eames, Kershaw and Coley, 2011a). To assess its applicability to the selected sites, the process was also applied to the 'baseline' scenarios (1961–1990) outputted by the Weather Generator, using the reference (training) data set from the 1961–1990 MIDAS observations (UK Met Office, 2012) from a nearby site.

5.2.3 Sites

The UK experiences a temperate oceanic climate (Peel, Finlayson and McMahon, 2007) with a strong influence from the south-westerly polar front jet stream. This causes frequent fluctuations and unsettled weather is typical. Its location between the Atlantic Ocean, continental Europe and the Scandinavian Peninsula causes significant precipitation differences between east and west, especially in coastal regions. Owing to the differences in latitude and the impact of occasional continental tropical air masses from the south, there can be significant thermal differences between northern and southern regions.

Eight sites were selected for this study to represent the geographical variation of built heritage sites in the UK (Figure 5.2). Site selection was constrained by the need to have sites with 30 year hourly wind and precipitation data in the MIDAS database (UK Met

Office, 2012). Due to this many of these eight have previously been used as central nodes in maps of driving rain (e.g. Prior, 1985; BSI, 1992) . The selected sites are representative of airfield conditions, i.e. unimpeded by urban canyons and reduced wind and precipitation. It should be noted that there were few locations with data that met the selection criteria in Northern Ireland. It is not suggested that the characteristics of the entire region are characterised by the properties observed for Aldergrove. This is important in the context of the strong winds typically experienced on the west coast of Ireland.

5.3 Results

5.3.1 Model validation

Eames et al. (Eames, Kershaw and Coley, 2011a; Eames, Kershaw and Coley, 2011b) have validated that probabilistic generation processes can be used to produce realistic hourly data series. To assess the applicability of this approach and estimate the error for the selected UK sites, the frequency (occurrence) of different meteorological conditions in the generated baseline data (1961–1990) were compared to the reference data for each site during the same time period.

To assess how similar the generated baseline time series are to the recorded meteorological conditions, the frequency (occurrence) of relevant parameters divided into bins or discrete values is presented in Figure 5.3. The parameters with their respective bin

Figure 5.2. Study sites used to evaluate future WDR exposure, representing the variability of exposures to precipitation and wind across the UK.

sizes and/or discrete value ranges are presented in Table 5.1. In Figure 5.3, the black line 45^{o} denotes a 1:1 ratio, while the red bold line is a logarithmic-transformed least-means correlation weighted according to frequency. How closely these lines lie to one another represents how well the generated data reproduces the characteristics of the measured reference data.

Table 5.1. The parameters employed to calculate the frequency of different meteorological conditions used in the comparison of the baseline generated time series and the recorded meteorological data.

Parameter	Time resolution	Type	Divisions, Interval
Wind direction	hourly	discrete	0^{o} to 350^{o}, 10^{o}
Wind speed	daily	bins	0 to 30 m s^{-1}, 1 m s^{-1}
Wind speed	hourly	bins	0 to 30 m s^{-1}, 1 m s^{-1}
Precipitation	daily	bins	0 to 50 mm h^{-1}, 1 mm h^{-1}
Precipitation	hourly	bins	0 to 30 mm h^{-1}, 1 mm h^{-1}

Some variation between the two data sets is to be expected, as the UKCP09 projections are provided at a resolution of 25 km $\times$ 25 km regions. Even though the Weather Generator allows for the selection of 5 km $\times$ 5 km, the climate predictions at this scale merely present the calculations undertaken at the larger scale. What is important is that the generated baseline data series have similar characteristics to the recorded meteorological data, even if they are not identical.

The most important parameters for calculating driving rain exposure with Equation 5.1 are the hourly mean wind speed, hourly precipitation, and predominant hourly wind direction. There is a very good relationship between the generated and down-sampled time series of hourly mean wind speeds and hourly precipitation. This is to be expected for the latter, as these values are a direct output of the Weather Generator. With regards to hourly wind speed, the strong correlation ($R^2_{weighted} = 0.91$) is the result of the probabilistic processes employed by Eames et al., and agrees with their assessments of reproducing wind speeds.

The generated daily precipitation is very similar to the measured daily precipitation. This is similar to the hourly precipitation, as the daily values are also a direct output of the

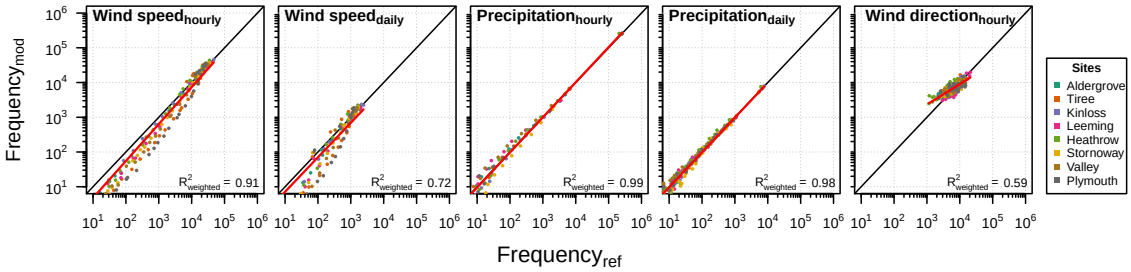

Figure 5.3. Comparison of the generated baseline time series (1960–1990) to the recorded meteorological data at sites within their respective prediction regions for eight UK sites. The bin frequency of the wind speed and precipitation is compared (daily and hourly), as well as the hourly wind direction.

Weather Generator and therefore derived directly from the UK Climate Projections from 2009. The discrepancy between modelled and measured data for both hourly and daily wind speeds is partially explained by the limitations of calculating them using PET, since this value is truncated at 0 (i.e. it cannot be negative) and is only generated to two decimal places (Eames, Kershaw and Coley, 2011a).

The distributions of wind speeds and precipitation are logarithmic, with low values much more common than high values. Extremes of hourly precipitation are well-reproduced in the generated baseline data sets. This is represented by $R^2_{weighted} = 0.99$, and negligible deviation from the 45° line (representing a 1:1 equivalency). In contrast, the probabilistic approach under-represents extreme hourly wind speeds. This is represented by a lower $R^2_{weighted} = 0.91$, and many parameters bins/discrete values deviating significantly from the diagonal 1:1 equivalency in Figure 5.3. It is important to note:

- these extreme high wind speed values occur very rarely, i.e. for less than 100 hours in 30 years;

- in Equation 5.1, an increase of 1 m s^{-1} in hourly wind speed for wind speeds greater than 20 will, at most, modify the WDR exposure by 5%;

- The extremes of hourly wind speeds are more pronounced for specific sites: for example, Plymouth (in dark gray points in Figure 5.3) consistently deviates further from the 1:1 equivalency, than other sites, i.e. it is the site at which extreme hourly wind speeds are most significantly under-represented.

The hourly wind direction warrants discussion, as the wind direction distribution is more regular than the other parameters. The wind directions generated by the Eames algorithm have a unique pattern that can be described as a saw-tooth: alternating higher and lower values for neighbouring wind directions. This is visible in Figure 5.4 and in the literature (Eames, Kershaw and Coley, 2011b, p. 131). These differences are most likely "due to the simplistic method used, where 1 h is not dependent on the next and because the interpolation does not follow the same probabilistic distribution' [as the other variables]" (Eames, Kershaw and Coley, 2011b, p. 130). Despite the saw-tooth pattern, the overall characteristics of site-specific wind directions are reproduced by the probabilistic process. It is useful to note that a 10^{o} difference in wind direction will, on average, change the cosine component (and therefore WDR exposure) of Equation 5.1 by 11%.

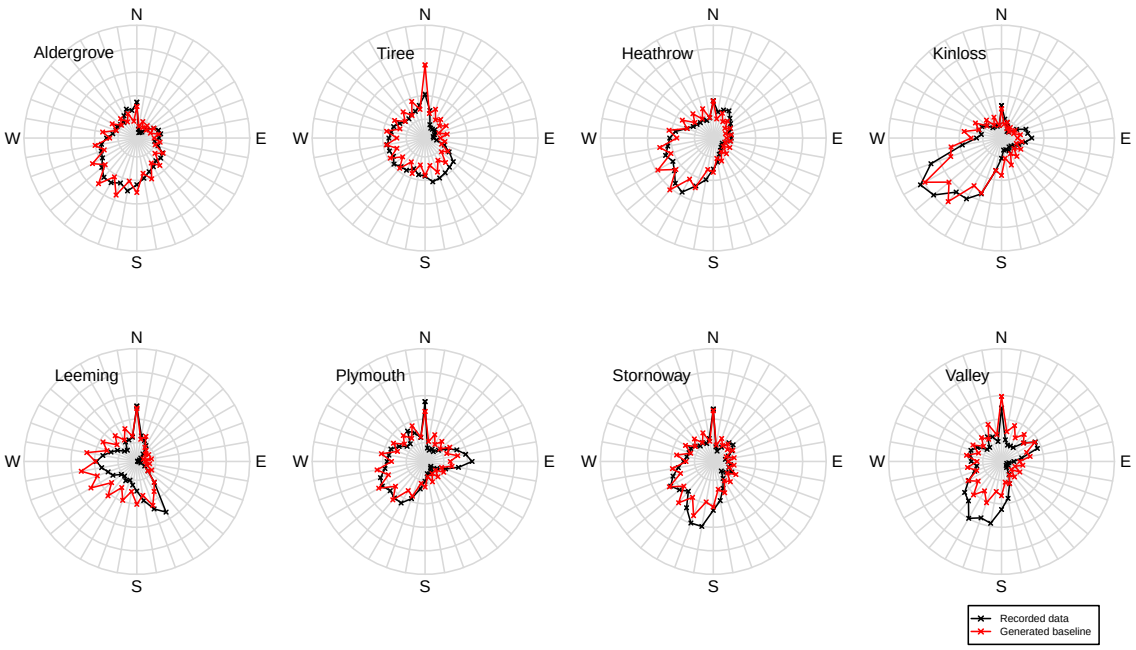

Figure 5.4. Comparison of the mean hourly wind speed distribution for the generated baseline time series (1961–1990) to the recorded meteorological data. 0^{o} represents a wind from the north.

5.3.2 Annual characteristics

The sites experienced varying annual WDR exposure during 1961–1990 (Table 5.2). In general, western coastal sites (Tiree, Stornoway, Valley, Plymouth) have on average received more than 380 L m^{-2} of annual WDR exposure. In contrast, inland and eastern sites in Britain (Kinloss, Leeming, and Heathrow) received less than 240 L m^{-2} of WDR annually. Aldergrove received an annual average WDR exposure of 330 L m^{-2}, which is significantly more than the other inland sites. This likely represents the overall higher exposure in Ireland due to weather systems arriving from the Atlantic Ocean in the west.

The sites with higher baseline WDR volumes are also those that are predicted to change most. This is most prominent in the WDR exposure of western sites of Wales and Scotland:

Valley and Tiree. Sites that have had mid-level exposure of roughly 370 L m^{-2} (i.e. Stornoway and Plymouth) are predicted to increase to the low 400s. In contrast, the more inland and eastern sites (Kinloss, Heathrow and Leeming) are not predicted to change very much.

The significant predicted changes in the annual WDR volumes calculated from the data in Table 5.2 and shown in Table 5.3 are between 7.2% and 25% for specific sites, but this does not reflect seasonal diversity.

It is generally accepted that, with future climate change, the meteorological conditions within different seasons will change, especially in winter (Watts et al., 2015; Hansen and Sato, 2016). This will also manifest as changes in the characteristics of wind-driven rain. To assess this, the calculated annual indices I_A were separated in Tables 5.2 and 5.3 into seasons based on calendar months: winter (DJF), spring (MAM), summer (JJA), autumn (SON). This analysis demonstrates that the predicted change in WDR exposure during different seasons is not proportional to the annual average change (Figure 5.5). There are strong polarising contrasts apparent for the winter and the summer, while the predicted changes in spring and autumn are closely related to the annual predicted changes.

The severity of predicted seasonal change is not the same across sites. For example, western coastal sites including Stornoway, Tiree, and Valley are predicted to experience as much as a 40% increase in WDR volume during the winter months. It is also predicted that Stornoway could experience almost 30% less WDR in the summer months, and slightly

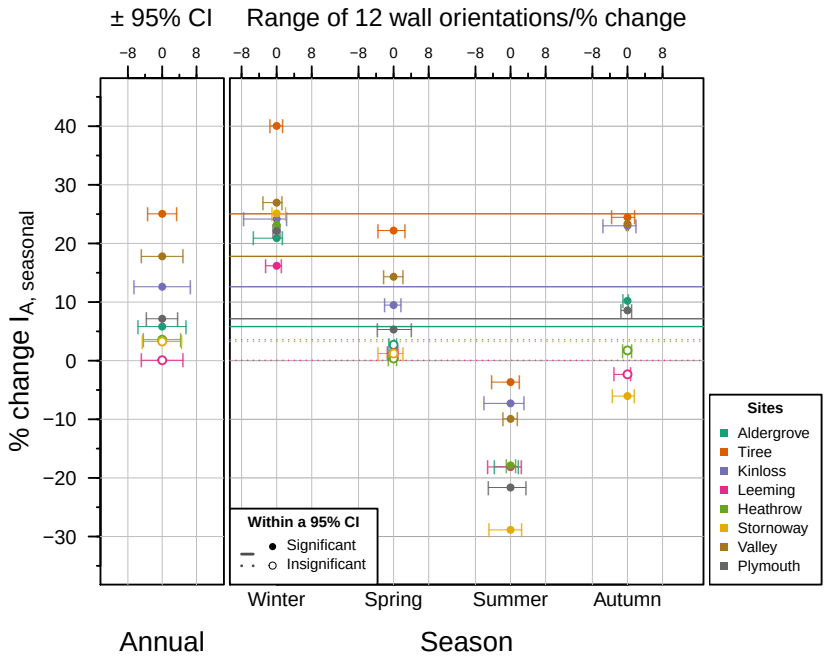

Figure 5.5. The predicted changes in average exposures of wind-driven rain, presented for annual behaviour and for individual seasons.

Table 5.2. Annual indices (I_A, total exposure to wind-driven rain) during the baseline (1961–1990) and under the prediction scenario (2070–2099) at the eight sites for all wall orientations.

	$I_{A,\text{baseline}}$ (1961–1990)					$I_{A,\text{scenario}}$ (2070–2099)				
Site	Annual $L\,m^{-2}$	Winter $L\,m^{-2}$	Spring $L\,m^{-2}$	Summer $L\,m^{-2}$	Autumn $L\,m^{-2}$	Annual $L\,m^{-2}$	Winter $L\,m^{-2}$	Spring $L\,m^{-2}$	Summer $L\,m^{-2}$	Autumn $L\,m^{-2}$
Aldergrove	330 ± 8.1	90 ± 3.1	70 ± 1.09	70 ± 1.5	90 ± 3.0	340 ± 9.0	110 ± 3.8	50 ± 1.4	50 ± 1.4	100 ± 3.4
Tiree	540 ± 7.1	180 ± 2.8	100 ± 0.64	80 ± 1.4	180 ± 3.0	680 ± 10	250 ± 4.6	80 ± 1.5	80 ± 1.5	220 ± 4.3
Kinloss	240 ± 6.5	60 ± 2.1	50 ± 1.1	60 ± 1.2	70 ± 2.4	270 ± 8.0	80 ± 2.8	50 ± 1.3	50 ± 1.3	90 ± 3.1
Leeming	210 ± 4.6	60 ± 1.6	50 ± 0.78	40 ± 0.93	60 ± 1.7	210 ± 4.8	60 ± 1.9	40 ± 0.93	40 ± 0.93	60 ± 1.7
Heathrow	200 ± 3.9	60 ± 1.2	50 ± 0.52	40 ± 0.91	60 ± 1.4	200 ± 4.2	70 ± 1.5	30 ± 0.96	30 ± 1.0	60 ± 1.6
Stornoway	390 ± 8.0	140 ± 2.8	80 ± 1.2	60 ± 1.7	110 ± 2.5	400 ± 8.7	170 ± 3.9	40 ± 1.5	40 ± 1.5	100 ± 2.7
Valley	520 ± 10	170 ± 4.7	110 ± 1.1	80 ± 0.84	160 ± 4.2	620 ± 13	220 ± 6.4	70 ± 0.93	70 ± 0.96	200 ± 5.5
Plymouth	380 ± 6.1	120 ± 2.1	70 ± 0.70	60 ± 1.3	120 ± 2.3	410 ± 6.9	150 ± 2.8	50 ± 1.3	50 ± 1.3	130 ± 2.8

lower than annual exposures during the autumn.

5.3.3 Spell volumes

The volume of water hitting surfaces during wind-driven rain spells is predominantly increasing. The intensity (or volume hereafter) of WDR spells during the winter, spring, and autumn is predicted to increase, while extreme events – such as the worst spell likely to occur in a three year period I_S – are predicted to increase by greater amounts. For some

Table 5.3. Predicted change in the annual spell index I_A (total wind-driven rain exposure) from 1961–1990 to 2070–2099 for all wall orientations. Italics indicate that the predicted change are statistically insignificant within a 95% CI.

Site	Annual %	Winter %	Spring %	Summer %	Autumn %
Aldergrove	5.8 ± 5.3	21 ± 7.4	*2.7 ± 3.1*	-18 ± 4.3	10 ± 6.8
Tiree	25. ± 3.2	40 ± 4.1	22 ± 2.1	-3.7 ± 3.5	24 ± 4.1
Kinloss	13 ± 6.1	24 ± 8.0	9.5 ± 4.4	-7.3 ± 4.6	23 ± 7.9
Leeming	*0 ± 4.6*	16 ± 6.2	*1.3 ± 3.4*	-18 ± 4.2	*-2.3 ± 5.9*
Heathrow	*3.6 ± 4.1*	23 ± 4.9	*0.38 ± 2.4*	-18 ± 4.8	*1.8 ± 5.4*
Stornoway	*3.3 ± 4.3*	25 ± 4.8	*1.2 ± 3.1*	-29 ± 5.5	-6.0 ± 4.8
Valley	18 ± 4.6	27 ± 6.4	14 ± 2.4	-10 ± 2.3	23 ± 5.9
Plymouth	7.2 ± 3.4	22 ± 4.0	5.3 ± 2.1	-22 ± 4.1	8.6 ± 4.2

sites, the summer months will have lower WDR exposure with regards to both general and extreme behaviour. At other sites, this change is insignificant. As established in BS 8104 and its preceding publications, façades facing the south-west will be more exposed to WDR, as they are more frequently hit by prevailing wind directions in the UK.

The worst spell likely to occur once every three years I_S is predicted to increase by 22% and 59% at specific sites (Table 5.4). Similarly, the mean exposure of spell-specific indices ($I'_{S,mean}$) is also predicted to increase, but by between 4.8% and 27%. This means that while larger differences are predicted in extreme events, the average WDR exposure is also predicted to increase.

Section 5.3.2 established the importance of assessing WDR exposures seasonally. This is also important for an assessment of the predicted characteristics of WDR spells. Figure 5.6 shows the volumes of the mean and the worst spell likely to occur at each site once every three years during different periods. When spells occurred over the duration of two seasons, they were categorised to the season in which most of the spell occurred. As established for the annual behaviour, annual predicted changes in spell exposure are not capturing the

Table 5.4. Predicted percent change in exposures to wind-driven rain from 1961–1990 to 2070–2099, for all wall orientations.

	Mean spell-specific index $I^{*}_{S,\mathrm{mean}}$					Once every three years spell I_S				
	Annual	Winter	Spring	Summer	Autumn	Annual	Winter	Spring	Summer	Autumn
Aldergrove	4.8 ± 1.9	23 ± 4.2	*-3.2 ± 3.3*	-21 ± 4.5	15 ± 4.4	23 ± 5.4	24 ± 7.9	*5.5 ± 6.5*	*-7.7 ± 9.5*	18 ± 7.8
Tiree	27 ± 4.1	44 ± 8.3	16 ± 5.1	*-3.4 ± 5.0*	46 ± 9.1	54 ± 8.5	55 ± 11.1	32 ± 8.9	*2.0 ± 8.9*	45 ± 10
Kinloss	13 ± 2.9	25 ± 4.6	10 ± 4.4	-10 ± 4.9	27 ± 6.8	29 ± 7.4	36 ± 11	21 ± 8.3	*6.2 ± 8.8*	25 ± 9.4
Leeming	4.8 ± 2.2	20 ± 4.9	*3.4 ± 4.0*	-12 ± 4.7	*3.8 ± 4.4*	*11 ± 27*	*17 ± 29*	9.0 ± 6.9	*-7.1 ± 9.8*	*4.4 ± 8.2*
Heathrow	13 ± 2.4	27 ± 4.7	*3.1 ± 3.8*	2.9 ± 6.5	11 ± 4.3	22 ± 5.2	27 ± 7.5	15 ± 8.0	11 ± 10	16 ± 8.3
Stornoway	8.0 ± 3.2	15 ± 5.1	*1.5 ± 4.2*	-18 ± 4.8	23 ± 6.7	30 ± 7.7	30 ± 9.4	*8.4 ± 8.8*	-13 ± 7.7	30 ± 8.5
Valley	13 ± 2.4	23 ± 4.8	7.6 ± 3.3	-10 ± 5.1	12 ± 5.0	24 ± 6.3	30 ± 9.1	21 ± 8.4	*-2.4 ± 9.9*	13 ± 8.4
Plymouth	14 ± 3.4	37 ± 7.3	*3.8 ± 4.0*	-12 ± 5.9	*2.0 ± 4.2*	25 ± 7.4	28 ± 9.7	22 ± 9.4	*-1.1 ± 13*	7.6 ± 7.9

differences between seasons. Notably, summer extreme events are predicted to become less intense, although this is insignificant for some sites and/or wall orientations.

During the baseline period 1961–1990, the worst spell likely to occur once every three years is likely to occur during the winter or autumn months. For this reason, there is little difference between these periods of time in Figure 5.6. In contrast, the extreme spell volumes occurring in spring and summer are significantly less severe.

As Figure 5.6 demonstrates, there are significant differences in spell volumes for different wall orientations during the baseline period. However, the predicted changes in volume for each wall orientation are similar to those presented in Table 5.4. This means that all façades of a building are predicted to see a similar percent change in their exposure, which will be varying severity depending on the established directional characteristics of WDR exposure.

Western sites have the highest baseline and predicted ‘once every three year’ spells, but these sites also have much higher mean I_S WDR exposures than their eastern and inland counterparts. The extreme event exposures (such as I_S) and the mean WDR exposure are not directly proportional. While there is a general relationship between the two, the

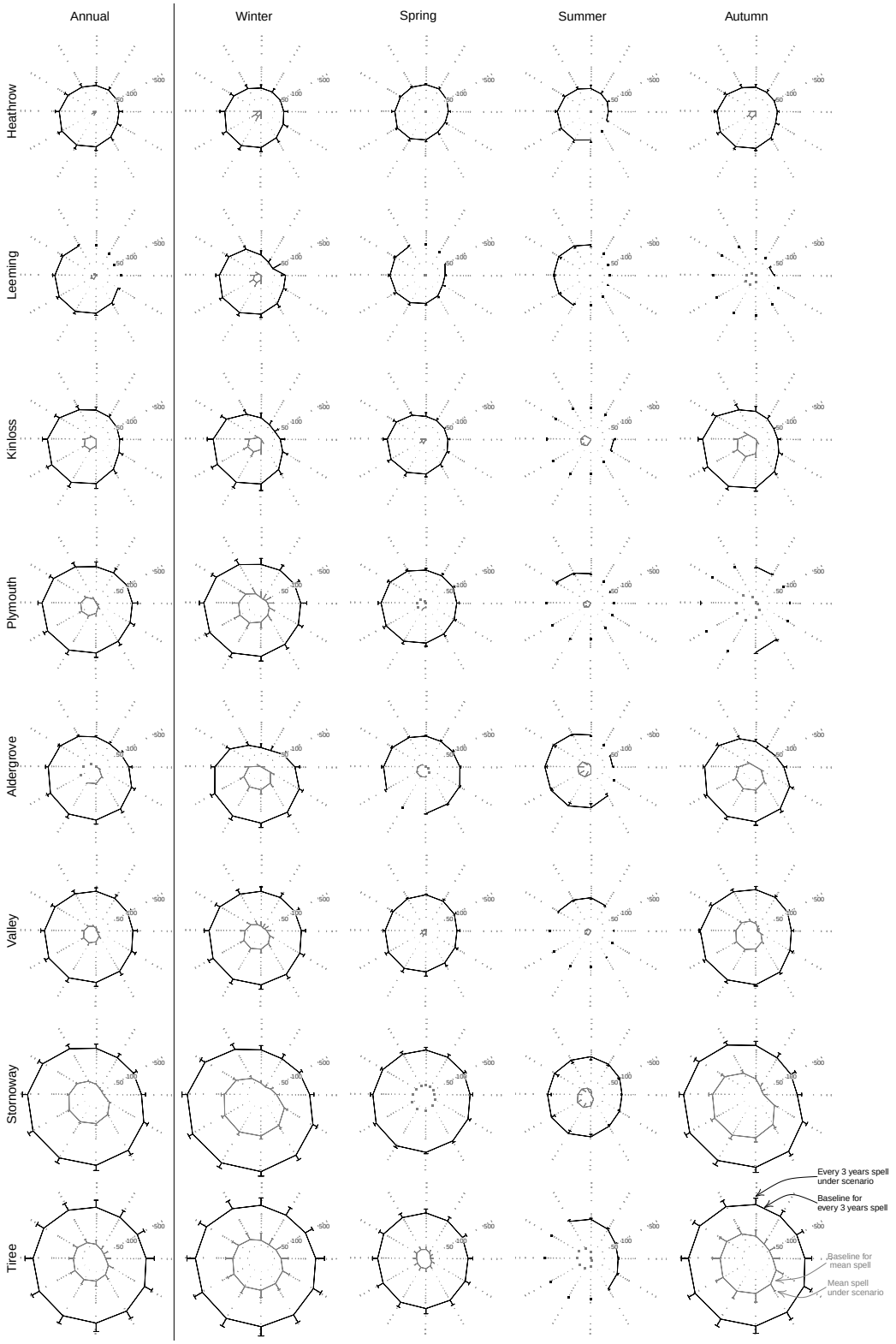

Figure 5.6. The volumes of the mean and the worst spell likely to occur once every three years at each site during different periods, represented by the gray and black circles, respectively. The whiskers indicate the predicted conditions in 2070–2099; unconnected points indicate change that was not significant within a 95% CI. The radial directions indicate wall orientations, where North = 0°.

volume of the mean WDR exposure varies relative to the 'once every three year' exposure. The predicted changes as percentages in the mean I'_S and the 'once every three year' spell volumes are much more similar, suggesting a common driving force that is likely annual precipitation.

5.3.4 Spell durations and inter-spell characteristics

Shorter wind-driven rain spells are predicted to become more common, with more time elapsing between them (Figure 5.7). Spells less than 10 h in duration were the most common type between 1961–1990, and they are predicted to occur much more frequently in the 2070–2099 scenario. For most locations, there is insignificant or slightly negative change in the occurrence of spells of medium length (lasting more than 10 h but less than 100 h). Longer spells (durations greater than 100 h) are predicted to occur much less frequently. Stornoway is unique in that mid-length spells (lasting more than 10 h but less than 100 h) are predicted to become much more common.

By definition, the minimum spell duration is the resolution of the meteorological measurements inputted into Equation 5.1, i.e. 1 h. The theoretical maximum duration for a rain spell (by the definition in ISO 15927) is the duration of the input meteorological data. In practice, rain spells very rarely extended beyond 1000 h. The few outlying spells that exceed 1000 h have been removed from the statistics presented herein – in general, they are found in regions with higher annual precipitation where gaps of 96 h or more without

any WDR exposure are less common.

Figure 5.7 shows the frequency in occurrence of spells of different lengths, in which each polar plot represents one site. The twelve axes within the polar plot represent wall orientations (see key in Figure 5.7). At all sites and wall orientations, the predicted change in occurrence of spells longer than 500 h is predominantly statistically insignificant. This is likely because they occur much less often than shorter spells.

There is little change predicted for the number of spells occurring per year at each site and wall orientation (approximately 2–3 spells per year, equivalent to less than 10%, at most, and insignificant for 3 of the sites). For the UK, a site and wall orientation, on average, experiences 23 rain spells (as defined by ISO 15927; Orr and Viles, 2018a; Chapter 4) for 1961–1990 and not predicted to change over the twenty-first century. Natural variation around this average is caused by two factors: annual precipitation and prevailing wind directions. For regions that experience higher than average annual precipitation, there are less likely to be periods of 96 h or longer without driving rain, so subsequent depressions would be bridged into a single spell. Also, walls oriented to be hit by prevailing UK wind patterns will less frequently meet the aforementioned condition for dividing exposure into spells.

If rain spells are predicted to become shorter but occur with the same annual frequency, it follows that there will be longer periods of time between them. Table 5.5 presents two metrics for quantifying this: the mean period of time elapsing between sequential WDR

Table 5.5. Period of time elapsing between sequential wind-driven rain spells from 1961–1990 and 2070–2099, with changes. The mean fraction of hours within rain spells represents the fraction of hours that were within rain spells on average out of the total number of hours occurring in a one-year period. All changes are statistically significant within a 95% CI.

	Mean inter-spell period			Mean fraction of hours within rain spells		
	1961-1990	2070-2099	Change	1961-1990	2070-2099	Change
	h	*h*	*h*	-	-	%
Aldergrove	180 ± 0.49	200 ± 2.6	26 ± 3.1	0.51 ± 0.002	0.43 ± 0.01	-15 ± 2.1
Tiree	170 ± 0.46	180 ± 1.9	14 ± 2.4	0.60 ± 0.002	0.57 ± 0.01	-5.0 ± 2.3
Kinloss	200 ± 0.66	220 ± 2.5	21 ± 3.2	0.42 ± 0.002	0.36 ± 0.01	-14 ± 2.1
Leeming	210 ± 0.89	240 ± 3.9	30 ± 4.8	0.37 ± 0.003	0.31 ± 0.01	-15 ± 3.6
Heathrow	220 ± 0.67	260 ± 4.4	34 ± 5.1	0.31 ± 0.001	0.27 ± 0.01	-11 ± 3.1
Stornoway	160 ± 0.54	180 ± 1.6	16 ± 2.2	0.65 ± 0.002	0.58 ± 0.01	-11 ± 1.0
Valley	180 ± 0.52	210 ± 2.8	28 ± 3.4	0.44 ± 0.002	0.38 ± 0.01	-12 ± 2.3
Plymouth	200 ± 0.61	240 ± 4.6	34 ± 5.2	0.37 ± 0.002	0.34 ± 0.01	-9.0 ± 3.2

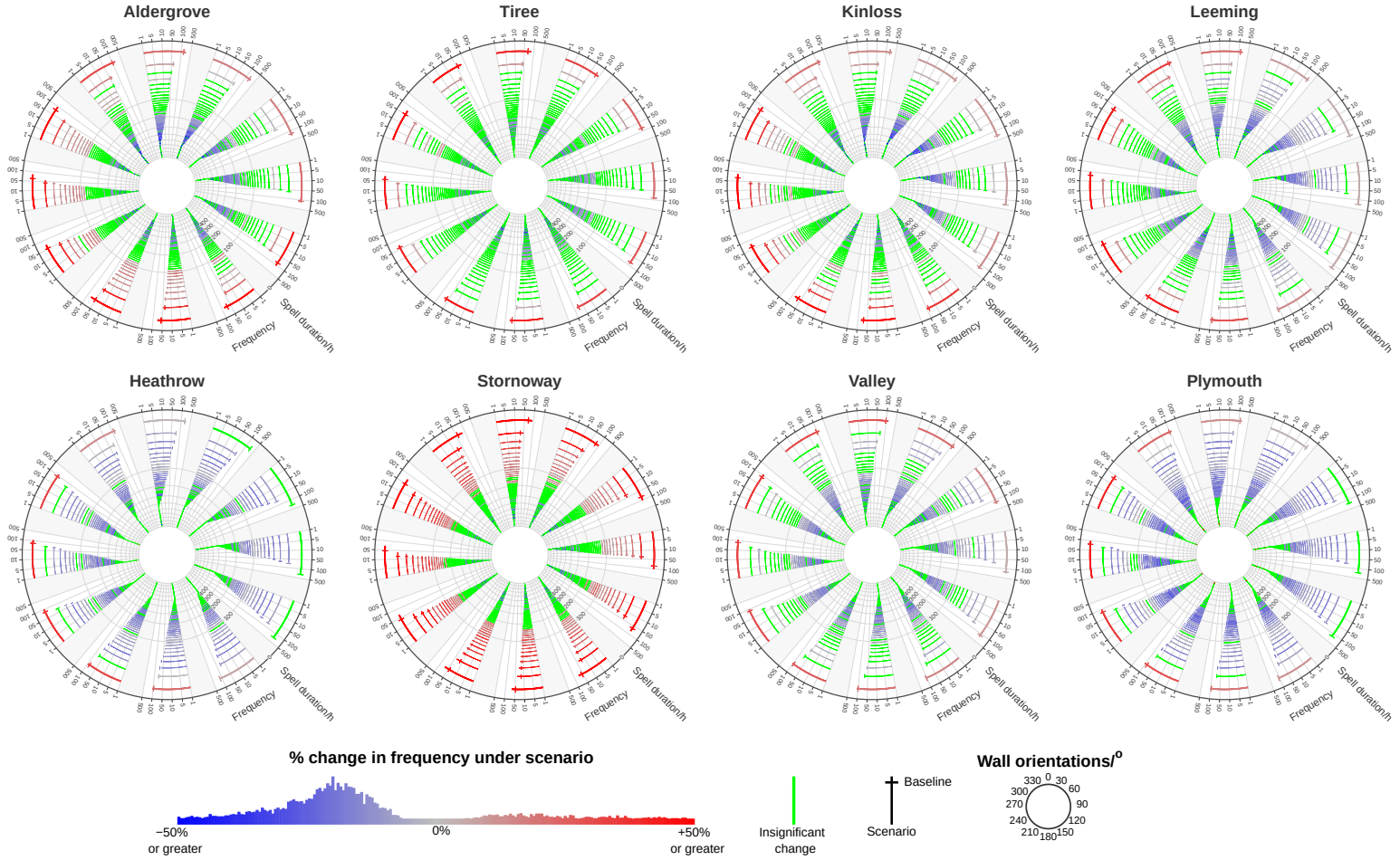

Figure 5.7. The frequency of wind-driven rain spells of different lengths at eight UK sites. The 12 'sub-axes' within each polar plotting area represent wall orientations (North = 0°). The 10 h bins are plotted as radial lines representing their mid-point, e.g. 5, 15, …, 995 h. The perpendicular axis represents the spell duration, and the radial axis represents their frequency of occurrence. The main line of the radial axis is the frequency under the predicted scenario, while the cross-line of the 't' is the baseline. The colour scale shows the predicted percentage change of frequency for the spell duration bins: red for increase, blue for decrease (with gray representing no change). Green is used to show when the change in occurrence was statistically insignificant.

spells, and the fraction of hours that were within rain spells on average out of the total number of hours occurring in a one-year period.

It can be observed that the inter-spell periods are increasing, on average, by approximately 1 day, representing a 10–15% increase in 2070–2099 upon 1961–1990. A concomitant decrease can be observed in the number of hours within an annual period that are within rain spells, as opposed to inter-spell periods.

5.3.5 Intra-spell characteristics

At all sites, regardless of spell length, the fraction of hours within spells during which there is WDR exposure occurring, the 'active fraction' is predicted to increase — except for long spells at Plymouth, which are predicted to decrease negligibly. The most significant increases in the active fraction are predicted to occur for the mid-length spells (longer than 10 h but less than 100 h long).

Sections 5.3.3 and 5.3.4 present predicted increases in the volume of rain spells and decreases in their duration. While these affect the wind-driven rain exposure at the single-spell level, they do not consider how the exposure might be distributed *within* an individual WDR spell.

To assess this, it is interesting to consider the 'active' fraction, defined as the number of hours within a rain spell during which there is exposure to wind-driven rain for a given location and wall orientation. Table 5.6 shows the active fraction at each site for short,

Table 5.6. Mean fraction of hours within spell with wind-driven rain.

	Short spells (less than 10 h)			Mid-length spells (longer than 10 h but less than 100 h)			Long spells (greater than 100 h)		
	1961-1990	2070-2099	Change	Baseline	2070-2099	Change	1961-1990	2070-2099	Change
	-	-	%	-	-	%	-	-	%
Aldergrove	0.89 ± 0.0016	0.92 ± 0.0026	3.3 ± 0.48	0.26 ± 0.0013	0.28 ± 0.0041	10 ± 2.1	0.13 ± 0.0003	0.14 ± 0.0013	4.9 ± 1.2
Tiree	0.87 ± 0.0019	0.92 ± 0.0032	5.3 ± 0.58	0.28 ± 0.0012	0.31 ± 0.0037	11 ± 1.8	0.14 ± 0.0003	0.15 ± 0.0011	5.2 ± 2.0
Kinloss	0.92 ± 0.0014	0.93 ± 0.0025	1.5 ± 0.42	0.22 ± 0.0010	0.26 ± 0.0036	20 ± 2.1	0.12 ± 0.0003	0.13 ± 0.0012	12 ± 1.3
Leeming	0.90 ± 0.0013	0.91 ± 0.0029	1.6 ± 0.47	0.24 ± 0.0009	0.26 ± 0.0036	11 ± 1.9	0.12 ± 0.0004	0.12 ± 0.0011	3.5 ± 1.2
Heathrow	0.89 ± 0.0012	0.92 ± 0.0030	3.3 ± 0.47	0.27 ± 0.0009	0.29 ± 0.0034	8.6 ± 1.6	0.13 ± 0.0004	0.13 ± 0.0012	3.4 ± 1.3
Stornoway	0.89 ± 0.0020	0.92 ± 0.0031	2.7 ± 0.56	0.25 ± 0.0014	0.29 ± 0.0036	19 ± 2.0	0.14 ± 0.0003	0.15 ± 0.0009	7.4 ± 0.91
Valley	0.89 ± 0.0013	0.92 ± 0.0025	3.6 ± 0.42	0.29 ± 0.0012	0.32 ± 0.0039	9.0 ± 1.7	0.14 ± 0.0003	0.14 ± 0.0012	3.2 ± 1.1
Plymouth	0.91 ± 0.0012	0.93 ± 0.0030	3.1 ± 0.46	0.32 ± 0.0012	0.33 ± 0.0049	5.0 ± 1.9	0.15 ± 0.0004	0.15 ± 0.0016	-1.7 ± 1.3

medium, and long WDR spells.

The active fractions for short spells are approximately 0.90, while for medium and long spells they are about 0.30 and 0.15, respectively. Longer spells have lower active fractions than their shorter counterparts, as they are more likely to bridge between multiple weather depressions but have periods with no WDR within them.

5.4 Discussion

Two points of discussion are necessary: a review of some of the factors that impact the semi-empirical calculations of WDR and predictions of wind-driven rain (Section 5.4.1), and a consideration of the implications of the predictions for cultural heritage and built infrastructure (Section 5.4.2). An important part of the latter is to highlight aspects of wind-driven rain that are not captured by the current standard metrics – imperative to characterising future risk if they are predicted to significantly change in frequency of occurrence and/or severity.

5.4.1 Factors impacting calculations and predictions of wind-driven rain

The predictions in this paper are based on a multi-stage method. Each of these stages has implicit assumptions, caveats, and/or limitations.

Availability and applicability of meteorological data

ISO 15927 requires at least 10 years (and ideally 20–30 years) of hourly meteorological data to account for annual variability of wind-driven behaviour. As a reference time frame of 1961–1990 was selected to be the same as the baseline provided by the UKCP09, sites with data fulfilling the criteria were limited. The weather station data used may not be representative of the 5 $\times$ 5 km grid used in UKCP09, and will also not accurately reflect the microclimates created in urban environments.

Limitations of the Weather Generator and the probabilistic generation of future weather timeseries

A report on the UKCP09 Weather Generator specifies that the fitted data "must be validated by the user" (Jones et al., 2009, p. 31). Section 5.3.1 demonstrated the time series created from the Weather Generator data did not simulate extremes of high wind speeds, which is also an acknowledged attribute of the Weather Generator (Jones et al., 2009). It should also be considered that both the Weather Generator and the Eames probabilistic

process are *learning* methods that lack a physical basis; therefore, any use of a training data set (e.g. one from 1961–1990) assumes that certain relationships and characteristics of the climate are also applicable for the future time periods of interest. Finally, the Weather Generator is "based on two models with time scales of one day to one month. The models are made to follow the average seasonalityvariability on time scales longer than a few weeks is not explicitly represented" (Jones et al., 2009, p. 32). As rain spells lasting longer than a few weeks rarely occur, the effect of this on the accuracy of the predictions is minimal.

Applicability of ISO 15927-3:2009

The methods in this standard are not applicable for (ISO, 2009, p. 1): a) mountainous areas with sheer cliffs or deep gorges, b) areas in which more than 25% of the annual rainfall comes from severe convective storms, and c) areas and periods when a significant proportion of precipitation is made up of snow or hail. Additional guidance is provided for data quality: a) indices calculated from inland stations are not representative of buildings in coastal locations (i.e. situated less than 8 km from the sea), b) in mountainous terrain calculated indices apply only to the immediate neighbourhood of the station, c) in predominantly flat regions (i.e. with variations in altitude less than 100 m), the calculated indices are valid up to 100 km from the measurement station. In hilly regions, the limits to validity are much less. It is not thought that any of the study sites should be discounted for these reasons.

Cosine rule

The cosine rule is used in semi-empirical calculations of wind-driven rain to incorporate the angle between the prevailing wind direction and wall orientation. A comparison of the cosine rule and numerical simulations of WDR exposure on building façades showed that it tends to overestimate WDR exposure at higher angles, and is not well-suited for "light to moderate horizontal rainfall intensities and for the higher wind-speed values" (Blocken and Carmeliet, 2006b, p. 1188). Despite these shortcomings, it remains the current standard for incorporating wall orientation into semi-empirical evaluation of WDR exposure.

Effect of droplet diameter

The wind-driven rain index assumes a rain-drop diameter of 1.2 mm, from which the coefficient in Equation 5.1 by the inverse of the terminal velocity V_T = 4.5 m s^{-1}. Depending on the type of precipitation (e.g. drizzle, cloudbursts, etc...) the WDR coefficient can vary as much as 50–200%, which can result in a halving or doubling the WDR exposure within that hour as calculated herein (Straube and Burnett, 1998). Future work is needed to explore whether information on the predominant type of hourly rainfall can be extracted from meteorological metadata, such as weather codes used by the Met Office. From this, a more accurate droplet diameter could be inferred, increasing the accuracy of semi-empirical representations of WDR.

5.4.2 Implications for risks to cultural heritage and built infrastructure

Characterising the properties of wind-driven rain spells in the future is an important component of understanding climate change risk. Moreover, the potential effects on built heritage should be inferred, to inform efficient and effective management of change.

The metrics used in current standards for assessing wind-driven rain exposure in the UK are relevant to two types of impact:

1. Annual index I_A: for assessing the average moisture content of masonry (BSI, 1984) and when "assessing the likely growth of messes and lichens" (BSI, 1992, p. 4);

2. Spell index I_S: indicates the likelihood of rain penetration through masonry and joints in other walling systems (ISO, 2009).

For both metrics, the risk is characterised by the volume of water calculated to impact a standard surface area. When considering the potential risks of wind-driven rain, it is proposed that there are three important properties of rain spells: a) volume of the exposure, b) the duration of the spell, and c) the active fraction – the fraction of hours within a spell for which there is actively exposure to wind-driven rain.

It is also important to consider run-off in considering the implications of these changes. The semi-empirical methods for calculating WDR are only applicable up to the point where WDR conceptually impacts a surface. They do not suggest that all of this water is absorbed

by the surface, as some of it will likely run over the surface. This has ramifications for the performance of building elements besides porous materials and will be discussed later in this section.

It is useful to consider the four categories of activity related to building performance presented in Table 5.7 and how these might change under future scenarios: building element failure, biological impacts, cycling, and deep-seated wetting. These activities are directly related to the properties of WDR spells. While there are many other mechanisms that can affect porous building materials and the building envelope – such as salt crystallisation and freeze-thaw effects – their relationships with WDR are more complex and cannot be so easily summarised. Table 5.7 and the discussions that follow demonstrate the necessity to consider additional characteristics of WDR rain spells in order to categorise the range of potential impacts on cultural heritage.

5.4.2.1 Applicability of current metrics

I_A is a catch-all metric that ambiguously represents many different kinds of impacts of wind-driven rain. The average annual wind-driven rain exposure is reflective of all types of spells, regardless of their duration and/or active fraction. By definition, it is weighted more heavily towards spells.

I_S is a metric for assessing the potential occurrence of water penetration through masonry and joints. It is defined as the "worst spell likely to occur once every three years",

Table 5.7. Likely change in predicted occurrence of mechanisms impacting building performance in 2070–2099 due to changes in wind-driven rain spells and temperature under a high emissions scenario.

Category	Mechanism of impact	Temperature*	Relevant properties of WDR spells				Likely change in predicted occurrence
			Volume	Duration	Inter-spell periods	Active fraction	
Building element failure	Ingress through junctions, cracks, etc. . .); Failure of moisture management systems (e.g. gutter overspill)	Negligible	Proportional	Inversely proportional	Inversely proportional	Proportional	Increase during winter, spring, and autumn months
Near-surface cycling	Repeated ingress and evaporation of water causing cycles of crystallisation and dissolution of soluble salts	Proportional; higher potential evaporation	Proportional	Inversely proportional	Proportional	Proportional for medium and long spells	Increases
Deep-seated wetting	Penetration through masonry to the interior; thermal bridging (Künzel and Kiessl, 1996); hygric and hydric swelling	Negligible	Proportional	Proportional	Inversely proportional	Proportional	Increase during winter, spring, and autumn months

** high emissions scenario for 2070–2099, UKCP09*

represented by a percentile of all spell exposures of the entire data set. By this definition, I_S reflects spells in which high quantities of water impact a surface. In practice, the spell that this percentile reflects is a spell of a very long duration, as there are more hours in which wind exposure can occur. This does not account for the relatively low active fraction that longer spells (greater than 100 h in duration) typically have: between 10–15%. Penetration through masonry units is more likely to occur during shorter – but more intense – spells, when sequential exposures to quantities of wind-driven rain exert pressures onto existing moisture within porous building materials, driving them deeper into the building envelope.

5.4.2.2 Building element failure

ISO 15927 acknowledges that the metrics defined within it do not encompass all potential impacts of wind-driven rain: for example, it specifies that building element failure, such as "rain penetration around the edges of doors and windows or similar cracks in building façadeson shorter periods of heavy rain and strong winds" (ISO, 2009, p. v). The failure of building elements could also be expanded to include the effects that follow on from overburdened drainage and moisture management systems. This could be due to insufficient maintenance and/or because the volume of WDR exposure in a given time frame exceed their capacity. When the building elements do not function properly, it can increase the amount of water that runs over a façade, which is often localised to particular areas of a construction.

Such instances are predicted to become more frequent, given that shorter rain spells (less than 10 h) are predicted to become more frequent and more intense. As these spells usually have WDR occurring in most of the hours within their duration (i.e. a high active fraction), there is little time for drainage systems and other building elements to shed water. Metrics are needed that can identify the risks of wind-driven rain to building element failure.

5.4.2.3 Near-surface cycling

Within standards for wind-driven rain assessment, the period between spells is defined as a minimum of 96 h as it is possible that periods up to this length with no driving rain are necessary before evaporative losses will exceed the ingress from rain exposure (Prior, 1985). While this represents the extreme scenario (and is, to a degree, arbitrary), surface evaporation is likely occurring within spells during the hours in which there is not wind-driven rain exposure – in addition to the inter-spell periods. Such movements of vapour and liquid water can be considered as moisture cycling, both at a micro-scale (within mm from the surface interface) and at the bulk scale.

The distribution of active hours within spells has not been assessed. Although the total fraction of active hours within spells is predicted to increase, further work is needed to understand how clustering or spreading of active hours within rain spells could lead to higher rates of micro-cycling of moisture at the surface and near the surface. Another

important component of this analysis would be to consider sub-hourly distributions of rainfall, which could further support moisture micro-cycling.

It is predicted that longer periods of time will elapse between spells, increasing, on average, by roughly one day across all eight UK sites studied here. This could allow for more significant cycling to occur between spells: for example, simple modelling of stone masonry walls shows that 24 h of evaporative drying can mean 0–3 mm [L m^{-2} day^{-1}] of potential evaporation (Hall et al., 2011).

5.4.2.4 Deep-seated wetting

Deep-seated wetting can be considered as a migration of moisture to and from depth within a masonry construction (Smith et al., 2011a). Smith et al. have highlighted the polarising behaviour between the wetness and dryness of winter and summer months that support an increased potential for seasonal-dependent deep-seated wetting. This would be propagated by an increase of active hours within mid-length and long spells, which could provide more opportunities for moisture gradients to be forced deeper into masonry. In contrast, longer spells are predicted to become less frequent, with longer periods of time between them. It is difficult to postulate which of these effects might dominate, but future work could attempt to model the potential evaporation and moisture ingress under various scenarios.

When it comes to assessing the potential for deep-seated wetting using the current definition of the airfield annual index in ISO 15927 and BS 8104, these changes are being

smoothed by an annual average, which is predicted to be 'net positive' for most sites, as the increases during winter months outweighs the decreases predicted for the summer months. Future WDR exposure should be calculated as seasonal indices, as these will more accurately capture the overall exposures to wind-driven rain. Annual and seasonal exposures for the baseline and scenario time periods are presented in Table 5.2, along with what these represent as percent changes (Table 5.3). The polarisation of winter and summer volumes strongly suggests that deep-seated wetting will likely become more serious and frequent for western sites in Scotland and Wales.

5.5 Conclusion

This study has evaluated the projected characteristics of WDR spells and exposure for eight UK sites towards the end of the twenty-first century under a high-emissions scenario. It was shown that the future UK climate is predicted to experience shorter wind-driven rain spells with higher volumes of exposure in more concentrated time periods, especially during winter and autumn months. These increases will be more severe for western and coastal locations that already experienced higher WDR exposure during the twentieth century. The projected impact on building exposure are higher frequency and severity of building element failure, near-surface cycling, and deep-seated wetting.

Combining probabilistic hourly time series generation with semi-empirical formulae of WDR exposure was a robust approach of assessing future exposure. The results

demonstrated that there will not only be changes in the quantity of exposure to WDR, but also in the temporal characteristics such as the length of WDR spells and the distribution of exposure within them.

Part III

Non-destructive measurement of the response of moisture regimes within stone masonry

6 | An 'isolated diffusion' gravimetric calibration procedure for radar and microwave moisture measurement in porous building stone

"Technology, like art, is a soaring exercise of the human imagination."

– DANIEL BELL (1991, p. 20)

Chapter has been submitted for review under the same title with the following co-authorship: Orr, S. A., M. Young, D. Stelfox, A. Leslie, J. Curran and H. Viles.

Abstract

Information about the presence and movement of water is crucial to understanding stone deterioration and rock weathering but hard to obtain. Non-destructive, non-invasive measurements of electromagnetic phenomena can provide proxy data on water contents within porous stone and rock. Commercial geophysical devices, such as radar and microwave moisture sensors, produce raw data or readings in arbitrary units, but can be related to absolute water contents through gravimetric calibration. Calibration procedures typically either equilibrate samples to a set of relative humidities (RH%) using salt solutions or environmental chambers (requiring specialised equipment), or monitor ambient drying which yields less homogenous moisture distributions and takes time. This study proposes and tests a cost- and time-effective 'isolated diffusion' gravimetric calibration procedure in which a set of samples are sealed at specific water contents and equilibrated. The procedure is compared to ambient drying over 120 h for three UK building stones and evaluated with modelled reflection coefficients and relative permittivities. The calibrations determined from isolated diffusion more closely follow modelled behaviour than those from ambient drying, as the calibrations developed from the latter were affected by uneven distributions of moisture. Calibrations for radar measurements developed from two types of back interfaces (air and metal) were very similar to one another, suggesting that measurements are consistent regardless of the type of back interface used. The isolated diffusion calibration procedure provides a cost-effective and simple method to facilitate comparison between different NDT methods and enables accurate measurement of water contents in porous geomaterials.

The methods section has been slightly modified to reduce repetition from Chapter 2.

6.1 Introduction

Stone is weathered by a range of physical, biological, and chemical processes – most of which are propagated or caused by the presence and movement of moisture. How water will contribute to or cause different deterioration mechanisms depends on its spatial and temporal patterning (Mamillan, 1991). Stone is very commonly employed in historic buildings and traditional constructions; in the built context, water can be introduced into a building fabric in several ways. Understanding these ingress pathways is fundamental to management and conservation of the historic built environment.

Determining where moisture is and in what quantity is difficult because there are few techniques that directly measure it. The most straightforward is gravimetry, i.e. measuring the mass of water. Using this method *in situ* requires invasive sampling (typically core drilling) resulting in irreversible changes to the fabric of a building. Invasive sampling or destructive testing constitutes a change in the historic building fabric and have limited spatial and temporal coverage. Even if undertaken for diagnostic purposes, this is restricted by administrative and ethical limitations.

Alternatively, indirect (non-destructive) testing methods can be used. Non-destructive testing (NDT) uses physical properties as proxies for moisture, such as electrical, visual, or thermal measurements. Many technologies have been developed or adapted for this purpose and have been thoroughly reviewed elsewhere (Saïd, 2007; Pinchin, 2008; Camuffo and

Bertolin, 2012). Geophysical techniques such as radar and microwave are useful as the influence of salinity is negligible on the measurements within most of the microwave frequency range (Klein and Swift, 1977).

The output from a non-destructive measurement can be a physical property (such as electrical resistivity) or some transformation related to it. This transformation can be beneficial when a device is primarily designed for use on a particular type of material, or if the range of the property between dry and saturated states overlaps with potential water contents. In the latter case, the arbitrary scale reduces the risk of mistaking the physical property measured for an inferred water content.

To better understand and compare these indirect measurements, they can be calibrated to gravimetric measurements of laboratory samples. This creates a relationship between the physical property (or arbitrary scale) and the water content on a mass or volume basis. Calibrations can also be compared to models. Many factors can influence gravimetric calibration results, including material properties, sample size, environmental conditions, frequency of measurement, and the range of water contents. An uneven distribution of moisture within a sample might result in a false relationship with the gravimetry, since gravimetry calculations assume a homogenous distribution. This is of particular concern for calibrations produced from ambient drying.

The benefits of employing multiple NDT techniques are widely acknowledged. Studies in the past have shown that applying multiple techniques will often provide the most

information, yielding the best assessments (Di Tullio et al., 2010; Válek et al., 2010; Martinho et al., 2014; Martínez-Garrido et al., 2018). Combining radar and microwave measurement systems characterises variation in moisture in two spatial scales. Unfortunately, this is complicated not only by the difficulty of interpreting results from a single method but also the harmonisation of the results (Binda, Cardani and Zanzi, 2010). Robust gravimetric calibration techniques can enable comparison by translating device output into absolute water contents as a common parameter. Thus, the choice of calibration procedure influences the precision and accuracy of multi-method surveys.

This study proposes a procedure for gravimetric calibration and demonstrates its implementation for radar and microwave measurements on three UK building stones. It is an innovative but straightforward method which to our knowledge has not yet been published using a vapour impermeable barrier to 'isolate' samples at a single water content – allowing equilibrium moisture diffusion throughout the sample. These calibrations are evaluated with models of effective dielectric permittivity and electromagnetic reflection and transmission coefficients to determine their applicability for evaluating and comparing radar and microwave moisture measurement.

Table 6.1. Hygric and physical properties of the three stone types investigated in this study.

Procedure	Number of samples	Density kg m^{-3}	water content$_{sat}$* %	effective porosity** %
Ambient drying				
Portland limestone	1	2378	4.9	11.7
Clipsham limestone	1	2371	4.7	11.2
Locharbriggs sandstone	1	1991	8.5	17.0
Isolated diffusion				
Portland limestone	6	2244-2291	5.1-5.2	11.5-11.8
Clipsham limestone	6	2363-2391	4.0-4.7	9.57-11.2
Locharbriggs sandstone	6	2033-2161	6.5-8.5	14.0-17.4

**by mass, dry basis*, water content$_{sat} = m_{water}/m_{bulk} \times 100\%$
***equivalent to saturated water content*, effective porosity $f = v_{water}/v_{bulk} \times 100\%$

6.2 Material and methods

6.2.1 Stones

This study investigated gravimetric calibrations for three stone types (Table 6.1): Portland limestone (base bed), Locharbriggs sandstone, and Clipsham limestone. These are common building and repair stones in the UK, which are susceptible to a range of weathering mechanisms. The samples were cubic (150 mm $\times$150 mm $\times$ 150 mm), as determined by the field of detection of the deepest microwave moisture sensor.

Portland

Commonly found throughout the world as a building and repair stone. In the UK, it has been used for prominent buildings such as St Paul's Cathedral, London (Inkpen et al., 2012). It is now quarried in the Isle of Portland off the south coast of England. It is an Upper Jurassic limestone that is dominated by small to medium grain sizes (Leary, 1983;

Jaynes and Cooke, 1987), with a matrix-rich compacted texture (Dubelaar et al., 2003). The base bed is homogenous with very few oolites or visible bedding planes.

Locharbriggs

A Permian sandstone from Dumfries, Scotland that has been quarried since the 18th century. It is a pink to red medium grained sandstone (Building Research Establishment, 2000) widely used across Scotland and England for traditional masonry styles and contemporary cladding. It is characterised by distinctive aeolian cross lamination and is composed mainly of quartz, with some feldspars and clays and very few small rock fragments (Pandey et al., 2014).

Clipsham

A Middle Jurassic, very pale cream and buff oolitic limestone from Lincolnshire, England. It is coarse-grained and contains many small patches of a light brown colour (Emery and Dickson, 1989). The oolites are of a variety of shapes and sizes and there are also shell fragments and very small pebbles. It was probably deposited in a moderately sub-tropical sea, where changes were frequent, making its texture liable to a certain amount of variation. Clipsham has been used extensively as a repair stone for other oolitic limestones in the south of England, but also as a historical building stone such as a 15th century tower at Eton College, Berkshire, near Windsor (Braun and Wilson, 1970).

6.2.2 Procedure

Two contrasting methods for gravimetric calibrations have been compared for radar and microwave techniques. The first procedure uses a stone sample dried over time in ambient conditions, while the second uses vapour impermeable materials to 'isolate' samples at a single water content – encouraging equilibrium moisture diffusion throughout the sample. These calibrations are evaluated with models of electromagnetic reflection and transmission coefficients and effective dielectric permittivity.

6.2.3 Equipment

Two commercial devices have been used: a high-resolution radar and a microwave moisture device, which has three sensors heads penetrating various depths. These techniques operate in a similar frequency range (1.6 GHz and 2.45 GHz, respectively) and use coupled antenna and receiver units to measure reflected electromagnetic energy.

6.2.3.1 Radar

In 1988, the measurement of electromagnetic 'echoes' from interfaces between material properties (Lai, Dérobert and Annan, 2018) was given the name 'ground penetrating radar' (Pilon, 1992), herein referred to as radar. Originally applied in near-surface geophysical investigations, it has become a powerful imaging and diagnostic technique in civil engineering for building applications (Lai, Dérobert and Annan, 2018). This study has

Table 6.2. Typical dimensional representations of GPR data.

Name	Alternate names	Dimensions	Source	Length
A-scan	trace (Giannopoulos, 2005), 'trace'-window, 'wiggle'-window (Tzanis, 2006), 1-D scan	1D	Individual measured reflection curve perpindicular to a source	Dependent on the time window and device resolution
B-scan	radargram (Lai, Dérobert and Annan, 2018), D-scan (Zahran, Shihab and Al-Nuaimy, 2002; Jalinoos et al., 2009), 2-D scan	2D	Series of A-scans	Dependent on the length of the transect and measurement spacing
C-scan	slice scan (Lai, Dérobert and Annan, 2018), 3-D scan	3D	Parallel series of B-scans or grid of parallel and perpendicular B-scans	Dependent on the line spacing and/or grid size

used a 1.6 GHz GPR antenna (Malå Geoscience, Malå, Sweden). Radar data are typically represented in one to three primary dimensions (Table 6.2).

B-scans and C-scans are frequently used for finding sub-surface features (e.g. embedded objects, pipes) and gradual changes (e.g. a sloped bedrock). They are typically presented as interpolated grayscale or colour scale/gradient visuals representing the reflection amplitudes. This approach can also be used to identify moisture gradients, e.g. capillary uptake(Venmans, Ven and Kollen, 2016) or *in situ* localised water contents (Alani, Aboutalebi and Kilic, 2013), since a higher water content causes the signal to take longer to travel the same physical distance. However, visual inspection of B-scans for moisture gradients can be influenced by edge effects or a sloping back (reflective) layer; in the latter case, it is incorrect to infer a moisture gradient from travel times unless the variation in physical distance is known.

To identify water contents, amplitudes and travel times of features can be extracted from individual A-scans (Figure 6.1). The amplitude of the direct wave is contributed to

by the surface reflection, i.e. the difference between the relative permittivity between the materials on either side of the surface interface ($\varepsilon_{r,air}$ and the bulk material $\varepsilon_{r,b}$). The higher the water content, the greater the difference between $\varepsilon_{r,air}$ and $\varepsilon_{r,b}$. This results in a reduced reflection amplitude, i.e. higher transmission.

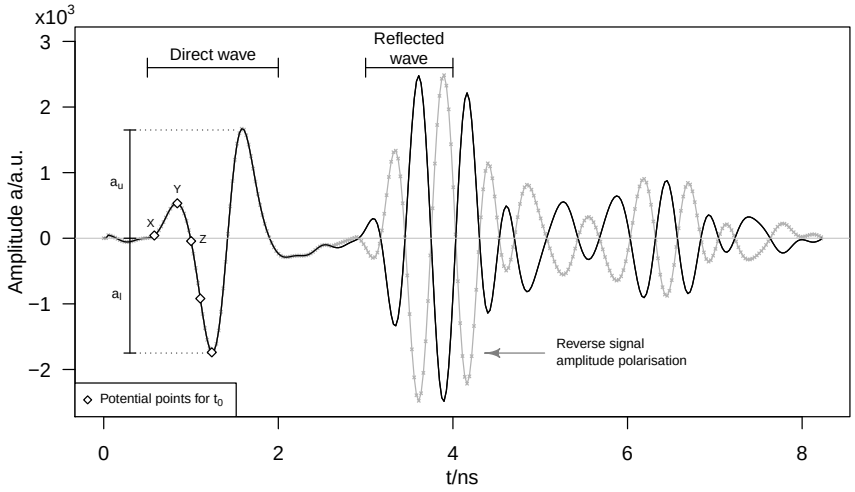

Figure 6.1. A demonstrative A-scan taken on an oven-dry sample of Portland limestone 150 mm×150 mm×150 mm. Similar features for those identified in the direct wave can be identified for the reflected wave. The potential points for t_0 were identified with a practitioner and expert survey (Yelf, 2004).

An electromagnetic signal will travel with a reduced velocity in a sample with higher water contents. This can be represented by the signal travel time between the direct wave (the reflection from the surface) and the reflected wave (the reflection generated by the interface at the back of the sample), also referred to as the reflector (Galagedara, Parkin and Redman, 2003) or 'back-wall reflection' (Lai et al., 2014). The travel time can be converted into an average velocity $\bar{v} = 2z/t$, with wall thickness t and travel time z, accounting for the time required for the signal to travel to the back interface and return to the antenna. Capitalising on $\bar{v} \approx c \times (\varepsilon_r)^{-1/2}$ where c is the speed of light, the real component of relative

permittivity (often referred to as the dielectric constant) can be expressed as:

$$\varepsilon_r' = \left(\frac{ct}{2z}\right)^2 \tag{6.1}$$

Both the amplitude and travel time method can be represented in a number of ways and are influenced by certain procedural details. The reflective wave can often be quite weak. To accommodate for this, a metal plate is placed at the back of the material to produce a strong reflectance. However, because a metal plate has infinite values of dielectric, it can reverse the signal amplitude polarity (Senin and Hamid, 2016), resulting in a transformed A-scan represented by the grey line in Figure 6.1. If this occurs, selecting the 'primary' peak of the wave can be ambiguous; in Figure 6.1, this could be represented by either the upper a_u or lower a_l amplitudes. It is advantageous to measure the wave amplitude with the peak-to-peak summed amplitude, i.e. with $a_p = a_u + a_l$ the absolute difference between the positive and negative peaks within the wave. To ensure the amplitudes are accurate, radar data undergoes a dewow process to align it to a zero baseline.

For calculating travel times, there is no consensus on where 'time zero' is within the direct wave (Yelf, 2004). Any number of parameters may be used, including (see Figure 6.1 for letter references): the time where the signal starts to raise over a predefined threshold (X), the time of the first extreme value (Y), or the first zero crossing after the first extreme value, approximately Z (Binda, 2005; Rodríguez-Abad et al., 2016).

Radar has most frequently been used to identify water contents in concrete using both amplitude and travel time changes (Laurens et al., 2005; Klysz and Balayssac, 2007; Senin and Hamid, 2016), but has also been effectively employed for geological materials at low frequencies (Olatinsu, Olorode and Oyedele, 2013) and brick specimens (Cetrangolo et al., 2017). Spectral analysis has been applied to A-scans (usually as a fast Fourier transform) to look at additional peak characteristics to the maxima and minima (Leucci, Masini and Persico, 2012; Lai et al., 2014).

6.2.3.2 Microwave moisture system

The MOIST350B (hf sensor; Leipzig, Germany) capitalises on the significant difference between the relative permittivity of water and most geological building materials in the microwave frequency region. The device works by producing an electromagnetic wave and measuring the proportion of energy that is reflected (the 'reflection coefficient') and measured by a receiving unit built into the sensor (Göller, 2006). A set of sensor heads penetrate to different depths by changing the field using combinations of certain antennae and applicators (Göller, 2001). Microwaves lose energy exponentially as they travel through materials like building stones (BSI, 2017). Therefore, all of the sensor heads (regardless of penetration depth), are sensitive to moisture near the surface. The three sensors used in this study have their respective penetration depth (Göller, 2012):

- R: up to 3 cm;
- D: up to 10 cm;

- P: up to 25 cm.

The microwave moisture system operates within a narrow frequency range around 2.45 GHz. This is the ISM radio band used for industrial, scientific and medical purposes (ITU, 2016). It is a convenient frequency to balance the depth penetration and sensitivity to changes in water content. The dielectric losses are greatest at approximately 20 GHz, but this would reduce the penetration depth to the mm range (Cole and Cole, 1941). As frequency decreases, the microwave reflectance becomes more dependent on conductivity, which is influenced by the presence of salts (Hussain, 2005; Lataste and Göller, 2018).

Each sensor head includes a set of calibrations for typical building materials where the reflection coefficient is transformed into a percent water content. While these are named for broad categories of materials (e.g. 'calcareous sandstone'), they were developed for one particular type of that material. In addition to these calibrations, a unitless moisture index (MI) can be used, which is a set of arbitrary units related more directly to the reflection coefficient. Both material-specific calibrations and the MI values are picked from the set of reflection coefficients generated within a frequency band around 2.45 GHz in a variety of ways specified by the manufacturer.

This microwave moisture system has been evaluated in laboratory and *in situ* with varying results. Blauer and Rousset decried strongly that the microwave system had "too big [sic] flaws to be used in … cultural heritage conservation" (Bläuer and Rousset, 2009, p. 32). They investigated how the microwave system monitored water vapour and liquid

water uptake in Swiss building stones with little success (Rousset and Bläuer, 2009). Their testing scenario is limited in two ways: 1) water in the vapour phase introduces small changes in the dielectric properties of air (Birnbaum and Chatterjee, 1952), and 2) monitoring capillary rise (which is characterised by strongly heterogenous distributions of water in a sample) introduces complex interactions with the aforementioned exponential loss pattern. Evaluations of brick have been more successful: the microwave system has shown good agreement with nuclear moisture density gauge readings but were noisier (Møller and Olsen, 2011). Gärtner, Plagge, and Sonntag produced very strong gravimetric calibrations from historic brick samples extracted from a German concert hall that were then applied to other parts of the same building (2010). However, we caution against the presentation of the calibrated sensor values they have employed: they have used the calibrations from four sensor heads to plot water contents at the maximum depths of penetration of each sensor. In reality, the moisture profile would be best represented by regression models of the four overlapping measurements, since they do not measure *at* a depth, but *to* a depth. More recently, unitless moisture indices measured on saturated and dry dolostone samples in layered configurations have agreed well with modelled microwave reflection coefficients (Kurik et al., 2017). In this research, the intermediate values (between dry and saturated states) were not examined.

6.2.4 Gravimetric calibration

6.2.4.1 General protocol

The two gravimetric calibration procedures (ambient drying vs isolated diffusion) differed in how the range of water contents was produced. Similar protocols were followed as part of each procedure. The tests were undertaken under laboratory conditions (18 to 22 ^{o}C and 40 to 60% RH). Mass measurements were taken with a balance capable of measuring up to 30 kg with a precision of $\pm$ 0.001 kg. The samples were oven-dried at 70 ^{o}C for 72 hours and weighed to obtain the dry mass. Samples were then immersed in distilled water for 72 hours and weighed to obtain the saturated[1] mass. For measurements taken immediately following the removal of samples from immersion, surface water was removed with an absorbent cloth.

In general, microwave fields are as wide as they are deep. To investigate the entire field of the P sensor, laboratory specimens would need to be at least 250 mm on each side, resulting in unwieldy samples weighing more than 30 kg each. Cubic samples of 150 mm in each dimension were selected as a compromise; it is presumed that the edge effects are negligible, since the dependence of microwave reflection decays exponentially with distance from the antenna.

Before each measurement, the mass of the sample was recorded to determine the water

[1] In this study we define the saturation mass as a *pseudo-saturated*, or reduced saturation state, ignoring the effects of air trapping (Gummerson, Hall and Hoff, 1980); see also (Hall and Hoff, 2012, p. 222).

content. The radar measurements comprised of 81 A-scans for each face, and were recorded for both a back wall interface of air and a 3 mm metal plate. The microwave measurements were taken at the centre of each face, with the sample placed on a large block of granite to minimise interference from edge and back-reflection effects. Each value was based on an average of three measurements.

6.2.4.2 Ambient drying procedure

This method, used as a comparison for the proposed calibration procedure, is a variation of the calibration protocol formalised by Eklund et al. (2013). The samples of stone were removed from immersion and monitored during 120 h of drying in ambient laboratory conditions. Drying was uninhibited for five faces but partially covered for the sixth face as the samples were placed on a metal grid. Measurements were taken on each of the six faces every 24 h.

6.2.4.3 Isolated diffusion procedure

This new method uses multiple samples of a geomaterial that are each set to a particular water contents including and between oven-dry and saturated states. After being removed from immersion, the mass of the samples was periodically monitored. Once they reached the desired average water content, they were sealed in layers of polyethylene with vapour-resistant tape roughly 2 mm thick. The samples were left for 168 h to ensure that water diffused before measurements were taken. The samples were stored in sealed states but

turned periodically (roughly every one to two weeks) to reduce gravitational effects.

One benefit of this procedure is that samples can be set to any range or subset water contents. In this study, five to six equally-spaced water contents ranging from oven-dry and saturated states were selected, depending on the stone type. If a sub-range of water contents was of particular interest, the procedure could be applied to these values instead of equally spaced water contents.

6.3 Theory/Calculation

This section introduces the theory that underpins the interactions between electromagnetic energy and porous media. Calculations of modelled dielectric constants and reflection coefficients in porous media systems are presented, which represent expected behaviour of the radar and microwave techniques, respectively, over a range of water contents.

Radar and microwaves are forms of electromagnetic energy governed by the same underlying principles. Models of how they should interact with porous media systems produce a reference of how the techniques should theoretically respond to different water contents in building stones. These can be compared to the device measurements to assess the effectiveness of the techniques and calibration procedures.

Electromagnetic waves travel through media depending on three properties: the electrical conductivity σ, the dielectric permittivity ε, and the magnetic permeability μ. In building stones, μ is equal to the permeability in free space since they are non-magnetic.

In the microwave frequency range, electromagnetic waves are influenced by both σ and ε and it is not possible to separate their effects. They are complex properties, the real and imaginary components denoted with prime $'$ and double prime $''$, respectively. A combined effective permittivity ε_e is derived from their summation (adapted from Laurens et al., 2005):

$$\begin{aligned}\varepsilon_e &= \varepsilon + \frac{\sigma}{j\omega} \\ &= (\varepsilon' - j\varepsilon'') + \frac{\sigma' + j\sigma''}{j\omega} \\ &= \left(\varepsilon' + \frac{\sigma''}{\omega}\right) - j\left(\varepsilon'' + \frac{\sigma'}{\omega}\right) \\ &= \varepsilon_e' - j\varepsilon_e''\end{aligned} \tag{6.2}$$

where the conductivity is divided by the imaginary number j and the angular frequency ω. Generally, permittivities are expressed relative to the permittivity of air ε_0 as ε_r, i.e.

$$\varepsilon_r = \frac{\varepsilon_e}{\varepsilon_0} = \frac{\varepsilon_e' - j\varepsilon_e''}{\varepsilon_0} = \varepsilon_r' - j\varepsilon_r'' \tag{6.3}$$

The real component ε_r' is the dielectric constant. The dielectric constant determines the wave speed in porous building materials, while the imaginary component represents absorption losses and affects the signal attenuation.

The dielectric constant is a bulk property. Many models have been developed for representing multi-phase systems (see Knoll, 1996; Martinez, Byrnes et al., 2001).

Recently, microwave reflections from porous building stones have been modelled (Kurik et al., 2017) with the two-phase mixed materials Maxwell Garnett formula (Garnett, 1904; Sihvola, 2000). However, the system is comprised of three phases: the solid mineral content, the liquid water content, and the vapour water/air mixture. To reflect this, a Lichtenecker-Rother mixing model (Lichtenecker and Rother, 1931) has been used:

$$\varepsilon_b^{\alpha} = \sum_i V_i \varepsilon_i^{\alpha} \tag{6.4}$$

where α is a 'geometrical' or constant shape factor; when $\alpha = 0.5$, the mixing model describes refractive mixing (Dobson et al., 1985). Among a number of mixing models, this model (with $\alpha = 0.5$) was shown to most closely match experimental data of Lundien (Lundien, 1966) and (Newton, 1977) (see Knoll, 1996). When this model was applied for wet soil by Birchak et al (Birchak et al., 1974) it included parameters for bound water: as this is negligible for the stones studied it has been omitted. We have defined a combined effective permittivity for the mineral-air combination ε'_m. Since we are only representing wave velocity, only the real component ε'_b of the bulk relative effective permittivity (the bulk dielectric constant) has been presented as:

$$\varepsilon'_{b,r} = \left[(1-f)\sqrt{\varepsilon'_{m,r}} + f\sqrt{\varepsilon'_{w,r}}\right]^2 \tag{6.5}$$

in which $\varepsilon'_{w,r}$ is the dielectric constant of fresh water ($\varepsilon'_{w,r} \approx 80$) and $\varepsilon'_{m,r}$ is the dielectric

constant of the combined solid-vapour phase material. At an oven-dry state $f \approx 0$, so Equation 6.5 simplifies to $\varepsilon'_{b,r} = \varepsilon'_{m,r}$, which can be determined from an appropriately-treated laboratory sample via Equation 6.1. Using the calculated value of $\varepsilon'_{b,r}$ the dielectric constant can be modelled for a given sample as a function of water content.

The bulk (or adjusted) dielectric constant of a multi-layered system can be represented using a parallel plate capacitor model (Zhao, 2015). The calculated dielectric constant from isolated diffusion was adjusted to account for the 2 mm thick layer of polyethylene between the sensor head and the sample surface:

$$\frac{1}{\varepsilon'_{r,adj}} = \frac{1}{\varepsilon'_{r,p}}\left[\frac{t_p}{t_p + t_b}\right] + \frac{1}{\varepsilon'_{r,b}}\left[\frac{t_b}{t_p + t_b}\right] \tag{6.6}$$

in which t represents the thickness of each layer and subscripts p and b represent the plastic and bulk layers, respectively.

How an electromagnetic wave will interact with an interface between regions of different dielectric properties is governed by the Fresnel equations – a broad set of principles describing the behaviour of light with different refractive indices n. By relating angles through Snell's law and assuming that the wave is entering the interface perpendicularly (i.e. $\theta_{\text{incident}} = \theta_{\text{reflected}} = \theta_{\text{refracted}} = 0$), $s-$ and $p-$polarisations are equal,

and the fraction of energy reflected can be represented by:

$$R = \left| \frac{n_2 - n_1}{n_2 + n_1} \right|^2 \tag{6.7}$$

By recognising that $n = cv^{-1}$ (and therefore $n = \sqrt{\varepsilon}$), this can be rewritten in terms of the relative permittivity, and used to model the reflection coefficient R. The transmission coefficient can similarly be determined from R, since $R + T = 1$. The scenario of an electromagnetic wave entering a building stone with $\varepsilon_{b,r}$ from ambient air $\varepsilon_{0,r}$ results in:

$$R = \left| \frac{\sqrt{\varepsilon_{b,r}} - \sqrt{\varepsilon_{0,r}}}{\sqrt{\varepsilon_{b,r}} + \sqrt{\varepsilon_{0,r}}} \right|^2 \tag{6.8}$$

in which $\varepsilon_{b,r}$ is the complex value, determined from the mixing model in Equation 6.4. As geomaterials are generally lossy dielectrics with a loss tangent $\tan\delta > 0.1 = \varepsilon_r'' / \varepsilon_r'$; when $\tan\delta > 0.1$ the contribution of the complex component of the effective permittivity to the reflection coefficient can be assumed to be constant over the realistic range of potential water contents in building stones.

This can be used to model the reflection and transmission coefficients of an electromagnetic wave over a range of water contents. The coefficients for layered media can be represented by a matrix product of the layers or determined sequentially (Hehl and Wesch, 1980; Mazilu, Miller and Donchev, 2001) or represented by a power series (Neas and Ohlídal, 2014). A simulation was produced in R (version 3.3.3) for this purpose, based on

the underlying mathematics in an archived online tool (Gallant, n.d.).

6.4 Results

Dielectric constants for dry samples (as determined with air- and metal-back measurements) are presented based on radar measurements (Section 6.4.1). These are used as the basis to model expected dielectric constants and reflection coefficients over a range of moisture contents for each stone type. These models are used as the comparative reference for evaluating calibrations of radar (Section 6.4.2) and microwave (Section 6.4.3) measurements, respectively.

6.4.1 Dry material dielectric constants

The dry dielectric constants ε'_b have been calculated with radar for three stone types (Table 6.3), by assuming $f = 0$ in Equation 6.5 as described in Section 6.3. These represent the dielectric constant of the combined solid-air mixture of given minerals and porosity. Locharbriggs sandstone has the lower dielectric constant of the three stone types studied partially due to its greater porosity and lower bulk density; the two limestones, Portland and Clipsham, have similar porosities and as a result, similar dielectric constants. It is important to note that the values presented in Table 6.3 were calculated based on different samples of each stone type (see Table 6.1), and errors might be introduced by natural variation in physical properties (e.g. heterogeneity). The material properties that influence

Table 6.3. Dielectric constants for three dry stone types (n=1) at 1.6 GHz calculated from radar travel times measured from two different calibration procedures.

	ε_r'			
	Air-back		Metal-back	
Stone	Ambient drying	Isolated diffusion	Ambient drying	Isolated diffusion
Portland	6.40	6.38	6.24	6.13
Clipsham	6.33	6.58	6.24	6.56
Locharbriggs	3.08	3.64	3.02	3.57

the dielectric constant of a material most significantly are its chemical composition and its density/structure (Nelson and Kraszewski, 1990); this is reflected by the relationship between the calculated dielectric constants and the bulk densities/effective porosities of the stone types (Table 6.1).

The calculated values of the dielectric constant are consistently lower for the metal-back measurements than those recorded with an air-back interface. Based on Equation 6.1, this implies a higher signal travel time. Additionally, the variation in dielectric constants between samples and back interfaces are small ($\Delta < 0.56$) compared to the differences induced by changes in water content. It is possible that the position of peaks within the A-scans has been influenced by the ringing reflections caused by the presence of metal. The air-back values for the dielectric constant were therefore considered to be more reliable and were used to build modelled values of dielectric constant and reflection coefficients over a range of water contents.

6.4.2 Radar calibrations

Values of the dielectric constant and the surface wave amplitude of the high resolution radar are more closely related to modelled values for the isolated diffusion method than the ambient drying method. Figure 6.2 demonstrates that values of the dielectric constant calculated from the ambient drying method are likely affected by an uneven distribution of moisture within the sample. This is represented by the parameters of linear regressions produced between the measured and modelled values of the dielectric constants (superimposed onto their respective subplots in Figure 6.2). Values of R^2 represent the linearity of the relationship, while m represents the slope. An m = 1 represent a 1:1 relationship between the values, while $m < 1$ and $m > 1$ represent under-measured and over-measured values, respectively. The R^2 for models produced from the isolated diffusion calibrations are consistently higher than their ambient drying counterparts, and have values of m closer to 1. In general, the m values of the isolated diffusion procedure are < 1, representing under-measurement.

At higher unsaturated water contents, values of ε_r' are lower than the modelled dielectric constants. This represents Stage I drying (Cooling, 1930; Scherer, 1990), in which the water content in the centre of the calibration sample has been reduced but the faces with evaporation remain psuedo-saturated with relatively constant flux. Since the radar measurements were taken at the centre of each face, the signal travel time is less than the

gravimetric value would imply. At lower non-zero water contents, the calibration samples are in Stage II drying, in which there is a steeper moisture gradient (i.e. retention) at depth. The travel times at the centre of each face pass through the moisture remaining at depth in the calibration sample, which does not reflect the overall lower gravimetric value influenced by lower water contents near edges. As the models were based on dry dielectric constants determined from the samples, the modelled dielectric constant will always intersect with the measured value at $f = 0$.

The calculated dielectric constants for Locharbriggs are more closely related to models with $\alpha = 0.4$ in Equation 6.5. It has been acknowledged that $\alpha > 0.5$ tends to result in an underestimation at higher water contents (Dobson et al., 1985; Knoll, 1996), a trend which is also observed for the calibration developed from ambient drying.

A similar comparison to dielectric constants can be drawn between measured surface wave amplitudes and transmission coefficients for the two calibration methods (Figure 6.3). The calibrations developed from isolated diffusion are consistent and more closely related to modelled transmission coefficients. The surface wave amplitudes are plotted against transmission waves as they are inversely proportional to the amount of reflection energy, i.e. proportional to transmitted energy. As with the measured dielectric constants, the heterogeneous distribution of moisture within the samples causes an under-measurement at higher water contents and an over-measurement at lower water contents (compared to gravimetry). The underestimation at higher unsaturated water contents is less prevalent

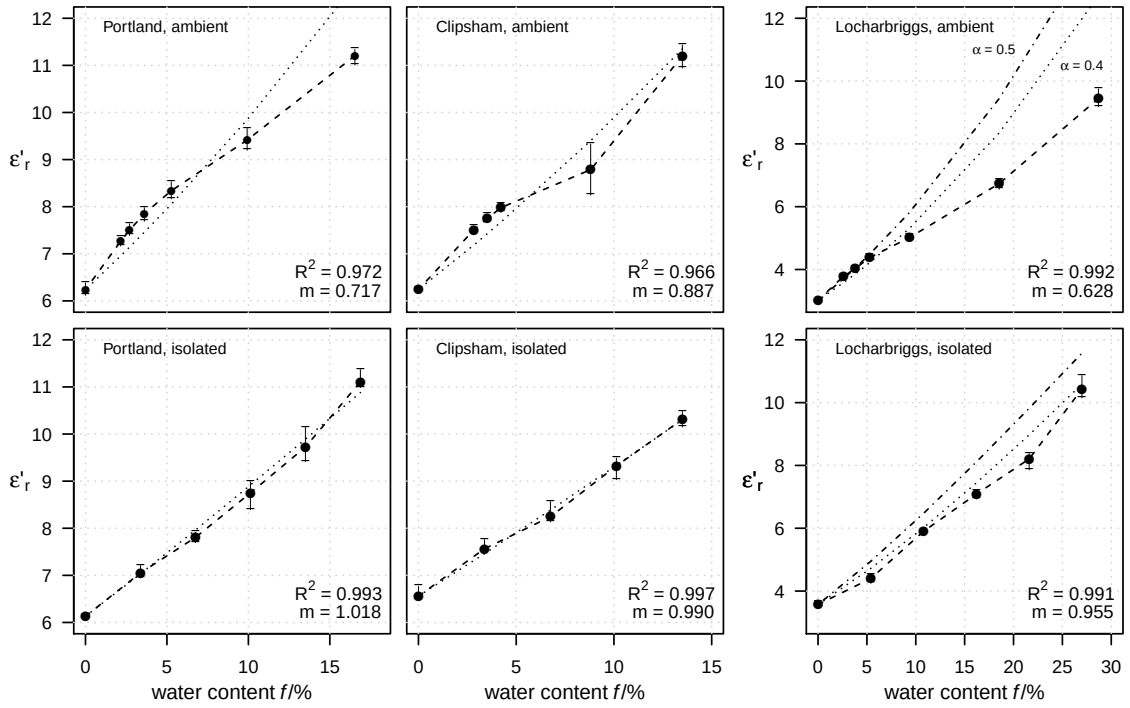

Figure 6.2. Dielectric constants for three UK building stones at 1.6 GHz over the ambient saturation range of water contents, as calculated from radar measurements taken using two calibration procedures. Dotted lines are modelled dielectric permittivities based on the mixing model in Equation 6.4. Vertical bars represent the range of measurements taken on each face of the sample. The same line types are used in both figures presenting results for Locharbriggs to represent values of α.

for the Portland calibration sample than that observed for the Clipsham and Locharbriggs sample. The deviations from the modelled transmission coefficients are more drastic for the surface wave amplitudes than the dielectric constants, except for the higher unsaturated water contents of the Portland calibration sample. Slopes of the linear regression results m are not presented in Figure 6.3 as these are less meaningful for the scaled transmission coefficients.

This deviation from modelled behaviour is likely caused by the non-linear interactions between distributions of moisture and reflection/transmission of electromagnetic energy that can cause unintuitive 'inversion' of the coefficients. These principle can be demon-

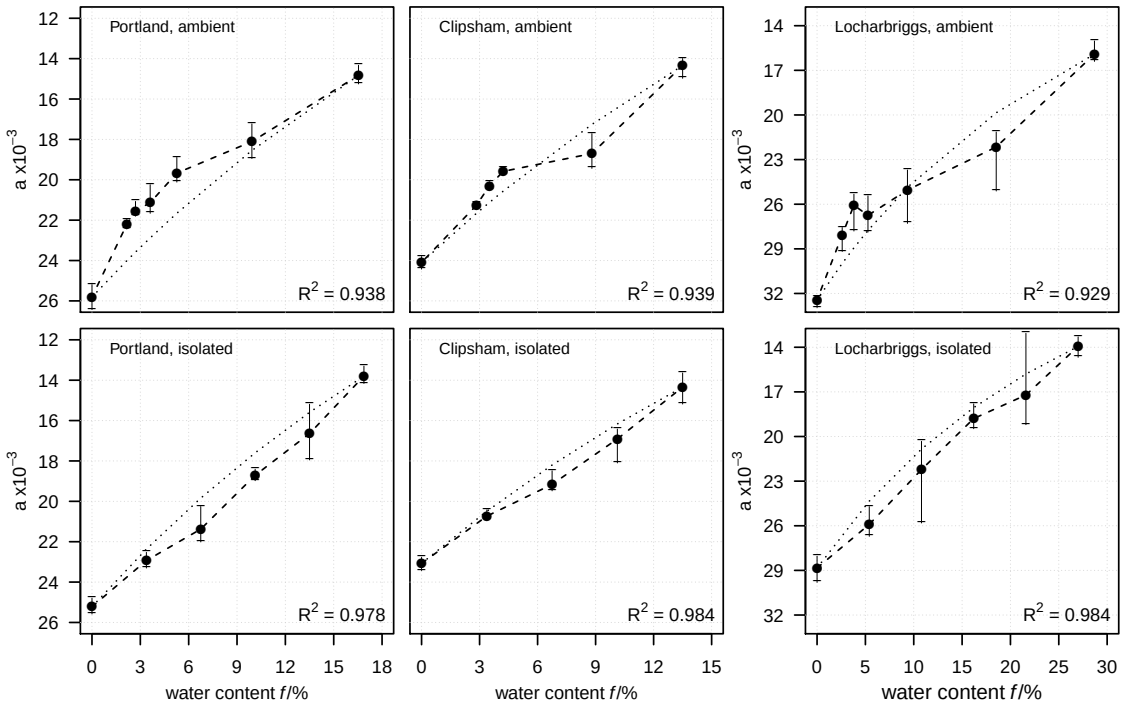

Figure 6.3. Surface wave amplitude for three stone types at 1.6 GHz over the ambient saturation range of water contents, as calculated from radar measurements taken on two calibration procedures. Dotted lines are modelled transmission coefficients based on the mixing model in Equation 6.4 assuming a loss tangent $\tan\delta = 0.1$, scaled between the extrema of the amplitudes. Vertical bars represent the range of measurements taken on each face of the sample.

strated by simple cases of two-layer systems of porous media at different water contents. Figure 6.4 shows the modelled reflection and transmission coefficients for a system with a total thickness of 150 mm and varying thickness of the upper layer. The solid line shows that, for a lower layer with a water content $f = 0$, the reflection coefficient can be reduced below the coefficient of a homogenous dry sample if there is a thin upper layer of water. Similarly, a lower layer with $f = 0.2$ covered by a thin dry upper layer can have a reflection coefficient amplified higher than a homogenous system with a higher water content. An amplifying inversion in the reflection coefficient is equivalent to a reducing inversion in the transmission coefficient, and vice versa. This inversion effect is likely exacerbating

the aforementioned under- and over-estimations caused by an uneven distribution of water within the calibration samples. This is represented by more significant deviations observed in the surface wave amplitude compared with the modelled transmission coefficients.

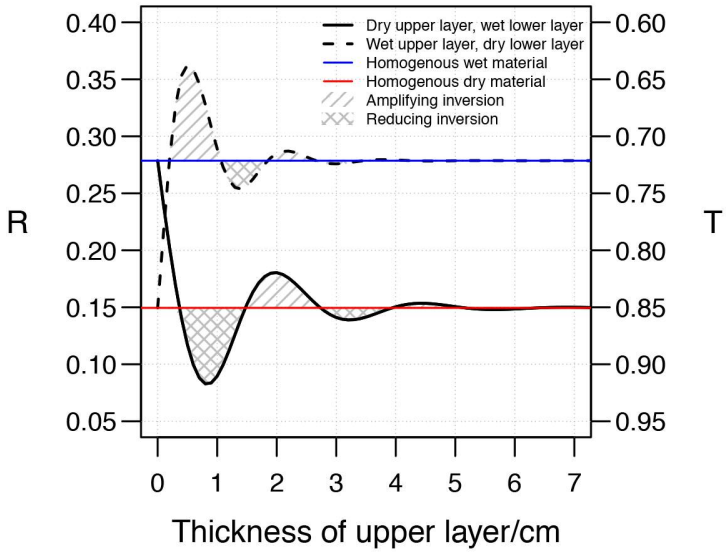

Figure 6.4. Modelled reflection and transmission coefficients, R and T respectively, for two configurations of layered systems of a porous materials with $\varepsilon_r = 6.3 - 0.63\text{j}$ (i.e. $\tan\delta = 0.1$). This demonstrates amplifying and reducing inversion of R for homogenous dry and wet ($f = 0.20$) geomaterials.

6.4.2.1 Comparison of radar features for air-back and metal-back measurements

The radar features calculated over the range of water contents were very similar for a back interface of both metal and air. This was assessed with linear regression models between the dielectric constants and first wave amplitudes determined for the two calibration methods and type of back interface (Table 6.4). The models had regression coefficients $R^2 > 0.99$, except the dielectric constant determined by isolated diffusion for Locharbriggs ($R^2 = 0.908$) and the surface wave amplitude for Portland under isolated diffusion conditions

Table 6.4. Linear regression models for the calibrations developed from measurements taken with a metal back as a function of air-back measurements.

	Ambient drying			Isolated diffusion		
	Portland	Clipsham	Locharbriggs	Portland	Clipsham	Locharbriggs
Dielectric constants						
R^2	0.999	0.997	0.999	0.997	1.000	0.908
Intercept	-0.046	0.356	0.043	-0.266	0.063	-0.672
Slope	0.990	0.948	0.987	1.026	0.987	1.051
Surface wave amplitudes						
R^2	0.994	0.997	0.992	0.855	1.00	1.00
Intercept	-872	-768	85.0	-973	295	351
Slope	1.02	1.03	0.978	1.05	0.982	0.982

($R^2 = 0.855$). The regression model slopes were 1 ± 0.05, representing a variability between measured parameters of less than 5%.

6.4.3 Microwave calibrations

The microwave sensor indices determined from isolated diffusion are generally more similar to the modelled reflection coefficients than those determined from the ambient calibration procedure for Portland and Clipsham samples. For the Locharbriggs, the correlation coefficients between the measured and modelled values are higher for the ambient drying procedure. Table 6.5 presents the linear regression parameters between the measured indices and the modelled reflection coefficients; slopes of the linear regression results m are not presented as these are less meaningful for the scaled reflection coefficients.

The combined effect of uneven distributions of water and inversion on sensor indices measured during ambient drying can be seen in Figure 6.5. As the indices are proportional to the reflection coefficients, the over- and under-estimations are transposed from those seen in the surface wave amplitudes and transmission coefficients: the higher unsaturated

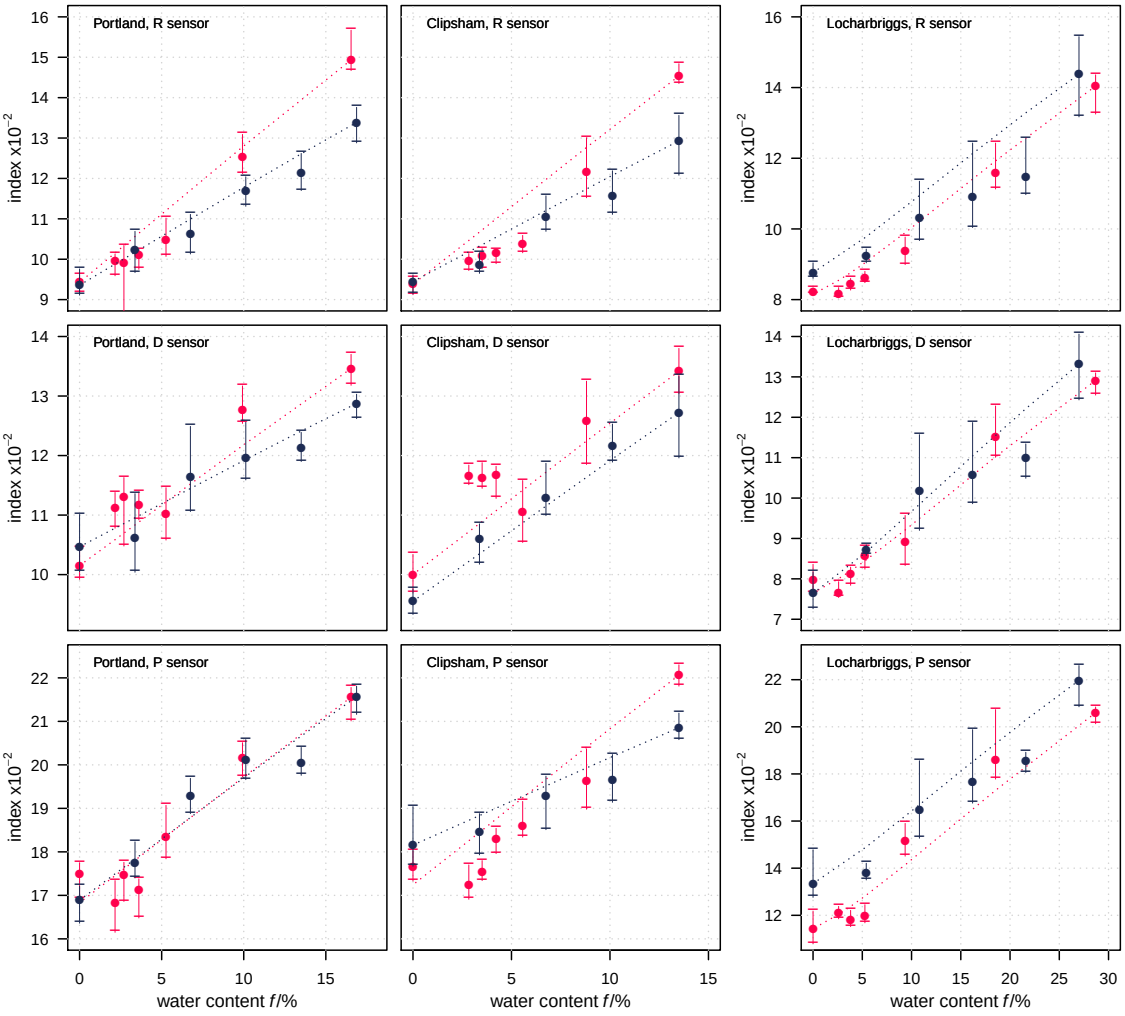

Figure 6.5. Microwave sensor indices for three stone types over the ambient saturation range of water contents for ambient drying (red) and isolated diffusion (blue). Dotted lines are modelled reflection coefficients based on the mixing model in Equation 6.4 assuming a loss tangent $\tan\delta = 0.1$, scaled between the extrema of the amplitudes. Vertical bars represent the range of measurements taken on each face of the sample.

water contents for some stone types and sensors are higher than a 1:1 proportional with the modelled coefficients: at lower non-zero water contents, the indices are below proportionality to reflection coefficients.

In some cases, proportionality to the modelled reflection coefficients dips below the homogenous dry calibration indices, e.g. Locharbriggs for the R and D sensor, and the two

Table 6.5. Linear regression model R^2 values for the measured microwave sensor indices as a function of modelled reflection coefficients *R* normalised to the extrema of the index measured for each sensor and stone type.

	Portland		Clipsham		Locharbriggs	
Microwave sensor	Ambient	Isolated	Ambient	Isolated	Ambient	Isolated
R	0.982	0.981	0.947	0.969	0.991	0.888
D	0.917	0.952	0.830	0.991	0.978	0.938
P	0.917	0.948	0.903	0.953	0.963	0.954

limestone types for the P sensor. There is also a corresponding strong amplifying inversion for the D sensor at non-zero lower water contents. As the depth penetration of the D sensor is between that of the R and P sensors, these corresponding inversions could be caused by higher moisture levels at mid-depths within the sample; unlike the examples presented in Figure 6.4, these would be represented by a scenario in which there were three layers of alternating lower, higher, and lower water contents respectively.

6.5 Discussion

6.5.1 Calibration procedures

In contrast with existing literature (Bläuer and Rousset, 2009; Rousset and Bläuer, 2009; Møller and Olsen, 2011), both ambient drying and isolated diffusion calibration procedures yielded high quality calibration curves that related well to gravimetry over the full range of water contents. The isolated diffusion procedure yielded more consistent calibration curves more closely related to modelled electromagnetic parameters.

Curves developed from the ambient drying procedure are impacted by a number of

factors. Most importantly, the distribution of moisture during the drying process meant that radar and microwave measurements taken at the centre of each face were not indicative of the gravimetry. This was exacerbated by the non-linear interactions of the electromagnetic waves with the distributions of moisture that can cause inversions of the signal reflection and transmission. It is likely that these effects are especially strong for the sample size and dimensions used, which was determined by the field of detection of the microwave measurement principle. The samples used herein have a volume-to-surface area ratio = 25. If samples have a smaller ratio, e.g. dimensions of 100 mm $\times$ 100 mm $\times$ 75 mm has a ratio $\approx$ 4 (Eklund et al., 2013), the effects of moisture distribution and inversion are likely less pronounced for geophysical measurement techniques such as capacitance.

Ambient drying measurements taken at equal time intervals (24 h, in the procedure used herein) results in fewer measurements at higher water contents and a concentration of measurements at lower water contents. Increasing the measurement frequency for the beginning of the drying process is limited by the time required to collect the measurements: the time interval between measurements must be sufficiently longer than the time required to collect data with a set of measurement techniques so that the differences between gravimetric comparisons are valid for the measurement period.

The isolated diffusion procedure shows significant promise for producing calibrations relevant to cultural heritage and other non-destructive investigations of geomaterials. If measurements in the field are taken over a plastic grid as a spatial reference, the data would

be more similar to calibration curves developed from the isolated diffusion procedure, which also introduces a plastic barrier between sensor and sample. The dielectric constant of most synthetic polymers is similar to that of polyethylene. If the calibrations and measurements were done with plastic grids of a different thickness, the parallel plate model (Equation 6.6) could be adapted to transform the measured readings into parameters equivalent with those of the calibration.

An important outcome of the calibrations developed for both radar features is that material heterogeneity between samples in the isolated diffusion method is negligible compared to the influence of changes in water content, which makes the isolated diffusion calibration technique viable. An important outcome of this result for heritage applications is that only one specimen is needed, which could support developing calibrations for scenarios in which sampling of materials is difficult. As the samples are in a state of near-equilibrium, the results of the isolated diffusion procedure are not impacted by time-dependent factors such as moisture loss–as is the case for ambient drying. It also facilitates inter-comparison of measurement techniques and the potential effect of environmental factors such as temperature and relative humidity. However, other calibration procedures, such as ambient drying, are still relevant and necessary for techniques that require direct contact with the sample surface, such as electrical resistance. Although it would be possible to remove the covering and re-seal the sample after the measurement, this would require more time and effort, and could affect the accuracy of future calibrations if moisture is

evaporated during the process.

Radar parameters calculated from air-back and metal-back measurements are comparable. This is important for field measurements where a metal-back may be necessary to produce a sufficiently strong back-wall reflection that can be detected, especially important in constructions with walls or structural elements with thickness greater than the calibration samples used (150 mm).

6.5.2 Comparison of radar and microwave measurements

The radar output—measured dielectric constants and surface wave amplitude—was more consistently related to the gravimetric calibrations than the output from the microwave device. It is likely that the radar is more consistently calibrated and related to models due to more focused spatial measurement scale involved in its measurement principle. The spatial capture of a single radar measurement within an A-scan is based on the separation of the signal producing and receiving component which is quite small in a 1.6 GHz antenna. In contrast, the microwave sensors are field-based, with a non-discrete sensing volume– albeit decreasing with distance from the applicator. It is plausible that the microwave sensing technique is therefore more sensitive to external influences in the periphery of the measurement area.

Despite this, the microwave measurement system can be a useful tool in building surveying. It can be used to provide representations of moisture variation within a building

fabric that are immediately interpretable on site. Measurements can be taken quickly over a flexible and large spatial scale as a range-finder method. Following this assessment, radar measurements could be taken for locations of specific interest. This is time-efficient, since the radar measurements typically involve the installation of a measurement grid or other system of alignment. The radar measurements requires further processing to produce numerical representations of the measured parameters, which means that results are not ready for interpretation while on site.

Importantly, the raw outputs from the two devices are not directly comparable. This demonstrates one utility of the calibration procedures: to use absolute water contents (as measured by gravimetry) as a common reference point to compare between the techniques. When comparing between radar and microwave measurements, it is important to remember proportionality. For example, the dielectric constants (derived from measured travel times) will be proportional to the microwave measurements. In contrast, any comparison or synthesis with the surface wave amplitude should involve an inverse transformation of one of the parameters, since they are inversely proportional.

The calibrations developed demonstrate that the calculated and measured electromagnetic properties are not directly comparable between stone types. This is especially apparent as a contrast between the two limestones and the Locharbriggs sandstone. The permittivities of these materials are greatly dependent on their mineral composition and porosity, which also manifest as significant contrasts in the dielectric constant, surface wave

amplitudes, and reflection/transmission coefficients. Natural building stones of similar mineralogies and porosities would therefore exhibit similar electromagnetic behaviour, i.e. parameters from non-destructive geophysical techniques would be similar. It is possible to predict what the dielectric constant–as the basis for most electromagnetic properties–will be, based on a given mineral composition and porosity (Martinez, Byrnes et al., 2001). This would enable an estimation of the ranges of non-destructive measurement techniques, based on prior knowledge of the range of other geomaterials.

6.6 Conclusion

Two calibration procedures based on ambient drying and isolated diffusion have produced calibration curves for radar and microwave techniques that relate well to gravimetry for three typical building stones in the UK. Both procedures produced comparable calibrations with air-back and metal-back interfaces. The isolated diffusion relates more closely to the modelled interactions of electromagnetic waves with porous media systems. The isolated diffusion procedure reduces the impact of uneven distribution of moisture within the samples and the potential for inversions of reflection and transmission. Thus, it is a viable low cost alternative for gravimetric calibration that provides robust gravimetric calibration. This procedure also more closely reflects the qualities of *in situ* measurements if they are taken over a plastic grid for alignment, consistency, and surface protection.

Ambient drying remains a valid calibration technique that is less time and resource

intensive than isolated diffusion. However, the calibration results for this procedure demonstrate the challenges of interpreting microwave moisture results when the distribution of moisture is uneven in a sample or *in situ* measurement. This procedure is especially relevant for measurement techniques that require direct surface contact or have smaller fields of detection. In the latter case, calibration curves can be developed on samples with smaller volume-to-surface area ratios which will be less impacted by uneven distributions of water within the samples.

These results demonstrate the utility of gravimetric calibrations for enabling comparability between measurement techniques and geomaterials. From these calibrations, mathematical relationships between sensor output and gravimetry can be developed. They enable a deeper understanding of the characteristic curves for different measurement devices and types of geomaterials, which supports accurate interpretation of survey information when it is not possible to develop material-specific calibrations.

7 | Moisture monitoring of stone masonry: a comparison of microwave and radar on a granite wall and a sandstone tower

"Technology changes all the time;
human nature, hardly ever."

– EVGENY MOROZOV (2011, p. 315)

This chapter is drafted with the intention of submission as a peer-reviewed research article under the same title with the following co-authorship: Orr, S. A., L. Fusade, M. Young, D. Stelfox, A. Leslie, J. Curran and H. Viles.

Abstract

Water is a fundamental control on the deterioration of historic stone masonry, of which wind-driven rain (WDR) is an important source in the UK. Non-destructive testing methods for moisture measurement can characterise the response of masonry to short (but intense) periods of wind-driven rain. An important part of this response is how masonry functions as a system of stone units and mortar joints, in which mortar can act as a conduit for moisture. While non-destructive techniques are common in moisture surveying of built heritage, there are no agreed best practice methods for collection, handling, and visual representation of data. This study explores the comparative advantages of microwave and radar measurements in two field experiments of exposure to short (but intense) simulated wind-driven rain exposure to demonstrate when and how they are most effectively employed. A novel method of representing data as percentiles is explored to facilitate effective communication of moisture measurements. In the case of the granite wall (e.g. with components of strongly contrasting hygric properties), microwave and radar provided similar information. The average travel time of the radar signal (from the back wall reflection) demonstrated that radar can non-destructively identify water penetration through mortar joints. In the sandstone tower, the microwave measurements were able to clearly identify four different moisture regimes as a result of different intensities of WDR exposure. The radar measurements were suited to identifying distinctions between localised moisture contents within masonry units and mortar joints, which characterised how the masonry was functioning as a holistic system. The measurements on both the granite wall and the sandstone tower demonstrated that the radar is influenced by environmental conditions which influence surface condensation and equilibrium moisture contents. Representing the measurements as percentiles improved visual representation of measurements with colour scales and minimised potential skewing of normalisation and scales from extreme values/outliers. This paper demonstrates that both microwave and radar techniques can be useful for monitoring moisture in stone masonry systems. Material characteristics of the masonry system and the objective(s) of the investigation should be considered during selection of the appropriate technique(s).

7.1 Introduction

Water is an integral component of direct and indirect weathering processes of historic building materials such as stone, which can cause deterioration of masonry (Hall et al., 2011). Wind-driven rain (WDR) is a significant source of moisture for buildings in the UK and other parts of Northern Europe (Sabbioni, Brimblecombe and Cassar, 2010, pp. 14–15), exposure to which is expected to become more severe and seasonally polarised over the 21st century as a result of climate change (Orr et al., 2018b; Chapter 5).

Non-destructive techniques can be an important part of managing moisture in built cultural heritage. These are indirect, non-invasive methods that use physical properties as proxies for the presence of water on and within porous building materials. The spatial capture/resolution and measurement principle of a technique determine how and when it is best applied in monitoring moisture regimes.

How data from a moisture survey is handled and visually represented depends on the objectives of the investigation. Representing data over space and/or time are two common forms of presentation; however, these aspects of communicating results are not formalised or explored widely in the current state-of-the-art of measuring moisture in buildings and building materials (Camuffo, 2018; Nilsson, 2018; Rosina et al., 2018).

Moisture-sensitive non-destructive methods are typically used to characterise the relative distribution of water across an entire façade (Pinchin, 2008). The unique systemic

qualities of stone masonry (units and joints) has either been considered negligible, i.e. measurements are interpolated across joints and masonry units, e.g. (Sass and Viles, 2010a, 2010b; Martínez-Garrido et al., 2018), or the joints are omitted from the survey, i.e. measurements are taken on individual masonry units alone (Válek et al., 2010). This disregards the potential benefit of capitalising on the spatial geometries of non-destructive techniques to assess the dynamic behaviour of masonry *systems*, as represented by interactions between masonry units and joints.

This study evaluates the performance of microwave sensors and radar for monitoring the movement of water in masonry constructions exposed to wind-driven rain. Scenarios of simulated short (but intense) wind-driven spells were developed for two contexts: a purpose-built wall of granite and lime mortar, and part of a nineteenth century sandstone tower that has been exposed to approximately 150 years of moisture-related weathering. A comparison of the spatial and temporal dynamics of the drying of these two constructions enables a discussion of their comparative advantages for characterising the behaviour of masonry systems exposed to wind-driven rain. The benefits and trade-offs of a proposed new method of representing measurements as percentiles are explored, as well as the combined benefit of using temporal and spatial graphical forms.

7.2 Material and methods

7.2.1 Experimental design

To assess the response of the masonry constructions to short (but intense) wind-driven rain spells realistic characteristics of rain (amount and intensity) and wind (speed and direction) were simulated in two field experiments (Table 7.1). Microwave sensors and radar were used to record moisture levels before and following the simulated wind-driven rain. The first experiment focused on a purpose-built test wall of granite masonry units located in Oxford, UK designed to reflect the wealth of built heritage in southwest England where very low porosity masonry units (e.g. granite) are surrounded by much more porous mortar joints and exposed to high amounts of driving rain. In this scenario, the mortar joints should experience high rates of moisture penetration. The second field experiment focused on the base of a pinnacle of a nineteenth century tower in Edinburgh constructed from sandstone which has experienced moisture-related weathering for over 150 years. This was accessed with scaffolding during a conservation project.

Both experiments are representative of conditions in regions in the UK that currently experience high wind-driven rain exposure (Orr and Viles, 2018a; Chapter 4) and are expected to suffer intensified WDR by the end of the 21st century (Orr et al., 2018b; Chapter 5). The experiments were designed to simulate characteristic durations and

Table 7.1. Experimental design of simulated WDR exposure to compare microwave and radar moisture measurement techniques.

Experiment site	Construction materials	Situation	Study area	Measurement spacing
Oxford	Granite and NHL lime mortar	Behaviour of masonry (units and joints) with strongly contrasting hygric properties	55 cm x 55 cm	5 cm grid (radar), 5 cm point spacing (microwave sensor)
Edinburgh				
Scenario A	Sandstone and NHL lime mortar	Behaviour of masonry (units and joints) with more similar hygric properties; four intensities of WDR spells	80 cm x 80 cm, including four zones of 30 cm x 30 cm	5 cm grid (radar), 10 cm point spacing (microwave sensor)
Scenario B	Sandstone, NHL lime mortar but with existing fragments of mortar of unknown composition	Behaviour of masonry (units and joints) with more similar hygric properties; behaviour of mortar joints in managing heavy WDR intensity	80 cm x 80 cm, including four zones of 30 cm x 30 cm	5 cm grid (radar), 10 cm point spacing (microwave sensor)

volumes of water in intense WDR events. The volume and duration of wind-driven rain applied was determined using a semi-empirical representation of WDR spells (ISO, 2009) based on hourly meteorological data obtained from the UK Met Office for a site in Devon (51.0886, -4.14743) from 2005 to 2015 (UK Met Office, 2006a, 2006b). The Devon climate was selected to reproduce a wind-driven rain exposure relevant to the purpose-built granite wall, which is a prevalent building material (constructed with lime mortar) in traditional buildings in that region. Recent work has demonstrated inaccuracies in a percentile-based approach when estimating extreme WDR events (Orr and Viles, 2018a; Chapter 4). For this reason, extreme value analysis (Pérez-Bella et al., 2012; Orr and Viles, 2018a; the latter is reprinted in Chapter 4) was employed. The most severe WDR spell lasting 5 h or less likely to occur once in any five-year period for a south-westerly oriented wall was 10.32 L m^{-2}. Similar short (but intense) spells have also been recorded in eastern Scotland. This exposure quantity was used to as a guideline for the simulated exposure, which were distributed over a three hour rain spell.

(a) (b)

Figure 7.1. The two masonry constructions evaluated in this study. (a) The purpose built granite wall; (b) New College, Edinburgh; the area circled in red represents the tower on which evaluations were undertaken. The latter is adapted from 'New College on the Mound, Edinburgh' by Kim Traynor, Wikimedia, CC BY-SA 3.0.

7.2.2 Oxford experiment: purpose-built granite test wall

A purpose-built test wall of granite and NHL (lime) mortar was constructed outside in a sheltered area in central Oxford to test the behaviour of masonry (units and joints) with strongly contrasting hygric properties. The test wall is 660 mm high, 620 mm wide and 150 mm thick and constructed out of Cornish granite blocks with a pointed dressing (see Figure 7.1). The units are embedded with joints approximately 2 cm wide of an NHL 3.5 lime mortar produced with quartz sand and calcitic aggregate. After construction, the wall was left to cure in ambient spring conditions in Oxford, UK for approximately 90 days. The wall was constructed and cured under a cover to minimise the impact of precipitation during curing and testing.

On the granite test wall, WDR was simulated using tap water applied through a full cone low-flow nozzle with a uniform spray distribution. A stop-valve timer released 15 s of simulated WDR every three minutes for 3.25 h, resulting in a total of 10.35 L m^{-2} of simulated WDR on the test wall façade.

7.2.3 Edinburgh experiment: New College, Edinburgh

Two scenarios were executed in the Edinburgh experiment, to evaluate the behaviour of masonry composed of units and joints with similar hygric properties. In Scenario A, three different levels of WDR intensity were simulated, while Scenario B evaluated the role of mortar joints in managing heavy WDR intensity (see Figure 7.2 and Table 7.1). Both scenarios included a control region comprised of masonry units and mortar units without WDR exposure.

New College (see Figure 7.1) is located in central Edinburgh, Scotland. It is the University of Edinburgh's School of Divinity, the current building of which was constructed in 1846 (Brown, 1996) primarily in Binny Sandstone; Binny is a Lower Carboniferous sandstone from Scotland (Craig, 1892). Despite Edinburgh's proximity to Britain's east coast, prevailing winds originate from the southwest (Iowa Environmental Mesonet, 2018). The eastern Scottish climate is characterised by moderate to heavy annual rainfall distributed throughout the year. New College is situated on an exposed site on the south side of the crag and tail formation crowned by Edinburgh Castle. This results in increased

intensity and quantity of wind-driven rain.

During the experiments, the New College building was undergoing stone replacement and mortar repointing due to significant moisture-related weathering. Wind-driven rain simulations were carried out on a pinnacle of the west tower, due to its exposed location relative to other parts of the building. The pinnacle is composed of large masonry units (30 cm in their shortest dimension), and had been partially repointed with an NHL lime mortar shortly before the experiments commenced. Some joints were not repointed; the pre-existing mortar is of an unknown composition and age.

During testing the pinnacle was sheltered from direct solar irradiation and rainfall by plastic netting installed for the maintenance and restoration work. WDR was simulated with a backpack sprayer pressurised to 2 bar with a hand-pump, which delivered water with a low through-put full-cone brass nozzle. The objectives of each scenario necessitated different configurations of WDR exposure and mortar joints (Table 7.2). The zones were studied simultaneously, to reduce the potential impact of environmental variability of rates of absorption and evaporation.

7.2.3.1 Monitoring

In both experiments, measurements were taken before the simulated WDR exposure and repeated at intervals afterwards. Measurements were taken at 5 or 10 cm grid/point spacing (see Table 7.1) with a microwave moisture device and a high resolution radar.

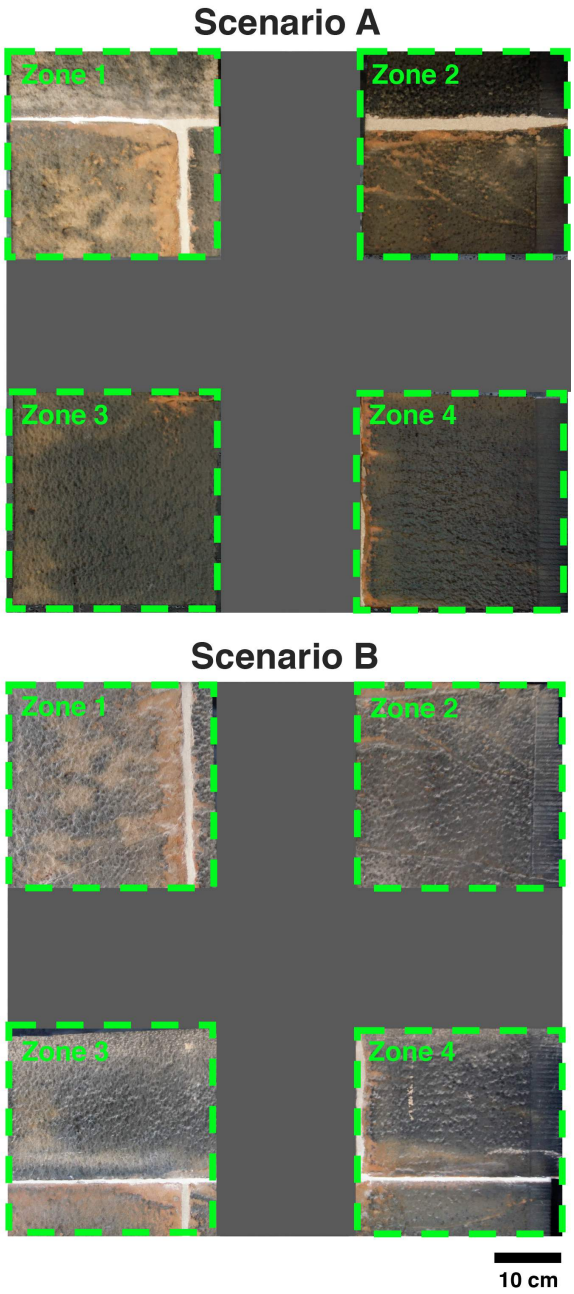

Figure 7.2. The measurement areas for the Edinburgh experiment, demonstrating the four zones in Scenario A and Scenario B. The cream-coloured/lighter portions are mortar joints and orange and blackened regions are the masonry units. The grey 'cross' represents 'no data' because of an impervious barrier applied directly to the façade surface between the zones which remained on the surface for the duration of the monitored drying.

Both techniques are non-invasive and have negligible influence from salinity due to their operating frequencies. For the Edinburgh experiment, measurements were also taken at

Table 7.2. Experimental design of the two scenarios designed for simulated WDR exposure of the sandstone tower.

Scenario	Motivation	Zone	Joints	WDR classification	WDR quantity (over 3 h) L m^{-2}
A	Investigation of four intensities of WDR spells	1	horizontal and vertical	control	0
		2	horizontal	light	2.5
		3	None	medium	5.0
		4	None	heavy	10
B	Investigation of different mortar joint configurations	1	vertical	control	0
		2	none	heavy	10
		3	vertical and horizontal	heavy	
		4	horizontal	heavy	10

hourly intervals during the simulated WDR spell to monitor moisture ingress. Temperature and relative humidity of the local environment and close to the masonry surface were recorded with iButtons hygrochrones and a weather station (Vaisala, Vantaa, FI).

MOIST350B

Produced by hf sensor, Leipzig, DE: the MOIST350B is a device that produces microwave fields of varying geometry sensitive to different depths (Göller, 2006, 2012). The recorded reflection values are based on average properties within the measurement area, but with decreasing sensitivity to moisture further away from the sensor (i.e. the surface). The sensors have been found to calibrate well over a range of water contents for building stones (Chapter 6). Two sensors were employed: one penetrating up to 2-3 cm (R1M) and another up to 20-30 cm (PM).

High resolution radar

Produced by Malå Geosciences, Malå, SE: a radar signal is produced by a 1.6 GHz antenna coupled with a receiver that measures the travel time of the signal. Changes in material properties cause large reflections within the signal (Lai, Dérobert and Annan, 2018). The travel time between reflections can be converted into an average velocity for a particular point within a construction, which under certain assumptions can be used to calculate the dielectric constant: a physical property that is strongly influenced by water content (Camuffo and Bertolin, 2012). Additionally, the amplitude of the surface (direct) wave is strongly dependent on water content and can be used as a proxy for near-surface water contents (Lai et al., 2014). Both radar characteristics have been shown to calibrate well over a range of moisture contents for porous building materials (Chapter 6) and are investigated here.

7.2.4 Percentile representation of measurements

How moisture measurement data are handled and visually represented is primarily driven by: (1) the spatial and temporal scale(s) used, and (2) the survey aim(s). Spatially, most applications of non-destructive techniques to monitor moisture have been at a façade (several m^2) scale (e.g. Martínez-Garrido et al., 2018). In these cases, the visualisation typically uses a scale of colour/shade (i.e. heat map) based on a uniform distribution

to represent variation of moisture levels. While this can be useful for communicating moisture distributions, colour scales are one of the least accurately used graphical forms (Cleveland and McGill, 1985; Carswell, 1992). Mapping non-uniformly distributed measurements onto a uniformly-distributed colour scale reduces the graphical resolution. This is especially apparent when measurements are skewed, e.g. if measurements are polarised to extremes. This skew also affects scatter plots of measurements over time, since a linear x-axis scale is typically used.

To improve upon this aspect of visual representation measurements can be converted to percentiles. A percentile is assigned to each measurement by ranking them in order of magnitude, from which a fraction or percentage of values for which a number is greater can be determined (the percentile). Representing measurements with percentiles has several benefits, including:

- equal resolution across the range of measurement values, regardless of the distribution, e.g. they will not be impacted by clusters or polarised data;
- reduced impact of extreme values/outliers on normalisation or scale limits;
- colour bins can be assigned to equally-sized percentile ranges, i.e. each colour represents an equal fraction of all measurements within the set.

The same percentiles can be used in other, more accurately used, forms of graphical representations, e.g. those based on positions with common aligned scales, such as multiple

bar charts or box plots with a single scale (Friel, Curcio and Bright, 2001), facilitating comparison between multiple visual representation formats of moisture measurements.

In this study both measurement principles are proportional to water contents, i.e. higher percentiles imply higher moisture levels. The percentile for each measurement has been determined from all measurements taken over the spatial and temporal range of each experiment/scenario. Since the measured variables have different units and ranges, the percentile representations have been compared to values normalised between 0 and 1. These visualisations are provided in Appendix B, and referred to at the relevant points in the text. As this normalisation would not impact the distribution of the measurement data, it can be used to evaluate how percentile representation changes the data visualisation, while also enabling comparison between different techniques and variables. Normalised values have been used in NDT applications, especially for evaluating multiple techniques/variables (e.g. Völker and Shokouhi, 2015b).

7.3 Results

This study explores the application of microwave and radar measurements in two types of constructions: a granite wall and a sandstone tower. Benefits and trade-offs of spatial and temporal graphical forms and percentile representation in each situation are discussed.

7.3.1 Oxford experiment

7.3.1.1 Comparison of microwave and radar: masonry with strongly contrasting component physical properties

The experiment on the granite wall demonstrates that the microwave near-surface sensor (R1M) and the radar direct (surface) wave amplitude produce similar data in this scenario. Despite using percentile representation, the spatial colour plots (Figure 7.3) have limited utility due to the high visual contrast between the granite and joints.

While a general comparison of moisture levels is possible, e.g. by 168 h the microwave measurements (Figure 7.3a,c) indicate more water has left joints towards the top of the wall than the bottom, shown by the lighter shading here, these spatial representations do not provide information on *rates* of moisture loss over time or comparisons of water contents of specific joints. However, spatial plots based on normalised measurements provide less information on localised variation than percentile representation due to an even greater polarisation between the granite and joints (Appendix B, Figure B.1).

Representing the measurements for regions of interest over time in barplots allows for quantitative and semi-quantitative comparison (Figure 7.4). Several observations are made:

- The surface microwave sensor (R1M) and the radar direct wave amplitude provide similar information (Figure 7.4b,c), e.g. the moisture levels over time exhibit similar behaviour;

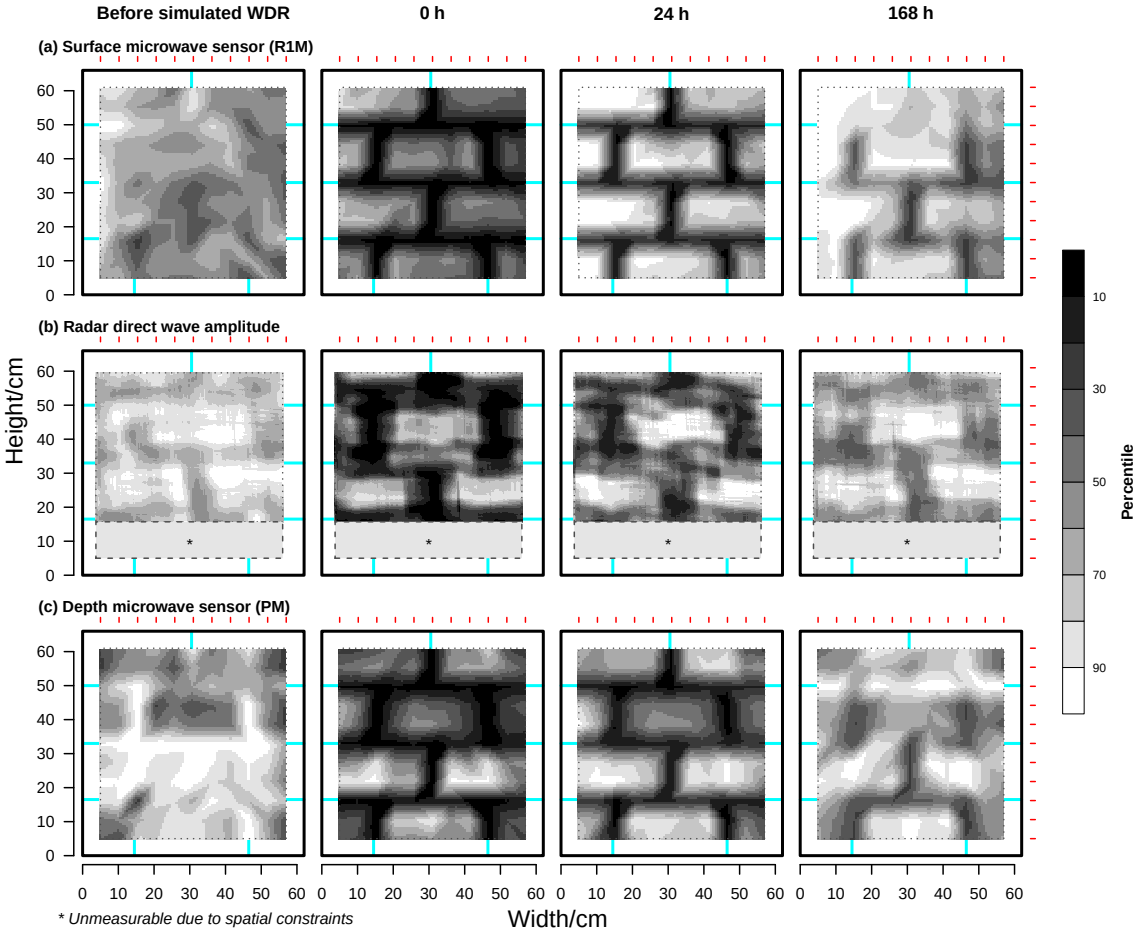

Figure 7.3. Spatial representations of a granite masonry wall drying after simulated WDR exposure, represented with percentiles. Measurements from the non-destructive techniques: (a) microwave surface sensor (R1M), (b) radar direct wave amplitude, and (c) microwave depth sensor (PM). The areas outside the dotted lines indicate areas of the wall that were not measured as they were too close to the edges. Blue lines indicate locations of mortar joints, while red lines indicate the measurement grid. The data is presented as normalised values in Figure B.1 (p. 322).

- The radar direct wave amplitude is more affected than the microwave sensors by environmental conditions (Figure 7.4a,c), e.g. responses to temperature and air humidity influencing surface condensation can be observed in the moisture levels;

- A similar influence of environmental conditions is observed on the surface microwave sensor (R1M) on the granite units (Figure 7.4a,b), suggesting that microwave measurements are also affected by surface condensate but dominated by

liquid water in the joints;

- The depth microwave sensor (PM) shows that the granite, as expected, absorbs very little water, as the moisture percentile of the median/mean are consistent over the duration of the experiment (Figure 7.4d);

- The similarity between the surface and depth microwave sensors (Figure 7.4b,d) demonstrates the cumulative nature of the sensors, i.e. they measure *to* a depth, not *at* at depth (with decreasing sensitivity); in this way, the depth sensor is influenced by near-surface water contents;

- Both microwave and radar measurements indicate vertical joints are wetter than horizontal ones (as represented by measurement percentiles, Figure 7.4b-d), likely due to prolonged contact while water runs over their surfaces.

The radar direct wave amplitude is more sensitive than the surface microwave sensor to changes in material properties. This is apparent in the outline of higher percentiles visible in the radar scan (Figure 7.3b, before simulated WDR) around mortar joints within the wall (c.f. the R1M measurements in Figure 7.3a which is a more homogenous blur). This is also represented in Figure 7.4b,c, by a greater difference between percentiles for joints and granite before simulated WDR. However, it should be noted that the granite percentiles are skewed (overestimated) in Figure 7.3. This is due to a greater number of a granite measurements that vertical/horizontal joints. In a scenario with

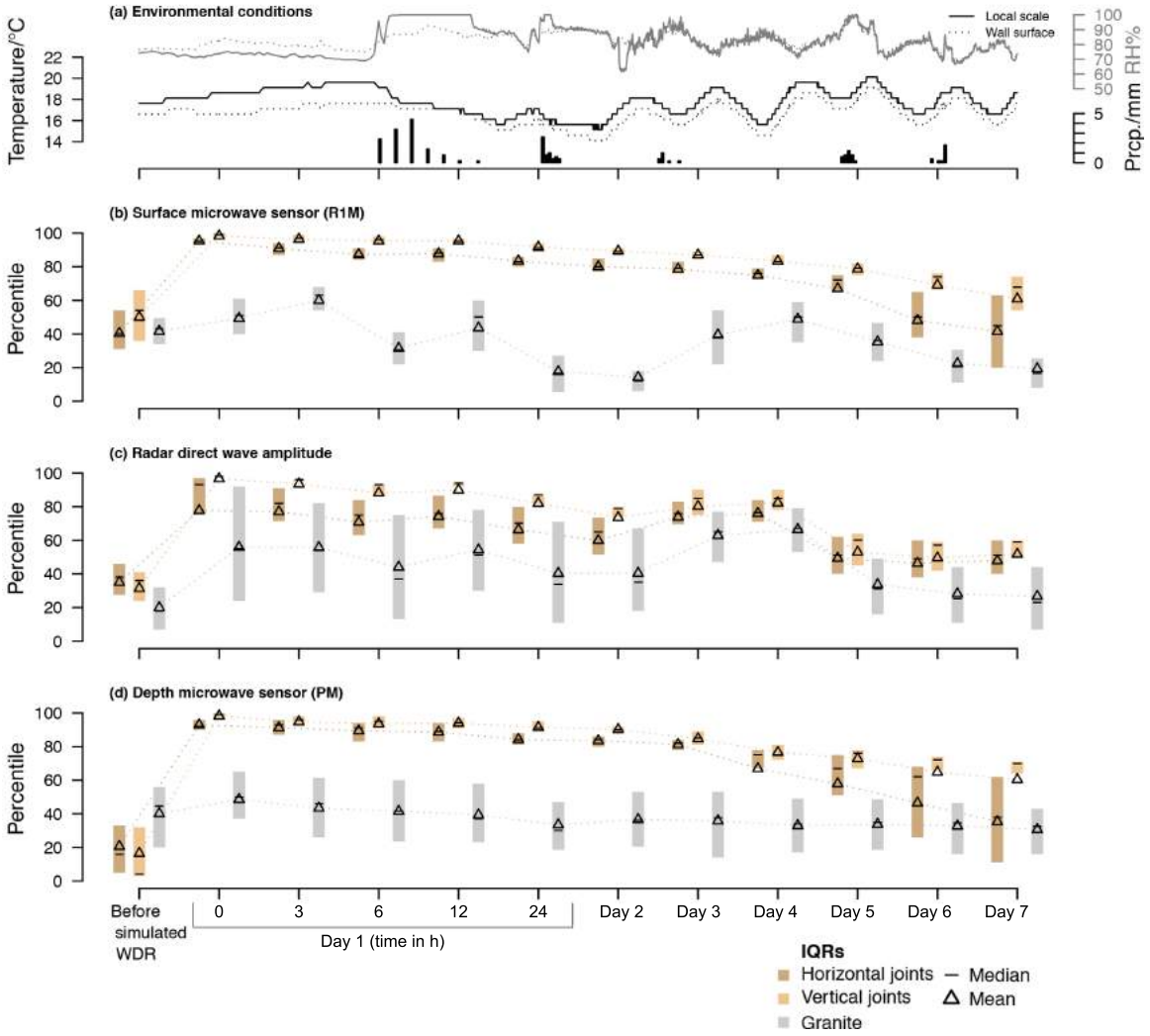

Figure 7.4. Temporal representations of components of a granite masonry wall during drying after simulated WDR exposure during the Oxford experiment. (a) Environmental conditions, (b) surface microwave sensor (R1M), (c) Radar direct wave amplitude, and (d) Depth microwave sensor (PM). The data is presented as normalised values in Figure B.2 (p. 323). Measurements were taken at increasing long intervals over the first day of drying (beginning at $t = 0$, 12:00h) to capture more rapid rates of moisture loss directly following the end of the simulated rain spell, and on subsequent days at approximately 12:00h.

significantly different numbers of measurements between subsets (i.e. regions of interest), representation with normalised values (or raw measurements) is preferred (Appendix B, Figure B.2). Normalised value representation demonstrates that the granite measurements are significantly lower than the surrounding mortar joints, which is not reflected in percentile representation due to skew caused by subgroup sizes.

The measurements suggest that the walls are transitioning between Stage I and Stage II drying (Cooling, 1930; Scherer, 1990) around 96 h after drying commenced (Figure 7.4). This provides validity for the moisture measurements since it conforms to theory. Stage I behaviour occurs when limited evaporation rates manifest as a brief period of pseudo steady-state drying during which there is a constant flux of water out of the surface (van Brakel, 1980); in contrast, Stage II drying is characterised by steeper moisture gradients at greater depths (Hall and Hoff, 2012, p. 205). The transition is marked by the end of plateaus and increasing slopes in the surface values (R1M and radar direct wave amplitude). It is interesting to note that during Stage II drying the horizontal joints have a higher rate of moisture loss than their vertical counterparts. This could suggest a cycle of moisture movement within the joints: during WDR exposure the vertical joints have a greater uptake, after which the evaporation rates from both are pseudo-steady state, until Stage II drying commences and higher evaporation rates are observed from horizontal joints. Similar performance of horizontal (bed) joints has been observed in measurements and modelled hygric responses of simple representations of masonry systems (Vereecken and Roels, 2013).

7.3.1.2 Identifying penetration through mortar joints using radar travel time

The penetration of liquid water through mortar joints can be identified with radar signal travel time, an additional variable to the direct wave amplitude. This evaluation is possible

when the signal penetrates to the back wall and produces a detectable reflection.

Penetration through mortar joints is especially important to consider in constructions such as the granite test wall, in which the mortar joints have a higher moisture burden than joints would if surrounding more porous stone units. As demonstrated in Figure 7.5c, visual inspection of the back face of the granite test wall reveals water penetration through the upper joints. This is also observed in total radar travel time (Figure 7.5b).

The spatial representation of the depth microwave sensor (PM) is a logical comparison, since it should also detect moisture at depth. The measurement percentiles for this technique (Figure 7.5a, also presented in Figure 7.3c) demonstrate higher implied water contents in the masonry joints, but it is important to note that microwave sensitivity moisture decreases as a function of depth (Camuffo and Bertolin, 2012), so these measurements are especially influenced by surface moisture. In contrast, the radar travel time is equally sensitive across the entire profile of the wall, since it is an average travel time across the depth of the masonry. Radar travel time is an effective assessment technique that allows water penetration through joints to be visualised.

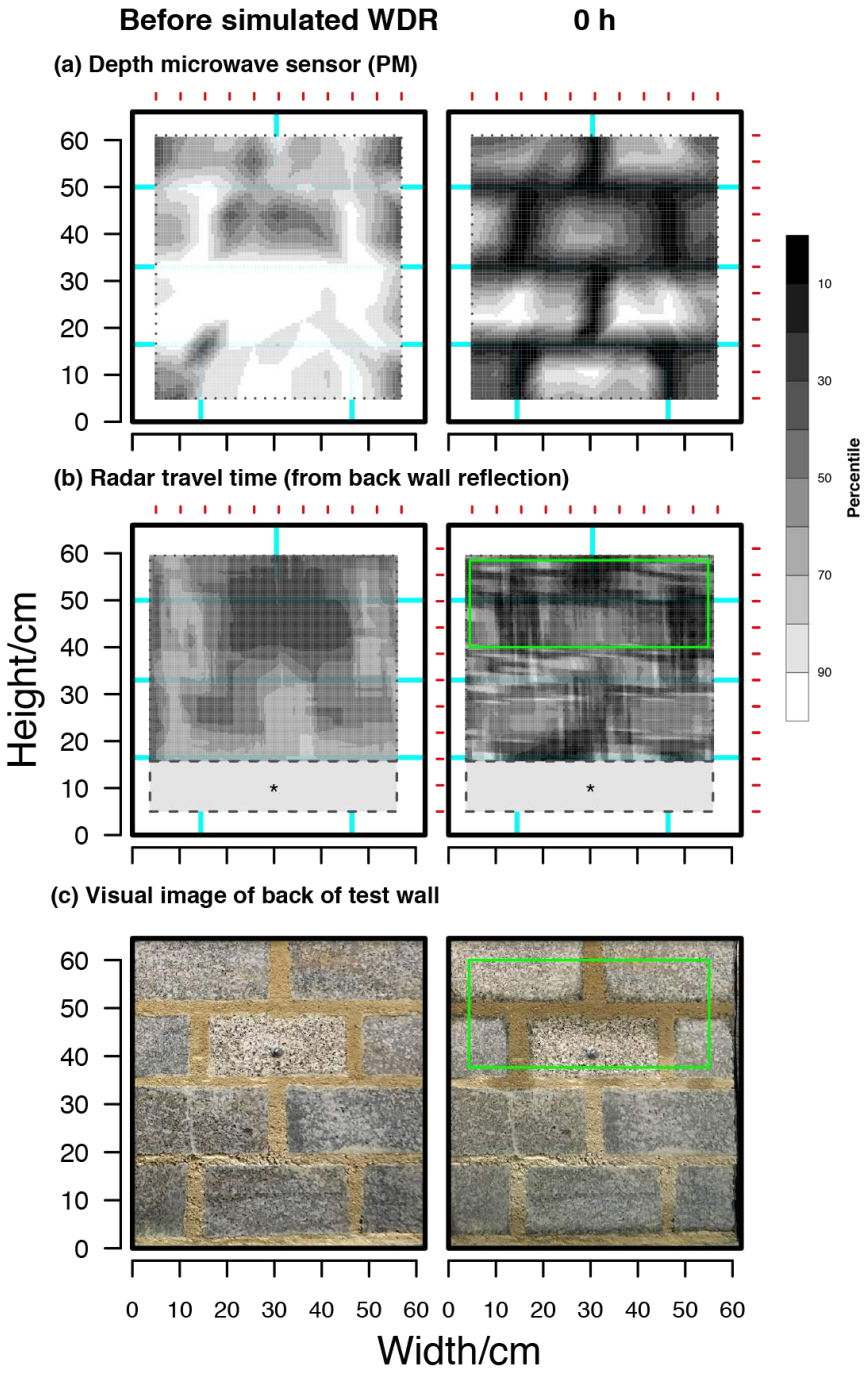

Figure 7.5. Spatial representations of moisture variation (in percentiles) across a granite masonry wall after simulated WDR exposure demonstrating penetration through joints and depth-focused electromagnetic measurements. (a) Depth microwave sensor (PM), (b) Radar travel time (from back wall reflection), and (c) Visual image of back of test wall. The green boxes highlight the area where colour change indicates water penetration and the resultant high measurement percentiles in radar travel time. See Figure 7.3 and its caption for an explanation of the colour scheme and scale employed; measurements with the surface microwave sensor (R1M) for the equivalent time periods are also presented.

7.3.2 Edinburgh experiment

7.3.2.1 Comparison of microwave and radar: masonry with similar component physical properties

Scenario A produced four different intensities of WDR exposure. This demonstrated that the microwave sensors distinguished four distinct 'zones' of moisture levels resulting from four levels of WDR exposure (Figures 7.6a,c and 7.7b,d). The radar direct wave amplitude exhibits more complex behaviour (Figures 7.6b and 7.7c).

The microwave sensor data demonstrates expected Stage I and Stage II drying (refer to Section 7.3.1.1 for explanation), with surface migration of water. Figure 7.7b,d illustrates that the microwave sensor measurements are similar between the four zones before the simulated WDR. During the 3 h spell, microwave measurements with the PM sensor, indicative of water contents at depth, increase rapidly in all zones except Zone 1 which did not receive any direct WDR exposure. During the spell, the surface microwave measurements were noticeably banded in the four zones; after the simulated WDR, the surface moisture levels homogenised to values above the 80th percentile after approximately 3 h of drying. However, they maintained the order of average moisture levels observed in each zone immediately following the end of simulated WDR. This homogenisation of surface microwave measurements was likely encouraged by moisture migration beneath the impervious barrier between the zones and in response to increased

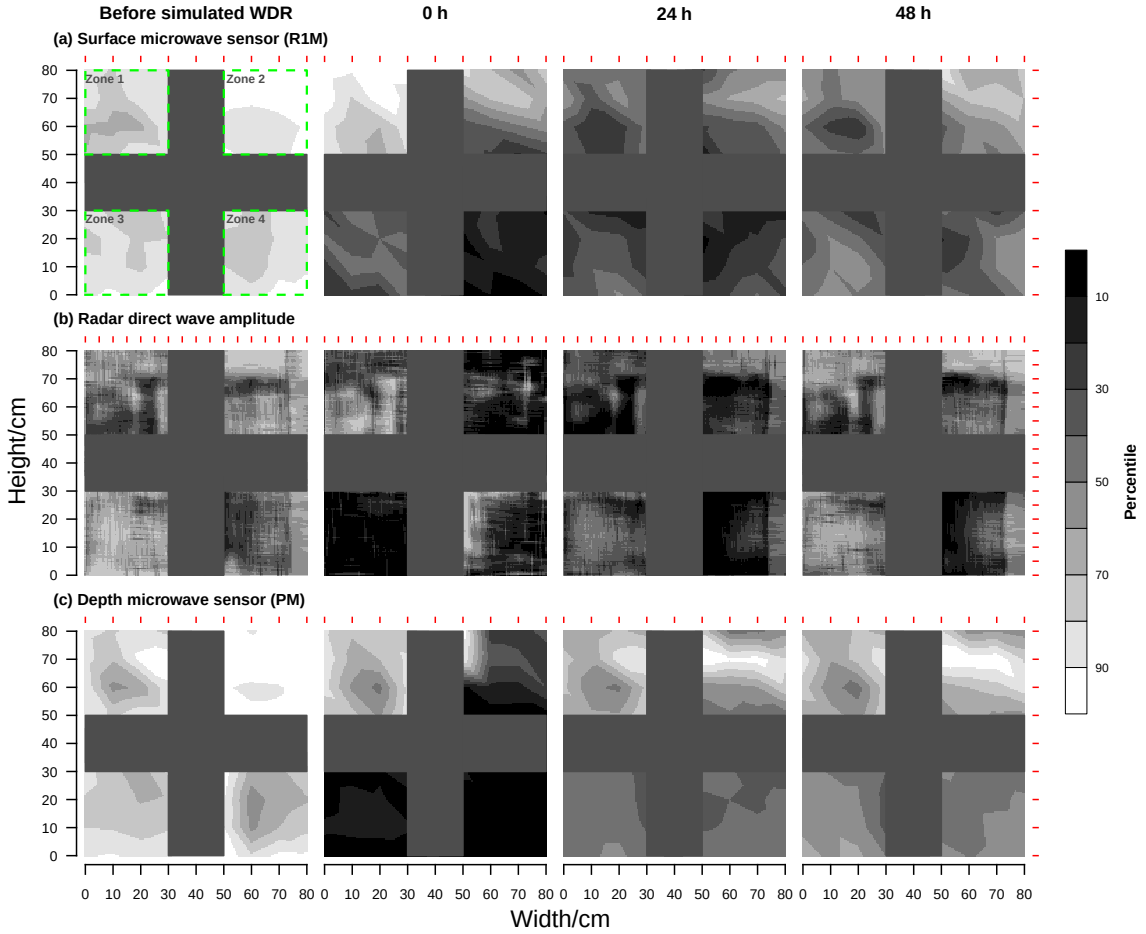

Figure 7.6. Spatial representations of moisture measurements during simulated WDR exposure for a part of New College, Edinburgh following four spell intensities (Scenario A). (a) Surface microwave sensor (R1M); (b) Radar direct wave amplitude. The grey 'cross' represents 'no data' because of an impervious barrier applied directly to the façade surface between the zones which remained on the surface for the duration of the monitored drying.

near-surface humidity.

In Scenario A, the radar direct wave amplitude measurements were similar to those of the depth microwave sensor. This contrasts the trends identified for the granite test wall (Oxford experiment), in which changes in surface measurements with environmental conditions were identified in both radar and microwave sensors. This suggests that the direct wave amplitude is sensitive to water contents up to a depth somewhere in between

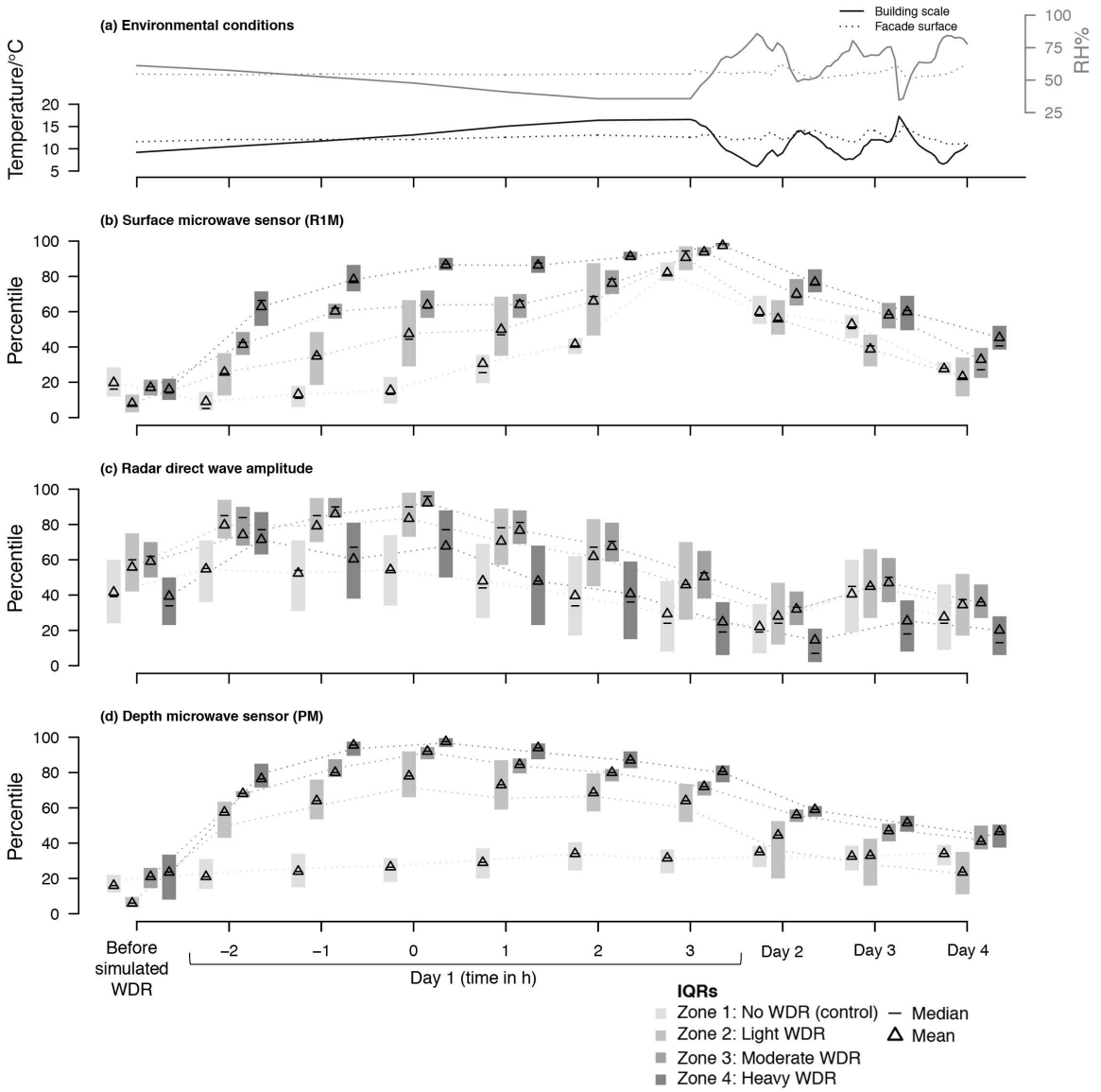

Figure 7.7. Temporal representations of moisture measurements during for a part of New College, Edinburgh following simulated WDR exposure at four spell intensities (Scenario A). (a) Environmental conditions; (b) Surface microwave sensor (R1M); (c) Radar direct wave amplitude; (d) Depth microwave sensor (PM). Negative time references represent hours within the spell ($t = 0$ is the beginning of the drying process). No precipitation was measured on site during the study time period.

that of the surface and depth microwave sensors. As such, it will exhibit properties more similar to one or the other depending on the moisture regime. The direct wave represents electromagnetic energy transmitted directly to the receiving antenna, as opposed to being a reflection from sub-surface changes in material properties (Sbartaï et al., 2007). It is

difficult to contextualise the radar direct wave amplitude in two-stage drying as no radar-based depth measurement was available for comparison. This is because the back wall reflection was not detectable. In Scenario A of the Edinburgh experiment, the percentiles are less affected by skew (as observed in the Oxford experiment) since they are comprised of equal number of measurements.

7.3.2.2 Assessing localised water contents of masonry units and mortar joints

Scenario B of the Edinburgh experiment examined the role of different mortar joint configurations in the response to heavy WDR exposure. The results demonstrated that both microwave sensors and the radar direct wave amplitude were able to detect differences in water contents between masonry units and mortar joints in a sandstone and lime mortar construction (Figure 7.8). However, the radar direct wave amplitude demonstrated a more significant contrast between the percentiles of masonry units and joints, enabling distinction between their hygric response.

The zones exhibited behaviour captured in both microwave and the radar measurements that can be rationalised by their joint configurations. As presented in Figure 7.8, Zone 1 (control) had low percentiles and comparable values between the units and the joints. Zone 2 (no joints) exhibited the highest percentiles within the stone units of the four zones. In contrast, Zone 3 (both a horizontal and vertical joint) had lower percentiles within the masonry units and the highest values of any zone within the joints. The percentiles of

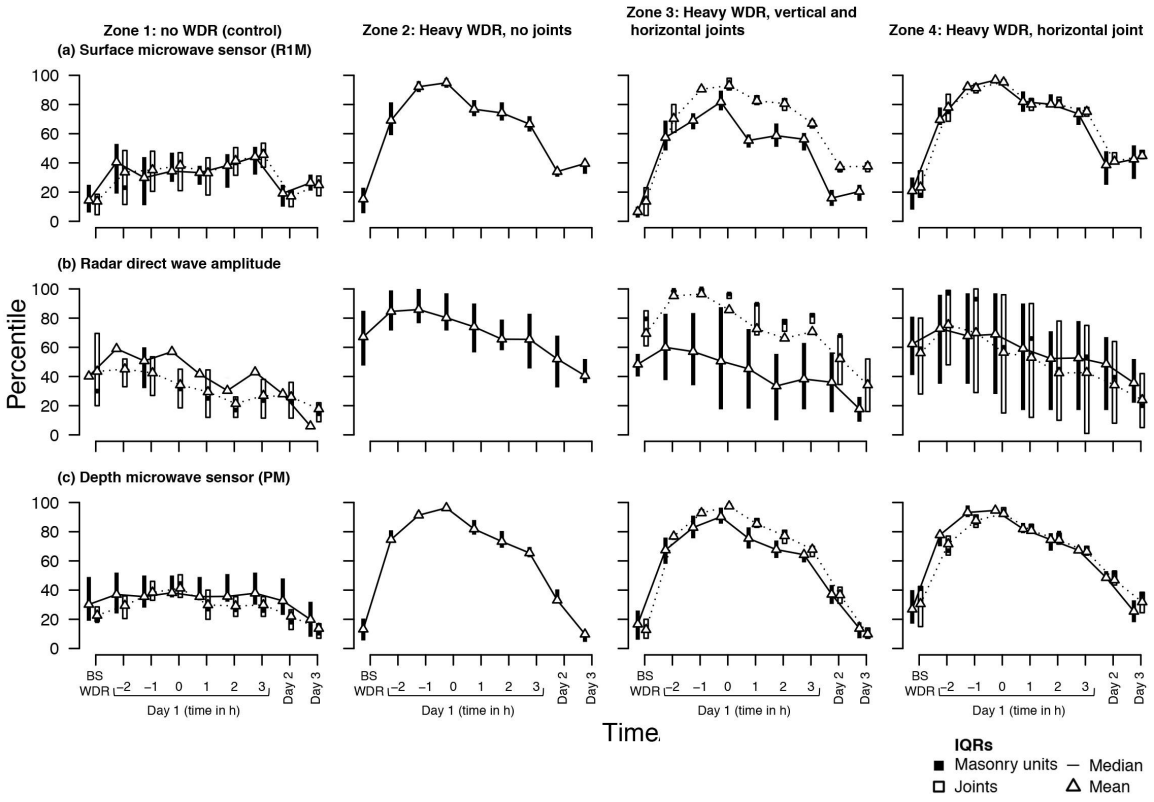

Figure 7.8. Measurement percentiles for two microwave sensors and a radar variable for mortar joint configurations within the sandstone façade of New College, Edinburgh (Scenario B). (a) Surface microwave sensor (R1M); (b) Radar direct wave amplitude; (c) Depth microwave sensor (PM). 'BS WDR' = Before Simulated WDR. Negative time references represent hours within the spell ($t = 0$ is the beginning of the drying process). The data is presented as normalised values in Figure B.3 (p. 324).

masonry units and mortar joints were very similar in Zone 4 (only a horizontal joint), emphasising the observations drawn from the granite test wall of the dominance of vertical joints with respect to moisture uptake.

Figure 7.8 demonstrates that the microwave sensors are very sensitive to changes in liquid water contents. This is represented by increases in percentiles from before simulated WDR to the first hour of the simulated spell of at least approximately 60% regardless of zone. This significant increase reduces the effectiveness of the temporal representation for distinguishing between measurement percentiles of the masonry units and the mortar

joints. In contrast, the radar direct wave amplitude exhibits a higher contrast between the joints and the masonry units in Zones 2 to 4. In this scenario, the percentile skew caused by higher numbers of measurements taken on the masonry units would have been significantly outweighed by the skew introduced by an extreme value in the surface microwave sensor (R1M) data set (Appendix B, Figure B.3); this type of problem is unavoidable without manual cleaning of data for outliers and extreme values, which is based on a subjective evaluation of measurement validity.

Scenario B further supports the theory that the radar direct wave amplitude is influenced by environmental conditions resulting in surface condensation. In the days before the measurements for Scenario B there had been heavy precipitation; although this did not impact directly on the façade, it affected local climate. Additionally, it is possible that the radar direct wave amplitude percentiles are higher before simulated WDR than for the microwave sensors as the surface water contents are fluctuating in response to condensate induced by higher values of relative humidity early mornings when each scenario began, whereas measurements on subsequent days were taken later in the day.

7.4 Discussion

7.4.1 Comparative advantages of radar and microwave techniques

Both microwave and radar methods can be a part of informative moisture monitoring in stone masonry. However, their respective properties and characteristics dictate how and in which type of scenarios they might best be employed (Table 7.3).

In cases with significant contrast in the hygric properties of masonry units and mortar joints (e.g. granite units and lime mortar), microwave and radar provide similar information on the general distribution of water. Both techniques can provide similar information on relative surface and depth moisture contents. Although the radar travel time can enable a streamlined analysis of water penetration through joints (and, average water contents across the depth of construction), a microwave depth sensor can provide slightly less useful (but still informative) output when the construction is too thick to produce a detectable back wall reflection.

The results of Scenario A of the Edinburgh experiment demonstrate that both radar and microwave techniques can be useful in evaluating the response of a construction with masonry units of higher sorptivity. The microwave sensor measurements provide uncomplicated information on relative levels of water content at a façade scale. This can

Table 7.3. A summary of recommended techniques and variables to use for specific investigation objectives depending on the masonry context.

Objective of investigation	Contrasting hygric properties of masonry units and mortar joints	Similar hygric properties of masonry units and mortar joints
General distributions	any (or in combination)	any microwave sensor (or in combination)
Penetration through mortar joints	radar total travel time	radar total travel time*
Localised contents in masonry stone units and mortar joints	any (or in combination)	radar direct wave amplitude
Surface condensation	radar direct wave amplitude or surface microwave sensor (R1M)	radar direct wave amplitude or surface microwave sensor (R1M)

**although not demonstrated here, this technique is applicable to various masonry configurations if the back wall can be detected at the operating frequency*

be applied in an effective monitoring strategy in several ways:

1. to perform a rapid initial survey across a façade, site, or building, to characterise the overall distribution of moisture and support an exploration of potential moisture sources

2. to undertake repeat measurements during a long-term (but periodic) monitoring exercise, which will be less influenced by recent and local environmental conditions, i.e. diurnal impact on measurements

During the Edinburgh experiment the microwave measurements were taken with 10 cm point-spacing, while the radar was taken over a grid with 5 cm line spacing. Although this does introduce an additional variable into comparison of the microwave and radar methods, it acknowledges practical surveying considerations. The microwave measurements take longer time to collect, since the sensor head must be moved and placed in a new position prior to each reading (in this experiment, 9 x 9 = 81 measurements). In contrast, the radar

antenna only need to be placed for each line (17 in each direction in this experiment) and it relatively easy to maintain alignment while collecting data along the transects.

There are a several reasons why radar is an ineffective technique for surveying at a façade scale when the hygric properties of unit and joint within the masonry are similar:

- the radar data requires more post-processing to produce useful information
- it is logistically less efficient than the handheld microwave sensor for rapidly collecting data in many areas (or across wide areas) of a façade or site
- it exhibits greater influence from environmental conditions and localised surface conditions, especially with regard to surface condensation

Radar can be used to evaluate the behaviour of masonry systems on a more localised scale than the façade or site. As demonstrated by Scenario B (and to a lesser extent the Oxford experiment), the radar measurements enable a discussion of how stone masonry functions as a *system* of units and joints functions. This has many potential applications, especially concerning decisions around retrofits and maintenance. For example, the analysis method used herein could be applied to evaluate the performance of original or repair mortar to inform whether repointing should be undertaken. It could also be used to evaluate the effectiveness of repointing after it has been implemented. As previously discussed, the radar travel time can also be used to identify regions where water has

penetrated through joints, which is of particular use in scenarios in which only one-sided access is possible (and therefore visual inspection for water penetration is infeasible).

7.4.2 Data visualisation and presentation

The results of this study demonstrate that, in moisture monitoring with non-destructive electromagnetic sensors, a combination of spatial and temporal representations of measurements provides useful information. For example, identifying the transition between Stage I and Stage II drying is easily done with a temporal representation of measurements. However, using a spatial representation of radar travel times allows for the locations within a masonry system which experience water penetration through joints to be rapidly identified. The visual representation technique needs to support the objectives of the monitoring exercise to provide useful information.

The use of measurement percentiles in spatial representations supports more accurate interpretation of data than if colour bins were assigned to the original measurement data, since this data is rarely uniformly distributed. Using percentile representation in both heat map and bar plots facilitates comparison between them. This is not ideal if the measurements are subset into subgroups of significantly different sizes, as this can introduce skew. However, in a case where the measurements include a significant outlier or an erroneous value, the skew introduced when normalising or determining scales would outweigh that which is introduced by using percentile representation.

When using percentile representation, it is important not to assume that the 80th percentile in one technique is equivalent or comparable to the 80th percentile in another. As well, the 100th percentile (i.e. the maximum), is only the maximum of the survey measurements, and does not represent a saturated state. This could be addressed if samples of sufficient size of the relevant material(s) can be obtained. From this, oven-dry and saturated measurements could be determined for each material, which can be included in the measurement set prior to determining percentiles.

7.5 Conclusion

In this study, the response to simulated wind-driven rain spells of two types of stone masonry provided insight into how and when non-destructive electromagnetic sensors are best employed as part of a monitoring strategy. In cases when the masonry units and mortar joints have significantly different hygric properties, both radar and microwave techniques provide useful information on the distribution. In more homogenous constructions, microwave sensors can provide useful information on the overall distribution of water across a façade, building, or site. Radar measurements are more suited to investigate localised variation of water contents to evaluate the behaviour of masonry systems, and investigate surface water contents due to condensation. They can also be used to identify areas in which water has penetrated through mortar joints to the interior of a construction.

Representing data in spatial and temporal visual forms facilitated a multi-perspective

approach that enriched the interpretation of the monitoring. Converting data into measurement percentiles improved the visual resolution of colour-based representations and reduced the impact of extreme outliers.

Both the evaluation of comparable advantages of moisture-sensitive non-destructive techniques and methods of data manipulation and visual representation are important components of multidisciplinary management of built cultural heritage and warrant further development.

Part IV

Implications for scientific research and practical heritage conservation

8 | Discussion, synthesis and future work

"You can flip a coin to change its face,
but it remains the same coin."

– DR DASHANNE STOKES (2016)

This chapter discusses the papers presented in Chapters 4 to 7. As Chapter 2 demonstrated, the bodies of literature on wind-driven rain exposure and moisture regimes within stone masonry are predominantly distinct from one another. To this end, this discussion creates connections between them through the components of this thesis, stimulates broader discussion, and recommends future directions for research. For a summary of methods and findings of each paper, please refer to the abstracts and conclusions presented at the beginning and end of their respective chapters, or the thesis conclusion (Chapter 9).

This thesis identifies different connections between the thesis components (exposure and response) and approaches (characterisation and methodological development) of thesis by:

- demonstrating how methods of investigating one component or approach can be informed by development/characterisation of the other;
- discussing ways in which the results of this thesis pertaining to one component or approach have implications for the other;
- identifying opportunities to further links between the components or approaches in

future work;

- highlighting challenges and opportunities common to the chosen assessment methodologies.

8.1 Exposure to wind-driven rain

Two aspects of exposure to wind-driven rain are explored in Chapters 4 and 5: the improvement of semi-empirical representation of wind-driven rain, and the impetus provided by the uncertainty of the 21st century climate in the UK.

8.1.1 Improving semi-empirical evaluation of wind-driven rain exposure

Semi-empirical evaluation of wind-driven rain is an important tool in characterising building exposure in the UK and should be further developed and improved. These methods have been undergoing development since their inception in the 1950s (Hoppestad, 1955), and can capitalise on developments in computational and processing capabilities. Although recent wind-driven rain exposure is not significantly different to that from the mid-21st century upon which BS 8104 was based (Chapter 4), future climate predictions suggest that exposures are, broadly speaking, becoming more intense and seasonally polarised (Chapter 5). This provides motivation to revisit, evaluate, and improve standards.

8.1.1.1 Improving the characterisation of wind-driven rain spells

Characterisation of wind-driven rain exposure can be improved by: (1) increasing the accuracy of the formulae used, and (2) exploring additional metrics to represent the diverse properties of wind-driven spells.

Increasing the accuracy of mathematical representation

Chapter 5 discussed the potential effect of droplet diameter on the semi-empirical representation of hourly exposure (ISO, 2009) used in Chapters 4 and 5. The droplet diameter distribution (and therefore median droplet diameter) is strongly dependent on the type of rainfall event (e.g. drizzle, cloudbursts, etc...). Within realistic bounds for droplet diameters, estimation of wind-driven rain exposure (e.g. Equation 4.1, p. 68) can be as much as half or double the quantity determined from the coefficient specified in current standards.

If the coefficient in the representation of exposure is determined from a more accurate droplet diameter for the time period of interest, the estimation of wind-driven rain quantity can be as much as half or double the value determined from current standards. Future work could emphasise the development of semi-empirical representation of wind-driven rain exposure that used a 'dynamic' coefficient that varies with droplet diameter. This coefficient could be derived from established relationships between drop size and rates

of precipitation (Marshall and Palmer, 1948; Best, 1950), or from reported weather conditions, e.g. the World Meteorological Organization's Table 4677 (2016). The WMO provides categorisation for different types of precipitation that could be linked to median droplet diameters based on observations (Lull, 1959). These categorisations are frequently reported by the weather stations in the UK and made available through UK Met Office. Additionally, experiments combining computational fluid dynamics (CFD) modelling approaches could determine the appropriate droplet diameters (and resultant coefficients from terminal velocities) based on rates of precipitation. These approaches could also enable semi-empirical representations of wind-driven rain to compute statistically probable *distributions* or ranges of wind-driven rain exposure, which would better align with current approaches in meteorological evaluation and climate change assessment.

Exploring additional metrics to reflect multi-dimensionality of wind-driven rain spells

Chapter 5 demonstrated the changing characteristics of spells of wind-driven rain. Some characteristics, including the quantity of exposure, are partially captured by current metrics employed in standards. Other aspects, such as duration and the 'consistency of hours within each spell during which there was wind-driven rain' occurring, are not. This thesis demonstrates the value of analysing the three primary aforementioned aspects (or 'dimensions') of wind-driven rain spells. Specifically, different types of impact (e.g.

building element failure, deep-seated wetting, penetration through joints, etc) are multi-dimensional. Thus, assessing the likelihood of their occurrence should also be multi-dimensional. This approach would: (a) build on the characterisation of future wind-driven rain properties (Chapter 5) to create stronger links to specific types of impact, and (b) further understanding of the relationship(s) between exposure and impacts (Chapter 4). These could be combined with records of building management issues to expand the links being made with the response of stone masonry beyond non-destructive monitoring to simulated situations (Chapters 6 and 7). This multi-dimensional approach is especially important to consider the impact(s) of short (but intense) spells of wind-driven rain, including penetration through joints (as demonstrated in Chapter 7). These types of wind-driven rain spells are not represented in current standards and require the development of specific strategies to be addressed with semi-empirical evaluation.

8.1.1.2 Statistical representation of extreme events

Since the development of BS 8104, there has been significant development in statistical representations of extreme weather events (Coles, 2001). These advances have been taken up in environmental applications, including flood occurrence (Madsen, Pearson and Rosbjerg, 1997; Engeland, Hisdal and Frigessi, 2004), but have not been taken up widely in wind-driven rain assessment. This is especially apparent in the percentile-based approach (and its limitations as identified in Chapter 4) specified in ISO 15927 (2009). The use of

an annual maxima series (AMS) approach in Chapters 4 and 5 demonstrate a progression towards current wider practice of representing extreme weather events. While the Gumbel distribution is used in combination with the AMS approach herein (and elsewhere, see, for example, Pérez-Bella et al., 2012, 2013), it does assume certain characteristics of the statistical distribution of extreme events. Further work could produce more generalised distributions with less assumptions about extreme wind-driven rain using the Generalised Extreme Value (GEV) distribution (Coles, 2001, pp. 47–48), or similar.

8.1.2 Climate change during the 21st century

The UK climate is changing, and is predicted to result in changes in wind-driven rain under a high emissions scenario over the 21st century (Chapter 5). However, some regions of the UK are experiencing disproportionate rates of change relative to others (Chapter 4). The predicted characteristics of WDR for 2070–2099 represent a trajectory that is already impacting building performance. The UKCP09 predictions represent change during the twenty-first century using 30 year periods, so the noise from annual variability is reduced. Figure 8.1 shows the predicted changes in summer and winter precipitation under a high emissions scenario. As precipitation is the core variable in both the UKCP09 models and the probabilistic generation process, the rate of change in precipitation can be considered as an indication of the rate of change of characteristics of wind-driven rain spells. Based on the predictions in Figure 8.1, conditions of precipitation and wind-driven rain for 2070–2099

under this scenario will be approached over the course of this century at an accelerating rate. Rates of change under different scenarios will vary, generating further work to determine how these predictions will manifest as future wind-driven rain exposure.

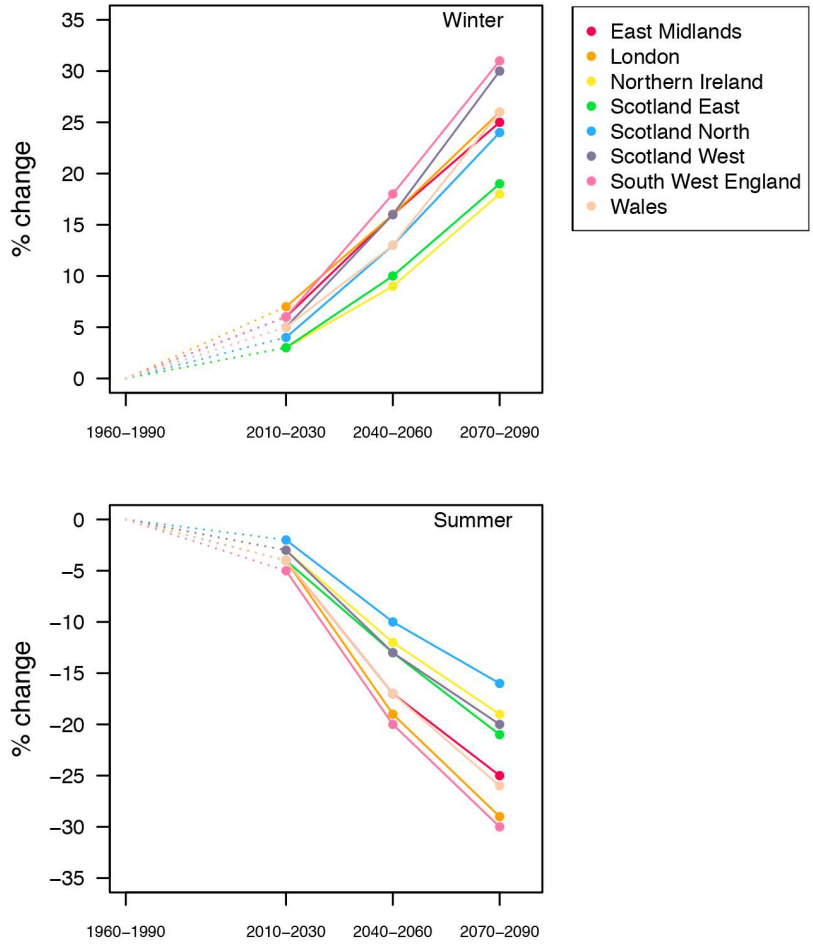

Figure 8.1. Predicted changes in summer and winter precipitation for the 21st century under a high emissions scenario (DEFRA, 2009).

Any output is only as good as the input. Stochastic models to create future weather data are in common use in building simulation (Guan, 2009; Eames, Kershaw and Coley, 2011b). These are necessary to produce time series at an hourly resolution, as such data is not readily available due to storage and computational limitations. This demonstrates

a disparity between the objectives of mainstream climate modelling and applied impacts, such as building sustainability. Future work could be collaborative efforts between these two disciplines to produce data in formats that are compatible with current practice in building science. This would support applied studies of the potential impacts of climate change on the traditional built environment.

8.2 Response of stone masonry

Standards that use semi-empirical evaluation of wind-driven rain, e.g. ISO 15927 (2009), often directly refer to the impact of wind-driven rain on masonry. Thus, the discussion here of changing aspects and the need for improved methods of assessment (as covered in Chapters 4 and 5) motivate improvement of methods that study moisture regimes in porous building stones (Chapters 6) and stone masonry systems (Chapter 7). Solid-wall constructions have an especially high risk of penetration through to the interior. The ability to characterise the hygric behaviour of these complex stone masonry systems produces an impetus for innovative uses of non-destructive moisture measurement techniques.

8.2.1 Identifying regions with higher prevalence of wind-driven rain

Chapters 4 and 5 demonstrate that the severity of a changing climate is (and will be, in future) unequal for regions of the UK. This provides motivation to develop non-destructive

techniques that are applicable to the buildings in these parts of the country. For example, developing methodologies that support the interpretation of moisture measurements taken on stone masonry with the particular properties found in these regions (e.g. granite-built structures prevalent in the southwest of England). Another important aspect of preparing for regional risks is characterisation of the properties of vernacular building stones (Chapter 6). This is especially important for sandstones commonly employed for building projects in Scotland, which exhibit significantly different dielectric properties to limestone. Characterising these properties supports accurate interpretation of measurements taken with non-destructive techniques.

8.2.2 Characterising the potential impact of periodicity on moisture monitoring

Chapter 7 demonstrated that short (but intense) wind-driven rain spells can result in water penetration through mortar joints and increased water contents for several days. These are the result of individual spells of wind-driven rain. Further study is needed to characterise the cumulative impact of series of wind-driven rain spells and seasonal exposures, especially with regards to deep-seated wetting (Smith et al., 2011a). This characterisation could incorporate a combination of modelling and measurement approaches, e.g. a combination of coupled heat and moisture modelling softwares with non-destructive techniques.

Furthering understanding of the periodicity of short- and long-term moisture regimes in

stone masonry through modelling approaches would enable more accurate interpretation of non-destructive moisture monitoring campaigns. This includes a range of scales of periodicity, including diurnal and seasonal behaviour. This would allow non-destructive measurement campaigns—short-term (as in Chapter 7) and longer-term—to be contextualised. This would reduce the potential for false diagnoses of moisture regimes due to misinterpretation of survey data, and produce maximum results while minimising maintenance efforts. This is especially important for long-term, but infrequent (non-continuous) campaigns, which (as discussed in Chapter 7) can be susceptible to influence/interference from short-term weather events and diurnal variation in environmental conditions.

8.2.3 Assessing the impact of urban scale and building geometry

Wind-driven rain exposure is influenced by a number of contextual aspects: ISO 15927 (2009) includes factors to account for surface roughness, topography, obstruction (e.g. built context), and a wall factor (to make estimations specific to a specific part of a building). However, the urban and built context is complex, and becoming ever more so with developments in architectural design and technological innovation. One opportunity facilitated by furthering capabilities of non-destructive techniques (Chapter 6) is to combine them with semi-empirical evaluation (Chapters 4 and 5) to characterise the effects of complex local environments on exposure to wind-driven rain.

8.3 Data handling and visualisation

New innovations and ever-increasing complexity in technological development and analytical methods demand new modes of data visualisation and handling.

8.3.1 Data handling

Collecting data can be quite straightforward; the difficult part is how to make it informative and useful. This is especially true for characterising climate change and dynamics of moisture regimes, for which rates of change and relative rates (in combination with representations of certainty) can be advantageous. One challenge within these applications is that many variables are non-uniformly distributed, since simple types of relativisation (e.g. absolute differences) might result in skewed representation of the properties of the datasets.

Chapter 4 demonstrated that using the Gumbel distribution was a viable alternative to percentile distributions for extreme event characterisation. Similarly, Chapter 5 also demonstrated the importance of contextualising changes in climate within the certainty of the predictions.

Chapter 6 demonstrated that non-destructive moisture-sensitive devices (such as microwave and radar measurements) can be well-calibrated well to a range of water contents in building stones. It also demonstrated the challenges of interpreting the readings from

devices that have non-linear responses to gradients of moisture across a depth. To this end, calibration is not always reliable or appropriate for more complex heritage applications. Thus, Chapter 7 demonstrated a novel method of representing measurements as percentiles that provides a relative measure that is independent on data distribution and less prone to influence from extreme values. Percentiles are appropriate in this scenario for some purposes as they are not affected by temporal frequency (as would be the case if assessing return periods of extreme wind-driven rain exposures).

8.3.1.1 Data fusion

The aim of using multiple non-destructive techniques in a moisture survey is to gain a more accurate, consistent, and useful output. In this regard, it can be considered an exercise in data fusion (Haghighat, Abdel-Mottaleb and Alhalabi, 2016). As discussed in Chapter 7, the output from moisture surveys is most typically presented visually, or, the data from different devices is presented individually. However, most interest in data fusion in non-destructive testing has traditionally been on data handling procedures and algorithms to more directly synthesise the output from multiple sources (Gros, 1997). This has been widely applied in civil engineering applications (Kohl et al., 2005; Heideklang and Shokouhi, 2013), e.g. detection of voids/reinforcements in concrete (Völker and Shokouhi, 2015a; Völker et al., 2018).

The challenge for implementing data fusion into monitoring of moisture regimes is that

the information benefit of applying algorithms cannot be evaluated without an accurate reference. For example, data fusion for reinforcements (e.g. rebar) can be assessed by producing a test specimen with the specified structural elements. While producing individual specimens of well-characterised moisture contents is feasible (e.g. Chapter 6), this is less straightforward for lateral and depth-resolved moisture regimes within masonry systems (such as those studied in Chapter 7). Future work could investigate whether three-dimensional models of coupled heat and moisture transfer could provide an accurate reference for the non-destructive measurements. This would enable assessment of the effectiveness of data fusion algorithms for multi-sensor approaches in moisture monitoring of stone masonry. Additionally, extensions of the the 'isolated diffusion' procedure could be explored, to determine if creating composite structures in a similar manner would be feasible.

Data fusion could also capitalise on the *differences* in sensitivity of different devices with regards to spatial resolution/capture and measurement principles. Data fusion could be employed to produce algorithms that look for 'disagreement'. For example, electromagnetic measurements could be grouped by their approximate depth of sensitivity and contrasted with other groups. Additionally, building on the work presented in Appendix C, the impact of salts could be explored by contrasting measurements that are not sensitive to salinity with those that are, and/or colour (i.e. visual imagery). This 'disagreement' could characterise a more dynamic picture of the relationship between moisture regimes,

salt weathering, and other aspects of stone weathering.

Of additional interest would be to explore opportunities within the growing field of hard/soft data fusion, which combines hard quantitative data (typically from sensors) with soft qualitative or semi-quantitative data based on human perception (Wolkenhauer, 2001; Wickramarathne et al., 2011). This could enhance the capabilities of non-destructive testing methods by capitalising on the breadth and depth of experiential knowledge about moisture ingress in the built environment represented in the building surveying and management community.

8.3.2 Visualisation strategies

There are several variables involved in the measurement and characterisation of moisture regimes and physical changes of stone masonry. Environmental conditions, such as temperature and humidity, exhibit spatial and temporal variation (Chapters 4 and 5). Equally, moisture surveys often incorporate data from many pieces of equipment (e.g. Chapter 7). This multi-dimensionality makes effective and and efficient communication of information difficult.

Visualisation is an under-explored topic in comprehensive moisture measurement literature (Nilsson, 2018) and wind-driven rain exposure (Blocken, 2014). Chapter 7 demonstrated the value of using multiple types of visualisation. These were most effectively employed in combination with appropriate data handling strategies (Section

8.3.1), and are equally important in the context of aspirations for data fusion (Section 8.3.1.1).

The multi-dimensionality of environmental conditions and rates of change is especially challenging to accurately represent. Figure 5.7 (on p. 123) demonstrates how innovative visualisations can distill multivariate data into effective forms of communication. This figure presents the baseline and predicted frequencies of occurrence of different wind-driven rain spell durations at 12 wall orientations at eight sites. This information could be represented by individual scatterplots of spell duration and one of: (1) baseline occurrence, (2) predicted future occurrence, or (3) percentage change in occurrence. This would require $8 \times 12 \times 3 = 288$ plots, as compared to the one (comprised of eight subplots) utilised herein.

The benefit of composite, effective visualisations is that they distill the 'overall messages' into a digestible format. Again using Figure 5.7 as the example, colour represents the percentage of change of predicted future occurrence to baseline conditions. It is evidentially clear that there are trends in this change related to wall orientation, and contrasts between sites. Similar approaches could be used to communicate non-destructive moisture measurement data, especially in scenarios where variation and contrast between regions of interest is paramount to the narrative.

8.4 Final remarks on discussion, synthesis, and future work

This chapter has discussed the papers that comprise the main body of research within this thesis in the context of the wider research field (Section 1.2 and Chapter 2). It has synthesised aspects of methodologies and characterisation within assessing wind-driven rain exposure and the response of stone masonry to it. This has demonstrated how these two components can inform one another. It has also discussed ways in which they hold implications for one another, and how future work could further links between them. Finally, this discussion has emphasised the common challenges faced within these components, especially data handling and visualisation, and provided suggestions of improvements to address these.

9 | Conclusion

"Each of us is carving a stone, erecting a column,
or cutting a piece of stained glass in the construction of
something much bigger than ourselves."

– RT HON ADRIENNE CLARKSON (2005)

This thesis has fulfilled the primary aim of evaluating and developing methodologies that contribute to improved assessment of exposure and response of stone masonry to wind-driven rain. It has assessed present and future wind-driven rain exposure in the UK and characterised hygric and physical properties of porous building stones and stone masonry systems demonstrating the utility of these methodologies. As a response to the practical challenges within heritage conservation faced by organisations such as Historic Environment Scotland and the Consarc Design Group, this thesis has emphasised semi-empirical evaluation and non-destructive techniques as practical and accessible tools widely used within the field. Each objective presented in Section 1.3 will be discussed in turn within their respective components.

9.1 Exposure to wind-driven rain

Objective A. To investigate current wind-driven rain exposure in the UK and evaluate the applicability of existing standards.

Extreme value analysis has been used to characterise extreme wind-driven rain

exposure for eight sites across the UK. The directional component (i.e. wall orientation) of exposure produces significant variation in the quantity, duration, and amount of wind-driven rain spells (Chapter 4). From 1986 to 2015, western coastal sites had high annual and spell exposure, especially for southern and western wall orientations in line prevailing wind directions. The intensity of exposure for northern and eastern wall orientations was more homogenous across the eight sites; the eastern coastal sites notably experienced the highest wind-driven rain exposure for eastern façades, demonstrating that wind speeds can have a dominating effect over prevailing wind directions.

Current standards are underestimating extreme wind-driven rain events such as the worst spell likely to occur in any given three year period when compared to a method based on extreme value analysis. In BS 8104, this shortcoming is likely caused by a poorly understood methodology to identify extreme events, as current wind-driven rain exposures are not significantly different from those of the mid-to-late twentieth century for many sites in the UK. For ISO 15927, this is influenced by its protocol that incorporates percentiles. Despite this, they remain a useful semi-qualitative tool for characterising annual exposure for average moisture contents and comparing relative exposures between sites.

Assessment of wind-driven rain exposure for design and risk analysis based on semi-empirical evaluations needs to incorporate methods that are not affected by random weather phenomena, such as extreme value analysis. Semi-empirical evaluations can be improved using these methods. Across the UK, the directional aspect (i.e. wall orientation) should

be considered as an important aspect in evaluating wind-driven rain exposure.

Objective B. To explore future wind-driven rain exposure in the UK and characterise the temporal attributes of wind-driven rain to develop new metrics.

Future wind-driven rain exposure has been characterised for eight UK sites towards the end of the twenty-first century under a high-emissions scenario by combining UKCP09 Weather Generator predictions with a probabilistic process (Chapter 5). The future UK climate is predicted to experience shorter wind-driven rain spells that have higher volumes of exposure in more concentrated time periods during winter and autumn months, but lower volumes during the summer – across all direction aspects (e.g. wall orientations). These increases will be more severe for western and coastal locations that already experienced higher wind-driven rain exposure during the twentieth century. This suggests higher risk due to increased frequency of more severe building element failure, near-surface cycling, and deep-seated wetting for stone masonry in the UK.

This demonstrates that there will not only be changes in the quantity of exposure to wind-driven rain, but also in the temporal characteristics, such as the length of wind-driven rain spells and the distribution of exposure within them. These require new temporal metrics to be developed and used to characterise the complex changes of wind-driven spell characterised predicted for the 21st century.

9.2 Response of moisture regimes within stone masonry

Objective C. To determine dielectric properties of three UK building stones and validate a rapid and cost-effective method of gravimetric calibration for non-destructive techniques.

A proposed cost- and time-effective 'isolated diffusion' gravimetric calibration procedure in which a set of samples are sealed at specific water contents and equilibrated has been validated (Chapter 6). A characterisation of dielectric properties enabled modelled behaviour over a range of moisture contents for each building stone to be developed. The calibrations determined from isolated diffusion more closely follow modelled behaviour than those from ambient drying, as the calibrations developed from the latter were affected by uneven distributions of moisture. Calibrations for radar measurements developed from two types of back interfaces (air and metal) were very similar to one another, suggesting that measurements are consistent regardless of the type of back interface used.

These results demonstrate the utility of gravimetric calibrations for enabling comparability between measurement techniques and geomaterials. The isolated diffusion calibration procedure provides a cost-effective and simple method to facilitate comparison between different NDT methods and enables accurate measurement of water contents in porous geomaterials. They enable a deeper understanding of the characteristic curves for different measurement devices and types of geomaterials, which supports accurate interpretation of

survey information when it is not possible to develop material-specific calibrations.

Objective D. To characterise moisture regimes within stone masonry systems based on comparative advantages of non-destructive electromagnetic techniques, and propose effective data handling and visualisation strategies.

The comparative advantages of microwave and radar measurements are examined in two field experiments of exposure to short (but intense) simulated wind-driven rain exposure to demonstrate when and how they are most effectively employed (Chapter 7). A novel method of representing data as percentiles is explored to facilitate effective communication of moisture measurements.

In this study, the response to simulated wind-driven rain spells of two types of stone masonry provided insight into how and when non-destructive electromagnetic sensors are best employed as part of a monitoring strategy. In cases when the masonry units and mortar joints have significantly different hygric properties, both radar and microwave techniques provide useful information on the distribution. In more homogenous constructions, microwave sensors can provide useful information on the overall distribution of water across a façade, building, or site, whereas radar measurements are more suited to investigate localised variation of water contents to evaluate the behaviour of masonry systems, and investigate surface water contents due to condensation. They can also be used to identify areas in which water has penetrated through mortar joints to the interior of a construction.

This demonstrates that both microwave and radar techniques can be useful for monitoring moisture in stone masonry systems. Material characteristics of the masonry system and the objective(s) of the investigation should be considered during selection of the appropriate technique(s).

Representing data in spatial and temporal visual forms facilitated a multi-perspective approach that enriched the interpretation of the monitoring. Converting data into measurement percentiles improved the visual resolution of colour-based representations and reduced the impact of extreme outliers.

Electromagnetic techniques should be selected in the context of material characteristics, and can especially be useful in combination in field studies of stone weathering. Radar and microwave techniques can be used in combination to evaluate the behaviour of masonry *systems* as a combination of stone masonry units and mortar joints. This is especially effective with the appropriate data handling and visualisation techniques, which should be explored further.

9.3 *Finale ultimo*[1]

There is a synergistic benefit in simultaneously developing methodologies and characterising exposure and response of stone masonry to wind-driven rain, which can be developed further in future work (Chapter 8). This is crucial, as the 21st century poses a great

[1] "Contemporary opera-goers are so accustomed to the idea of a finale being final that they may be surprised to discover that there is also such a thing as a *Finale ultimo*" (Kolodin, 1976, p. 185).

challenge to the resilience of stone masonry. There are predicted pressures of a changing climate. There is also the threat that existing stone masonry buildings are perceived as burdens, instead of opportunities, within sustainable development. These pressures are faced by monumental sites: the great cathedrals and palaces representing the triumph of technical and artistic pursuits of the past millennium. These pressures are equally pertinent for the vernacular and everyday place, which arguably play a much more significant role in daily life. Without these structures, an integral component of understanding our current and future relationship with the environment in the Anthropocenic context will be forfeited.

The opportunities afforded by data-driven advances and technological innovation to address these changes cannot be ignored. Ever increasing access to information, modes of analysis, and novel assessment tools present an inspiring array of possibilities to further understanding, conservation, and management of the historic built environment. These opportunities are imperative for heritage science, the progression of which depends on bridging the artificial gap between the 'two cultures' of the sciences and humanities. Breaking through this false dichotomy is the key to sustainability.

"Nothing is more dangerous than a dogmatic worldview–
nothing more constraining, more blinding to innovation,
more destructive of openness to novelty."

– PROF STEPHEN JAY GOULD (1997, p. 96)

References

Abuku, M., H. Janssen and S. Roels. (2009). 'Impact of wind-driven rain on historic brick wall buildings in a moderately cold and humid climate: Numerical analyses of mould growth risk, indoor climate and energy consumption'. *Energy and Buildings* 41 (1): 101–110. doi:10.1016/j.enbuild.2008.07.011.

Alani, A. M., M. Aboutalebi and G. Kilic. (2013). 'Applications of ground penetrating radar (GPR) in bridge deck monitoring and assessment'. *Journal of Applied Geophysics* 97:45–54. doi:10.1016/j.jappgeo.2013.04.009.

Alves, C., C. Figueiredo, A. Maurício, M. A. S. Braga and L. Aires-Barros. (2011). 'Limestones under salt decay tests: assessment of pore network-dependent durability predictors'. *Environmental Earth Sciences* 63 (7): 1511–1527. doi:10.1007/s12665-011-0915-1.

Antill, S. J., and H. A. Viles. (2003). 'Examples of the use of computer simulation as a tool for stone weathering research'. *Building and Environment* 38 (9/10): 1243–1250. doi:10.1016/S0360-1323(03)00081-7.

Antretter, F., F. Sauer, T. Schöpfer and A. Holm. (2011). 'Validation of a hygrothermal whole building simulation software'. In *Proceedings of the 12th Conference of the*

International Building Performance Simulation Association (Building Simulation, BS 2011), Sydney, Australia, November 14–16, 2011, 14:1694–1701.

Archie, G. E. (1942). 'The electrical resistivity log as an aid in determining some reservoir characteristics'. *Transactions of the AIME* 146 (01): 54–62. doi:10.2118/942054-G.

Arkell, W. J. (1947). *Oxford Stone*. London, UK: Faber & Faber.

ASHRAE. (2009). *Criteria for Moisture-Control Design Analysis in Buildings*. ASHRAE Standard 160. American Society of Heating, Refrigerating and Air-Conditioning Engineers.

Ashurst, J., and F. G. Dimes. (1998). *Conservation of Building and Decorative Stone*. Vol. 2. Oxford, UK: Butterworth-Heinemann.

Ashurst, N. (2016). *Cleaning Historic Buildings: Substrates, Soiling and Investigation*. 2nd ed. Vol. 1. Abingdon, UK: Routledge.

ASTM International. (2013a). *Standard Practice for Field Calibration and Application of Hand-Held Moisture Meters*. ASTM Standard 7438–13. West Conshohocken, PA, USA: ASTM International.

— . (2013b). *Standard Test Method for Laboratory Standardization and Calibration of Hand-Held Moisture Meters*. ASTM Standard D4444–13. West Conshohocken, PA, USA: ASTM International.

— . (2016). *Standard Test Methods for Direct Moisture Content Measurement of Wood and Wood-Based Materials*. ASTM Standard D4442–16. West Conshohocken, PA, USA: ASTM International.

— . (2018). *Standard Test Method for Field Determination of Water (Moisture) Content of Soil by the Calcium Carbide Gas Pressure Tester*. ASTM Standard D4944–18. West Conshohocken, PA, USA: ASTM International.

Baheru, T., A. G. Chowdhury, G. Bitsuamlak, F. J. Masters and A. Tokay. (2014). 'Simulation of wind-driven rain associated with tropical storms and hurricanes using the 12-fan Wall of Wind'. *Building and Environment* 76:18–29. doi:10.1016/j.buildenv.2014.03.002.

Ball, R. J., G. C. Allen, G. Starrs and W. J. McCarter. (2011). 'Impedance spectroscopy measurements to study physio-chemical processes in lime-based composites'. *Applied Physics A* 105 (3): 739–751. doi:10.1007/s00339-011-6509-7.

Barreira, E., R. M. S. F. Almeida and J. M. P. Q. Delgado. (2016). 'Infrared thermography for assessing moisture related phenomena in building components'. *Construction and Building Materials* 110:251–269. doi:10.1016/j.conbuildmat.2016.02.026.

Barrow, F. L. (1927). 'The measurement of moisture movements in building materials'. *Journal of Scientific Instruments* 4 (15): 475–480.

Bayram, F. (2012). 'Predicting mechanical strength loss of natural stones after freeze–thaw in cold regions'. *Cold Regions Science and Technology* 83/84:98–102. doi:10.1016/j.coldregions.2012.07.003.

Beckett, H. E. (1938). *Building Research Note, No. 755*. Tech. rep. Watford, UK: Building Research Station.

Beguin, D. (1986). 'Étude pour la France du risque de mouillage par la pluie des parois verticales de la construction'. *Cahiers du Centre Scientifique et Technique du Bâtiment*, no. 2106.

Beijer, O. (1977). 'Concrete walls and weathering'. In *Proceedings of the RILEM/ASTM/CIB Symposium on Evaluation of the Performance of External Vertical Surfaces of Buildings, Espoo, Finland, 23–31 August & 1-2 September, 1977*, 66–76.

Bell, D. (1991). *The Winding Passage: Sociological Essays and Journeys*. Piscataway, NJ, USA: Transaction Publishers.

Beloin, N. J., and F. H. Haynie. (1975). 'Soiling of Building Materials'. *Journal of the Air Pollution Control Association* 25 (4): 399–403. doi:10.1080/00022470.1975.10470099.

Benavente, D., G. Cultrone and M. Gómez-Heras. (2008). 'The combined influence of mineralogical, hygric and thermal properties on the durability of porous building

stones'. *European Journal of Mineralogy* 20 (4): 673–685. doi:10.1127/0935-1221/2008/0020-1850.

Bergman, N., and T. J. Foxon. (2018). 'Reorienting Finance Towards Energy Efficiency: The Case of UK Housing'. *SWPS* 05. doi:10.2139/ssrn.3109500.

Best, A. C. (1950). 'The size distribution of raindrops'. *Quarterly Journal of the Royal Meteorological Society* 76 (327): 16–36. doi:10.1002/qj.49707632704.

Bianco, L. (2017). 'Portland Stone and the Architectural History of London: An overview'. *Mesto a Dejiny—The City and History* 6 (1): 33–47.

Binda, L. (2005). 'MD.E.1: Determination of moisture distribution and level using radar in masonry built with regular units', *Materials and Structures* 38 (276): 283–288. doi:10.1617/14268.

Binda, L., and A. Anzani. (1997). 'Structural behaviour and durability of stone masonry'. In *Saving our architectural heritage: the conservation of historic stone structures*, 112–48. New York, NY, USA: Wiley.

Binda, L., L. Cantini and C. Tedeschi. (2013). 'Diagnosis of Historic Masonry Structures Using Non-Destructive Techniques'. In *Nondestructive Testing of Materials and Structures*, ed. by O. Büyüköztürk, M. A. Tademir, O. Güne and Y. Akkaya, 6:1089–1102. RILEM Bookseries. Amsterdam, Netherlands: Springer. doi:10.1007/978-94-007-0723-8_152.

Binda, L., G. Cardani and L. Zanzi. (2010). 'Nondestructive testing evaluation of drying process in flooded full-scale masonry walls'. *Journal of Performance of Constructed Facilities* 24 (5): 473–483. doi:10.1061/(ASCE)CF.1943-5509.0000097.

Birchak, J. R., C. G. Gardner, J. E. Hipp and J. M. Victor. (1974). 'High dielectric constant microwave probes for sensing soil moisture'. *Proceedings of the IEEE* 62 (1): 93–98. doi:10.1109/PROC.1974.9388.

Birnbaum, G., and S. K. Chatterjee. (1952). 'The dielectric constant of water vapor in the microwave region'. *Journal of Applied Physics* 23 (2): 220–223. doi:10.1063/1.1702178.

Bjelland, T., and I. H. Thorseth. (2002). 'Comparative studies of the lichen-rock interface of four lichens in Vingen, western Norway'. *Chemical Geology* 192:81–98. doi:10.1016/S0009-2541(02)00193-6.

Bläuer, C., and B. Rousset. (2009). 'Attempt to use microwave moisture mapping system (MOIST 200B) to control and monitor the water uptake of stones in frame of cultural heritage conservation'. In *Proceedings of the 12th International Conference on Microwave and High Frequency Heating (AMPERE 2009), Karlsruhe, Germany, 7–10 September, 2009*, 29–32.

Blocken, B. (2014). '50 years of Computational Wind Engineering: Past, present and future'. *Journal of Wind Engineering and Industrial Aerodynamics* 129:69–102. doi:10.1016/j.jweia.2014.03.008.

Blocken, B., M. Abuku, S. Roels and J. Carmeliet. (2009). 'Wind-driven rain on building facades: some perspectives'. In *Proceedings of the 5th European and African Conference on Wind Engineering, Florence, Italy, July 19–23, 2009*, 5:19–23.

Blocken, B., and J. Carmeliet. (2002). 'Spatial and temporal distribution of driving rain on a low-rise building'. *Wind and Structures* 5 (5): 441–462.

— . (2004). 'A review of wind-driven rain research in building science'. *Journal of Wind Engineering and Industrial Aerodynamics* 92 (13): 1079–1130. doi:10.1016/j.jweia.2004.06.003.

— . (2005). 'High-resolution wind-driven rain measurements on a low-rise building—experimental data for model development and model validation'. *Journal of Wind Engineering and Industrial Aerodynamics* 93 (12): 905–928. doi:10.1016/j.jweia.2005.09.004.

— . (2006a). 'On the accuracy of wind-driven rain measurements on buildings'. *Building and Environment* 41 (12): 1798–1810. doi:10.1016/j.buildenv.2005.07.022.

— . (2006b). ‘On the validity of the cosine projection in wind-driven rain calculations on buildings’. *Building and Environment* 41 (9): 1182–1189. doi:10.1016/j.buildenv.2005.05.002.

— . (2010). ‘Overview of three state-of-the-art wind-driven rain assessment models and comparison based on model theory’. *Building and Environment* 45 (3): 691–703. doi:10.1016/j.buildenv.2009.08.007.

Blümich, B., S. Anferova, K. Kremer, S. Sharma, V. Herrmann and A. Segre. (2003). ‘Unilateral nuclear magnetic resonance for quality control’. *Spectroscopy* 18 (2): 18–73.

Blümich, B., J. Perlo and F. Casanova. (2008). ‘Mobile single-sided NMR’. *Progress in Nuclear Magnetic Resonance Spectroscopy* 52 (4): 197–269. doi:10.1016/j.pnmrs.2007.10.002.

Bomberg, M., and C. J. Shirtliffe. (1978). ‘Influence of moisture and moisture gradients on heat transfer through porous building materials’. In *Proceedings of the Symposium on Heat Transmission Measurements, Philadelphia, PA, USA, 19–20 September, 1977*, ed. by R. Tye.

Bonazza, A., P. Brimblecombe, C. M. Grossi and C. Sabbioni. (2007). ‘Carbon in black crusts from the Tower of London’. *Environmental Science & Technology* 41 (12): 4199–4204. doi:10.1021/es062417w.

Bortolotti, V., M. Camaiti, C. Casieri, F. D. Luca, P. Fantazzini and C. Terenzi. (2006). 'Water absorption kinetics in different wettability conditions studied at pore and sample scales in porous media by NMR with portable single-sided and laboratory imaging devices'. *Journal of Magnetic Resonance* 181 (2): 287–295. doi:10.1016/j.jmr.2006.05.016.

Braun, R. C., and M. J. G. Wilson. (1970). 'The removal of atmospheric sulphur by building stones'. *Atmospheric Environment* 4 (4): 371–378. doi:10.1016/0004-6981(70)90082-X.

Briggen, P. M., B. Blocken and H. L. Schellen. (2009). 'Wind-driven rain on the facade of a monumental tower: Numerical simulation, full-scale validation and sensitivity analysis'. *Building and Environment* 44 (8): 1675–1690. doi:10.1016/j.buildenv.2008.11.003.

Brimblecombe, P. (1994). 'The Balance of Environmental Factors Attacking Artefacts', ed. by W. E. Krumbein, P. Brimblecombe, D. E. Cosgrove and S. Staniforth, 67–80. Durability and Change: The Science, Responsibility, and Cost of Sustaining Cultural Heritage. Berlin, Germany: John Wiley.

Brimblecombe, P. (2014). 'Refining climate change threats to heritage'. *Journal of the Institute of Conservation* 37 (2): 85–93. doi:10.1080/19455224.2014.916226.

British Geological Survey. (2015). 'Building stones in Edinburgh from the Carboniferous of West Lothian'. [HTML], accessed July 15, 2018. url: http://earthwise.bgs.ac.uk/index.php/Building_stones_in_Edinburgh_from_the_Carboniferous_of_West_Lothian.

Brocken, H. J. P., O. C. G. Adant and L. Pel. (1997). 'Moisture transport properties of mortar and mortar joint: a NMR study'. *Heron* 42 (1): 55–69.

Brown, B. (1988). *Field measurements to gauge catch ratios of free-space driving rain on house walls at exposed estates in Dorset*. Note 127/88. Watford, UK: Building Research Establishment.

Brown, S. J. (1996). 'The Disruption and the Dream: The Making of New College, 1843–1861'. In *Disruption to Diversity: Edinburgh Divinity 1846-1996.* Ed. by G. D. Wright David F.; Badcock, 29–50. London, UK: T&T Clark.

BSI. (1970). *Methods of test for resistance to air and water penetration. Permeable walling constructions (water penetration)*. BS 4315-2:1970. British Standards Institution.

— . (1984). *Method for assessing exposure to wind-driven rain*. BS DD93:1984. British Standards Institution.

— . (1992). *Code of practice for assessing exposure of walls to wind-driven rain*. BS 8104:1992. British Standards Institution.

— . (2001). *Hygrothermal performance of building components and building elements. Determination of the resistance of external wall systems to driving rain under pulsating air pressure*. BS EN 12865:2001. British Standards Institution.

— . (2017). *Conservation of cultural heritage. Methods of measurement of moisture content, or water content, in materials constituting immovable cultural heritage*. BS EN 16682:2017. British Standards Institution.

Building Research Establishment. (2000). 'Technical Data Sheet: Locharbriggs Sandstone'. [HTML], accessed March 22, 2018. url: http://projects.bre.co.uk/ConDiv/stonelist/locharbriggs.html.

Burkinshaw, R., and M. Parrett. (2003). *Diagnosing Damp*. London, UK: RICS Books.

Camaiti, M., V. Bortolotti and P. Fantazzini. (2015). 'Stone porosity, wettability changes and other features detected by MRI and NMR relaxometry: a more than 15-year study'. *Magnetic Resonance in Chemistry* 53 (1): 34–47. doi:10.1002/mrc.4163.

Camuffo, D. (1995). 'Physical weathering of stones'. *Science of The Total Environment* 167 (1): 1–14. doi:10.1016/0048-9697(95)04565-I.

— . (1998). *Microclimate for Cultural Heritage*. Amsterdam, Netherlands: Elsevier.

— . (2013). *Microclimate for Cultural Heritage: Conservation, Restoration, and Maintenance of Indoor and Outdoor Monuments*. 2nd ed. New York, NY, USA: Elsevier Science.

— . (2018). ‘Standardization activity in the evaluation of moisture content’. *Journal of Cultural Heritage* 31:S10–S14. doi:10.1016/j.culher.2018.03.021.

Camuffo, D., and C. Bertolin. (2012). ‘Towards standardisation of moisture content measurement in cultural heritage materials’. *E-Preservation Science* 9:23–35.

Capitani, D., N. Proietti, M. Gobbino, L. Soroldoni, U. Casellato, M. Valentini and E. Rosina. (2009). ‘An integrated study for mapping the moisture distribution in an ancient damaged wall painting’. *Analytical and Bioanalytical Chemistry* 395 (7): 2245–2253. doi:10.1007/s00216-009-3170-5.

Cardani, G., L. Cantini, S. Munda, L. Zanzi and L. Binda. (2013). ‘Non Invasive Measurements of Moisture in Full-Scale Stone and Brick Masonry Models After Simulated Flooding: Effectiveness of GPR’. In *Nondestructive Testing of Materials and Structures*, ed. by O. Büyüköztürk, M. A. Tademir, O. Güne and Y. Akkaya, 6:1143–1149. RILEM Bookseries. Amsterdam, Netherlands: Springer Netherlands. doi:10.1007/978-94-007-0723-8_159.

Carswell, C. M. (1992). ‘Choosing specifiers: An evaluation of the basic tasks model of graphical perception’. *Human Factors* 34 (5): 535–554. doi:10.1177/001872089203400503.

Cartz, L. (1995). *Nondestructive testing*. Geauga County, OH, US: ASM International.

Cassar, M. (2005). *Climate Change and the Historic Environment*. Report. London, UK: UCL Centre for Sustainable Heritage.

CEN. (1997). *Hygrothermal performance of buildings – Climatic data – Part 3 : Calculation of a driving rain index for vertical surfaces from hourly wind and rain data*. Draft prEN 13013-3. Comité Européen de normalisation.

Cerný, R., J. Semerak, J. Toman and P. Häupl. (1995). 'A capacitive method for measuringthe moisture content in envelope parts of building structures'. In *Proceedings of the International Symposium Non-Destructive Testing in Civil Engineering (NDT-CE), Berlin, Germany, September 26–28, 1995*, 995–1002.

Cerný, R. (2009). 'Time-domain reflectometry method and its application for measuring moisture content in porous materials: A review'. *Measurement* 42 (3): 329–336. doi:10.1016/j.measurement.2008.08.011.

Cetrangolo, G. P., L. D. Domenech, G. Moltini and A. A. Morquio. (2017). 'Determination of Moisture Content in Ceramic Brick Walls Using Ground Penetration Radar'. *Journal of Nondestructive Evaluation* 36 (1): 12. doi:10.1007/s10921-016-0390-4.

Chabriac, P.-A., A. Fabbri, J.-C. Morel, J.-P. Laurent and J. Blanc-Gonnet. (2014). 'A procedure to measure the in-situ hygrothermal behavior of earth walls'. *Materials* 7 (4): 3002–3020. doi:10.3390/ma7043002.

Chang, E. K. M., Y. Guo and X. Xia. (2012). 'CMIP5 multimodel ensemble projection of storm track change under global warming'. *Journal of Geophysical Research: Atmospheres* 117 (D23). doi:10.1029/2012JD018578.

Charola, A. E., and R. Ware. (2002). 'Acid deposition and the deterioration of stone: a brief review of a broad topic'. *Geological Society of London, Special Publications* 205 (1): 393–406. doi:10.1144/GSL.SP.2002.205.01.28.

Charola, A. E. (2000). 'Salts in the Deterioration of Porous Materials: An Overview'. *Journal of the American Institute for Conservation* 39 (3): 327–343. doi:10.2307/3179977.

Chartered Institute for Buildings Services Engineers. (2017). 'Test Reference Years'. [HTML], accessed September 6, 2017. url: www.cibse.org.

Choi, E. C. C. (1991). 'Numerical simulation of wind-driven rain falling onto a 2-D building'. In *Proceedings of the The Asian Pacific Conference on Computational Mechanics, Hong Kong, Hong Kong, December 11–13, 1991*, 1721–1727.

— . (1993). 'Simulation of wind-driven-rain around a building'. *Computational Wind Engineering* 1:721–729. doi:10.1016/0167-6105(93)90342-L.

— . (1994a). 'Determination of wind-driven-rain intensity on building faces'. *Journal of Wind Engineering and Industrial Aerodynamics* 51 (1): 55–69. doi:10.1016/0167-6105(94)90077-9.

— . (1994b). ‘Parameters affecting the intensity of wind-driven rain on the front face of a building’. *Journal of Wind Engineering and Industrial Aerodynamics* 53 (1–2): 1–17. doi:10.1016/0167-6105(94)90015-9.

— . (1997). ‘Numerical modelling of gust effect on wind-driven rain’. *Journal of Wind Engineering and Industrial Aerodynamics* 72:107–116. doi:10.1016/S0167-6105(97)00246-8.

Christensen, J. H., K. K. Kanikicharla, G. Marshall and J. Turner. (2013). ‘Climate phenomena and their relevance for future regional climate change’. In *Climate Change 2013: The Physical Science Basis. Contribution of Working Group I to the Fifth Assessment Report of the Intergovernmental Panel on Climate Change*, ed. by T. F. Stocker, D. Qin, G.-K. Plattner, M. M. B. Tignor, S. K. Allen, J. Boschung, A. Nauels, Y. Xia, V. Bex and P. M. Midgley. Cambridge, UK and New York, NY, USA: Cambridge University Press.

Christian, J. E. (1993). ‘A search for moisture sources’. In *Bugs, Mold & Rot II: Proceedings of a Workshop on Control of Humidity for Health, Artefacts, and Buildings, Oak Ridge, TN, USA, November 16–17, 1993*, 71–81.

Clarke, B. L., and J. Ashurst. (1972). *Stone Preservation Experiments*. Watford, UK: Building Research Establishment.

Clarkson, A. (2005). 'Her Excellency the Right Honourable Adrienne Clarkson Speech on the Occasion of the Order of Canada Investiture'. [HTML], accessed September 3, 2018. url: http://archive.gg.ca/media/doc.asp?lang=e&DocID=4396.

Cleveland, W. S., and R. McGill. (1985). 'Graphical perception and graphical methods for analyzing scientific data'. *Science* 229 (4716): 828–833. doi:10.1126/science.229.4716.828.

Climent, M., S. Lindmark and L.-O. Nilsson. (2018). 'Calibration techniques'. Chap. 4 in *Methods of Measuring Moisture in Building Materials and Structures: State-of-the-Art Report of the RILEM Technical Committee 248-MMB*, ed. by L.-O. Nilsson, 27–37. New York, NY, USA: Springer International.

Cole, K. S., and R. H. Cole. (1941). 'Dispersion and absorption in dielectrics I. Alternating current characteristics'. *The Journal of Chemical Physics* 9 (4): 341–351. doi:10.1063/1.1750906.

Coles, S. (2001). *An Introduction to Statistical Modeling of Extreme Values*. London, UK: Springer.

Colman, S. M. (1981). 'Rock-weathering rates as functions of time'. *Quaternary Research* 15 (3): 250–264. doi:10.1016/0033-5894(81)90029-6.

Cooke, R. U., R. J. Inkpen and G. F. S. Wiggs. (1995). 'Using gravestones to assess changing rates of weathering in the United Kingdom'. *Earth Surface Processes and Landforms* 20 (6): 531–546. doi:10.1002/esp.3290200605.

Cooling, L. F. (1930). 'Contribution to the study of florescence. II. The evaporation of water from bricks'. *Transactions of the British Ceramic Society* 29:39–54.

Cotic, P., Z. Jaglicic, E. Niederleithinger, U. Effner, S. Kruschwitz, C. Trela and V. Bosiljkov. (2013). 'Effect of moisture on the reliability of void detection in brickwork masonry using radar, ultrasonic and complex resistivity tomography'. *Materials and Structures* 46 (10): 1723–1735. doi:10.1617/s11527-012-0011-3.

Council of Europe. (1985). *Convention for the Protection of the Architectural Heritage of Europe*. CETS 121. Brussels, Belgium: Council of Europe.

Craig, G. (1892). 'On building stones used in Edinburgh: their geological sources, relative durability and other characteristics'. *Transactions of the Edinburgh Geological Society* 6 (4): 254–273.

Crispim, C. A., and C. C. Gaylarde. (2005). 'Cyanobacteria and Biodeterioration of Cultural Heritage: A Review'. *Microbial Ecology* 49 (1): 1–9. doi:10.1007/s00248-003-1052-5.

Cunnane, C. (1973). 'A particular comparison of annual maxima and partial duration series methods of flood frequency prediction'. *Journal of Hydrology* 18 (3): 257–271. doi:10.1016/0022-1694(73)90051-6.

D'Ayala, D., and Y. D. Aktas. (2016). 'Moisture dynamics in the masonry fabric of historic buildings subjected to wind-driven rain and flooding'. *Building and Environment* 104:208–220. doi:10.1016/j.buildenv.2016.05.015.

Davis, R. E., G. R. McGregor and K. B. Enfield. (2016). 'Humidity: A review and primer on atmospheric moisture and human health'. *Environmental Research* 144:106–116. doi:10.1016/j.envres.2015.10.014.

De Rose, D., N. Pearson, P. Mensinga and J. F. Straube. (2014). 'Towards a limit states approach to insulating solid masonry walls in a cold climate'. In *14th Canadian Conference on Building Science and Technology, Toronto, ON, Canada, October 29–30, 2014*.

DEFRA. (2009). 'UK Climate Projections 2009'. [HTML], accessed September 6, 2017. url: http://ukclimateprojections.defra.gov.uk/.

Derome, D., A. Teasdale-St-Hilare and P. Fazio. (2001). 'Methods for the assessment of moisture content of envelope assemblies.' In *Proceedings of ASHRAE/DOE Buildings VIII, Thermal Performance of the Exterior Envelopes of Whole Buildings, Clearwater Beach, FL, USA, December 2–7, 2001*.

Derome, D., A. Kubilay, T. Defraeye, B. Blocken and J. Carmeliet. (2017). 'Ten questions concerning modeling of wind-driven rain in the built environment'. *Building and Environment* 114:495–506. doi:10.1016/j.buildenv.2016.12.026.

Di Tullio, V., N. Proietti, M. Gobbino, D. Capitani, R. Olmi, S. Priori, C. Riminesi and E. Giani. (2010). 'Non-destructive mapping of dampness and salts in degraded wall paintings in hypogeous buildings: the case of St. Clement at mass fresco in St. Clement Basilica, Rome'. *Analytical and Bioanalytical Chemistry* 396 (5): 1885–1896. doi:10.1007/s00216-009-3400-x.

DiGiovanni, D. A., A. J. Gatesman, R. H. Giles and W. E. Nixon. (2013). 'Backscattering of ground terrain and building materials at submillimeter-wave and terahertz frequencies'. *Proceedings of the SPIE — Passive and Active Millimeter-Wave Imaging XVI* 8715. doi:10.1117/12.2015772.

Dill, M. J. (2000). *A review of testing for moisture in building elements*. London, UK: CIRIA.

Divya, N. K., and P. Ramanathan. (2017). 'Non-destructive methods for the measurement of moisture contents – a review'. *Sensor Review* 37 (1): 71–77. doi:10.1108/SR-01-2016-0032.

Dobson, M. C., F. T. Ulaby, M. T. Hallikainen and M. A. El-Rayes. (1985). 'Microwave dielectric behavior of wet soil-Part II: Dielectric mixing models'. *IEEE Transactions on Geoscience and Remote Sensing*, no. 1: 35–46. doi:10.1109/TGRS.1985.289498.

Doehne, E. (2002). 'Salt Weathering: A Selective Review'. In *Natural stone, weathering phenomena, conservation strategies and case studies*, ed. by S. Siegesmund, S. A. Vollbrecht and T. Weiss, 51–64. Geological Society of London.

Doehne, E., and C. A. Price. (2010). *Stone Conservation: An Overview of Current Research*. 2nd ed. Research in Conservation. Los Angeles, CA, USA: Getty Conservation Institute.

Drury, P., and A. McPherson. (2008). *Conservation principles: policies and guidance for the sustainable management of the historic environment*. London, UK: English Heritage.

Du, H., C. P. Underwood and J. S. Edge. (2012). 'Generating design reference years from the UKCP09 projections and their application to future air-conditioning loads'. *Building Services Engineering Research and Technology* 33 (1): 63–79. doi:10.1177/0143624411431775.

Dubelaar, C. W., S. Engering, R. P. J. Van Hees, R. Koch and H. G. Lorenz. (2003). 'Lithofacies and petrophysical properties of Portland Base Bed and Portland Whit Bed limestone as related to durability'. *Heron* 48 (3): 221–229.

Eames, M., T. Kershaw and D. Coley. (2011a). 'The creation of wind speed and direction data for the use in probabilistic future weather files'. *Building Services Engineering Research and Technology* 32 (2): 143–158. doi:10.1177/0143624410381624.

Eames, M., T. Kershaw and D. Coley. (2011b). 'On the creation of future probabilistic design weather years from UKCP09'. *Building Services Engineering Research and Technology* 32 (2): 127–142. doi:10.1177/0143624410379934.

Ecorys. (2012). *The Economic Impact of Maintaining and Repairing Historic Buildings in England*. A Report to the Heritage Lottery Fund and English Heritage. London, UK: Heritage Lottery Fund.

Edis, E., I. Flores-Colen and J. de Brito. (2015). 'Quasi-quantitative infrared thermographic detection of moisture variation in facades with adhered ceramic cladding using principal component analysis'. *Building and Environment* 94 (1): 97–108. doi:10.1016/j.buildenv.2015.07.027.

Eidmann, G., R. Savelsberg, P. Blümler and B. Blümich. (1996). 'The NMR-MOUSE^{TM}, a mobile universal surface explorer'. *Journal of Magnetic Resonance* 122:104–109.

Eklund, J. A., H. Zhang, H. A. Viles and T. Curteis. (2013). 'Using handheld moisture meters on limestone: Factors affecting performance and guidelines for best practice'. *International Journal of Architectural Heritage* 7 (2): 207–224. doi:10.1080/15583058.2011.626491.

Ekström, M., P. D. Jones, H. J. Fowler, G. Lenderink, T. A. Buishand and D. Conway. (2007). 'Regional climate model data used within the SWURVE project 1: projected changes in seasonal patterns and estimation of PET'. *Hydrology and Earth System Sciences Discussions* 11 (3): 1069–1083. doi:10.5194/hess-11-1069-2007.

El Beyrouty, K., and A. Tessler. (2013). *The economic impact of the UK heritage tourism economy*. Tech. rep. Oxford, UK: Oxford Economics.

Eldridge, H. J. (1976). *Common defects in buildings*. London, UK: HM Stationery Office.

Emery, D., and J. A. D. Dickson. (1989). 'A syndepositional meteoric phreatic lens in the Middle Jurassic Lincolnshire Limestone, England, UK'. *Sedimentary Geology* 65 (3–4): 273–284. doi:10.1016/0037-0738(89)90029-8.

Engeland, K., H. Hisdal and A. Frigessi. (2004). 'Practical extreme value modelling of hydrological floods and droughts: a case study'. *Extremes* 7 (1): 5–30. doi:10.1007/s10687-004-4727-5.

English Heritage. (2012). *Practical building conservation: Stone*. Ed. by D. Odgers and A. Henry. Farnham, UK: Ashgate.

— . (2014). *Practical building conservation: Building Environment*. Ed. by R. Pender, B. Ridout and T. Curteis. Farnham, UK: Ashgate.

Erkal, A., D. D'Ayala and L. Sequeira. (2012). 'Assessment of wind-driven rain impact, related surface erosion and surface strength reduction of historic building materials'. *Building and Environment* 57:336–348. doi:10.1016/j.buildenv.2012.05.004.

Espinosa-Marzal, R. M., and G. W. Scherer. (2010). 'Mechanisms of damage by salt'. *Geological Society of London, Special Publications* 331 (1): 61–77. doi:10.1144/SP331.5.

Fatoric, S., and E. Seekamp. (2017). 'Are cultural heritage and resources threatened by climate change? A systematic literature review'. *Climatic Change* 142 (1): 227–254. doi:10.1007/s10584-017-1929-9.

Fazio, P., S. R. Mallidi and D. Zhu. (1995). 'A quantitative study for the measurement of driving rain exposure in the Montreal region'. *Building and Environment* 30 (1): 1–11. doi:10.1016/0360-1323(94)E0028-P.

Federici, J. F. (2012). 'Review of Moisture and Liquid Detection and Mapping using Terahertz Imaging'. *Journal of Infrared, Millimeter, and Terahertz Waves* 33 (2): 97–126. doi:10.1007/s10762-011-9865-7.

Fisher, R. A., and L. H. C. Tippett. (1928). 'Limiting forms of the frequency distribution of the largest or smallest member of a sample'. *Mathematical Proceedings of the Cambridge Philosophical Society* 24 (2): 180–190. doi:10.1017/S0305004100015681.

Fister, W., T. Iserloh, J. B. Ries and R.-G. Schmidt. (2012). 'A portable wind and rainfall simulator for in situ soil erosion measurements'. *Catena* 91:72–84. doi:10.1016/j.catena.2011.03.002.

Flammarion, C. (1905). *L'atmosphère et les grands phénomènes de la nature*. Paris, France: Hachette.

Forster, A. M., and K. Carter. (2011). 'A framework for specifying natural hydraulic lime mortars for masonry construction'. *Structural Survey* 29 (5): 373–396. doi:10.1108/02630801111182411.

Fowler, H. J., and M. Ekström. (2009). 'Multi-model ensemble estimates of climate change impacts on UK seasonal precipitation extremes'. *International Journal of Climatology* 29 (3): 385–416. doi:10.1002/joc.1827.

Franzen, C., and P. W. Mirwald. (2009). 'Moisture sorption behaviour of salt mixtures in porous stone'. *Geochemistry* 69 (1): 91–98. doi:10.1016/j.chemer.2008.02.001.

Franzini, M., C. Gratziu and M. Spampinato. (1984). 'Degradazione del marmo per effetto di variazioni di temperatura'. *Rendiconti della Società Italiana di Mineralogia e Petrologia* 39:47–58.

Friel, S. N., F. R. Curcio and G. W. Bright. (2001). 'Making sense of graphs: Critical factors influencing comprehension and instructional implications'. *Journal for Research in mathematics Education*: 124–158. doi:10.2307/749671.

Galagedara, L. W., G. W. Parkin and J. D. Redman. (2003). 'An analysis of the ground-penetrating radar direct ground wave method for soil water content measurement'. *Hydrological Processes* 17 (18): 3615–3628. doi:10.1002/hyp.1351.

Gallant, M. I. (n.d.). 'Layer Reflectance Calculator'. [HTML] Accessed via www.archive.org, April 11, 2018. url: http://www.jensign.com/reflect/r8TA.html.

Garden, G. K. (1963). *Rain penetration and its control*. 401–404. CBD40. Division of Building Research, National Research Council of Canada.

Garnett, J. C. M. (1904). 'XII. Colours in metal glasses and in metallic films'. *Philosophical Transactions of the Royal Society of London A: Mathematical, Physical and Engineering Sciences* 203 (359–371): 385–420. doi:10.1098/rsta.1904.0024.

Garratt, J., and F. Nowak. (1991). *Tackling Condensation: A Guide to the Causes Of, and Remedies for Surface Condensation and Mould in Traditional Housing*. Report 174. Watford, UK: Building Research Establishment.

Gärtner, G., R. Plagge and H. Sonntag. (2010). 'Determination of moisture content of the outer wall using hf-sensor technology'. In *Proceedings of the 1st European Conference on Moisture Measurement, Weimar, Germany, October 5–7, 2010.*

Gauri, K. L. (1978). 'The preservation of stone'. *Scientific American* 238 (6): 126–136.

Ge, H., V. Chiu and T. Stathopoulos. (2017). 'Effect of overhang on wind-driven rain wetting of facades on a mid-rise building: Field measurements'. *Building and Environment* 118:234–250. doi:10.1016/j.buildenv.2017.03.034.

Ge, H., V. Chiu, T. Stathopoulos and F. Souri. (2018). 'Improved assessment of wind-driven rain on building façade based on ISO standard with high-resolution on-site weather data'. *Journal of Wind Engineering and Industrial Aerodynamics* 176:183–196. doi:10.1016/j.jweia.2018.03.013.

Geisel, T. S. (1979). *Oh Say Can You Say?* New York, NY, USA: Random House.

Ghandehari, M., C. S. Vimer, I. Ioannou, A. Sidelev, W. Jin and P. Spellane. (2012). 'In-situ measurement of liquid phase moisture in cement mortar'. *NDT&E International* 45 (1): 162–168. doi:10.1016/j.ndteint.2011.09.011.

Giannopoulos, A. (2005). 'Modelling ground penetrating radar by gprMax'. *Construction and Building Materials* 19 (10): 755–762. doi:10.1016/j.conbuildmat.2005.06.007.

Giarma, C., and D. Aravantinos. (2014). 'On building components' exposure to driving rain in Greece'. *Journal of Wind Engineering and Industrial Aerodynamics* 125:133–145. doi:10.1016/j.jweia.2013.11.014.

Göller, A. (2001). 'Moisture mapping—getting 2D and 3D moisture distribution by microwave measurements'. In *Proceedings of the Fourth International Conference on*

Electromagnetic Wave Interaction with Water and Moist Substances, Weimar, Germany, May 13–16, 2001, ed. by K. Kupfer, 282–289.

— . (2006). 'Microwave Scanning Technology for Material Testing'. In *Proceedings of the 9th European Conference on NDT (EC-NDT 2006), Berlin, Germany, September 25–29, 2006*.

— . (2012). 'MOIST SCAN – Multilayer microwave moisture scans at buildings, masonry and civil structures'. In *Proceedings of the 14th International Conference and Exhibition on Structural Faults and Repair, Edinburgh, UK, July 3–5, 2012*.

Gómez-Heras, M., B. J. Smith and R. Fort. (2008). 'Influence of surface heterogeneities of building granite on its thermal response and its potential for the generation of thermoclasty'. *Environmental Geology* 56:547–560. doi:10.1007/s00254-008-1356-3.

Gómez-Heras, M., and S. McCabe. (2015). 'Weathering of stone-built heritage: A lens through which to read the Anthropocene'. *Anthropocene* 11:1–13. doi:10.1016/j.ancene.2015.12.003.

Goudie, A. S., and H. A. Viles. (1997). *Salt Weathering Hazards*. Chichester, UK: Wiley.

Gould, S. J. (1997). *Dinosaur in a haystack : reflections in natural history*. London, UK: Penguin.

Griffin, P. S., N. Indictor and R. J. Koestler. (1991). 'The biodeterioration of stone: a review of deterioration mechanisms, conservation case histories, and treatment'. *International Biodeterioration* 28 (1–4): 187–207. doi:10.1016/0265-3036(91)90042-P.

Grinzato, E., N. Ludwig, G. Cadelano, M. Bertucci, M. Gargano and P. Bison. (2011). 'Infrared thermography for moisture detection: a laboratory study and in-situ test'. *Materials Evaluation* 69 (1): 97–104.

Gros, X. E. (1997). *NDT Data Fusion*. London, UK: Arnold.

Grossi, C. M., R. M. Esbert, F. Daz-Pache and F. J. Alonso. (2003). 'Soiling of building stones in urban environments'. *Building and Environment* 38 (1): 147–159. doi:10.1016/S0360-1323(02)00017-3.

Guan, L. (2009). 'Preparation of future weather data to study the impact of climate change on buildings'. *Building and Environment* 44 (4): 793–800. doi:10.1016/j.buildenv.2008.05.021.

Gumbel, E. J. (1941). 'The return period of flood flows'. *The annals of mathematical statistics* 12 (2): 163–190. doi:10.1214/aoms/1177731747.

— . (1958). *Statistics of extremes*. New York, NY, USA: Columbia University Press.

Gummerson, R. J., C. Hall and W. D. Hoff. (1980). ‘Capillary water transport in masonry structures: building construction applications of Darcy’s law’. *Construction Papers* 1 (1): 17–27.

Gummerson, R. J., C. Hall, W. D. Hoff, R. Hawkes, G. N. Holland and W. S. Moore. (1979). ‘Unsaturated water flow within porous materials observed by NMR imaging’. *Nature* 281:56–57. doi:10.1038/281056a0.

Guttman, N. (2010). *Guide to Climatological Practices*. Tech. rep. 100. Geneva, Switzerland: World Meteorological Organisation.

Haarsma, R. J., W. Hazeleger, C. Severijns, H. Vries, A. Sterl, R. Bintanja, G. J. Oldenborgh and H. W. Brink. (2013). ‘More hurricanes to hit western Europe due to global warming’. *Geophysical Research Letters* 40 (9): 1783–1788. doi:10.1002/grl.50360.

Haghighat, M., M. Abdel-Mottaleb and W. Alhalabi. (2016). ‘Discriminant Correlation Analysis: Real-Time Feature Level Fusion for Multimodal Biometric Recognition’. *IEEE Transactions on Information Forensics and Security* 11 (9): 1984–1996. doi:10.1109/TIFS.2016.2569061.

Hall, C., A. Hamilton, W. D. Hoff, H. A. Viles and J. A. Eklund. (2011). ‘Moisture dynamics in walls: Response to micro-environment and climate change’. *Proceedings*

of the Royal Society A: Mathematical, Physical and Engineering Sciences 467 (2125): 194–211. doi:10.1098/rspa.2010.0131.

Hall, C., and W. D. Hoff. (2002). *Water Transport in Brick, Stone, and Concrete*. London, UK and New York, NY, USA: Spon Press.

— . (2012). *Water Transport in Brick, Stone and Concrete*. 2nd ed. London, UK and New York, NY, USA: Spon Press, Taylor & Francis Group.

Hall, C., and W. D. Hoff. (2007). 'Rising damp: capillary rise dynamics in walls'. *Proceedings of the Royal Society of London A: Mathematical, Physical and Engineering Sciences* 463 (2084): 1871–1884. doi:10.1098/rspa.2007.1855.

Hall, K. (1999). 'The role of thermal stress fatigue in the breakdown of rock in cold regions'. *Geomorphology* 31 (1-4): 47–63. doi:10.1016/S0169-555X(99)00072-0.

Hansen, J., and M. Sato. (2016). 'Regional climate change and national responsibilities'. *Environmental Research Letters* 11 (3): 034009.

Hauschild, T., and F. Menke. (1998). 'Moisture measurement in masonry walls using a non-invasive reflectometer'. *Electronics Letters* 34 (25): 2413–2414. doi:10.1049/el:19981694.

Hehl, K., and W. Wesch. (1980). 'Calculation of optical reflection and transmission coefficients of a multi-layer system'. *physica status solidi (a)* 58 (1): 181–188. doi:10.1002/pssa.2210580122.

Heideklang, R., and P. Shokouhi. (2013). ‘Application of data fusion in nondestructive testing (NDT)’. In *Proceedings of the 16th International Conference on Information Fusion (FUSION 2013), Istanbul, Turkey, July 9–12, 2013*, 835–841.

Hilaire, J., and H. Savina. (1988). *Pluie battante sur une façade d’immeuble*. Tech. rep. Nantes, Frances: CSTB.

Hillerman, T. (1990). *Coyote Waits*. New York, NY, USA: Harper & Row.

Historic England. (2017). *Strategic Stone Study: A Building Stone Atlas of North Yorkshire East and York*. First published by English Heritage 2012, rebranded by Historic England in December 2017. London, UK: Historic England.

Historic Environment Scotland. (2018). *A climate change risk assessment*. Research and Study Report. Edinburgh, UK: Historic Environment Scotland.

Högberg, A. B., M. K. Kragh and F. J. van Mook. (1999). ‘A comparison of driving rain measurements with different gauges’. In *Proceedings of the 5th Symposium of Building Physics in the Nordic Countries, Gothenburg, Sweden, August 24–26, 1999*, 361–368.

Hoke, G. D., and D. L. Turcotte. (2004). ‘The weathering of stones due to dissolution’. *Environmental Geology* 46 (3/4): 305–310. doi:10.1007/s00254-004-1033-0.

Holm, A., and H. M. Künzel. (2003). ‘Two-dimensional transient heat and moisture simulations of rising damp with WUFI 2D’. In *Research in Building Physics:*

Proceedings of the 2nd International Conference on Building Physics, Antwerp, Belgium, September 14–18, 2003, 363–67.

Holmes, C. (2015). *Future changes in wind and rain and the implications for wind driven rain*. Tech. rep. Boston, MA, US: ClimateXChange.

Holmes, S., and M. Wingate. (2002). *Building with Lime: A Practical Introduction*. 2nd ed. Bradford, UK: ITDG.

Holtorf, C. (2006). 'Can less be more? Heritage in the age of terrorism'. *Public Archaeology* 5 (2): 101–109. doi:10.1179/pua.2006.5.2.101.

Hooff, T. van, B. Blocken and M. van Harten. (2011). '3D CFD simulations of wind flow and wind-driven rain shelter in sports stadia: Influence of stadium geometry'. *Building and Environment* 46 (1): 22–37. doi:10.1016/j.buildenv.2010.06.013.

Hoppestad, S. (1955). *Slagregn i Norge.* Tech. rep. 13. Oslo, Norway: Norges Byggforskningsinstitutt.

Houghton, H. G. (1968). 'On precipitation mechanisms and their artificial modification'. *Journal of Applied Meteorology* 7 (5): 851–859.

Houze Jr, R. A. (1997). 'Stratiform precipitation in regions of convection: A meteorological paradox?' *Bulletin of the American Meteorological Society* 78 (10): 2179–2196.

Howell, J. (1995). 'Moisture measurement in masonry: Guidance for surveyors'. In *COBRA 1995*, 145–148. London, UK: The Royal Institution of Chartered Surveyors.

Huang, S. H., and Q. S. Li. (2010). 'Numerical simulations of wind-driven rain on building envelopes based on Eulerian multiphase model'. *Journal of Wind Engineering and Industrial Aerodynamics* 98 (12): 843–857. doi:10.1016/j.jweia.2010.08.003.

Hughes, J., C. Groot, K. Van Balen, B. Bicer-Simsir, L. Binda, J. Elsen, R. Hees, T. Von Konow, J. Erik Lindqvist, P. Maurenbrecher, I. Papayianni, M. Subercaseaux, C. Tedeschi, E.-E. Toumbakari, M. Thompson, J. Válek and M. Veiga. (2012). 'RILEM TC 203-RHM Repair mortars for historic masonry: The role of mortar in masonry: an introduction to the requirements for the design of repair mortars'. *Materials and Structures* 45:1287–1294.

Hughes, T., G. K. Lott, M. J. Poultney and B. J. Cooper. (2013). 'Portland Stone: A nomination for "Global Heritage Stone Resource" from the United Kingdom'. *Episodes* 36 (3): 221–226.

Hundt, J., and J. Buschmann. (1971). 'Moisture measurement in concrete'. *Materials and Structures* 4 (4): 253–256. doi:10.1007/BF02478952.

Hussain, M. G. M. (2005). 'Mathematical model for the electromagnetic conductivity of lossy materials'. *Journal of Electromagnetic Waves and Applications* 19 (2): 271–279. doi:10.1163/1569393054497311.

ICOMOS-ISCS. (2008). 'Illustrated Glossary on Stone Deterioration Patterns'. In *Monuments & Sites*, ed. by V. Vergès-Belmin, vol. 15. ICOMOS (International Council on Monuments and Sites) and ISCS (International Scientific Committee for Stone).

Inkpen, R. J., H. A. Viles, C. Moses, B. Baily, P. Collier, S. T. Trudgill and R. U. Cooke. (2012). 'Thirty years of erosion and declining atmospheric pollution at St Paul's Cathedral, London'. *Atmospheric Environment* 62:521–529. doi:10.1016/j.atmosenv.2012.08.055.

Iowa Environmental Mesonet. (2018). 'Wind Roses for Edinburgh Airport'. [HTML], accessed July 15, 2018. url: https://mesonet.agron.iastate.edu/sites/windrose.phtml?network=GB__ASOS&station=EGPH.

IPCC. (2013). 'Summary for Policymakers'. In *Climate Change 2013: The Physical Science Basis. Contribution of Working Group I to the Fifth Assessment Report of the Intergovernmental Panel on Climate Change*, ed. by T. Stocker, D. Qin, G.-K. Plattner, M. Tignor, S. Allen, J. Boschung, A. Nauels, Y. Xia, V. Bex and P. Midgley, 3–32. Cambridge, UK: Cambridge University Press.

ISO. (2003). *Wood-based panels – Determination of moisture content*. ISO 16979:2003. International Standards Organisation.

— . (2009). *Hygrothermal performance of buildings - Calculation and presentation of climatic data – Part 3: Calculation of a driving rain index for vertical surfaces from hourly wind and rain data*. ISO 15927-3: 2009. International Standards Organisation.

ITU. (2016). *ITU Radio Regulations*. Geneva, Switzerland: International Telecomunication Union. doi:11.1002/pub/80da2b36-en.

Jackson, M. (2005). 'Embodied energy and historic preservation: A needed reassessment'. *APT Bulletin: The Journal of Preservation Technology* 36 (4): 47–52.

Jain, S. K., and V. P. Singh. (2003). *Water Resources Systems Planning and Management*. Amsterdam, Netherlands: Elsevier.

Jalinoos, F., R. Arndt, D. Huston and J. Cui. (2009). 'Structural Health Monitoring by Periodic NDE: NDE for Bridge Maintenance'. *Materials Evaluation* 67 (11): 1300–1307.

Jaynes, S. M., and R. U. Cooke. (1987). 'Stone weathering in southeast England'. *Atmospheric Environment* 21 (7): 1601–1622. doi:10.1016/0004-6981(87)90321-0.

Jenkins, G., M. Perry and J. Prior. (2009). *The climate of the UK and recent trends*. Tech. rep. Newcastle, UK: UK Met Office.

Jones, P. D., C. G. Kilsby, C. Harpham, V. Glenis and A. Burton. (2009). *UK Climate Projections science report: Projections of future daily climate for the UK from the Weather Generator*. University of Newcastle.

Kaatze, U., and C. Hübner. (2010). 'Electromagnetic techniques for moisture content determination of materials'. *Measurement Science and Technology* 21 (8): 082001. doi:10.1088/0957-0233/21/8/082001.

Kahraman, S. (2007). 'The correlations between the saturated and dry P-wave velocity of rocks'. *Ultrasonics* 46 (4): 341–348. doi:10.1016/j.ultras.2007.05.003.

Keim, A. W. (1902). *The Prevention of Dampness in Buildings*. 2nd ed. London, UK: Scott, Greenwood & Son.

Kendon, E. J., N. M. Roberts, H. J. Fowler, M. J. Roberts, S. C. Chan and C. A. Senior. (2014). 'Heavier summer downpours with climate change revealed by weather forecast resolution model'. *Nature Climate Change* 4:570–576. doi:10.1038/nclimate2258.

Kendon, L., J. Murphy, H. Fowler, N. Roberts and S. Blenkinsop. (2015). 'UKCP09 in light of new CONVEX results'. In *Proceedings of the CONVEX2015 Workshop, London, UK, January 14, 2015*.

Kerr, D., R. Matthews and T. Kirmayr. (1997). 'To develop a European standard dynamic watertightness test for curtain walling'. In *Proceedings of the 2nd European and*

African Conference on Wind Engineering, Genova, Italy, June 22–26, 1997, 2:1051–1058.

— . (1998). 'To develop a European standard dynamic watertightness test for curtain walling'. In *Proceedings of the 4th UK Conference on Wind Engineering, Bristol, UK, September*, 2–4.

Kharin, V. V., F. W. Zwiers, X. Zhang and G. C. Hegerl. (2007). 'Changes in Temperature and Precipitation Extremes in the IPCC Ensemble of Global Coupled Model Simulations'. *Journal of Climate* 20 (8): 1419–1444. doi:10.1175/JCLI4066.1.

Kilic, G. (2014). 'Using advanced NDT for historic buildings: Towards an integrated multidisciplinary health assessment strategy'. *Journal of Cultural Heritage*. doi:10.1016/j.culher.2014.09.010.

Klein, L., and C. Swift. (1977). 'An improved model for the dielectric constant of sea water at microwave frequencies'. *IEEE Journal of Oceanic Engineering* 2 (1): 104–111. doi:10.1109/JOE.1977.1145319.

Klysz, G., and J.-P. Balayssac. (2007). 'Determination of volumetric water content of concrete using ground-penetrating radar'. *Cement and Concrete Research* 37 (8): 1164–1171. doi:10.1016/j.cemconres.2007.04.010.

Knoll, M. D. (1996). ‘A petrophysical basis for ground penetrating radar and very early time electromagnetics: Electrical properties of sand-clay mixtures’. PhD thesis, University of British Columbia.

Knowler, A. E. (1927). ‘On the measurement of the electrical resistance of porous materials’. *Proceedings of the Physical Society* 40 (1): 37–40. doi:10.1088/0959-5309/40/1/307.

Kohl, C., M. Krause, C. Maierhofer and J. Wöstmann. (2005). ‘2D- and 3D-visualisation of NDT-data using data fusion technique’. *Materials and Structures* 38 (9): 817–826. doi:10.1007/BF02481654.

Kolodin, I. (1976). *The opera omnibus: four centuries of critical give and take*. Boston, MA, USA: Dutton.

Kralj, B., G. N. Pande and J. Middleton. (1991). ‘On the mechanics of frost damage to brick masonry’. *Computers & Structures* 41 (1): 53–66. doi:10.1016/0045-7949(91)90155-F.

Krügener, K., M. Schwerdtfeger, S. F. Busch, A. Soltani, E. Castro-Camus, M. Koch and W. Viöl. (2015). ‘Terahertz meets sculptural and architectural art: Evaluation and conservation of stone objects with T-ray technology’. *Scientific Reports* 5:14842. doi:10.1038/srep14842.

Kruschwitz, S. (2007). ‘Assessment of the Complex Resistivity Behaviour of Salt Affected Building Materials’. PhD thesis, Technischen Universität Berlin.

— . (2015). ‘NDT for microstructure and moisture investigation of porous building material’. In *Proceedings of the International Symposium Non-Destructive Testing in Civil Engineering (NDT-CE 2015), Berlin, Germany, 15–17 Sep 2015*, 535–539.

Kruschwitz, S., E. Niederleithinger, C. Trela and J. Wöstmann. (2012). ‘Use of complex resistivity tomography for moisture monitoring in a flooded masonry specimen’. *Journal of Infrastructure Systems* 18 (1): 2–11. doi:10.1061/(ASCE)IS.1943-555X.0000053.

Kubilay, A., D. Derome, B. Blocken and J. Carmeliet. (2013). ‘CFD simulation and validation of wind-driven rain on a building facade with an Eulerian multiphase model’. *Building and Environment* 61:69–81. doi:10.1016/j.buildenv.2012.12.005.

— . (2015). ‘Wind-driven rain on two parallel wide buildings: Field measurements and CFD simulations’. *Journal of Wind Engineering and Industrial Aerodynamics* 146:11–28. doi:10.1016/j.jweia.2015.07.006.

Kucera, V., J. Tidblad, K. Kreislova, D. Knotkova, M. Faller, D. Reiss, R. Snethlage, T. Yates, J. Henriksen, M. Schreiner, M. Melcher, M. Ferm, R.-A. Lefévre and J. Kobus. (2007). ‘UN/ECE ICP Materials Dose-response Functions for the

Multi-pollutant Situation'. In *Acid Rain - Deposition to Recovery*, ed. by P. Brimblecombe, H. Hara, D. Houle and M. Novak, 249–258. Amsterdam, Netherlands: Springer. doi:10.1007/978-1-4020-5885-1_27.

Künzel, H. M., and K. Kiessl. (1996). 'Calculation of heat and moisture transfer in exposed building components'. *International Journal of Heat and Mass Transfer* 40 (1): 159–167. doi:10.1016/S0017-9310(96)00084-1.

Kupfer, K. (1997). *Materialfeuchtemessung: Grundlagen - MeSSverfahren - Applikationen - Normen*. Tübingen, Germany: Expert.

Kurik, L., T. Kalamees, U. Kallavus and V. Sinivee. (2017). 'Influencing factors of moisture measurement when using microwave reflection method'. *Energy Procedia* 132:159–164. doi:10.1016/j.egypro.2017.09.675.

Kylili, A., P. A. Fokaides, P. Christou and S. A. Kalogirou. (2014). 'Infrared thermography (IRT) applications for building diagnostics: A review'. *Applied Energy* 134:531–549. doi:10.1016/j.apenergy.2014.08.005.

Lacy, R. E. (1951). 'Observations with a directional raingauge'. *Quarterly Journal of the Royal Meteorological Society* 77 (332): 283–292. doi:10.1002/qj.49707733213.

— . (1965). 'Driving-rain maps and the onslaught of rain on buildings'. In *Proceedings of the RILEM/CIB Symposium on Moisture Problems in Buildings, Rain Penetration, Helsinki, Finland, August 16–19, 1965*, Paper 3-4.

— . (1976). *Driving-rain index*. Tech. rep. Watford, UK: Building Research Establishment.

— . (1977). *Climate and building in Britain*. London, UK: Her Majesty's Stationery Office.

Lacy, R. E., and H. C. Shellard. (1962). 'An index of driving rain'. *The meteorological magazine* 91 (1080): 177–184.

Lai, W. W.-L., X. Dérobert and P. Annan. (2018). 'A review of Ground Penetrating Radar application in civil engineering: A 30-year journey from Locating and Testing to Imaging and Diagnosis'. *NDT&E International* 96:58–78. doi:10.1016/j.ndteint.2017.04.002.

Lai, W. W.-L., T. Kind, S. Kruschwitz, J. Wöstmann and H. Wiggenhauser. (2014). 'Spectral absorption of spatial and temporal ground penetrating radar signals by water in construction materials'. *NDT&E International* 67:55–63. doi:10.1016/j.ndteint.2014.06.009.

Larsen, P. K. (2012). 'Determination of Water Content in Brick Masonry Walls using a Dielectric Probe'. *Journal of Architectural Conservation* 18 (1): 47–62. doi:10.1080/13556207.2012.10785103.

Lataste, J.-F., and A. Göller. (2018). 'Microwave Reflection'. Chap. 16 in *Methods of Measuring Moisture in Building Materials and Structures: State-of-the-Art Report of*

the RILEM Technical Committee 248-MMB, ed. by L.-O. Nilsson, 123–140. New York, NY, USA: Springer.

Laurens, S., J. P. Balayssac, J. Rhazi, G. Klysz and G. Arliguie. (2005). 'Non-destructive evaluation of concrete moisture by GPR: experimental study and direct modeling'. *Materials and structures* 38 (9): 827–832. doi:10.1007/BF02481655.

Lawson, C. L., and R. J. Hanson. (1995). *Solving Least Squares Problems*. Philadelphia, PA, USA: Society for Industrial and Applied Mathematics.

Laycock, E. A., and C. Wood. (2014). 'Understanding and controlling the ingress of driven rain through exposed, solid wall masonry structures'. *Geological Society of London, Special Publications* 391 (1): 175–191. doi:10.1144/SP391.1.

Leadbetter, M. R. (1991). 'On a basis for 'Peaks over Threshold' modeling'. *Statistics and Probability Letters* 12 (4): 357–362. doi:10.1016/0167-7152(91)90107-3.

Leary, E. (1983). *The building limestones of the British Isles*. Watford, UK: Building Research Establishment.

Leblon, B., O. Adedipe, G. Hans, A. Haddadi, S. Tsuchikawa, J. Burger, R. Stirling, Z. Pirouz, K. Groves, J. Nader and A. LaRocque. (2013). 'A review of near-infrared spectroscopy for monitoring moisture content and density of solid wood'. *The Forestry Chronicle* 89 (05): 595–606. doi:10.5558/tfc2013-111.

Lerma, J. L., M. Cabrelles and C. Portalés. (2011). 'Multitemporal thermal analysis to detect moisture on a building façade'. *Construction and Building Materials* 25 (5): 2190–2197. doi:10.1016/j.conbuildmat.2010.10.007.

Leucci, G., N. Masini and R. Persico. (2012). 'Timefrequency analysis of GPR data to investigate the damage of monumental buildings'. *Journal of Geophysics and Engineering* 9 (4): S81–S91. doi:10.1088/1742-2132/9/4/S81.

Lewry, A. J., J. Asiedu-Dompreh, D. J. Bigland and R. N. Butlin. (1994). 'The effect of humidity on the dry deposition of sulfur dioxide onto calcareous stones'. *Construction and Building Materials* 8 (2): 97–100. doi:10.1016/S0950-0618(09)90018-6.

Liberatore, D., G. Spera and M. Cotugno. (2003). 'A new penetration test on mortar joints'. In *Proceedings of the RILEM TC 177-MDT Workshop on On-Site Control and Non-Destructive Evaluation of Masonry Structures, Mantova, Italy, 12–14 November 2001*, 191–202.

Lichtenecker, K., and K. Rother. (1931). 'Die Herleitung des logarithmischen Mischungs-gesetzes aus allgemeinen prinzipien der stationaren Stormung.' *Physikalische Zeitschrift* 32:255–260.

Litti, G., S. Khoshdel, A. Audenaert and J. Braet. (2015). 'Hygrothermal performance evaluation of traditional brick masonry in historic buildings'. *Energy and Buildings* 105:393–411. doi:10.1016/j.enbuild.2015.07.049.

Litvan, G. G. (1980). 'Freeze-thaw durability of porous building materials'. In *Durability of building materials and components*. West Conshohocken, PA, USA: ASTM International.

Livingston, R. A. (1999). 'Nondestructive Testing of Historic Structures'. *Archives and Museum Informatics* 13 (3): 249–271. doi:10.1023/A:1012416309607.

Lopez, C. R. (2011). 'Measurement, analysis, and simulation of wind driven rain'. PhD thesis, University of Florida.

Lott, G. (2011). 'The Building Stone Industry in Britain: Past and Present'. [HTML], accessed November 20, 2014. url: http://www.englishstone.org.uk/documents/dimension%20stone.html.

— . (2013). 'Sourcing stone for the conservation and repair of historical buildings in Britain'. *Quarterly Journal of Engineering Geology and Hydrogeology* 46 (4): 405–420. doi:10.1144/qjegh2013-004.

Lott, G. K., and C. Richardson. (1997). 'Yorkshire stone for building the Houses of Parliament (1839–c. 1852)'. *Proceedings of the Yorkshire Geological Society* 51 (4): 265–272. doi:10.1144/pygs.51.4.265.

Lowndes, C. A. S. (1962). 'Wet spells at London'. *The meteorological magazine* 91 (1080): 98–104.

Lull, H. W. (1959). *Soil compaction on forest and range lands*. 768. Forest Service, US Department of Agriculture.

Lundien, J. R. (1966). *Terrain analysis by electromagnetic means: Report 2, Radar responses to laboratory prepared soil samples*. Technical report 3-693. Vicksburg, MS, USA: U.S. Army Engineer Waterways Experiment Station.

Madsen, H., C. P. Pearson and D. Rosbjerg. (1997). 'Comparison of annual maximum series and partial duration series methods for modeling extreme hydrologic events: 2. Regional modeling'. *Water Resources Research* 33 (4): 759–769. doi:10.1029/96WR03848.

Maierhofer, C., and S. Leipold. (2001). 'Radar investigation of masonry structures'. *NDT&E International* 34 (2): 139–147. doi:10.1016/S0963-8695(00)00038-4.

Maierhofer, C., J. Wöstmann, C. Trela and M. Röllig. (2008). 'Investigation of moisture content and distribution with radar and active thermography'. In *Proceedings of the International RILEM Conference on Site Assessment of Concrete, Masonry and Timber Structures (SACoMaTiS 2018), Varenna, Como Lake, Italy, 1–2 September, 2008*, ed. by L. Binda, M. di Prisco and R. Felicetti, 34:411–420.

Mamillan, M. (1991). 'Alteration et Durabilité des Pierres'. In *Réhabilitation et restauration des ouvrages et des structures [Rehabilitation and restoration of structures and structures], Paris, France, June 18–19, 1991*.

Manual on Codes: International Codes. (2016). Vol. I.1. WMO-No.306. Geneva, Switzerland: World Meteorological Organization.

Marsh, P. H. (1977). *Air and rain penetration of buildings*. Lancaster, UK and New York, NY, USA: Construction Press.

Marshall, J. S., and W. M. Palmer. (1948). 'The distribution of raindrops with size'. *Journal of Meteorology* 5 (4): 165–166. doi:10.1175/1520-0469(1948)005<0165:TDORWS>2.0.CO;2.

Martínez-Garrido, M., R. Fort, M. Gómez-Heras, J. Valles-Iriso and M. Varas-Muriel. (2018). 'A comprehensive study for moisture control in cultural heritage using non-destructive techniques'. *Journal of Applied Geophysics* 155:36–52. doi:10.1016/j.jappgeo.2018.03.008.

Martínez-Martínez, J., D. Benavente, M. Gómez-Heras, L. Marco-Castaño and M. Á. García-del-Cura. (2013). 'Non-linear decay of building stones during freeze–thaw weathering processes'. 25th Anniversary Session for ACI 228 – Building on the Past for the Future of NDT of Concrete, *Construction and Building Materials* 38:443–454. doi:10.1016/j.conbuildmat.2012.07.059.

Martinez, A., A. P. Byrnes et al. (2001). *Modeling dielectric-constant values of geologic materials: An aid to ground-penetrating radar data collection and interpretation*. Lawrence, KS, USA: Kansas Geological Survey, University of Kansas.

Martinho, E., F. Alegria, A. Dionisio, C. Grangeia and F. Almeida. (2012). '3D-resistivity imaging and distribution of water soluble salts in Portuguese Renaissance stone bas-reliefs'. *Engineering Geology* 141–142:33–44. doi:10.1016/j.enggeo.2012.04.010.

Martinho, E., F. Alegria, C. Grangeia, A. Dionisio and F. Almeida. (2010). 'Electrical resistivity imaging: Overview and a case study in stone cultural heritage', ed. by E. H. Duke and S. R. Aguirre, 199–230. 3D Imaging: Theory, Technology, and Applications. Hauppauge, NY, USA: Nova Science Publishers.

Martinho, E., A. Dionísio, F. Almeida, M. Mendes and C. Grangeia. (2014). 'Integrated geophysical approach for stone decay diagnosis in cultural heritage'. *Construction and Building Materials* 52:345–352. doi:10.1016/j.conbuildmat.2013.11.047.

Masschaele, B., M. Dierick, L. Van Hoorebeke, V. Cnudde and P. Jacobs. (2004). 'The use of neutrons and monochromatic X-rays for non-destructive testing in geological materials'. *Environmental Geology* 46 (3): 486–492. doi:10.1007/s00254-004-1050-z.

May, N., and C. H. Sanders. (2017). *Moisture in buildings: an integrated approach to risk assessment and guidance*. White Paper. London, UK: BSI Group.

Mazilu, M., A. Miller and V. T. Donchev. (2001). 'Modular method for calculation of transmission and reflection in multilayered structures'. *Applied Optics* 40 (36): 6670–6676.

McCabe, S., P. Brimblecombe, B. J. Smith, D. McAllister, S. Srinivasan and P. A. M. Basheer. (2013). 'The use and meanings of 'time of wetness' in understanding building stone decay'. *Quarterly Journal of Engineering Geology and Hydrogeology* 46 (4): 469–476. doi:10.1144/qjegh2012-048.

Mendell, M. J., J. M. Macher and K. Kumagai. (2018). 'Measured moisture in buildings and adverse health effects: A review'. *Indoor Air* 28 (4): 488–499. doi:10.1111/ina.12464.

Ministry of Housing, Communities & Local Government. (2016). *English House Survey: Energy efficiency*. London, UK: Ministry of Housing, Communities & Local Government.

Mol, L., M. Gómez-Heras, C. Brassey, O. Green and T. Blenkinsop. (2017). 'The benefit of a tough skin: bullet holes, weathering and the preservation of heritage'. *Royal Society open science* 4 (2): 160335. doi:10.1098/rsos.160335.

Moldenhauer, L., R. Helmerich, E. Köppe, F. Haamkens and J. Wittmann. (2017). 'Experimental feasibility study about moisture in building materials measured with

bluetooth'. *Materials Today: Proceedings* 4 (5): 5889–5892. doi:10.1016/j.matpr.2017.06.064.

Møller, E. B., and B. Olsen. (2011). 'Rising damp, a reoccurring problem in basements–a case study with different attempts to stop the moisture'. In *Proceedings of the 9th Nordic Symposium on Building Physics (NSB 2011), Tampere, Finland, May 29–June 2, 2011*.

Mook, F. J. van. (2002). 'Driving rain on building envelopes'. PhD thesis, Technische Universiteit Eindhoven.

Moonen, P., T. Defraeye, V. Dorer, B. Blocken and J. Carmeliet. (2012). 'Urban Physics: Effect of the micro-climate on comfort, health and energy demand'. *Frontiers of Architectural Research* 1 (3): 197–228. doi:10.1016/j.foar.2012.05.002.

Morozov, E. (2011). *The Net Delusion: How Not to Liberate The World*. London, UK: Penguin Books Limited.

Morris, S. (2004). *Portland : An illustrated history*. Dorset, UK: Dovecote Press.

Moses, C., D. Robinson and J. Barlow. (2014). 'Methods for measuring rock surface weathering and erosion: A critical review'. *Earth-Science Reviews* 135:141–161. doi:10.1016/j.earscirev.2014.04.006.

Murphy, J. M., D. M. Sexton, G. J. Jenkins, B. B. Booth, C. C. Brown, R. T. Clark, M. Collins, G. R. Harris, E. J. Kendon, R. A. Betts et al. (2009). *UK climate*

projections science report: climate change projections. Tech. rep. Exeter, UK: Met Office Hadley Centre.

Mylona, A. (2012). 'The use of UKCP09 to produce weather files for building simulation'. *Building Services Engineering Research and Technology* 33 (1): 51–62. doi:10.1177/0143624411428951.

Nadarajah, S. (2006). 'The exponentiated Gumbel distribution with climate application'. *Environmetrics* 17 (1): 13–23. doi:10.1002/env.739.

Nadarajah, S., and S. Kotz. (2004). 'The beta Gumbel distribution'. *Mathematical Problems in Engineering* 2004 (4): 323–332. doi:10.1155/S1024123X04403068.

Nakicenovic, N., and R. Swart. (2000). *Special report on emissions scenarios*. A special report of working Group III. Geneva, Switzerland: Intergovernmental Panel on Climate Change.

Narula, P., K. Sarkar and S. Azad. (2017). 'Driving rain indices for India at $1^\circ \times 1^\circ$ gridded scale'. *Journal of Wind Engineering and Industrial Aerodynamics* 161:1–8. doi:10.1016/j.jweia.2016.12.005.

Neas, D., and I. Ohlídal. (2014). 'Consolidated series for efficient calculation of the reflection and transmission in rough multilayers'. *Optics Express* 22 (4): 4499–4515. doi:10.1364/OE.22.004499.

Nelson, S. O., and A. W. Kraszewski. (1990). 'Dielectric properties of materials and measurement techniques'. *Drying technology* 8 (5): 1123–1142. doi:10.1080/07373939008959939.

Newman, A. J. (1987). 'Microclimate and its effects on durability [of buildings]'. *Chemistry and Industry*: 583–93.

Newton, R. W. (1977). *Microwave remote sensing and its application to soil moisture detection*. Technical Report RSC-81. College Station, TX, USA: Texas A & M University.

Nguyen, T. Q., J. Petkovic, P. Dangla and V. Baroghel-Bouny. (2008). 'Modelling of coupled ion and moisture transport in porous building materials'. *Construction and Building Materials* 22 (11): 2185–2195. doi:10.1016/j.conbuildmat.2007.08.013.

Nicolai, A., J. Grunewald, R. Plagge and G. Scheffler. (2008). 'An efficient numerical solution method and implementation for coupled heat, moisture and salt transport: The Delphin Program. Research Report on Priority Program DFG SPP 1122'. In *Simulation of Time Dependent Degradation of Porous Materials*, ed. by E.-M. R. Franke L Dekkelmann G, 85–100. 85–100.11. Göttingen, Germany: Cuvillier.

Niemz, P., and D. Mannes. (2012). 'Non-destructive testing of wood and wood-based materials'. *Journal of Cultural Heritage* 13 (3): S26–S34. doi:10.1016/j.culher.2012.04.001.

Nik, V. M. (2017). 'Application of typical and extreme weather data sets in the hygrothermal simulation of building components for future climate – A case study for a wooden frame wall'. *Energy and Buildings* 154:30–45. doi:10.1016/j.enbuild.2017.08.042.

Nik, V. M., S. O. Mundt-Petersen, A. Sasic Kalagasidis and P. De Wilde. (2015). 'Future moisture loads for building facades in Sweden: Climate change and wind-driven rain'. *Building and Environment* 93:362–375. doi:10.1016/j.buildenv.2015.07.012.

Nik, V. M., and A. Sasic Kalagasidis. (2014). 'Wind Driven Rain and Climate Change: A Simple Approach for the Impact Assessment and Uncertainty Analysis'. In *Proceedings of 10th Nordic Symposium on Building Physics, Lund, Sweden, June 15–19, 2014*, 574–581.

Nilsson, L. O. (2018). *Methods of Measuring Moisture in Building Materials and Structures: State-of-the-Art Report of the RILEM Technical Committee 248-MMB*. New York, NY, USA: Springer.

Oakeshott, W. F. (1975). *Oxford stone restored: the work of the Oxford Historic Buildings Fund, 1957-1974*. Oxford, UK: Trustees of the Oxford Historic Buildings Fund.

Olatinsu, O. B., D. O. Olorode and K. F. Oyedele. (2013). 'Radio frequency dielectric properties of limestone and sandstone from Ewekoro, Eastern Dahomey Basin'. *Advances in Applied Science Research* 4:150–158.

Oliver, A. C. (1988). *Dampness in Buildings*. Oxford, UK: BSP Professional Books.

— . (1997). *Dampness in Buildings*. Ed. by J. Douglas and S. Stirling. Chichester, UK: Wiley.

Olmi, R., S. Priori, D. Capitani, N. Proietti, L. Capineri, P. Falorni, R. Negrotti and C. Riminesi. (2011). 'Innovative techniques for sub-surface investigations'. *Materials Evaluation (Technical Focus Issue: Moisture Detection Techniques)* 69 (1): 89–96.

Orr, S. A. (2015). *Comparative synthesis of handheld damp meters and infrared thermography with 2D-resistive tomography: informing moisture monitoring of historic masonry*. MRes Thesis. University College London.

Orr, S. A., and H. Viles. (2018a). 'Characterisation of building exposure to wind-driven rain in the UK and evaluation of current standards'. *Journal of Wind Engineering and Industrial Aerodynamics* 180:88–97. doi:10.1016/j.jweia.2018.07.013.

Orr, S. A., H. A. Viles, A. Leslie and D. Stelfox. (2016). 'Comparability of non-invasive moisture measurement techniques on masonry during artificial post-rainspell drying'. In *Proceedings of the 13th International Congress on the Deterioration and Conservation of Stone, Paisley, UK, 5–10 September, 2016*, 2:431–438.

Orr, S. A., M. Young, S. Stelfox, J. Curran and H. Viles. (2018b). 'Wind-driven rain and future risk to built heritage in the United Kingdom: Novel metrics for characterising rain spells'. *Science of The Total Environment* 640–641:1098–1111. doi:10.1016/j.scitotenv.2018.05.354.

Osmond, S. D. (1995). *Assessment of the full scale micro climate around buildings*. Note N47/95. Unpublished. Watford, UK: Building Research Establishment.

Osmond, S. (1996). *Assessment of the full scale micro climate around buildings*. Note N91/96. Unpublished. Watford, UK: Building Research Establishment.

Pakkala, T. A., A.-M. Lemberg, J. Lahdensivu and M. Pentti. (2016). 'Climate change effect on wind-driven rain on facades'. *Nordic Concrete* 31:31–49.

Pande, A., and C. S. Pande. (1962). 'Physical methods of moisture measurement'. Published in four parts. *Instrument Practice* 16 (7): 896–903, 988–995, 1104–1110, 1246–1250.

Pandey, S. C., A. M. Pollard, H. A. Viles and J. H. Tellam. (2014). 'Influence of ion exchange processes on salt transport and distribution in historic sandstone buildings'. *Applied Geochemistry* 48:176–183. doi:10.1016/j.apgeochem.2014.07.001.

Peel, M. C., B. L. Finlayson and T. A. McMahon. (2007). 'Updated world map of the Köppen-Geiger climate classification'. *Hydrology and Earth System Sciences* 11 (5): 1633–1644. doi:10.5194/hess-11-1633-2007.

Pel, L. (1995). ‘Moisture transport in porous building materials’. PhD thesis, Technische Universiteit Eindhoven. doi:10.6100/IR431403.

Pérez-Bella, J. M., J. Domínguez-Hernández, E. Cano-Suñén, J. J. del Coz-Díaz and Á. Martín-Rodríguez. (2014). ‘Procedure for a detailed territorial assessment of wind-driven rain and driving-rain wind pressure and its implementation to three Spanish regions’. *Journal of Wind Engineering and Industrial Aerodynamics* 128:76–89. doi:10.1016/j.jweia.2014.02.008.

Pérez-Bella, J. M., J. Domínguez-Hernández, E. Cano-Suñén, J. J. del Coz-Díaz and F. P. Á. Rabanal. (2017). ‘On the significance of the climate-dataset time resolution in characterising wind-driven rain and simultaneous wind pressure. Part II: directional analysis’. *Stochastic Environmental Research and Risk Assessment*: 1–17. doi:10.1007/s00477-017-1479-8.

Pérez-Bella, J. M., J. Domínguez-Hernández, B. Rodríguez-Soria, J. J. del Coz-Díaz and E. Cano-Suñén. (2012). ‘Estimation of the exposure of buildings to driving rain in Spain from daily wind and rain data’. *Building and Environment* 57:259–270. doi:10.1016/j.buildenv.2012.05.010.

— . (2013). ‘Combined use of wind-driven rain and wind pressure to define water penetration risk into building façades: the Spanish case’. *Building and Environment* 64:46–56. doi:10.1016/j.buildenv.2013.03.004.

Persoon, J., T. van Hooff, B. Blocken, J. Carmeliet and M. H. de Wit. (2008). 'On the impact of roof geometry on rain shelter in football stadia'. *Journal of Wind Engineering and Industrial Aerodynamics* 96 (8): 1274–1293. doi:10.1016/j.jweia.2008.02.036.

Pettersson, K., S. Krajnovic, A. S. Kalagasidis and P. Johansson. (2016). 'Simulating wind-driven rain on building facades using Eulerian multiphase with rain phase turbulence model'. *Building and Environment* 106:1–9. doi:10.1016/j.buildenv.2016.06.012.

Phillipson, M. C., P. H. Baker, M. Davies, Z. Ye, A. McNaughtan, G. H. Galbraith and R. C. McLean. (2007). 'Moisture measurement in building materials: an overview of current methods and new approaches'. *Building Services Engineering Research and Technology* 28 (4): 303–316. doi:10.1177/0143624407084184.

Pilon, J. A. (1992). *Ground penetrating radar*. Ottawa, ON, Canada: Geological Survey of Canada.

Pinchin, S. E. (2008). 'Techniques for monitoring moisture in walls'. *Studies in Conservation* 53 (S-2): 33–45. doi:10.1179/sic.2008.53.Supplement-2.33.

Platt, S. D., C. J. Martin, S. M. Hunt and C. W. Lewis. (1989). 'Damp housing, mould growth, and symptomatic health state.' *BMJ* 298 (6689): 1673–1678.

Pollard, C. W. (2000). *The Soul of the Firm*. Grand Rapids, MI, USA: Zondervan.

Prior, J. (1983). 'Improved (directional) driving rain indices for the United Kingdom - computation, mapping and applications.' In *Proceedings of a Symposium on Building Climatology, Moscow, Russia, September 20–24, 1982*, III:187–199. International Council for Building Research, Studies and Documentation (CIB).

— . (1985). *Directional driving rain indices for the United Kingdom : computation and mapping (Background to BSI Draft for Development DD93)*. Watford, UK: Building Research Establishment.

Prior, J., and A. J. Newman. (1988). 'Driving Rain — Calculations and measurements for buildings'. *Weather* 43 (4): 146–155. doi:10.1002/j.1477-8696.1988.tb03895.x.

Proietti, N., D. Capitani, S. Cozzolino, M. Valentini, E. Pedemonte, E. Princi, S. Vicini and A. L. Segre. (2006). 'In Situ and Frontal Polymerization for the Consolidation of Porous Stones: A Unilateral NMR and Magnetic Resonance Imaging Study'. *The Journal of Physical Chemistry B* 110 (47): 23719–23728. doi:10.1021/jp063219u.

Quincot, G., M. Azenha, J. Barros and R. Faria. (2011). *State of the art–Methods to measure moisture in concrete*. Report. Guimarães, Portugal: Projetos De Investigação Científica E Desenvolvimento Tecnológico.

Radford, A. (2001). *A guide to dry stone walling*. Marlborough, Wiltshire, UK: Crowood.

Ray, P. (1986). *Mesoscale Meteorology and Forecasting*. Boston, MA, USA: American Meteorological Society.

Reid, J., and S. Garvin. (2011). *Wind driven rain: assessment of the need for new guidance*. Tech. rep. A1533015. East Kilbride, Scotland: Building Research Establishment Scotland.

Rodgers, G. G. (1977). 'Theoretical studies of the interaction of wind flow with precipitation elements in determining the deposition of rain, snow and ice on buildings and structures'. *Sixth Course Airflow and Building Design, University of Sheffield*.

Rodgers, G. G., G. Poots, J. K. Page and W. M. Pickering. (1974). 'Theoretical predictions of raindrop impaction on a slab type building'. *Building Science* 9 (3): 181–190. doi:10.1016/0007-3628(74)90016-4.

Rodríguez-Abad, I., G. Klysz, R. Martínez-Sala, J. P. Balayssac and J. Mené-Aparicio. (2016). 'Application of ground-penetrating radar technique to evaluate the waterfront location in hardened concrete'. *Geoscientific Instrumentation, Methods and Data Systems* 5 (2): 567–574. doi:10.5194/gi-5-567-2016.

Rodriguez-Navarro, C., E. Hansen, E. Sebastian and W. S. Ginell. (1997). 'The Role of Clays in the Decay of Ancient Egyptian Limestone Sculptures'. *Journal of the American Institute for Conservation* 36 (2): 151–163. doi:10.2307/3179829.

Roels, S., J. Carmeliet, H. Hens, O. Adan, H. Brocken, R. erný, Z. Pavlik, A. T. Ellis, C. Hall, K. Kumaran et al. (2004). 'A comparison of different techniques to quantify

moisture content profiles in porous building materials'. *Journal of Thermal Envelope and Building Science* 27 (4): 261–276. doi:10.1177/1097196304042117.

Roife, V. S. (1980). 'State of moisture content measurement in the building materials industry'. *Measurement Techniques* 23 (3): 264–266.

Rosina, E., and E. Grinzato. (2001). 'Infrared and Thermal Testing for Conservation of Historic Buildings'. *Materials Evaluation* 59 (8): 942–954.

Rosina, E., A. Sansonetti, N. Ludwig and (eds.) (2018). 'MODIHMA 2018 Innovative Techniques for MOisture Detection in HIstorical MAsonry'. Ed. by E. Rosina, A. Sansonetti and N. Ludwig. *Journal of Cultural Heritage* 31 (Supplement): S1–S88.

Ross, M. (2003). *Planning and the heritage: policy and procedures*. Abingdon, UK: Routledge.

Ross, R. J., and R. F. Pellerin. (1994). *Nondestructive testing for assessing wood members in structures: A review*. General technical report 70. Madison, WI, USA: Forest Products Laboratory, U.S. Forest Service.

Rousset, B., and C. Bläuer. (2009). *R.0014.01f: Cathédrales de Bâle, de Berne, de Fribourg et de Lausanne: Project de contrôle et de suivi des consolidants: résultats des teste de laboratoire*. Research Report. Fribourg, Switzerland: Conservation Science Consulting Sàrl.

Ruedrich, J., and S. Siegesmund. (2007). ‘Salt and ice crystallisation in porous sandstones’. *Environmental Geology* 52 (2): 343–367. doi:10.1007/s00254-006-0585-6.

Rüther, P., and B. Time. (2015). ‘External wood claddings–performance criteria, driving rain and large-scale water penetration methods’. *Wood Material Science & Engineering* 10 (3): 287–299. doi:10.1080/17480272.2015.1063688.

Sabbioni, C., P. Brimblecombe and M. Cassar. (2010). *The Atlas of Climate Change Impact on European Cultural Heritage: Scientific Analysis and Management Strategies*. Anthem Atlas and Reference Series. Bath, UK: Anthem.

Sacre, C. (1982). ‘Concomitance de la pluie et du vent en France, approche statistique’. *Cent. Sci. Tech. Batim* 232:1792.

Saïd, M. N. A. (2004). *Moisture measurement guide for building envelope applications*. Research Report 190. Ottawa, ON, Canada: Institute for Research in Construction, National Research Council Canada.

— . (2007). ‘Measurement methods of moisture in building envelopes–a literature review’. *International Journal of Architectural Heritage* 1 (3): 293–310. doi:10.1080/15583050701476754.

Salzman, L. F. (1992). *Building in England Down to 1540: A Documentary History*. New ed. Oxford Reprints Series. Oxford, UK: Oxford University Press.

Sandberg, P. J. (1974). 'Driving rain distribution over an infinitely long high building; Computerized calculations'. In *Proceedings of the 2nd International CIB/RILEM Symposium on Moisture Problems in Buildings, Rotterdam, Netherlands September 10–12,1974*, Paper 1-1-2.

Sanders, C. (2004). *Comparison of the 'British Standard' and 'French' methods for estimating driving rain impacts on walls*. Report, IEA Annex 41 meeting A41-T3-UK-04-2. Glasgow, UK: IEA.

Sandrolini, F., and E. Franzoni. (2006). 'An operative protocol for reliable measurements of moisture in porous materials of ancient buildings'. *Building and Environment* 41 (10): 1372–1380. doi:10.1016/j.buildenv.2005.05.023.

Santos, C. P., L. Matias, A. C. Magalhães and M. R. Viega. (2003). 'Application of thermography and ultra-sounds for wall anomalies diagnosis: a laboratory research study'. In *International Symposium on Non-Destructive Testing in Civil Engineering (NDT-CE 2003), Berlin, Germany, September 16–19, 2003*.

Sass, O. (1998). 'Die Steuerung von Steinschlagmenge undverteilung durch Mikroklima, Gesteinsfeuchte und Gesteinseigenschaften im westlichen Karwendelgebirge (Bayerische Alpen).' PhD thesis, Ludwig-Maximilians-Universität München.

Sass, O., and H. A. Viles. (2006). 'How wet are these walls? Testing a novel technique for measuring moisture in ruined walls'. *Journal of Cultural Heritage* 7 (4): 257–263. doi:10.1016/j.culher.2006.08.001.

— . (2010a). 'Two-dimensional resistivity surveys of the moisture content of historic limestone walls in Oxford, UK: Implications for understanding catastrophic stone deterioration'. *Geological Society of London, Special Publications* 331:237–249. doi:10.1144/SP331.22.

— . (2010b). 'Wetting and drying of masonry walls: 2D-resistivity monitoring of driving rain experiments on historic stonework in Oxford, UK'. *Journal of Applied Geophysics* 70 (1): 72–83. doi:10.1016/j.jappgeo.2009.11.006.

Sbartaï, Z. M., S. Laurens, J. Rhazi, J. P. Balayssac and G. Arliguie. (2007). 'Using radar direct wave for concrete condition assessment: Correlation with electrical resistivity'. *Journal of Applied Geophysics* 62 (4): 361–374. doi:10.1016/j.jappgeo.2007.02.003.

Schaffer, R. J. (1932). *The Weathering of Natural Building Stones*. Building Research Special Reports 18. Watford, UK: Building Research Establishment.

Scherer, G. W. (1990). 'Theory of Drying'. *Journal of the American Ceramic Society* 73 (1): 3–14. doi:10.1111/j.1151-2916.1990.tb05082.x.

Schmidt, C. (1976). *Restoration and Preservation*. Lebanon, PA, USA: Schmidt.

Scholten, T., C. GeiSSler, J. Goc, P. Kühn and C. Wiegand. (2011). 'A new splash cup to measure the kinetic energy of rainfall'. *Journal of Plant Nutrition and Soil Science* 174 (4): 596–601. doi:10.1002/jpln.201000349.

Sebastián, E., G. Cultrone, D. Benavente, L. L. Fernandez, K. Elert and C. Rodriguez-Navarro. (2008). 'Swelling damage in clay-rich sandstones used in the church of San Mateo in Tarifa (Spain)'. *Journal of Cultural Heritage* 9 (1): 66–76. doi:10.1016/j.culher.2007.09.002.

Senin, S. F., and R. Hamid. (2016). 'Ground penetrating radar wave attenuation models for estimation of moisture and chloride content in concrete slab'. *Construction and Building Materials* 106:659–669. doi:10.1016/j.conbuildmat.2015.12.156.

Sexton, D. M. H., and J. Murphy. (2010). *UKCP09: Probabilistic projections of wind speed*. Tech. rep. Exeter, UK: Met Office Hadley Centre.

El-Sherbiny, Y. (2018). 'Erosive wear of different facade finishing materials'. *HBRC Journal* In Press, Corrected Proof. doi:10.1016/j.hbrcj.2018.04.001.

Siegesmund, S., and R. Snethlage, eds. (1994). *Stone in Architecture; properties, durability*. 3rd ed. New York, NY, USA: Springer.

Sihvola, A. (2000). 'Mixing rules with complex dielectric coefficients'. *Subsurface Sensing Technologies and Applications* 1 (4): 393–415. doi:10.1023/A:1026511515005.

Singh, J. (1994). 'The built environment and the development of fungi'. In *Building Mycology: Management of Decay and Health in Buildings*, 1–21. Abingdon, UK: Taylor & Francis.

Slawski, M., and M. Hein. (2013). 'Non-negative least squares for high-dimensional linear models: Consistency and sparse recovery without regularization'. *Electronic Journal of Statistics* 7:3004–3056.

Slight, H. A. (1989). 'The measurement of moisture content'. *Measurement and Control* 22 (2): 42–44.

Smith, B. J., S. McCabe, D. McAllister, C. Adamson, H. A. Viles and J. M. Curran. (2011a). 'A commentary on climate change, stone decay dynamics and the 'greening' of natural stone buildings: New perspectives on 'deep wetting''. *Environmental Earth Sciences* 63 (7): 1691–1700. doi:10.1007/s12665-010-0766-1.

Smith, B. J., S. Srinivasan, S. McCabe, D. McAllister, N. M. Cutler, P. A. M. Basheer and H. A. Viles. (2011b). 'Climate Change and the Testing of Complex Moisture Regimes in Building Stone: Preliminary Observations on Possible Strategies'. *Materials Evaluation (Technical Focus Issue: Moisture Detection Techniques)* 69 (1): 49–57.

Smith, B. J., and H. A. Viles. (2006). 'Rapid, catastrophic decay of building limestones: Thoughts on causes, effects and consequences'. In *Proceedings of the International*

Heritage, Weathering and Conservation Conference (HWC 2006), June 21-24, 2006, Madrid, Spain, 1:191–197. Madrid.

Smith, R. L. (1989). 'Extreme value analysis of environmental time series: an application to trend detection in ground-level ozone'. *Statistical Science* 4 (4): 367–377.

— . (1990). 'Extreme value theory'. *Handbook of Applicable Mathematics* 7:437–471.

Solla, M., S. Lagüela, M. X. Álvarez, H. Lorenzo and B. Riveiro. (2012). 'A multidisciplinary non-destructive approach to analyze moisture in historic masonry structures: Integration of both field and synthetic GPR data generated from photogrammetric and infrared imaging'. In *Proceedings of the 14th International Conference on Ground Penetrating Radar (GPR 2012), Shanghai, China, June 4–8, 2012*, 585–590.

Solli, B., M. Burström, E. Domanska, M. Edgeworth, A. González-Ruibal, C. Holtorf, G. Lucas, T. Oestigaard, L. Smith and C. Witmore. (2011). 'Some Reflections on Heritage and Archaeology in the Anthropocene'. *Norwegian Archaeological Review* 44 (1): 40–88. doi:10.1080/00293652.2011.572677.

Sondheim, S., and J. Lapine. (2000). *Sunday in the Park with George [Libretto]*. Applause Musical Library. Milwaukee, WI, USA: Applause Theatre & Cinema Books.

Souster, C. G. (1979). 'A theoretical approach to predicting snow loads and driving rain deposition on buildings.' PhD thesis, University of Sheffield.

Spencer, H. (1861). *Education: intellectual, moral, and physical*. London, UK: Williams / Norgate.

Steiger, M. (2003). 'Salts and Crusts'. In *The Effects of Air Pollution on the Built Environment*, ed. by P. Brimblecombe, 2:133–181. Air Pollution Reviews. London, UK: World Scientific. doi:10.1142/9781848161283_0005.

Steiger, M., A. E. Charola and K. Sterflinger. (2011). 'Weathering and Deterioration'. Chap. 4 in *Stone in Architecture: Properties, Durability*, ed. by S. Siegesmund and R. Snethlage, 227–316. Berlin/Heidelberg, Germany: Springer. doi:10.1007/978-3-642-14475-2_4.

Stein, T. H. M., R. J. Hogan, P. A. Clark, C. E. Halliwell, K. E. Hanley, H. W. Lean, J. C. Nicol and R. S. Plant. (2015). 'The DYMECS Project: A Statistical Approach for the Evaluation of Convective Storms in High-Resolution NWP Models'. *Bulletin of the American Meteorological Society* 96 (6): 939–951. doi:10.1175/BAMS-D-13-00279.1.

Stelfox, D. (2018). *Personal correspondence, 1 February 2018.* Interview.

Stokes, D. (2016). 'We Need To Move Beyond LGBT Alphabet Soup And Slurs. The Huffington Post.' [HTML], accessed September 3, 2018. url: https://www.huffingtonpost.com/dashanne-stokes/we-need-to-move-beyond-lg_b_10465840.html.

Straube, J. F. (1998). 'Moisture control and enclosure wall systems'. PhD thesis, University of Waterloo.

— . (2002). 'Moisture in buildings'. *ASHRAE Journal* 44 (1): 15–19.

Straube, J. F., and E. F. P. Burnett. (1997). 'Driving rain and masonry veneer'. In *Proceedings of the ASTM Symposium on Water Leakage Through Building Facades (Special Technical Publication 131), March 17, 1996, Orlando, FL, USA*, 73–87.

— . (1998). 'Driving rain and masonry veneer'. In *Water leakage through building facades, Special Technical Publication, ASTM STP 1314*, 73–87. ASTM International.

— . (2000). 'Simplified prediction of driving rain on buildings'. In *Proceedings of the 1st International Building Physics Conference, September 18–21, 2000, Eindhoven, Netherlands*, 375–382.

Stubbs, M. (2004). 'Heritage-sustainability: developing a methodology for the sustainable appraisal of the historic environment'. *Planning Practice & Research* 19 (3): 285–305. doi:10.1080/0269745042000323229.

Su, S. L., D. N. Singh and M. S. Baghini. (2014). 'A critical review of soil moisture measurement'. *Measurement* 54:92–105. doi:10.1016/j.measurement.2014.04.007.

Suchocki, C., and J. Katzer. (2018). 'Terrestrial laser scanning harnessed for moisture detection in building materials – Problems and limitations'. *Automation in Construction* 94:127–134. doi:10.1016/j.autcon.2018.06.010.

Svahn, H. (2006). *Non-Destructive Field Tests in Stone Conservation*. Final Report for the Research and Development Project 3. Stolkholm, Sweden: Riksantikvarieämbetet.

Skora, J., J. Vorel, T. Krejí, M. ejnoha and J. ejnoha. (2009). 'Analysis of coupled heat and moisture transfer in masonry structures'. *Materials and Structures* 42 (8): 1153–1167.

Tada, S., and K. Watanabe. (1998). 'An overview of principles and techniques of moisture properties measurement for building materials and components'. In *Proceedings of the France–Japan Workshop on Mass-Energy Transfer and Deterioration of Building Materials and Components, Tsukuba, Japan, January 22–23, 1998*, 37–75.

Tang, W., C. I. Davidson, S. Finger and K. Vance. (2004). 'Erosion of limestone building surfaces caused by wind-driven rain: 1. Field measurements'. *Atmospheric Environment* 38 (33): 5589–5599. doi:10.1016/j.atmosenv.2004.06.030.

Tedoldi, F. (2002). 'Il progetto Eureka-Mouse: un metodo di Risonanza Magnetica Nucleare al servizio del Patrimonio Artistico'. *Rend. Sci. Istituto Lombardo B* 136:239–256.

Thornbush, M., and H. Viles. (2005). 'The Changing Façade of Magdalen College, Oxford: Reconstructing Long-Term Soiling Patterns from Archival Photographs and

Traffic Records'. *Journal of Architectural Conservation* 11 (2): 40–57. doi:10.1080/13556207.2005.10784944.

Tidblad, J., and V. Kucera. (2007). 'Dose-response functions and tolerable levels for corrosion in the multi-pollutant situation'. *Pollution atmosphérique* 49 (Oct): 87–93.

Timmons, S. (1976). *Preservation and conservation: principles and practices : proceedings of the North American International Regional Conference, Williamsburg, Virginia, and Philadelphia, Pennsylvania, September 10–16, 1972*. Preservation Press, National Trust for Historic Preservation in the United States.

Traversetti, L., F. Bartoli and G. Caneva. (2018). 'Wind-driven rain as a bioclimatic factor affecting the biological colonization at the archaeological site of Pompeii, Italy'. *International Biodeterioration & Biodegradation* 134:31–38. doi:10.1016/j.ibiod.2018.07.016.

Trotman, P. M., and H. Harrison. (2004). *Understanding dampness*. Watford, UK: BREbookshop.

Tsoka, S., and T. K. Thiis. (2018). 'Calculation of the driving rain wall factor using ray tracing'. *Journal of Wind Engineering and Industrial Aerodynamics* 179:190–199. doi:10.1016/j.jweia.2018.06.008.

Tsuchikawa, S., and H. Kobori. (2015). 'A review of recent application of near infrared spectroscopy to wood science and technology'. *Journal of Wood Science* 61 (3): 213–220. doi:10.1007/s10086-015-1467-x.

Twelmeier, H., S. T. Sperbeck and H. Budelmann. (2008). 'Restoration Mortar for Historical Masonry–Durability Prediction by means of numerical and Engineering Models'. In *14th International Brick and Block Masonry Conference, incorporating the 8th Australasian Masonry Conference, Sydney, Australia, February 13–20, 2008*.

Tzanis, A. (2006). 'MATGPR: A freeware MATLAB package for the analysis of common-offset GPR data'. *Geophysical Research Abstracts* 8 (09448).

UK Climate Projections. (2012). 'Weather Generator'. [HTML], accessed September 20, 2017. url: http://ukclimateprojections.metoffice.gov.uk/23261.

— . (2014). 'UK Climate Projections, UKCP09: Science & modelling FAQ'. [HTML], accessed November 19, 2018. url: http://ukclimateprojections.metoffice.gov.uk/22602#answer22704.

UK Met Office. (2006a). 'Met Office Integrated Data Archive System (MIDAS) UK Hourly Rainfall Data'. badc.nerd.ac.uk.

— . (2006b). 'Met Office Integrated Data Archive System (MIDAS) UK Hourly Weather Observation Data'. badc.nerd.ac.uk.

— . (2012). *Met Office Integrated Data Archive System (MIDAS) Land and Marine Surface Stations Data (1853-current)*.

— . (2018). 'How we measure wind'. [HTML], accessed November 19, 2018. url: https://www.metoffice.gov.uk/guide/weather/observations-guide/how-we-measure-wind.

Underwood, J. S., and V. Meentemeyer. (1998). 'Climatology of wind-driven rain for the contiguous United States for the period 1971–1995'. *Physical Geography* 19 (6): 445–462. doi:10.1080/02723646.1998.10642661.

University of the West of England. (2011). 'Evolution of Building Elements: External Walls'. [HTML], accessed august 21, 2018. url: https://fet.uwe.ac.uk/conweb/house_ages/elements/section2.htm.

Vadodaria, K., D. L. Loveday, V. Haines, V. Mitchell, B. Mallaband and S. H. Bayer. (2010). 'UK solid-wall dwellings-thermal comfort, energy efficiency refurbishment and the user perspective-some preliminary analysis from the CALEBRE project'. In *Proceedings of a Conference "Adapting to Change: New Thinking on Comfort", Cumberland Lodge, Windsor, UK, April 9–11, 2010*. London: Network for Comfort / Energy Use in Buildings (NCEUB).

Válek, J., S. Kruschwitz, J. Wöstmann, T. Kind, J. Valach, C. Köpp and J. Lesák. (2010). 'Nondestructive Investigation of Wet Building Material: Multimethodical Approach'.

Journal of Performance of Constructed Facilities 24 (5): 462–472. doi:10.1061/(asce)cf.1943-5509.0000056.

van Brakel, J. (1980). 'Mass transfer in convective drying'. *Advances in Drying* 1:217–267.

Vasconcelos, G., P. B. Lourenço, C. A. S. Alves and J. Pamplona. (2008). 'Ultrasonic evaluation of the physical and mechanical properties of granites'. *Ultrasonics* 48 (5): 453–466. doi:10.1016/j.ultras.2008.03.008.

Venmans, A. A. M., R. van de Ven and J. Kollen. (2016). 'Rapid and Non-intrusive Measurements of Moisture in Road Constructions Using Passive Microwave Radiometry and GPR–Full Scale Test'. *Procedia engineering* 143:1244–1251. doi:10.1016/j.proeng.2016.06.111.

Vereecken, E., and S. Roels. (2012). 'Review of mould prediction models and their influence on mould risk evaluation'. *Building and Environment* 51:296–310. doi:10.1016/j.buildenv.2011.11.003.

— . (2013). 'Hygric performance of a massive masonry wall: How do the mortar joints influence the moisture flux?' *Construction and Building Materials* 41:697–707. doi:10.1016/j.conbuildmat.2012.12.024.

Verstrynge, E., R. Adriaens, J. Elsen and K. Van Balen. (2014). 'Multi-scale analysis on the influence of moisture on the mechanical behavior of ferruginous sandstone'.

Construction and Building Materials 54:78–90.

doi:10.1016/j.conbuildmat.2013.12.024.

Viles, H. A. (2012). 'Microbial geomorphology: A neglected link between life and landscape'. Special Issue of Zoogeomorphology and Ecosystem Engineering Proceedings of the 42nd Binghamton Symposium in Geomorphology, Mobile, AL, USA, October 21–23, 2011, *Geomorphology* 157/158:6–16.

doi:10.1016/j.geomorph.2011.03.021.

— . (2013). 'Durability and conservation of stone: Coping with complexity'. *Quarterly Journal of Engineering Geology and Hydrogeology* 46 (4): 367–375.

doi:10.1144/qjegh2012-053.

Vitruvius. (n.d.). *De architectura, "II.8.7"*.

Völker, C., and P. Shokouhi. (2015a). 'Data aggregation for improved honeycomb detection in concrete using machine learning - Based algorithms'. In *Proceedings of the International Symposium Non-Destructive Testing in Civil Engineering (NDT-CE 2015), Berlin, Germany, September 15–17, 2015*, 1–8.

— . (2015b). 'Multi sensor data fusion approach for automatic Honeycomb detection in concrete'. *NDT&E International* 71:54–60. doi:10.1016/j.ndteint.2015.01.003.

Völker, C., S. Kruschwitz, G. Ebell and J. Shen. (2018). 'Towards Data Based Corrosion Analysis of Concrete with Supervised Machine Learning'. In *Proceedings of the*

NDE/NDT for Highway and Bridges: Structural Materials Technology (SMT 2018) and the International Symposium for Non-Destructive Testing in Civil Engineering (NDT-CE 2018), New Brunswick, NJ, USA, August 27–29, 2018. New Brunswick, New Jersey, USA.

Walker, R., S. Pavía and M. Dalton. (2016). 'Measurement of moisture content in solid brick walls using timber dowel'. *Materials and Structures* 49 (7): 2549–2561. doi:10.1617/s11527-015-0667-6.

Wang, Z. (1990). 'Effects of different pore fluids on seismic velocities in rocks'. *Canadian Journal of Exploration Geophysics* 26:104–112.

Warnes, A. R. (1926). *Building stones, their properties, decay, and preservation*. London, UK: E. Benn Ltd.

Warscheid, T., and J. Braams. (2000). 'Biodeterioration of stone: a review'. *International Biodeterioration & Biodegradation* 46 (4): 343–368. doi:10.1016/S0964-8305(00)00109-8.

Waters, C. N., J. Zalasiewicz, C. Summerhayes, A. D. Barnosky, C. Poirier, A. Gauszka, A. Cearreta, M. Edgeworth, E. C. Ellis, M. Ellis, C. Jeandel, R. Leinfelder, J. R. McNeill, D. d. Richter, W. Steffen, J. Syvitski, D. Vidas, M. Wagreich, M. Williams, A. Zhisheng, J. Grinevald, E. Odada, N. Oreskes and A. P. Wolfe.

(2016). 'The Anthropocene is functionally and stratigraphically distinct from the Holocene'. *Science* 351 (6269). doi:10.1126/science.aad2622.

Waters, E. H. (1965). 'Measurement of moisture in concrete and masonry with special reference to neutron scattering techniques'. *Nuclear Structural Engineering* 2 (5): 494–500. doi:10.1016/0369-5816(65)90077-3.

Watkins, R., G. J. Levermore and J. B. Parkinson. (2011). 'Constructing a future weather file for use in building simulation using UKCP09 projections'. *Building Services Engineering Research and Technology* 32 (3): 293–299. doi:10.1177/0143624410396661.

Watts, G., R. W. Battarbee, J. P. Bloomfield, J. Crossman, A. Daccache, I. Durance, J. A. Elliott, G. Garner, J. Hannaford, D. M. Hannah et al. (2015). 'Climate change and water in the UK–past changes and future prospects'. *Progress in Physical Geography* 39 (1): 6–28. doi:10.1177/0309133314542957.

Weber, R. A. (2013). 'Building envelope design guide—Masonry wall systems'. [PHP], accessed August 21, 2018. url: https://web.archive.org/web/20130314154143/http://wbdg.org/design/env_wall_masonry.php.

Weritz, F., S. Kruschwitz, C. Maierhofer and A. Wendrich. (2009). 'Assessment of Moisture and Salt Contents in Brick Masonry with Microwave Transmission,

Spectral-Induced Polarization, and Laser-Induced Breakdown Spectroscopy'. *International Journal of Architectural Heritage* 3 (2): 126–144. doi:10.1080/15583050802278992.

Wheatley, D., and C. Bickerton. (2017). 'Subjective well-being and engagement in arts, culture and sport'. *Journal of Cultural Economics* 41 (1): 23–45. doi:10.1007/s10824-016-9270-0.

Wickramarathne, T. L., K. Premaratne, M. N. Murthi, M. Scheutz, S. Kübler and M. Pravia. (2011). 'Belief theoretic methods for soft and hard data fusion'. In *Proceedings of the IEEE International Conference on Acoustics, Speech and Signal Processing (ICASSP), Prague, Czech Republic, May 22–27, 2011*, 2388–2391. doi:10.1109/ICASSP.2011.5946964.

Wilhelm, K. (2016). 'Improving non-destructive techniques for stone weathering research *in situ*'. PhD thesis, University of Oxford.

Wilhelm, K., H. Viles and O. Burke. (2016). 'The Influence of Salt on Handheld Electrical Moisture Meters: Can They Be Used to Detect Salt Problems in Porous Stone?' *International Journal of Architectural Heritage* 10 (6): 735–748. doi:10.1080/15583058.2015.1109733.

Wilkinson, J., D. De Rose, J. F. Straube and B. Sullivan. (2009). 'Measuring the impact of interior insulation on solid masonry walls in a cold climate'. In *Proceedings of the*

12th Canadian Building Science & Technology Conference, Montreal, QC, Canada, May 6–8, 2009, 97–110.

Wilks, D. S., and R. L. Wilby. (1999). 'The weather generation game: a review of stochastic weather models'. *Progress in Physical Geography* 23 (3): 329–357. doi:10.1177/030913339902300302.

Winkler, E. M. (1966). 'Important agents of weathering for building and monumental stone'. *Engineering Geology* 1 (5): 381–400. doi:10.1016/0013-7952(66)90003-2.

Winkler, E. M. (1987). 'Weathering and weathering rates of natural stone'. *Environmental Geology and Water Sciences* 9 (2): 85–92. doi:10.1007/BF02449939.

Wolkenhauer, O. (2001). 'On Information Fusion in the Life-Sciences'. In *Data Fusion and Perception*, ed. by G. Della Riccia, H.-J. Lenz and R. Kruse, 121–134. Vienna, Austria: Springer. doi:10.1007/978-3-7091-2580-9_7.

Woodcock, N. H., and R. A. Strachan. (2012). *Geological History of Britain and Ireland*. Chichester, UK: Wiley.

Wormald, R., and A. L. Britch. (1969). 'Methods of measuring moisture content applicable to building materials'. *Building science* 3 (3): 135–145. doi:10.1016/0007-3628(69)90026-7.

Xu, W., R. F. Adler and N.-Y. Wang. (2014). 'Combining Satellite Infrared and Lightning Information to Estimate Warm?Season Convective and Stratiform Rainfall'. *Journal of*

Applied Meteorology and Climatology 53 (1): 180–199. doi:10.1175/JAMC-D-13-069.1.

Yee, C. (1946). *The silent traveller in Oxford*. 3rd ed. London, UK: Methuen.

Yelf, R. (2004). 'Where is true time zero?' In *Proceedings of the Tenth International Conference on Ground Penetrating Radar (GPR 2004), Delft, The Netherlands, June 21–24, 2004*, 279–282. Delft.

Young, M. E. (2015). *Thermal Imaging in the Historic Environment*. Short Guide 10. Edinburgh, UK: Historic Environment Scotland.

Young, M. E., D. C. M. Urquhart and R. A. Laing. (2003). 'Maintenance and repair issues for stone cleaned sandstone and granite building façades'. *Building and Environment* 38 (9-10): 1125–1131. doi:10.1016/S0360-1323(03)00084-2.

Zahiri, Z., D. F. Laefer and A. Gowen. (2018). 'The feasibility of short-wave infrared spectrometry in assessing water-to-cement ratio and density of hardened concrete'. *Construction and Building Materials* 185:661–669. doi:10.1016/j.conbuildmat.2018.07.082.

Zahran, O., S. Shihab and W. Al-Nuaimy. (2002). 'Comparison between surface impulse ground penetrating radar signals and ultrasonic time-of-flight diffraction signals'. In *Proceedings of the 7th IEEE High Frequency Postgraduate Student Colloquium, London, UK, September 8–9, 2002*. IEEE.

Zappa, G., L. C. Shaffrey, K. I. Hodges, P. G. Sansom and D. B. Stephenson. (2013). 'A multimodel assessment of future projections of North Atlantic and European extratropical cyclones in the CMIP5 climate models'. *Journal of Climate* 26 (16): 5846–5862. doi:10.1175/JCLI-D-12-00573.1.

Zhao, J. H., E. Rivera, A. Mufti, D. Stephenson and D. J. Thomson. (2012). 'Evaluation of dielectric based and other methods for moisture content measurement in building stones'. *Journal of Civil Structural Health Monitoring* 2 (3-4): 137–148. doi:10.1007/s13349-012-0024-1.

Zhao, T. (2015). 'Effective medium modeling and experimental characterization of multilayer dielectric with periodic inclusion'. PhD thesis, Iowa State University.

Part V

Appendices

A | Geological Strata of Great Britain

This appendix is a map of geological strata on the island of Great Britain, demonstrating the diversity of ages and rock types.

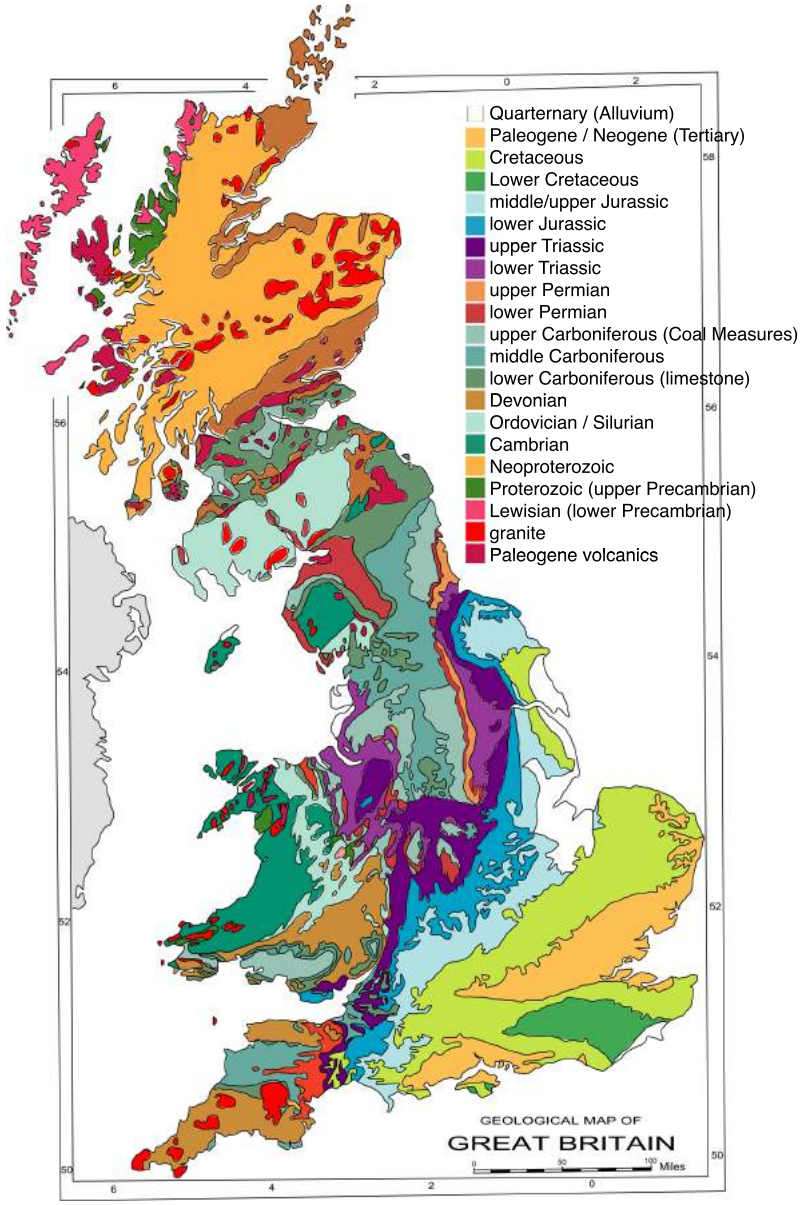

Figure A.1. The geological strata of Great Britain. Adapted from 'Geology map of Great Britain, which is part of the United Kingdom' by AlexD, Wikimedia, CC BY-SA 3.0.

B | Supplementary Information to Paper IV: normalised value representation of moisture measurement data

This appendix was prepared as Supplemental Information for Paper IV (Chapter 7) and presents figures similar to a subset of those presented in Chapter 7 but using normalised values instead of percentile representation.

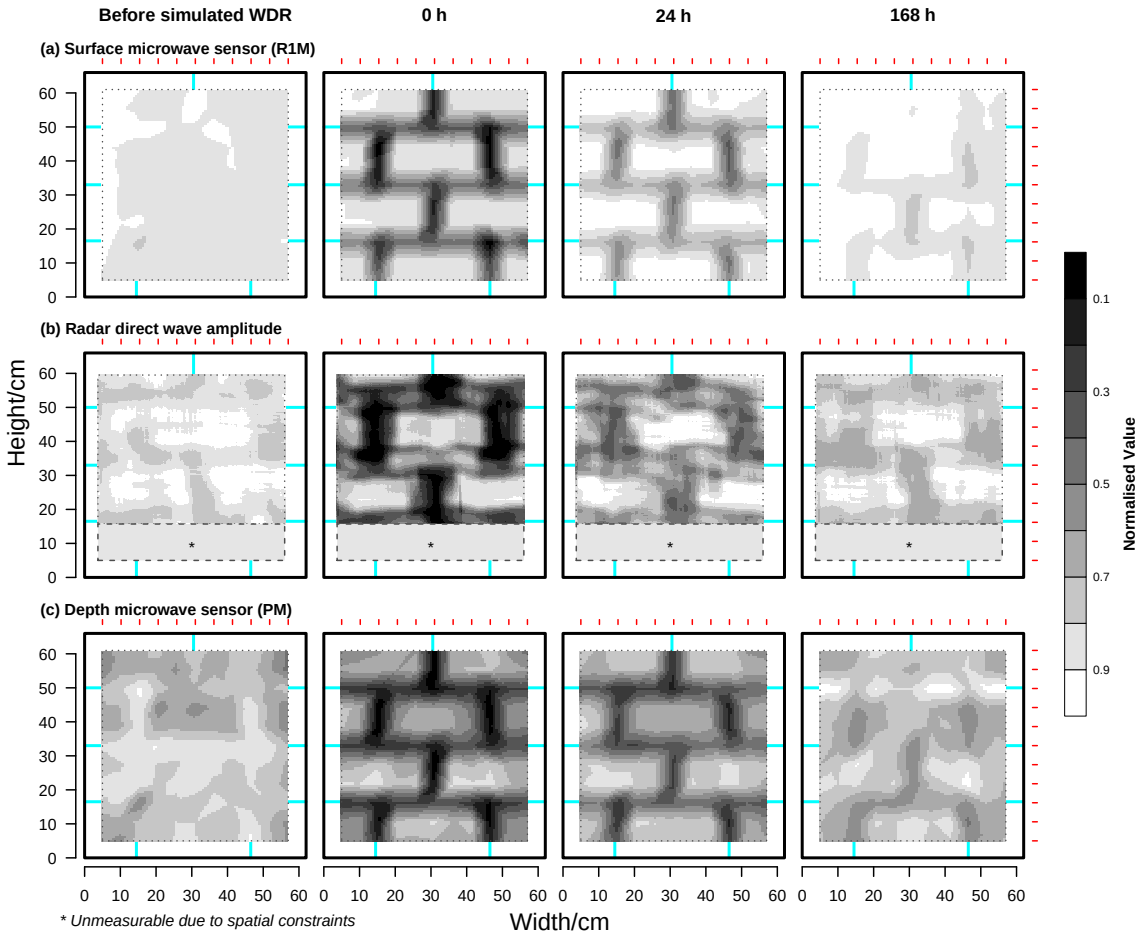

Figure B.1. Spatial representations of a granite masonry wall drying after simulated WDR exposure, represented with normalised values. Measurements from the non-destructive techniques: (a) microwave surface sensor (R1M), (b) radar direct wave amplitude, and (c) microwave depth sensor (PM). The areas outside the dotted lines indicate areas of the wall that were not measured as they were too close to the edges. Blue lines indicate locations of mortar joints, while red lines indicate the measurement grid. This figure is identical to Figure 7.3 (p. 192) except that the latter uses percentile representation.

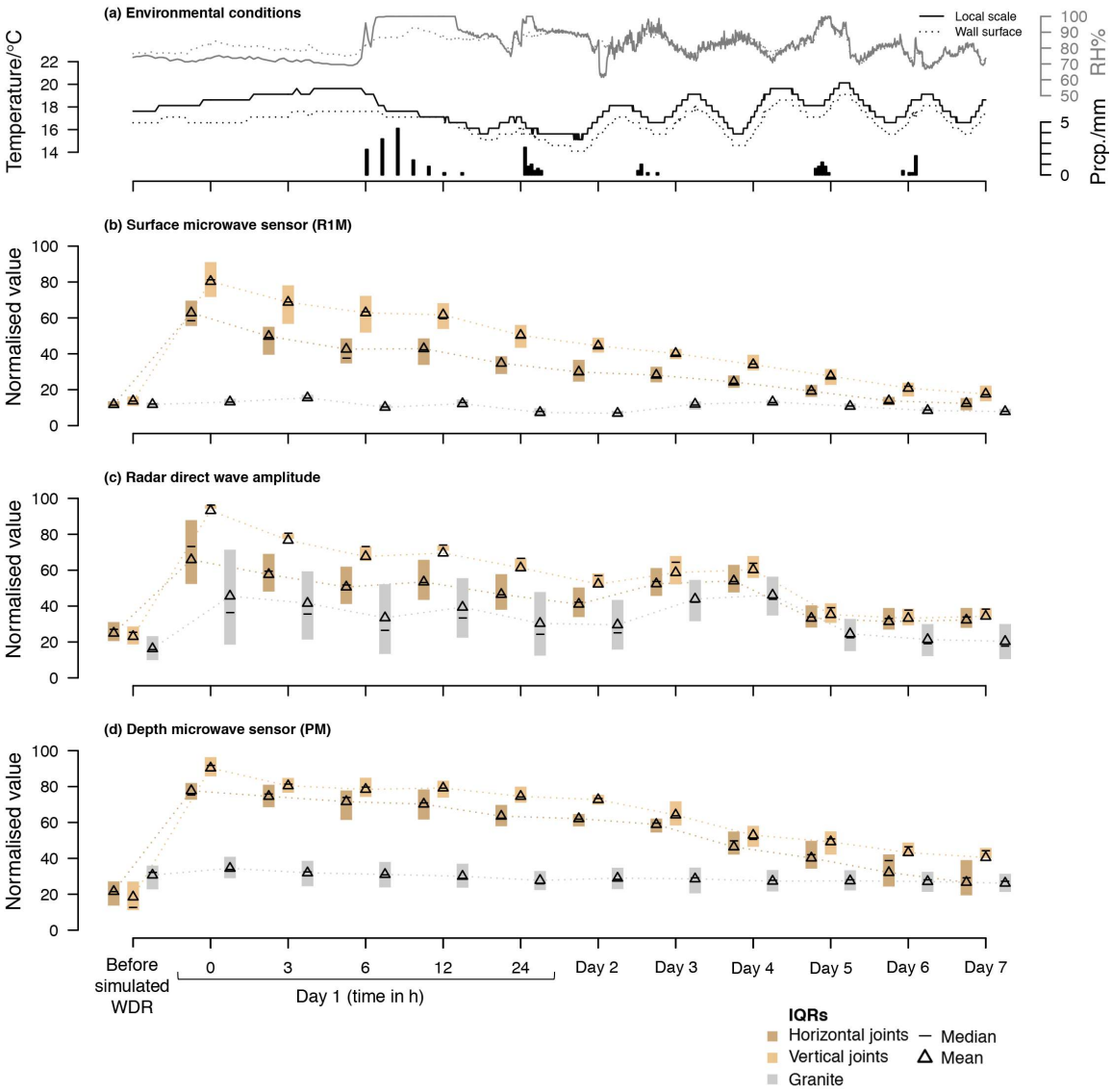

Figure B.2. Temporal representations of components of a granite masonry wall during drying after simulated WDR exposure during the Oxford experiment. (a) Environmental conditions, (b) surface microwave sensor (R1M), (c) Radar direct wave amplitude, and (d) Depth microwave sensor (PM). This Figure is identical to Figure 7.4 (p. 194) except that the latter uses percentile representation.

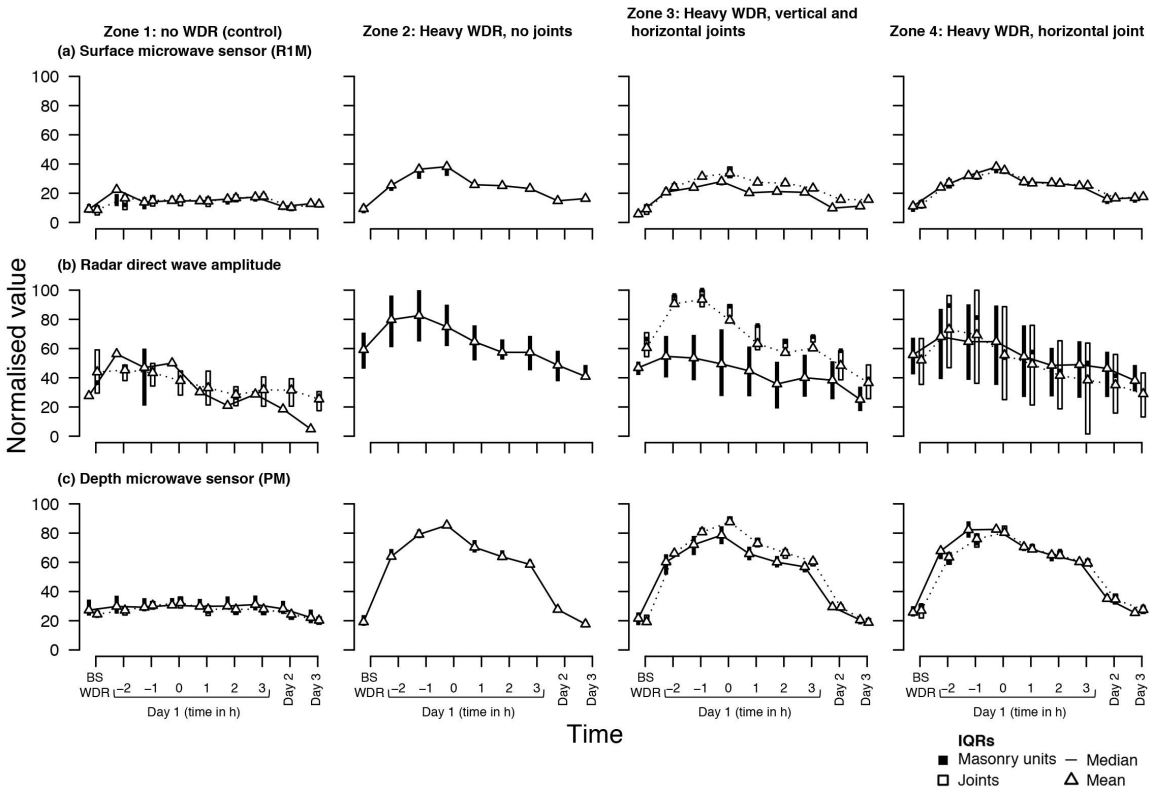

Figure B.3. Measurement percentiles for two microwave sensors and a radar variable for mortar joint configurations within the sandstone façade of New College, Edinburgh (Scenario B). (a) Surface microwave sensor (R1M); (b) Radar direct wave amplitude; (c) Depth microwave sensor (PM). 'BS WDR' = Before Simulated WDR. Negative time references represent hours within the spell ($t = 0$ is the beginning of the drying process). This figure is identical to Figure 7.8 (p. 202) except that the latter uses percentile representation.

C | Pilot study: comparability of non-destructive moisture measurement techniques on masonry during simulated wetting

Published as: Orr, S. A., H. A. Viles, A. Leslie, and D. Stelfox. (2016). 'Comparability of non-invasive moisture measurement techniques on masonry during artificial post-rainspell drying', In *Proceedings of the 13th International Congress on the Deterioration and Conservation of Stone, Paisley, UK, 5–10 September, 2016*, 2:431–438.

Abstract

Detecting the presence of moisture in historical masonry is essential to understanding how a structure interacts with the environment, and diagnosing the potential for damage from a range of physical, chemical, and biological processes. In-situ, non-invasive diagnostic techniques have been developed in preference to methods that require irreversible modifications to a structure. These techniques include: electrical resistivity, microwaves, and infrared thermography. Independently, these approaches provide limited snapshots of surficial and internal moisture regimes; this project sought to assess the comparability of multiple techniques. Simulated post-rain spell drying was monitored over 48 h on limestone and sandstone monoliths in a controlled laboratory environment and also in ambient conditions on purpose-built masonry located in Oxfordshire, UK. Repeat measurements were taken using electrical resistance tomography (ERT), electrical and microwave moisture meters, and infrared thermography. Three aspects of comparability are discussed: i) data transformations and geological comparability, ii) depth-resolving meter readings, iii) the localised benefits of employing multiple technologies and instruments.

This chapter is a reprint of Orr et al. (2016). It presents the results of a pilot study of this thesis incorporating both electrical resistive and electromagnetic techniques.

C.1 Introduction

Water is an important factor in stone deterioration, acting as a primary and secondary agent in a range of chemical, physical, and biological deterioration mechanisms. The role of water in specific mechanisms depends on its spatial and temporal patterning (Mamillan, 1991). To this end, it is necessary to be able to detect and monitor local variation of water within stonework and masonry structures.

Non-invasive moisture monitoring techniques have been developed for the historical environment as an alternative to invasive techniques. These include electrical resistance tomography (ERT), which has been employed to successfully monitor short-term moisture regimes in historic masonry (Martinho et al., 2010). In contrast, thermography and handheld moisture meters (or 'damp' meters) have been adopted from civil engineering, but are primarily intended for use on twentieth-century materials. Handheld meters have been assessed for relative performance and best practice (Eklund et al., 2013) for use on stone but their applicability to masonry with regards to how they compare to more robust analytical equipment is yet to be established.

This paper compares two handheld moisture meters and infrared thermography to electrical resistance tomography to investigate moisture dynamics, discussing aspects of technological comparability for complex masonry constructions and information gained by combining multiple devices.

C.2 Material and methods

C.2.1 Materials

Two stone monoliths were used: a sandstone block measuring 55 x 32 x 25.5 cm (obtained from a quarry) and a limestone block (from a waste site) measuring 71 x 38 cm in height and length respectively (see Figure C.1a), with an uneven width varying from 9 to 20 cm. The limestone block has a discolouration running down the front surface suggesting near-surface physical inconsistencies, and could be indicative of defects at further depths.

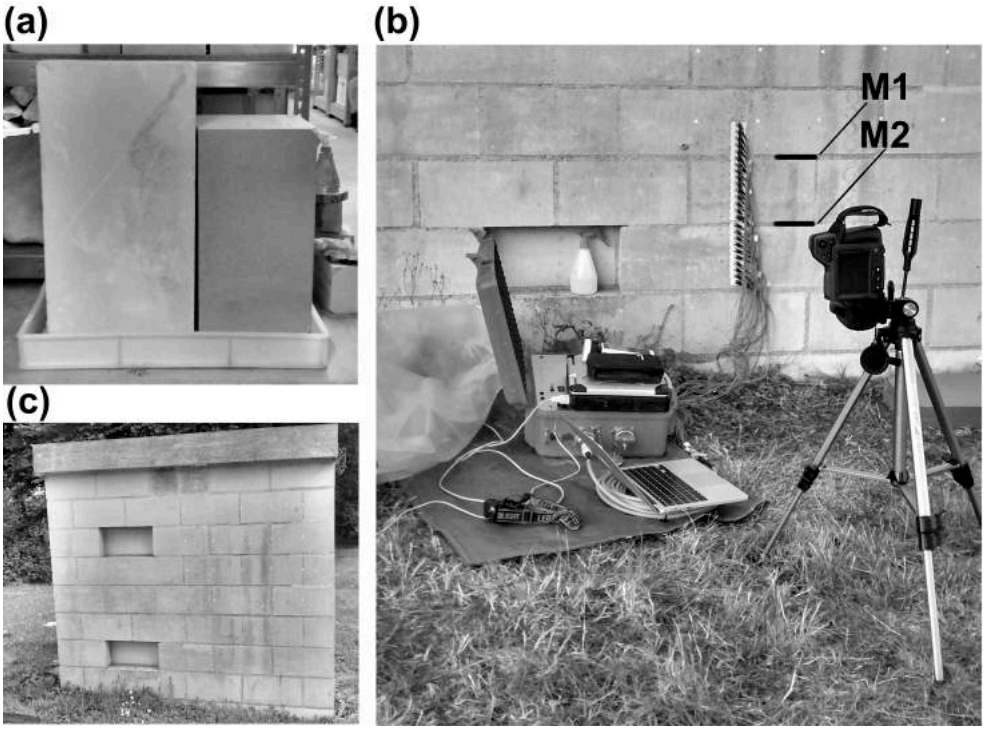

Figure C.1. The monoliths (left, limestone; right, sandstone) (a) and the traditional masonry construction (b). An example of the simultaneous instrument set-up with positions of the mortar joints: M1 and M2 (c).

The masonry construction is 1.8 m high and 2.0 m wide, and comprises a single skin of

Elm Park limestone ashlar blocks (20 x 20 x 40 cm) with 2 cm lime mortar joints (Figure C.1b). It is located in a field with sparse tree cover in Oxfordshire, England. Measurements were taken in July 2015. The wall has an exposed western faade that receives direct sunlight between 13:00–15:00 h and 17:00–19:00 h daily in summer if not obscured by cloud cover.

C.2.2 Experimental protocol

This study monitored drying for 48 h after simulated rain events across 48 cm vertical transects of 25 evenly-spaced 2 cm nodes. The ERT apparatus could not be removed from the stone surface for the employed time scales, so handheld meter measurements were taken on a parallel transect separated from the former by 8 cm (Figure C.1c). Preliminary testing on the monoliths demonstrated two ERT transects separated by 15 cm and equally-distanced from the edges were highly correlated, and had similar wetting and drying properties (Orr, 2015). Thus, the parallel transects were considered to be comparable representations of drying processes, with error $\leq 15\%$. The monoliths were equilibrated and tested under stable temperature and RH.

Moisture instrument readings were taken along the transects at hourly intervals for the initial 12 h of drying, after which measurements were taken at 3, 6, 12 and 24 h; this timescale captures the dynamic nature of surface desorption through evaporation. For unsaturated flow in porous media the cumulative moisture migration i (in this case, i_{drying}) can be defined as $i_{dry} = Rt^{1/2}$, in which R is a material property of desorptivity equal to the

Boltzman transformation $\phi = xt^{1/2}$ integrated over a moisture content θ differential for a vertical distance x in time t (Hall and Hoff, 2012, p. 114). This relationship dictates that rates of desorption decrease significantly with time; deviations typically occur in fabricated materials and were unexpected for the selected stones (Hall and Hoff, 2012, p. 129).

A driving rain index was derived to determine the quantity of water that should be applied to emulate driving rain spells based on EN ISO 15927-3:2009 (ISO, 2009) for the Oxfordshire field site. Meteorological data was taken from the UK MIDAS database at a site 20 km from the site; in predominantly flat regions, indices are applicable up to 100 km away. The following parameters were employed:

- Roughness factor for Tier II terrain for 'farm land with boundary hedges, occasional small farm structures, houses or trees'
- Wall geometry factor = 0.4, reflecting the lower portion of a 'two-story building with flat roof (pitch $< 20°$)'
- Topography and obstruction factors = 1, ie. no index reductions

The determined spell index I_S is the 67th percentile of I_S, representing the maximum value of I'_S likely to occur in a three year period. A wall spell index = 6.5 L m^{-2} hr^{-1} (calculated for 1985–2014) of distilled water was applied over 1 h with a small pressured spray bottle in roughly rectangular areas surrounding the transects.

C.2.3 Instrumentation

A GeoTom device (Geolog2000; Augsburg, Germany) was used to collect the two-dimensional resistance profiles in conjunction with crocodile clip shielded cables and self-adhesive electrocardiogram electrodes affixed to the stone surface. Adhesive electrodes were used instead of drilled-in steel electrodes as they are non-invasive, and have been shown to have similar contact resistance to implanted steel electrodes (Sass and Viles, 2006). Data were collected with a linear Wenner array and inverted into apparent resistivity models using RES2DINV v. 3.59 (GeoTomo Software; Malaysia).

Electrical resistance is also influenced by material properties, physical characteristics, and salts (Martinho et al., 2010) which creates ambiguity leading to misinterpretation of direct-current measurements (Kruschwitz, 2007, p. 2). However, ERT has been shown to relate to moisture contents with gravimetric calibration methods (Sass, 1998) through an extension of Archie's Law relating saturation and resistivity with the appropriate assumptions (Sass and Viles, 2010b) . Lime mortar has been shown to have commensurate dielectric properties to limestone (Ball et al., 2011). In addition to ERT, the following were used to monitor moisture:

- Surveymaster Protimeter (GE Measurement & Control; Billerica, MA, USA) includes a pin-type resistance meter with a sensor consisting of two 10 mm long stainless steel pins spaced approximately 14 mm apart, a wood moisture equivalent

(WME) from 0–100.

- T610 (Trotec; Marchtrenk, Austria) produces a microwave field penetrating 20–30 cm that is subsequently reflected and converted into nominal values from 0–200.

- T460 thermal imaging camera (FLIR; Wilsonville, OR, USA) was used to capture surface temperatures of the monoliths and masonry wall areas surrounding the transects; it has a thermal sensitivity of < 0.03 °C and an output resolution of 240 x 320 pixels.

C.3 Results and discussion

C.3.1 Data transformations

ERT timeseries were logarithmically transformed and normalised to initial, pre-wetting stage resistivities (ρ_{pw}). These do not represent completely 'dry' states; the pre-wetting measurements represent the stone at a particular phase of hygrothermal transition. The transformed resistivities $\rho_i' = -log_{10}(\rho_i/\rho_{pw})$ enabled comparison between the monoliths and the masonry construction at depths with pseudo-values linearly proportional to moisture contents. Values of ρ_i' theoretically range within (∞, 0); as $\rho' \rightarrow 0$ the resistivity (and thus purported moisture content) are returned to the pre-wetting stage. Practically, values of ρ' did not exceed 2.

Inversion uncertainties were greater for the pre-wetting states, tending to increase

over the duration of the drying process: this is likely caused by the software's difficulty with handling the geological realism of inverting very dry stone (Sass and Viles, 2010b). This complicated obtaining appropriate values of ρ_{pw}; however, the benefit of lognormal transformation is that the pre-wetting denominator induces only a vertical shift of ρ' in the lognormal dimension. While pre-wetting resistivities can be analysed, two parameters independent of this enable valuable discussion: i) the shape of the drying curve, and ii) $\Delta\rho_{f-0}$.

The meter readings v exhibit linear behaviour similar to the ERT depth ρ' curves (Figure C.2). This suggests that the instrument readings calibrate linearly to moisture contents. This implies that relative meter readings (additive/subtractive from a reference value, ie. Δv_{ref-i}) can be considered proportional to moisture contents. While the idea of 'relative readings' is not novel in moisture meter best practice, previous guidance has suggested using (Burkinshaw and Parrett, 2003, p. 76); this relationship is not ideal for interpreting the readings of some handheld meters.

The surface resistance meter captured a constant surface value of moisture before decreasing to the pre-wetting conditions, which corresponds to the inversion of the ERT surface measurement. It has been shown that this meter model is able to produce WMEs higher than these values on English limestones (Eklund et al., 2013), so it was not suspected to represent moisture contents out of instrumental range.

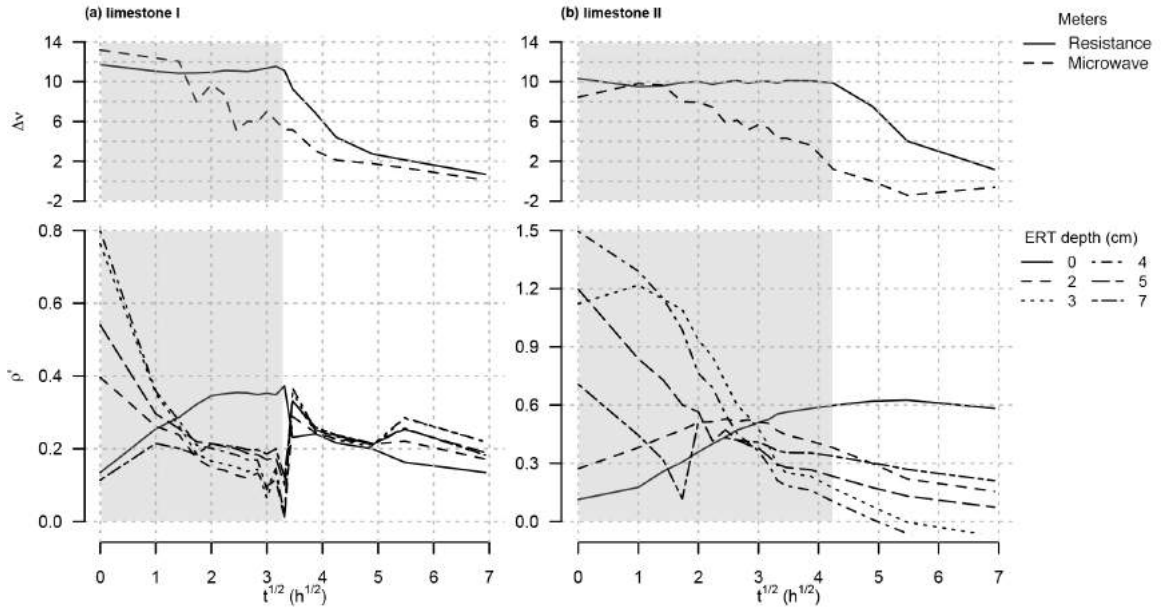

Figure C.2. Transformed meter readings Δv and ERT depth moisture profiles ρ' for two iterations of the limestone monolith moisture regimes.

C.3.2 Depth-resolved damp meter modelling

No single ERT depth profile was found to characterise the moisture meter readings over the total drying duration in isolation: there were periods when certain depths had Pearson's $R > 0.8$, but negative coefficients indicated relationships to a lack of moisture following a migration to adjacent depth(s). To this end, multiple linear regression models were created using non-negative least squares (NNLS) regression for each of the monolith and stone masonry experimental runs.

NNLS is a least squares regression in which coefficients are restricted to positive values, based on an algorithm developed by Lawson and Hanson (1995). As the residuals of a NNLS regression are not normally distributed, typical evaluation parameters (eg.

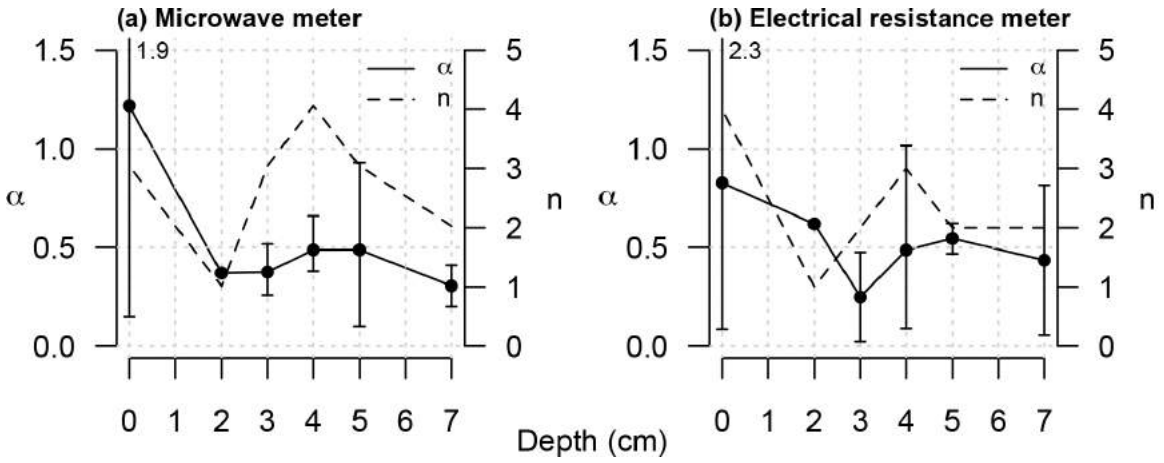

Figure C.3. NNLS regression results for handheld meters: Coefficients and quantity of regression models incorporating depth. Vertical bars indicate maxima and minima.

confidence intervals, p-values) are not applicable, so each predictor column (ERT depths) and the meter reading vectors were normalised between 0 and 1 (Slawski and Hein, 2013): regressions coefficients represent the relative contributions of independent variables.

Both handheld meters exhibited decreasing correlation with the ERT as depth increased, an effect that was seen more strongly with the microwave meter (Figure C.3).

C.3.3 Multi-instrument utility

The surface resistance meter captured distinct mortar behaviour due to the high resolution and localised readings. In contrast, the microwave meter and ERT did not capture distinct moisture movements through the mortar as clearly due to wider detection range and smoothing techniques, respectively.

Passive IR thermography was able to capture early rapid edge-adjacent evaporation transitioning to front surface evaporation in the stone monoliths, in addition to subsequent

higher moisture concentrating at the base, adjacent to an impermeable plastic barrier (Figure C.4). These phenomena are difficult to assess or characterise with other non-destructive techniques due to interference from the adjacent air space.

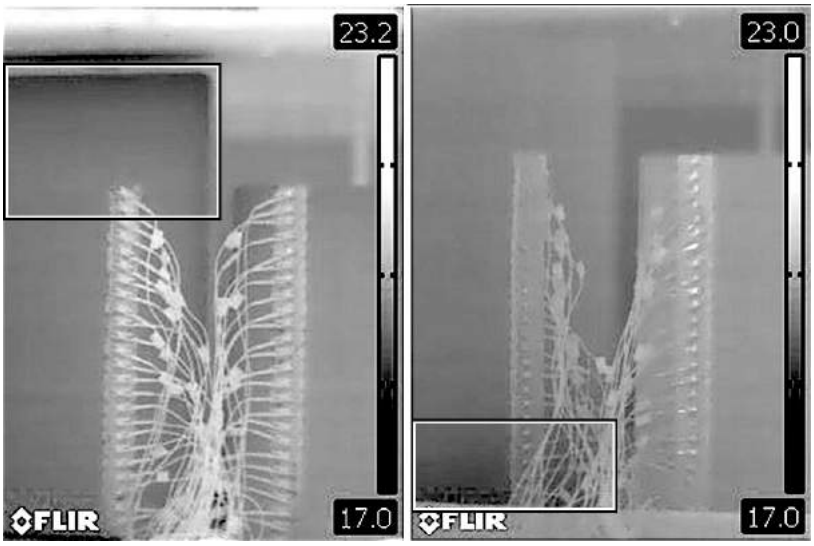

Figure C.4. A distinct transfer of significant moisture migration at monolith edges mid-drying (left) and collected base water at 48 h (right) is highlighted in boxes, where darker zones represent areas of higher moisture content.

Mortar-adjacent behaviour was assessed by comparing the mortar moisture contents to the adjacent ashlar units: positive values represent mortar readings greater than the surrounding areas, as would be expected for a more porous building material designed to aid moisture migration through masonry.

The early electrical mortar readings were commensurate to the surrounding stone representing similar moisture contents during the latent phase of activity, after which mortar moisture contents increase (Figure C.5). Differences in dielectric properties can be discounted as a crucial factor: pre-wetting readings differed by 0.1 WME between the mortar joints and the surrounding stonework, respectively. The microwave meter captures

the mortar joint behaviour to a lesser extent: there is significant variation above and below the mortar joint during the latent phase of moisture transport but mortar meter readings are similar to the electrical resistance meter after $t^{1/2} = 2$. In contrast, ERT does not exhibit any distinct near-mortar behaviour.

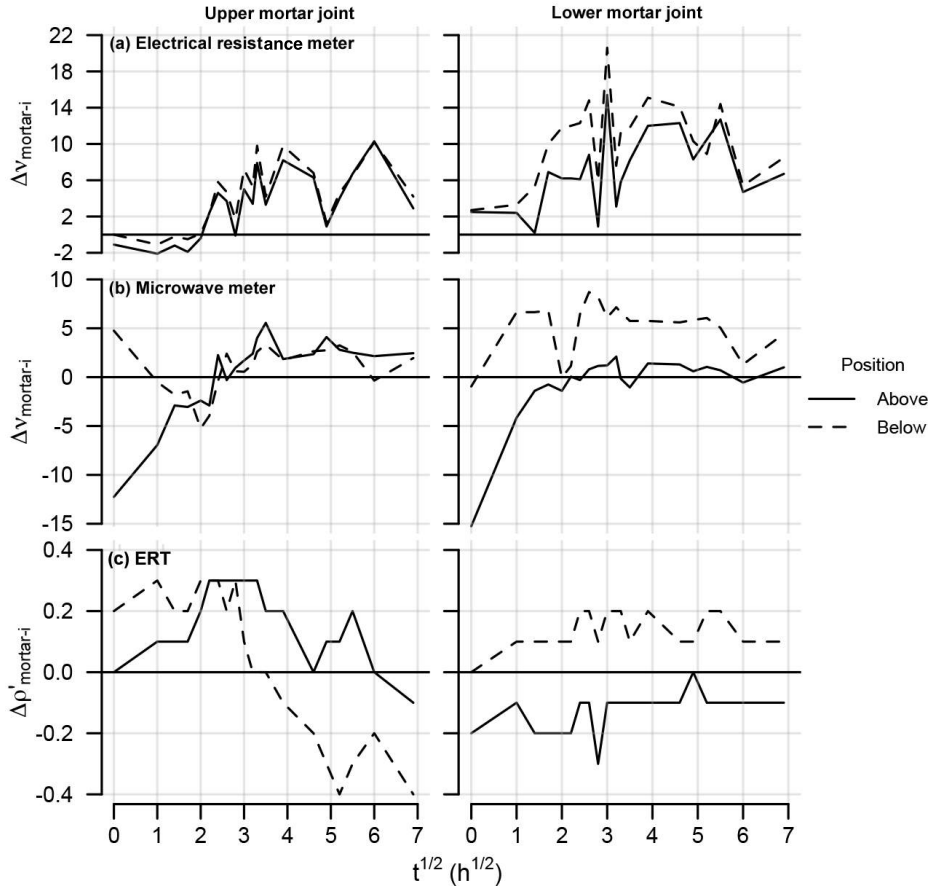

Figure C.5. Differential instrument readings above and below mortar joints within the stone for the electrical resistance meter (a), the microwave meter (b), and ERT (c). Values are presented relative to the upper (M1) and lower (M2) mortar joint values (see Figure C.1c); positive values represent higher moisture than the surrounding areas.

C.4 Conclusions

Spatial and temporal comparisons of data from handheld moisture meters and infrared thermography with electrical resistance tomography produced valuable information on how instrument measurements interacted with the masonry elements.

Distinct mortar joint and near-edge behaviour was distinguished by the handheld meters and infrared thermography, identifying important characteristics of moisture migration that would have otherwise been unnoticed by ERT.

Although handheld meter signals may penetrate a certain range, they are less attuned to detecting water at greater depths as their readings are more representative of near-surface moisture regimes.

Identifying building elements and conditions for which instrument types are most applicable enables efficient moisture surveys, but interpretation should consider different building materials and, if possible, incorporate laboratory validation.

D | Statements of substantive contributions from paper co-authors

This appendix includes signed statements from the co-authors of the papers included herein confirming that, as represented by first authorship, the candidate has made a substantive contribution.

As a co-author on the following publication(s) (published and/or in preparation), I undersign to confirm that the first author **Scott Allan Orr** has made a substantive contribution to the conceptualisation, data collection, analysis, writing, and revising of the manuscript(s).

Orr, S.A. and Viles, H., 2018. Characterisation of building exposure to wind-driven rain in the UK and evaluation of current standards. *Journal of Wind Engineering and Industrial Aerodynamics*, 180, pp. 88-97. DOI: 10.1016/j.jweia.2018.07.013

Orr, S.A., Young, M., Stelfox, D., Curran, J. and Viles, H., 2018. Wind-driven rain and future risk to built heritage in the United Kingdom: Novel metrics for characterising rain spells. *Science of the Total Environment*, 640, pp. 1098-1111. DOI: 10.1016/j.scitotenv.2018.05.354

Orr, S.A., Young, M., Stelfox, D., Leslie, A., Curran, J. and Viles, H. An 'isolated diffusion' gravimetric calibration procedure for radar and microwave moisture measurement in porous building stone. In review.

Orr, S.A., Fusade, L., Young, M., Stelfox, D., Leslie, A., Curran, J. and Viles, H. Moisture monitoring of stone masonry: a comparison of microwave and radar on a granite wall and a sandstone tower. In preparation.

_____Professor Heather Viles, Head of School of Geography and the Environment

(name and position)

_____ 30th August 2018

(signature and date)

Figure D.1. Co-author statement from Professor Heather Viles, Head of School of Geography and the Environment, University of Oxford.

As a co-author on the following publication(s) (published and/or in preparation), I undersign to confirm that the first author **Scott Allan Orr** has made a substantive contribution to the conceptualisation, data collection, analysis, writing, and revising of the manuscript(s).

Orr, S.A., Young, M., Stelfox, D., Curran, J. and Viles, H., 2018. Wind-driven rain and future risk to built heritage in the United Kingdom: Novel metrics for characterising rain spells. *Science of the Total Environment*, 640, pp. 1098-1111. DOI: 10.1016/j.scitotenv.2018.05.354

Orr, S.A., Young, M., Stelfox, D., Leslie, A., Curran, J. and Viles, H. An 'isolated diffusion' gravimetric calibration procedure for radar and microwave moisture measurement in porous building stone. In review.

Orr, S.A., Fusade, L., Young, M., Stelfox, D., Leslie, A., Curran, J. and Viles, H. Moisture monitoring of stone masonry: a comparison of microwave and radar on a granite wall and a sandstone tower. In preparation.

__Dr Maureen E Young (Conservation Scientist, Historic Environment Scotland)_____
(name and position)

M.E. Young 6/9/18__
(signature and date)

Figure D.2. Co-author statement from Dr Maureen Young, Conservation Scientist at Historic Environment Scotland.

As a co-author on the following publication(s) (published and/or in preparation), I undersign to confirm that the first author **Scott Allan Orr** has made a substantive contribution to the conceptualisation, data collection, analysis, writing, and revising of the manuscript(s).

Orr, S.A., Young, M., Stelfox, D., Curran, J. and Viles, H., 2018. Wind-driven rain and future risk to built heritage in the United Kingdom: Novel metrics for characterising rain spells. *Science of the Total Environment*, 640, pp. 1098-1111. DOI: 10.1016/j.scitotenv.2018.05.354

Orr, S.A., Young, M., Stelfox, D., Leslie, A., Curran, J. and Viles, H. An 'isolated diffusion' gravimetric calibration procedure for radar and microwave moisture measurement in porous building stone. In review.

Orr, S.A., Fusade, L., Young, M., Stelfox, D., Leslie, A., Curran, J. and Viles, H. Moisture monitoring of stone masonry: a comparison of microwave and radar on a granite wall and a sandstone tower. In preparation.

Dawson Stelfox, Conservation Architct, Consarc Design Group Ltd

31st August 2018

Figure D.3. Co-author statement from Mr Dawson Stelfox, Chairman of the Consarc Design Group.

As a co-author on the following publication(s) (published and/or in preparation), I undersign to confirm that the first author **Scott Allan Orr** has made a substantive contribution to the conceptualisation, data collection, analysis, writing, and revising of the manuscript(s).

Orr, S.A., Young, M., Stelfox, D., Curran, J. and Viles, H., 2018. Wind-driven rain and future risk to built heritage in the United Kingdom: Novel metrics for characterising rain spells. *Science of the Total Environment*, 640, pp. 1098-1111. DOI: 10.1016/j.scitotenv.2018.05.354

Orr, S.A., Young, M., Stelfox, D., Leslie, A., Curran, J. and Viles, H. An 'isolated diffusion' gravimetric calibration procedure for radar and microwave moisture measurement in porous building stone. In review.

Orr, S.A., Fusade, L., Young, M., Stelfox, D., Leslie, A., Curran, J. and Viles, H. Moisture monitoring of stone masonry: a comparison of microwave and radar on a granite wall and a sandstone tower. In preparation.

JOANNE CURRAN (ASSOCIATE)

(name and position)

Joanne Curran 31/08/2018.

(signature and date)

Figure D.4. Co-author statement from Dr Joanne Curran, Associate of the Consarc Design Group.

As a co-author on the following publication(s) (published and/or in preparation), I undersign to confirm that the first author **Scott Allan Orr** has made a substantive contribution to the conceptualisation, data collection, analysis, writing, and revising of the manuscript(s).

Orr, S.A., Young, M., Stelfox, D., Leslie, A., Curran, J. and Viles, H. An 'isolated diffusion' gravimetric calibration procedure for radar and microwave moisture measurement in porous building stone. In review.

Orr, S.A., Fusade, L., Young, M., Stelfox, D., Leslie, A., Curran, J. and Viles, H. Moisture monitoring of stone masonry: a comparison of microwave and radar on a granite wall and a sandstone tower. In preparation.

Alick Leslie,

Senior Buildings Conservation Advisor, Historic England_____

(name and position)

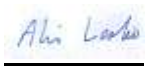

4th September 2018_____

(signature and date)

Figure D.5. Co-author statement from Dr Alick Leslie, formerly the Director of Conservation Science at Historic Environment Scotland.

As a co-author on the following publication(s) (published and/or in preparation), I undersign to confirm that the first author **Scott Allan Orr** has made a substantive contribution to the conceptualisation, data collection, analysis, writing, and revising of the manuscript(s).

Orr, S.A., Fusade, L., Young, M., Stelfox, D., Leslie, A., Curran, J. and Viles, H. Moisture monitoring of stone masonry: a comparison of microwave and radar on a granite wall and a sandstone tower. In preparation.

Lucie Fusade
Doctoral student School of Geography and the Environment

(name and position)


31/08/2018

(signature and date)

Figure D.6. Co-author statement from Ms Lucie Fusade, Doctoral Student in the School of Geography and the Environment, University of Oxford.

"But life is too short and precious for us to pass through it without leaving a few footprints behind us . . . Why should I not leave a few words to mark one period in my brief life? Even a bird's clawprints remain for a little time in the snow. Let these impressions of my short years in Oxford remain as long."

– CHIANG YEE 蔣彝, 'The Silent Traveller' (1946, p. 2)